# UNIVERSITA' DELLA CALABRIA

Dipartimento di Biologia, Ecologia e Scienze della Terra

## Dottorato di Ricerca in

Scienze della Vita

XXXIII **CICLO**

**Settore Scientifico Disciplinare:** MED/04

# TORSIN A ACTING AS A MECHANOSENSOR MODULATES NUCLEAR TRANSPORT IN PATHOPHYSIOLOGICAL CONDITIONS

**Coordinatore:** Ch.mo Prof. Maria Carmela Cerra

**Supervisore**: Ch.mo Prof. Marcello Maggiolini

**Dottorando:** Dott.ssa Giulia Raffaella Galli

Anno accdemico 2020/2021

# Index

**Chapter 3**

## Chapter 4

# *Abstract*

Gli esseri umani e l'ambiente circostante comunicano anche attraverso forze meccaniche. Gli input meccanici provenienti dal mondo che ci circonda svolgono un ruolo cruciale nei processi fisiologici e nel mantenimento dell'omeostasi dell'organismo umano. D'altra parte, difetti nelle proprietà meccaniche delle cellule o alterazioni delle forze meccaniche sono coinvolti nelle cause di diverse patologie tra cui il cancro. Le cellule del nostro corpo rispondono attivamente alle forze meccaniche, traducendo tali stimoli in segnali biochimici e nella regolazione dell'espressione genica. Il nucleo, costituito da due membrane separate che controllano il trasporto delle molecole, svolge un ruolo centrale nelle vie della meccano-trasduzione. Il trasporto nucleare delle molecole è meccanicamente sensibile ed è costituito da varie proteine coinvolte nel trasferimento di forze tra il citoscheletro e l'interno del nucleo.

La ricerca condotta ha riguardato il ruolo dell'ATP-ase Torsin A come potenziale meccano-sensore in grado di rispondere ai cambiamenti della rigidità del substrato e modulare la traslocazione di proteine attraverso i pori nucleari. Sono stati pertanto studiati i cambiamenti nell'accumulo nucleare di MRTFA e YAP, poiché tali fattori di trascrizione sono fortemente sensibili ai segnali meccanici e risultano coinvolti nella progressione tumorale. Gli esperimenti sono stati eseguiti piastrando le cellule su gel di poliacrilammide con rigidità variabile e modulando i livelli di espressione di Torsin A attraverso tecniche di silenziamento genico ed over-espressione. In seguito ai cambiamenti di espressione di Torsin A è stata osservata un'alterazione nella traslocazione nucleare dei fattori di trascrizione summenzionati, supportando l'ipotesi

che Torsin A può agire nella meccano-sensibilità per il trasporto nucleare. L'utilizzo di costrutti mutanti di Torsin A ha ulteriormente consentito di dimostrare che Torsin A è coinvolta nel trasporto nucleare. Successivamente, sono stati anche valutati cambiamenti nella posizione di Torsin A in cellule piastrate su gel a diversa rigidità. Poiché il comportamento di Torsin A è fortemente dipendente dal cofattore noto come Lull1, che permette la traslocazione di Torsin A dal reticolo plasmatico all'involucro nucleare, la posizione di Torsin A in presenza e in assenza di tale cofattore è stata dunque valutata in cellule piastrate su gel a diversa rigidità. I risultati ottenuti hanno suggerito che la posizione di Torsin A è dipendente dalla presenza del cofattore Lull1. Inoltre, è stato osservato che l'accumulo di Torsin A nell'involucro nucleare diminuisce inibendo l'attività di Importin ß, indicando dunque che Importin ß è coinvolta nella localizzazione di Torsin A. È stato infine osservato che l'accumulo perinucleare di Torsina A è inversamente associato alla polimerizzazione dell'actina. Tali risultati indicano che Torsin A è un meccano-sensore in grado di rispondere ai cambiamenti della rigidità del substrato e di modulare la traslocazione nucleare di proteine coinvolte in importanti processi biologici.

# Chapter 1

## 1.Introduction

### 1.1 Physical forces in physiology

Every day human beings perceive mechanical forces from the surrounding environment, and this ability is crucial for their interaction with the physical world. All cells and species across the developmental continuum, from the most primitive to the most evolved, are mechanically adaptive [1, 2]. The mechanical stimuli coming from the world around us, are converted into biological responses, which play a fundamental role in the physiological processes. Furthermore, mechanical forces reveal to be an essential regulator of development and homeostasis of the human body. The sense of hearing and equilibrium, which is the product of electrochemical reactions to sound waves, pressure and gravity, is one of the clearest examples to understand how physical external forces influence physiology. Specifically, the hair cells called stereocilia located in the inner ear, contract, responding to mechanical forces, contract. The movements of these cells activate intracellular processes that lead to the mechanical opening of ion channels which in turn allow the entry of calcium and other ions that serve as a signal for the activation of downstream cascades [2, 3].The restoration of pressure at rest is another example of how the physiological functions of the human organism are influenced by mechanical forces. Similarly, the link between mechanical forces and organism is essential to touch sensation and proprioception, which is the internal sensing of the relative location of one part of the body [4,5]. Mechanical signals also play a crucial role in controlling physiological

phenomena in other complex tissues that are not specifically involved in sensory functions. For instance, skeletal and cardiac muscles adapt to increased load, e.g., by vigorous resistance training, with hypertrophic development, whereas immobilized muscles atrophy over time [6]. Particularly intriguing is the role played by physical forces in the cardiovascular system, in fact the anatomy and physiology of the heart and vasculature are affected by blood pressure and shear stress [7-10] and low interstitial flow rates are necessary to promote lymphangiogenesis [11]. In addition, in the mature cardiovascular system, manifestations of mechanical forces such as laminar shear stress and circumferential artery stretching are believed to have an atheroprotective effect on endothelial cells. According to this concept, atherosclerotic lesions are also found in particular positions with interrupted flow patterns known as turbulent, characterized by a low and oscillatory shear stress on the endothelium. Bone tissue is another example of the role of mechanical signals in tissue maintenance. The compact bone is made up of concentric layers of bone matrix interspersed by narrow cavities known as lacunae. These lacunae harbour osteocytes and are connected via a network of interconnected channels called canaliculi. During locomotion, compression forces are generated by muscle contractions which, together with gravity, cause small deformations of the poro-elastic bone, resulting in pressure differences that guide the flow of interstitial fluid through the lacuna-canalicular network. Experimental evidence demonstrated that this load-induced fluid flow, promotes localized bone remodelling by imparting dynamic mechanical properties to cartilage [12]. Additionally, the developmental physiology of the lung during maturation is affected by the constant changing in mechanical stress and strain induced by the cyclic. Likewise, the main cells that form cartilage, known as chondrocytes, are accustomed

to the widespread distension and contraction of the lungs [13]. Similarly, the flow of urine within the renal tubules plays a key role in the regulation of renal morphogenesis, since this cell experiences the shear tension of the fluid due to the bending of primary cilia [14].

### 1.1.2 Physical forces in diseases

The mechanical properties of tissues can be largely different. Cell and tissue mechanics have a key role in cell growth and differentiation, as well as in the development of disease [15]. In tissue homeostasis conditions, mechanical properties of tissues are mostly invariant, although this scenario changes in pathological contexts. Recently, in vitro experiments have shown how the stiffness of the underlying substrate helps to assess the shape and function of cells in a highly cell-specific manner that is likely to have significance to their function in *vivo*. On the other hand, the rigidity of the tissues, such as breast, lung, liver, kidney and some blood vessels, varies from 0.2–4.0 kPa [16] and the stiffness variance for individual tissue types is often small, within 10–15%of the mean value [17]. In normal conditions, regulated stiffness helps to preserve a particular differentiated cell phenotype and decreases the progression of the cell cycle to maintain homeostasis. Increased stiffness in the range of 12 kPa or higher can lead to aberrant cell cycle progression and potentially irregular tissue [18-21].

Cardiac myocytes need a particular mechanical environment to develop and function in the best way. Cardiac muscle tissue in physiologic condition has a stiffness of 10–15 kPa and thus embryonic cardiac myocytes that are grown under 'normal' matrix

conditions, i.e. on matrixes with a stiffness of ~11 kPa, retain their differentiated state and beat. Nevertheless, if myocytes are grown on a substrate with a stiffness which can be compared to that of a myocardial infarction scale (35–70 kPa), they lose their striation, their beating frequency diminished, and the fraction of cells that beat decreases from usually more than 30% to less than 10% [22]. The cardiac muscle must be relaxed so that the ventricles can be filled. In the case of pressure-overloaded heart disease, the ventricle is stiffer than normal, resulting in diastolic heart failure. Muscle strips from these hearts have been shown to be substantially stiffer than regular or volume-overloaded muscles [23].

The enhanced stiffness may be due to muscle hypertrophy, which is characterized by an increase in the number of elastic units arranged in parallel. However, it has been found that the muscle strips of the overloaded hearts maintain their increased stiffness after myofibrils and titin, the proteins responsible for the elastic properties of muscle fibers, have been removed, indicating that the increased stiffness of the diseased tissue is due to changes in the matrix rather than in the cardiac muscle cells. The quantity of collagen was comparable to that of normal cardiac muscle, suggesting that increased matrix stiffness could not be? As a consequence, the difference in matrix stiffness is most likely due to changes in the matrix, such as increased cross-linking. However, in heart failures with dilated ventricles and decreased ability to relax or produce strength, muscle strips were found to be weaker than average. Arterial stiffness, which is clinically measured as pulse wave velocity (PWV), is another independent risk factor and induces adverse cardiovascular effects, such as myocardial infarction, heart failure and stroke [24, 25]. Its growth is determined by a variety of factors, such as ageing, blood pressure, hereditary factors and systemic diseases [26, 27]. Increased aortic

stiffness induces increased cardiac activity and reduced coronary artery perfusion by altering the timing of aorta pressure pulse-wave reflection [26]. Cardiac-generated pressure waves in combination with irregular mechanical properties of the arterial system cause cardiac hypertrophy, i.e., thicker heart muscle, leading to a stiffer heart, reduced cardiac output, and increased blood supply of cardiac muscle mass.

Standard liver elastic modulus is 0.4–0.6 Pa but can increase to as much as 15 kPa after injury and fibrosis [17, 28]. Like several other types of cells that keep a segregated state and hardly ever divide under normal conditions, liver cells, including hepatocytes, stellate cells and portal fibroblasts, lose their differentiated characteristics and start to divide more rapidly in response to matrix stiffness [29]. In vivo work showed that after intentional liver injury, measurements of tissue shear modulus become substantially stiffer before increased concentrations of collagen are detected, a surprising finding since increased stiffness is usually associated with increased fibrous tissue (collagen). This increase in stiffness can be prevented by lysyl oxidase inhibitors, an enzyme that cross-links collagen [17].

These findings suggest that increased matrix stiffness is an early response to injury in this model and is associated with increased collagen cross-linking prior to changes in matrix component synthesis.

Another evidence of the role of mechanics in disease is the decreased stiffness of the renal glomerular podocytes, which are cells that support the glomerular capillaries, resulting in kidney disease. For instance, it has been shown that conditionally immortalized glomerular podocytes from the mouse model of HIV-associated nephropathy (HIVAN) are significantly softer than normal podocytes measured by atomic force microscopy (AFM) and microaspiration [30]. At a disease stage that

displayed no observable pathological changes, the glomeruli of these mice were 30% softer than normal glomeruli [31]. Glomeruli and podocytes in other disease are also slightly weaker than normal cells, suggesting that the increased mechanical deformation of podocytes and glomeruli may be a common feature of a variety of kidney diseases. This could make these structures more vulnerable to hemodynamic injury or may reflect a mechanical condition that is inhospitable to normal glomerular cells, resulting in apoptosis.

### 1.1.2.1 Physical forces in cancer

It has been observed over the last decade that mechanical features of the microenvironment of the tumour, like matrix stiffness [32] topography [33], containment [34], shear stress [35], mechanical stretching [36] can affect the behaviour of cancer cells. For example, highly metastatic melanoma cells can be selected by growing them in a soft fibrin matrix [37]. By regulating integrin expression and signalling, high stiffness of the breast tumour microenvironment promotes malignant mammary epithelium phenotype [21,38]. The extracellular matrix (ECM) can stimulate cancer progression [38]. The fine tuning of mechanical micro-environmental cues is vital to influence cancer growth and development [39]. It has been proposed that increased matrix stiffness is the first step towards promoting the invasive epithelial cell phenotype through increased integrin-induced signalling. This is likely to be accomplished by increasing resistance to internally produced voltage, thereby enhancing myosin activity [40]. In addition, studies of animal tumour models have shown that increased collagen cross-linking and stiffening by lysyl oxidase oxidation

induced invasiveness of oncogene-activated epithelial cells, developed larger focal adhesions and promoted phosphoinositide 3-kinase activity [21].

Tumors are often usually stiffer than underlying healthy tissues [41] and stiffness is used for clinical diagnosis, most simply by tissue palpation [42], but also by X-ray and ultrasound techniques [43]. Many factors may affect the production of a rigid, fibrotic microenvironment in tumors, including changes in the cellular and extracellular matrix (ECM) constituents of the tumour and disrupted interstitial fluid balance. These changes can also promote a variety of cellular functions that lead to tumour progression and metastases. Targeting tumour stiffening is therefore an emerging approach to therapeutic intervention.

Standard breast tissue is elastic, around 0.2 kPa, while breast tumors are much stiffer, around 4 kPa [44, 16]. Dense and potentially rigid breast tissue raises the likelihood that a patient may develop breast cancer. Experiments employing substrates of different degrees of stiffness offer clues as to the underlying molecular effects of increased matrix stiffness on breast tissue. For example, normal epithelial breast cells that have been plated on substrates with increasing stiffness within the range of 0.17–1.2 kPa have increased abnormalities, including loss of normal acinar structure, increased extracellular signal-regulated kinase (ERK) and Rho activity [45].

## 1.2 Mechanotransduction

The cells which are in our body continuously communicate between each other's and with the extracellular environment through signals which they send and receive. This interaction is essential because it balances homeostasis. The signals used by the cells

can be classified in three principal kinds: chemical, electrical and mechanical. A signalling molecule, such as a hormone, is usually involved in a chemical pathway; it binds to its specific receptor and causes an intracellular biochemical cascade amplified by other messenger molecules. Electrical signals are typical of the nervous system where electro-chemical gradients, used by neurons to propagate action potentials at high speed, manipulate the flow of ions. The mechanical signalling is a topic of interest in mechanobiology, where the reciprocal relationship between the cells and their surrounding microenvironment is described. The latest research in mechanobiology have found out a net of mechanical signals which from the organ-level organisation goes down to the molecular step. The physical stimuli may appear in the form of shear stress, compression and stretching forces. As the biochemical receptors detect chemical signals, the mechanosensors expressed by the cells identified the physical stimuli. These sensors take part in a mechanical signalling network and contribute to make changes in gene expression. Thus, mechanobiology studies the cellular regulation from a new point of view and certainly provides new information and knowledge about the way the cells work. Considered that cells do not exist as isolated unities, physical forces become extremely relevant. For example, compression forces induce the expression of a gene called Twist, needed in the mesodermal differentiation, so they playing a fundamental role in cell fate determination.

Further studies on the understanding of the mechanical bases of the biological process, integrated with genetic and biochemical knowledge, will allow us to better understand cellular functioning. Starting from the consideration that interconnection between mechanosensitive components allows rapid transduction of extracellular clues to the nucleus on the micro to millisecond time scale, a further advantage of mechanical

signalling is speed. Furthermore, as common messenger molecules are used by both mechanical and biochemical networks, the crosstalk between signalling cascades is allowed, creating a sophisticated regulatory network in the cell. The process by which cells sense mechanical stimuli and respond to them through biochemical signals is known as mechanotransduction. On the cell membrane, focal adhesion (FA) complexes transmit mechanical stimuli through the dynamic cytoskeleton to the nucleus via the linker of nucleoskeleton and cytoskeleton (LINC) complexes and nuclear lamina [46] (Figure 1.2.1.).
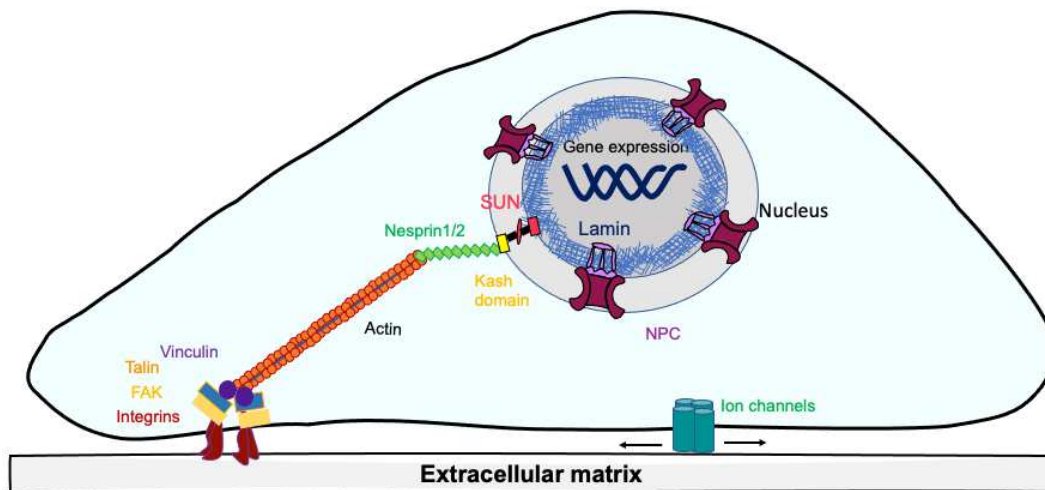


*Figure 1.2.1.: Diagram of a cell indicating the main actors of mechanotrasdution Stretch-activated ion channels are located on the cell membrane. Integrins, focal adhesion kinases, talin and vinculin form the focal adhesion (FA) complexes coupling the extracellular matrix to the cytoskeleton. F-actin fibres connect the FA complex to the nucleus. Force transfer into the nucleoplasm is mediated by the LINC complex on the nuclear membrane – composed of nesprins and SUN proteins. The lamin proteins lines the nuclear membrane, and couple cytoskeletal forces to the chromatin.*

## 1.2.1 Mechanosensing elements

An important mechanosensing element is the FA complex. The cell attaches to neighbouring cells and to extracellular matrix (ECM) through FA complexes. The complex, with the role in linking the ECM with the intracellular cytoskeleton consists of over 100 different proteins such as integrins. [9]. Integrins in the FA complex allow it to bind to the ECM and connect to the actin cytoskeleton by adaptor proteins such as Talin and Vinculin [47, 48]. By changing the composition of their proteins, the FA complexes process mechanical details. For example, tension reveals the vinculin binding sites on Talin [49]. During this process traction forces which allow the cells to migrate forward, are generated.

Cytoskeleton is essential in conveying mechanical stimuli to the nucleus. Actin filaments, microtubules and intermediate filaments are the three forms of cytoskeletal filaments. They are not static structures that inherently resist deformation. Instead, they may be assembled and disassembled according to the need of the cell. Particularly the polymerisation kinetics of actin is affected and altered by the force [50]. The direct association between cytoskeletal actin and transcription factors is a very good example of mechanical biochemical crosstalk, as the changes detected by the cytoskeleton and induced by the force directly affect the position of transcription factors. In this way, mechanical stimuli are transduced through a biochemical signal that controls the form of the expressed genes.

## 1.2.2 LINC complex

The LINC complex, a protein complex found on the nuclear envelope (NE) with physical connection to the cytoskeleton and nuclear laminate, allows extracellular forces to be transferred to the nucleus. The NE is a phospholipid membrane made up of a double layer divided by a perinuclear space of 30-50 nm, with an outer nuclear membrane (ONM) continuous with a rough endoplasmic reticulum (ER) [51]. Physical signals from the ECM and the cytoplasm can reach the nuclear interior thanks to the LINC complex. The LINC complex consists of SUN (Sad1p, UNC84) proteins on the inner membrane (INM) and nesprin (nuclear envelope spectrin repeats) on the ONM. Nesprins have C-terminal KASH (Klarsicht / ANC-1 / Syne Homology) domains which bind to SUN proteins. This bond binds the nesprins to the ONM [52]. A possible function of SUN is to controls the size of the perinuclear area [53]. As a result, the LINC complex is ready to interact with the cytoskeleton via nesprins and with the nuclear interior via the SUN proteins [54, 55] and contributes to form a direct mechanical connection between the actin cytoskeleton and the chromatin in the nucleus. This requires a stable structure. Thus, trimers of SUN proteins and nesprins interact to form heterohexamers, which can arrange into higher order 2D arrays to reinforce the connection [56].

Studies have also shown the relationship between the LINC complex and the cell transcriptome, suggesting that it has an important function in the mechanical regulation of gene expression [57]. The pattern of gene expression can be altered by force through the regulation of the position of mechanosensitive transcription regulators. These transcription factors, which can be both activators and repressor, may be associated with cytoskeletal actin. As a consequence, force-induced changes to actin

polymerisation or LINC complex organisation will influence their cellular localisation and affect and control the gene expression. The mediating force transfer to chromatin is the lamina forming the nucleoskeleton. LaminA/C/B form a dense network of intermediate filaments in the nucleus. They cover the INM, acting as a scaffold to preserve nuclear structure and rigidity while cells are under mechanical stress [58]. The nucleus has to resist deformation because when the nuclear barrier is damaged a double-stranded DNA breaks may take place. Thus, NE rupture events are quickly remedied by the ESCRT (endosomal sorting complexes needed for transport) complex [59]. Not only are lamins important for structural stability, but they are also involved in relevant processes such as stem cell differentiation [60], DNA transcription [61] and cell cycle regulation [62], because they're in close touch with the genome.

Chromatin in the nucleus is organized in a non-random manner, partly by interacting with laminates to form laminate-associated domains (LADs) that are   silenced in transcription [63]. As a result, laminates make the mechanical cues from the ECM and cytoskeleton affect the gene expression through chromatin organisation.

### 1.2.3 Mechanosensitive Transcription Factors

Another layer of regulation of gene expression in response to mechanical signals is added regulating the position and the function of transcription factors. Mechanosensitive transcription factors are necessarily receptive to variations in the forces perceived by the cell, as the polymerization of the actin cytoskeleton varies according to the extracellular mechanical cues.

Mechanical stimuli and extracellular signals impact on both MRTF-A, also termed megakaryocytic acute leukaemia (MAL) and the YAP transcriptional regulatory networks, which are involved in the response to mechanical stress. Both MRTFA and YAP have an RPEL pattern on their N-terminus which bind to the hydrophobic cleavage of G-actin [64, 65]. The rigidity of the substrate activates MRTF-A and YAP nuclear translocation [66, 67]. The expression of these mechanosensitivity transcription factors may be affected by substrate rigidity, which can also regulate the cellular position through actin dynamics. For instance, in the comparison between cells grown on stiff (75 kPa) and on soft polyacrylamide gels (5kPa), the expression of YAP results increased in cells grown on stiff gels [68].

In this research we trace the nuclear shuttling of MRTFA and YAP. They take part in signalling pathways that modify cytoskeleton dynamics according to mechanical signals and has downstream effects on cellular motility [69, 70] and differentiation [71, 72].

They are a relevant example of a mechanosensitive transcription factors that are part of the crosstalk between biophysical and biochemical signalling networks.

### 1.2.3.1 YAP and MRTFA in cancer

YAP and MRTF- A signallings are a both involved in cancer [73, 74]. They interact inducing cancer cell invasion in vitro and breast cancer metastasis to the lung in vivo [75].

MRTF- A, was identified as a chromosome 22 encoded fusion partner of the t (1;22) (p13; q13) translocation which is responsible of acute megakaryoblastic leukaemia in

infants and children. When MRTFA, on chromosome 1 A is fused to the RNA-binding motif protein 15 (RBM15), also called OTT gene encodes for protein RBM15-MKL1 which has potential oncogenic properties [76, 77]. Scientific studies report MRTF-A as a promoter tumour cell invasion and metastasis [78], and is also known that the MRTF-A overexpression promote metastasis-relevant traits in thyroid cancer cells [79]. New evidences demonstrate an involvement of MRTF- A also in prostatic cancer, in fact the use of selectively compounds that target the Rho/MKL1 signalling inhibits the invasion of prostate cancer cell in a Matrigel model of metastasis [80]. In addition, it has been demonstrated that the block of MRTF-A signalling by using anti-fibrotic agents, improves the possibilities of therapeutic intervention decreasing the activation of pancreatic stellate cells in the tumour microenvironment [81] and also significantly reduces the development of bleomycin-induced dermal fibrosis in vivo [82].

MRTF-A signalling is also involved in the aggressive phenotype of metastatic melanoma, for this reason targeting the MRTF-A transcriptional pathway appears as a novel approach for melanoma therapeutics [83, 84].

On the other hand, YAP has been previous characterized as effector of the Hippo growth control pathway [85] and it also responds to Rho-GTPase signalling. It translocates in the nucleus responding to high cytoskeletal tension induced by mechanical cues [86 ,87]

YAP is a known transcription factor activated in human cancer, with the role to instruct malignant properties such as proliferation, cell survival, chemoresistance and metastasis [88-93].The prime candidates to over - activate YAP in cancer cell are mechanical imputes from the aberrant tumour microenvironment, including aberrant

tissue organization, accumulation of stromal cells, inflammation, increased compression forces and interstitial pressure, metalloprotease-mediated ECM remodelling by cancer activated fibroblasts (CAFs) and overall ECM stiffening [94, 95, 21]. In addition, recent studies suggest that YAP mechanical activation in cancer cells is relevant to acquire chemoresistance [96, 97]. In several tumours properties rely on activation of YAP in fibroblasts (CAFs) such as the increase of ECM stiffness and the change of the cellular composition of tumour niches by secreting chemokine are responsible for tumour invasion and angiogenesis [98].

Scientific evidences show that the use of the YAP inhibitor Verteporfin in preclinical model of kidney fibrosis is efficient [99] and in addition it is used in a pre-clinical model of melanoma to prevent the development of the fibrotic phenotype due to oncogenic BRAF inhibition [100].

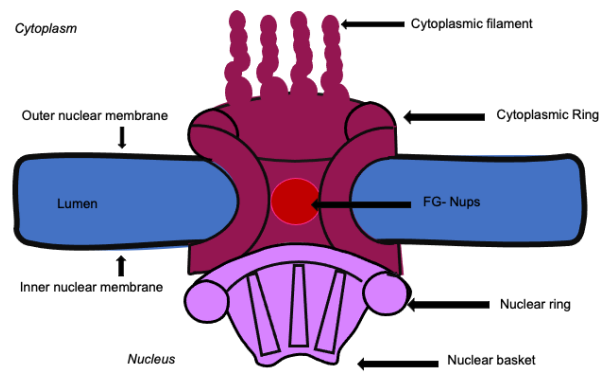## 1.3 The Nucleus as a Mechanosensor

The most important function of the nucleus is to store chromatin; besides it is the site where processes such as DNA replication, transcription and repair take place. But, considering its responses to physical stimuli, another important function that it has is mechanosensation. Nuclear mechanotransduction shows how forces can affect, in a direct way, both the organisation of protein on the nuclear envelop (NE) and the chromatin within it, modulating gene expression. This process is quick, and it is made possible by the LINC complexes, which enable forces to pass from the cytoskeleton to the nucleoskeleton trough the NE [101]. Lamins also exhibit mechano-sensing skills. Studies have shown that laminate A / C phosphorylation is encouraged in cells with

lower cytoskeletal stress, such as those grown on soft substrates. Phosphorylation of laminaA / C encourages the disassembly of laminate and thus the sum of laminate scales with extracellular stiffness [102]. When lamins or lamin-binding proteins such as laminate-associated polypeptide 1 (LAP1) and emerin are malfunctioning, many diseases named laminopathies are reported and these are involved in mechanical control of gene expression [103].

## 1.3.1 Mechanosensitivity of Nuclear Transport

Gene expression patterns can be modulated in response to force also involving the nuclear transport process. Transcription factors are not always localised into the nucleus, so, for this reason, to activate gene expression, they might be transferred through the nuclear envelope. Once transcribed, the messenger RNA (mRNA) exported from the nucleus is converted to proteins by ribosomes localised in the cytoplasm. The compartmentalization of transcription and translation regulators helps cells to regulate each stage of gene expression spatially and temporally. Due to its wide-ranging consequences for gene expression and hence cellular

function, the import and export of materials around the NE are strictly regulated processes. It is very important to consider that it is a membrane that does not allow the molecules to flow freely from and to the nucleus. That is why nuclear import and export of cargo is a complex process involving proteins in the NE, such as nuclear pores, and regulatory molecules near the NE. This regulation is influenced in part by the nuclear pore complexes (NPCs) located on the NE. Molecules smaller than 40kDa, ions and other metabolites, can easily pass through the nuclear membrane [104], on

the contrary larger macromolecules are selected from the nuclear pore. Approximately 30 nucleoporins (Nup) subunits take part in the NPCs.It is linked to the nuclear membrane by the transmembrane Nups, while the main channel, where cargo selection is believed to occur, consists of phenylalanine-glycine (FG) repeats [105] (Figure 1.3.1.1). The mechanism of selection of nuclear pores is not completely known, the main structure being the entropic energy barrier formed by the fluctuating FG-repeat [106]. NPCs response to force undergo conformational changes and stretch [107.], modifying their permeability. There are studies that associated these force-induced changes in the structure of NPCs with increased nuclear imports of certain proteins [66]. Important factors in the mechanism of selection of the NPC are the characteristics of the cargo. Surface residues of proteins have been shown to alter their translocation rates by up to two orders of magnitude [108]. More recent studies have identified the NPC's mechanosensitive cargo selection as nuclear translocation rate can be affected by the nanomechanical stability of a molecule [67] and have provided further proof that mechanical signals strongly influence nuclear transport process.

*Figure 1.3.1.1.: schematic representation of Nuclear Pore Complex (NUP) with NUPS.*

## 1.4 Torsin

Nuclear transport is a very complicated process, and it requires precise regulation. It is mechanosensitive, infact it is based on the selection of the NPC, whose permeability can vary according to the applied force and the rigidity of the translocating cargo. Nevertheless, only a few mechanosensors with a role in nuclear transport have been detected, so our knowledge about the mechanical regulation of nuclear transport is not complete yet.

In consideration of the fact that it is located at the rough ER and the NE, where it is linked to the LINC complexes and cytoskeleton, Torsin A, an ATPase, may be investigated as an ideal protein probably responsive to force and of relevance to nuclear transport.

## 1.4.1 Torsin A Structure

Torsin A structure can be divided into three sections:

- The N-terminus signal sequence guides Torsin A to the ER lumen.

- Sensor I motif contains the patterns Walker A and B which activate the operation of ATPase.

- Sensor II motif necessary to communicate with its cofactors (Figure 1.4.1.1.).

The structures of the complex may not be indicative of Torsin A in vivo because the experimental conditions required the use of binding agents. However, three main models have been proposed:

- Torsin A forms homo-hexamers in blue native PAGE (polyacrylamide gel electrophoresis) experiments [109].

-  Torsin A forms a trimer with its cofactors [110].

- Torsin A-cofactor heterodimer [110].



| Structural domain | SS | HD | | WA | SENSOR I MOTIF | WB | | SENSOR II MOTIF |

*Figure 1.4.1.1.: Representation of Torsin A sequence. SS: signal sequence, HD: hydrophobic domain, WA: Walker A domain, WB: Walker B domain*

## 1.4.2 Torsin A Function

Torsins are ATPases which belong to the AAA+ (ATPases associated with a range of cellular activities) superfamily proteins. Human genome encodes for four Torsins isoforms (Tor1A, Tor2A, Tor3A, TorB). Torsin has several potential roles, including the control of protein folding as molecular chaperone [111], synaptic vesicle trafficking [112] and protein degradation through the ER-associated pathway [113].

Torsin A needs two cofactors for its ATP- ase function:

- LAP1 located at the INM, where it interacts with nuclear lamins.
- The luminal domain-like LAP1 (LULL1) found throughout the ER.

The cofactors structure in the luminal domains includes the catalytic arginine finger for the hydrolysis step, this motif is commonly conserved in AAA+ proteins but it is not present in Torsin [114]. The disparity in position depends on their N-terminal domains [54].

LAP1 is involved with Torsin A to position the actin-associated nuclear (TAN) transmembrane lines that connect the nucleus to the cytoskeletal actin. TAN lines are composed of nesprin-2 G and SUN2, both components of the LINC complex and are anchored to lamins filaments in the nucleoskeleton [116]. LULL1 is the strongest activator of Torsin A [117] and it is also involved in Torsin A redistribution to the INM [118] (Figure 1.4.2.1.).
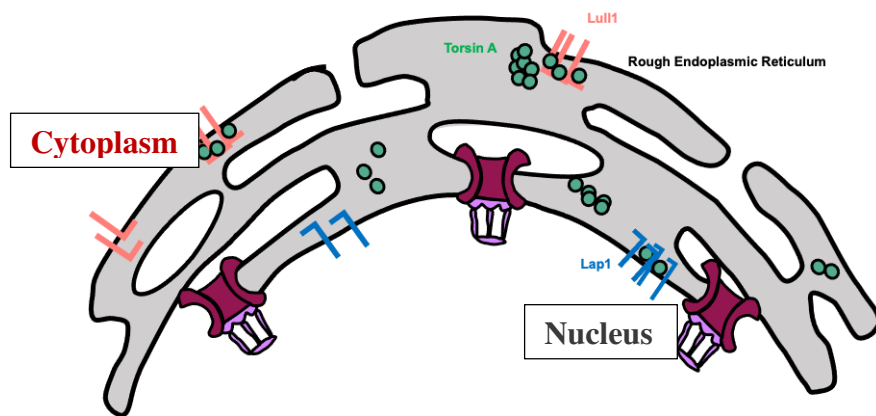
*Figure 1.4.2.1.:  a scheme which represents the localisation of Torsin A and its cofactors on the nuclear double membrane and rough ER.*

**1.4.3. Relationship between Torsin A and Nuclear Structure**

This study wants to investigate the effects of Torsin A on the molecular nuclear translocation through the nuclear membrane. As it is the unique AAA+ ATPase which is located both in the ER lumen and the perinuclear space [119], Torsin A can easily interact with proteins part of the LINC complex, such as the KASH domains of nesprins [120]. Moreover, as already described, Torsin A uses its cofactor LAP1 to interact, in an indirect way, with the cytoskeleton and the nucleus. Additionally, Torsin A is also involved in the nuclear pore biogenesis, as cells that do not have functioning Torsin A have faulty NPCs because of a lack of Nup358 [121]. These structural connections with key elements of the mechanotransduction pathways support the function of Torsin A as a mechanosensor (Figure 1.4.3.1.).
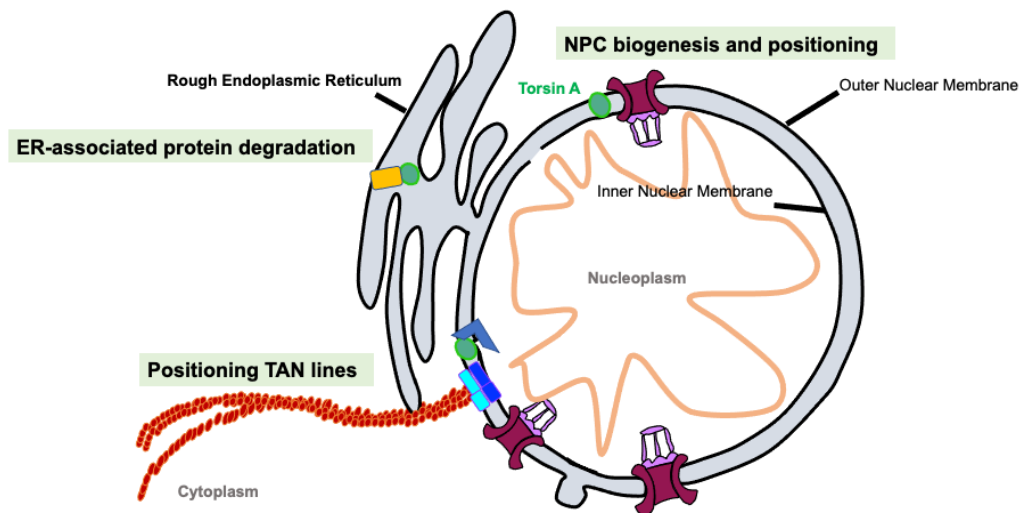
*Figure 1.4.3.1.: scheme describing the Roles of Torsin A in a cell.*

Past studies indicate that modulating the NE architecture Torsin A plays a role both in nuclear import and export processes. As far as nuclear import is concerned, the loss of OOC5 is the counterpart of Torsin A in C. Elegans have been shown to cause nucleoporin mislocation. This has contributed to disturbances in nuclear pore assembly and irregular import Kinetics [122]. Torsin A knockout phenotype contains nuclear envelope (NE) defects, indicating a role in keeping NE integrity. Specifically, INM blebbing is observed, although this phenotype is confined to neural tissue.

Unlike other types of cells that produce other isoforms, Torsin A [109] is strongly expressed by neurons. They could also be more seriously affected as there are no other isoforms able to compensate the knockout. Furthermore, since Torsin A is a protein that strategically has contact with elements of the LINC complex cytoskeleton, it will be possible to evaluate a direct response of Torsin A to mechanical stimuli from the external environment.

### 1.4.4 Relationship between Torsin A and Translocating Cargo

Torsin A, by acting on the substrate of the cargo as a molecular chaperon, can have a role in the control of nuclear translocation. As an ATPase, Torsin A catalyses the release of energy by ATP hydrolysis, which can be used to control folding, cellular localization and protein aggregation [123].

Chaperones can be divided into three key categories based on their purpose:

- Holdases that binding to non-native proteins, thus preventing their aggregation [124].

- Unfolding which are enzymes that effectively drive protein unfolding using ATP energy and transform it to natively folded proteins [125].

- Disaggregase [126].

These chaperones actively unfold large protein aggregates and enable spontaneous native folding of proteins. If Torsin A, as a chaperone, impact on the folded state or oligomeric assembly of its substrates, can alter the rate and number of proteins entering the nucleus via nuclear pores. The structure of Torsin A suggests that it works as a holder chaperone. Differently from the other members of the AAA+ family, Torsin A does not present the aromatic pore loops which is necessary to form a central channel for substrate translocation [127]. It also lacks a substrate-binding domain [128]. Therefore, it is probable that the interaction of Torsin A with substrates are temporary, as the ones of holder molecular chaperons. By doing research about the response of Torsin A to mechanical stimuli, we might find out a new mechanosensing pathway which directly impact on the nuclear translocation of cargo such as MRTFA and YAP.

**1.4.5 Torsin A in diseases**

Torsin A, from a medical perspective, has been involved in many illnesses because of its possible role in controlling nuclear transport and reshaping the nuclear architecture. Most specifically, the Torsin A mutant triggers the majority of causes of early onset torsional dystonia [128]. Early-onset primary dystonia (DYT1), a rare neurodevelopmental condition is characterized by involuntary, sustained muscle contractions that typically begin in the lower limbs and follow the autosomal inheriting mode [129].

Dystonia mutant involves the inframe deletion of glutamic acid at the C- terminus. The loss of this acid patch is important because it is located on the luminal face of Torsin A where it prevents the mutant from interacting with the cofactors of Torsin A [117]. In the absence of a wilde-type Torsin A, the neural INM evaginates abnormally during development [121]. Experimental evidence shows a close link between psychiatric comorbidities in patients with dystonia, thus suggesting that major depression and DYT1 share equal genetic risk factors [130]. In fact, mouse models of DYT1 show alterations in serotonergic transmission, in line with depressive illness [131]. In addition, hypometabolism in the subgenual cingulate cortex of subjects with GAG deletion, which corresponds to the metabolic changes typically observed in depressed subjects, supports the correlation. Torsin A is also involved in the ethology of recurrent major depression, in addition to its established impact on DYT1 [132]. Besides Torsin A is involved in Parkinson's disease. This pathology is characterized by the degeneration of dopaminergic nigrostriatal neurons [133]. Lewy bodies are the main neuropathological evidence of Parkinson's disease. The role of Lewy bodies in the neurodegenerative process is unknown, but various experimental evidences have

made it possible to identify various associated proteins including ubiquitin, α-synuclein and 3-nitorothyrosine [133, 134]. Lewy bodies have also been reported in patients with Dystonia. Several studies also show that Torsin A co-localizes with α-synuclein [135] and that increasing the expression of Torsin A wilde type reduces the number of inclusion bodies, thus showing the ability of Torsin A to be an holdase, a molecular chaperone that has the task of preventing the aggregation of target molecules. Torsin A also influences the positioning of nuclear pore complex (NPCs). This disease phenotype further supports the notion that Torsin A is of structural significance to the NE and may therefore have an effect on nuclear transport.

# Aim of the study

The aim of this study was to investigate the potential role elicited by Torsin A as a potential mechanosensor in osteosarcoma cancer cell line U2OS. We aimed to understand whether Torsin A can respond to changes in stiffness of the substrate by modulating the nuclear translocation of mechanosensitive transcription factors involved in cancer progression. Moreover, we aimed to evaluate the influence of mechanical cues on Torsin A localization. Our results further extend the mechanisms by which Torsin A could affect important biological processes such the nuclear shuttling of transcription factors in response to the mechanical cues in pathophysiological conditions.

# Chapter 2

## 2. Materials & Methods

All reagents used are from Sigma-Aldrich unless otherwise stated.

### 2.1. Cell Culture

All experiments conducted on this project were used U20S Osteosarcoma cell line purchased from American Type Culture Collection (ATCC) and MALGFP- U2OS stable cell lines were a gentle gift from Dr Maria Kristine Vartiainen. All tissue culture was conducted in sterile conditions in a laminar flow hood, and cells stored at 37°C at 5% atmosphere $CO_2$ in the incubator. Cells were maintained in 5 mL DMEM complete medium supplemented with 100 U/mL penicillin (Invitrogen), 100 µg/mL streptomycin (Invitrogen), 2 µM glutamine (Invitrogen) and 10% fetal bovine serum (FBS). Cells were split and seeded in to a new flask when they reached 80% confluency. They were incubated at 37 °C in trypsin for 5 minutes to detach them from the flask surface before resuspension. Cells were seeded in to new flasks labelled with their new passage number in a 1:5 dilution.

### 2.2. Transient transfections

Transfection is a process that allows the introduction of exogenous genetic material into the eukaryotic cell. In the case of a transient transfection, the exogenous genetic material does not integrate into the genome of the cell, but it remains as an extrachromosomal fragment: in this case the characteristic introduced by the transfection will persist for only 72 hours. The transfer of nucleic acids presents an

important problem which is due to the negative charges into the phosphate groups of the molecules. The exogenous material cannot overcome the cell membrane owing to these charges and Because of electrostatic repulsive forces. The anionic groups of the DNA are hidden by the use of cationic lipids which represent one of the most common methods of transfection. The cationic lipids associate to form liposomes, that is amphipathic lipid molecule. This technique is included in the chemical ones of transfection.

The amphipathic lipids molecules when in contact with the aqueous environment, create a phospholipid bilayer similar to cell membranes. Furthermore, the charged molecules, such as DNA, can be contained in the liposomes which show their polar heads turned towards the inner of the vesicle and once fused with the plasma membrane, transport the exogenous material within the cell. The cationic lipids most commonly used are characterized by some features such as high efficiency; low cytotoxicity, quick and simple protocol for usage and some of them also have the possibility to be used in the presence of serum.

## 2.2.1 Plasmid Constructs

GFP – Empty Vector has been generated in the Professor Sergi Garçia-Manyes, MRTFA - GFP plasmids were a gentle present from Maria Vartiainen [136]. GFP - TorA plasmids encoding wild-type TorA or its mutants (TorA wild-type, TorA-ΔE, TorA E171Q and TorA K108A) were a kind gift from Rose Goodchild [137]. pm_ScarlettYAP has been generated in the Professor Sergi Garçia-Manyes lab from the 2 different components: YAP from life technologies and pmScarlet empty vector

was a kind gift from David j Williamson and MKL1- flag purchase from Addgene. They were mixed for 15 minutes with the transfection reagent FuGENE (Promega) and after that it was added to the cells.

## 2.2.2 Gene silencing experiments

$3 \times 10^5$ cells were put per well of a 6-well plate which contained 2 mL of medium. 10 nM of siRNA (Dharmacon) targeting Torsin A, LULL1 and were used for knockdown. siRNA was mixed for 15 minutes with Opti-MEM (Gibco) and transfection reagent Hiperfect (Qiagen) before being added to the respective wells. To perform a negative control Non-targeting siRNA (siNT) was used. Sequences of the siRNA used are listed below in Table1.

**Table 1: siRNA sequences used in knockdown experiments**

| siRNA Oligo | Sequences target( 5'-3') |
|---|---|
| Control(ON targetPlus- NontargetPool) | |
| TorA | ACCGGAACCUCAUUGAUUA |
| | UGGCACAGCAGCUUAAUUG |
| | GAGGUCCAUCUUCAUAUUU |
| | CAUCUUAAAUGCCGUGUUU |
| Lull1 | CCACUUUGAUCUUCUAUAA |
| | GACACCAUGAGACAGAUUA |
| | GUGCAGAUACAGGUGAUAA |

## 2.3 Immunofluorescence

These experiments were conducted using the GFP-Torsin A and MKL1- flag. U2OS cells were transfected and plated on glass. Fixed cells are permeabilized with

0.1% Triton for 15 minutes. Aiming to reduce non-specific background staining, the samples were blocked in PBS composed by 2.5 % bovine serum albumin for 1 hour at room temperature. Cells were then incubated for 1 hour with the primary antibody ANTI-FLAG® antibody produced in rabbit (F7425-.2MG, Millipore Sigma). After incubation in the primary antibody, the cells are washed thrice in PBS before being incubated with the secondary fluorescence conjugate antibody Donkey Anti-Rabbit IgG H&L (Alexa Fluor® 594) (ab150076) at room temperature for 1 hour. Cells were incubated in DAPI solution for 3 minutes then washed three times with PBS.

## 2.4 Modulation of the cytoskeleton by using drug Assay

These experiments were conducted using the GFP-Torsin A. U2OS cells were transfected and plated on gels with different stiffness.

*Jasplakinolide treatment:*

After 3hour on gels at 37°C, 0.1 µM Jasplakinolide (Abcam) was added to the cells, for the control of cells tested, cells were incubated for 1hour in 0.1 µM DMSO and they were kept at 37°C for 1hour. Cells were washed thrice whit PBS and incubated with Alexa Fluor® 594 phalloidin (Thermo Fisher Scientific) solution for 1 hour to visualize F-actin in cell cultures. They were fixed in 4% paraformaldehyde and mounted on microscopy slides according to the protocol. Cells were incubated in DAPI solution for 3 minutes then washed three times with PBS and analysed.

*Latranculin B treatment:*

After 3hour on gels at 37ºC, 0.1 µM Latranculin B (Abcam) was added to the cells, for the control of cells tested, cells were incubated for 1hour in 0.1 µM DMSO and they were kept at 37ºC for 1hour.  Cells were washed thrice whit PBS and incubated with Alexa Fluor® 594 phalloidin (Thermo Fisher Scientific) solution for 1 hour to visualize F-actin in cell cultures.  They were fixed in 4% paraformaldehyde and mounted on microscopy slides according to the protocol. Cells were incubated in DAPI solution for 3 minutes then washed three times with PBS and analysed.

*Nocodazole:*

After 3 hours on gels at 37ºC, 0.1 µM Nocodazole (Sigma-Aldrich) was added to the cells, for the control of cells tested, cells were incubated for 1hour in 0.1 µM DMSO and they were kept at 37ºC for 1hour, after that they were fixed in 4% paraformaldehyde and mounted on microscopy slides according to the protocol. Cells were incubated in DAPI solution for 3 minutes then washed three times with PBS and analysed.

## 2.5  Modulation of Torsin A import in the Nuclear envelop Assay

These experiments were conducted using the GFP-Torsin A. U2OS cells were transfected and plated on gels with different stiffness.

*Importanzole:*

After 3hour on gels at 37ºC, 0.1 µM Importazole (Sigma-Aldrich) was added to the cells, for the control of cells tested, cells were incubated for 1hour in 0.1 µM

DMSO and they were kept at 37°C for 1hour, after that they were fixed in 4% paraformaldehyde and mounted on microscopy slides according to the protocol. Cells were incubated in DAPI solution for 3 minutes then washed three times with PBS and analysed.

## 2.6 Substrate Rigidity Experiments

In these experiments, as a stimulus for MRTFA and YAP shuttling to the nucleus polyacrylamide gels of different stiffness were used.  Differences in nuclear translocation were compared across two knockdown conditions or across two Overexpression condition. Substrate rigidity experiments were also used as a stimulus for Torsin A localisation. Differences in Torsin A localisation were compared across two knockdown condition, two overexpression or by using different drugs. Polyacrylamide gels were prepared on Functionalised coverslips. The Functionalisation was performed as follows: 1 mL of 0.1M NaOH was put on each 22 mm square coverslip and incubated at room temperature for 5 minutes. NaOH was eliminated and the coverslips were put in jars in which there were 10 mL of 0.5% (3-aminopropyl) trimethoxy-silane in $dH_2O$. This step was carried out in the chemical hood and at RT for 30 minutes. Then the coverslips were washed with $dH_2O$ 6 times. And after that they were transferred into jars containing 0.5% glutaraldehyde in 10 mL of PBS for other 30 minutes. Even this step was carried out in the chemical hood and at RT. At least, they were washed thrice with $dH_2O$ and dried completely. A mix of 40% acrylamide, 2% bis-acrylamide, 1M HEPES, APS and TEMED was made according to Table 3 to produce polyacrylamide gels of proper rigidities. Then, APS

and TEMED were added immediately before pouring 35 µL of the solution on the functionalized side of each coverslip. A 25 mm round coverslip was placed on top of the gel and used as a mold. Gels were left to polymerize for 30 minutes at room temperature and then washed with 50 mM of pH 7.0 HEPES. Sulfo-SANPAH was added on the top of each gel for succinimide-mediated cross- linking. Gels were then exposed to UV light (7500 $\mu J/cm^2$). Cross-linked gels were washed in 50 mM HEPES at pH 8.2. Each gel was coated with 180 µL of 25 µg/mL fibronectin. these steps were carried out in the tissue culture hood. They were left for at least 2 hours at 37°C in the incubator and then washed twice with sterile PBS. At this point, the cells could be seeded onto the gels, or stored at 4°C for up to one week.

**Table 2: Polyacrylamide gel mix. Volumes in µL**

| Rigidity (kPa) | Water | 40% Acrylamide | 2% Bis - acrylamide | 1M HEPES | 10% APS | TEMED |
|---|---|---|---|---|---|---|
| 4 | 794 | 100 | 85 | 10 | 10 | 1 |
| 81 | 514 | 250 | 215 | 10 | 10 | 1 |

## 2.7 Preparation for Microscopy

First of all, the cells were fixed by using in 4% paraformaldehyde in PBS for 15 minutes. A chemical cross linking was introduced by Paraformaldehyde which also preserves the cellular reactions which occur at the point of fixation. After that the cells were washed 3 times with PBS. DAPI staining at 1:3000 dilution was also carried out. Cells were incubated in DAPI solution for 3 minutes then washed three times with

PBS. As mounting medium, ProLong glass antifade mountant (Thermo Fisher Scientific) was employed. By using forceps, Coverslips of cells were placed cell- side down on a 10 μL drop of mounting medium. Before fluorescence microscopy imaging the slides were left to dry in the dark overnight.

## 2.8 Fluorescence Microscopy

The fixed fluorescent cells were observed through The Nikon Eclipse-Ti epifluorescence microscope. The Hamamatsu C11440 digital camera at 60x magnification (Nikon objective lens) using Zeiss Immersol 518 F oil as immersion medium was used to acquired images. The exposure time for fluorescent imaging was set at 300 ms. A number of images per cell was taken one recording the fluorescence emitted by the GFP-tagged Torsin A wild type and mutants constructs; one recording the fluorescence emitted by GFP-tagged MRTFA constructs; one recording the fluorescence emitted by the pm-Scarlett YAP and the last one for the nuclear fluorescence from DAPI. The fluorescence intensities were quantified by using FIJI. First background intensity was subtracted from the images. The cell was drawn by hand and the integrated pixel intensity of the whole cell was measured in the GFP channel or Scarlett one (it depends on the experiment). The nucleus of the corresponding cell was drawn on DAPI image to be positioned in a more accurate way. The outlined coordinates were imported onto the GFP image or the Scarlett image and fluorescence intensity was measured. Nuclear fluorescence intensity was subtracted from the whole cell intensity with the aim to obtain cytoplasmic fluorescence values.

$$I_{cytoplasm} = I_{cell} - I_{nucleus}$$

Nuclear and cytoplasmic intensities were divided by their respective areas.The normalised nuclear intensity was divided by normalised cytoplasmic intensity to obtain a ratio indicating the fraction of nuclear MRTFA or YAP.

$$NI_{nucleus} = I_{nucleus} / Area_{nucleus}$$

$$NI_{cytplasm} = I_{cytplasm} / Area_{cytplasm}$$

$$Nucleus / Cytplasm = NI_{nucleus} / NI_{cytplasm}$$

**2.9 Statistical Analysis**

GraphPad was used to perform statistical tests. To determine if the data sets follow a Gaussian distribution normality tests were run. If data are normally distributed, the ANOVA test was selected to compare between datasets. Otherwise, the Kruskal-Wallis test, a non-parametric test was used to determine if the datasets are significantly different from each other, where $p < 0.05$ is the threshold for significance.

**2.10 Western Blot**

A solution containing radioimmunoprecipitation (RIPA) buffer and inhibitor cocktail tablets (Roche) were used to lyse the cells. After that, cells were scraped off the plate using a cell scraper and stored at -20°C. With the aim to denature the proteins, the samples were treated by sonication and heated at 95°C in Laemmli sample buffer for 5 minutes. Proteins were separated from the lysates in a running buffer at 185 V for

40 minutes, resolved on a 10% SDS- polyacrylamide gel, transferred to a nitrocellulose membrane for 100 minutes at 100 V for western blotting and subsequentially non-specific binding sites on the membrane were blocked by using a solution of 5% milk in PBS - Tween for 1 hour at room temperature. Membrane was incubated overnight at 4 °C with antibodies against Torsin A (Cell Singalling D-M2A8), and Histone3 (Cell Singalling 9715) in a 5% milk solution. The day after, the membrane was washed three times with PBS and probed with horseradish peroxidase-linked secondary antibodies Anti - mouse (GE Healtcare: NA931V) and Anti – Rabbit (GE Healtcare: NA931V) for 1 hour at room temperature. To visualise the signal was used the Pierce Enhanced Chemiluminescence (ECL) detection system (Thermo Fisher).  An equal volume of detection reagent 1 and 2 of the Pierce ECL kit was mixed together and used to cover completely the membrane for 3minutes at room temperature. The blot was visualised by chemiluminescent imaging.

# Chapter 3

## 3. Results

### 3.1 Verification of siRNA Knockdown

Aiming to investigate the role of Torsin-A in nuclear translocation, we downregulated the expression of Torsin-A by using specific siRNA and quantify changes to the nuclear accumulation of MRTFA and YAP in U2OS osteosarcoma cell lines by fluorescence analysis. We first verified the efficiency of siRNA transfection by performing western blot analysis. Having both Torsin A and the usual housekeeping gene GAPDH a too similar molecular weight, Histone 3 was used as a control. Comparing the protein level of Torsin A siControl to the siTorsin A lane in we showed an efficient knockdown of Torsin A protein in U2OS cell lines (Figure 1A).
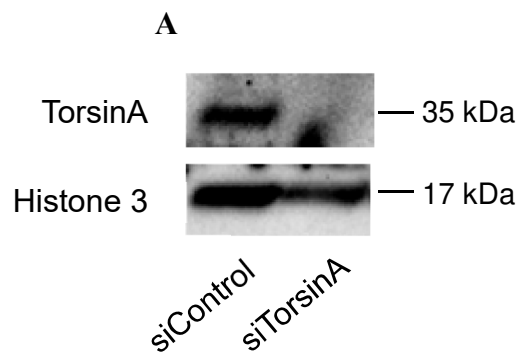


*Figure 1: (A) Western blot of MRTFA-GFP cells used in substrate rigidity experiments to verify Torsin A knockdown. As control Histone 3 was used.*

LULL1 is the major cofactor of Torsin A and it is also involved in Torsin A localization. The LULL1 knockdown was not verified because the primers of Lull1 formed dimers during qPCR. New primers will need to be designed and tested.

Although the change in phenotype in the siLULL1 experimental conditions sections indicates that siRNA silencing was effective, it is essential to verify the knockdown with new primers.

**3.2 Torsin A modulates MRTFA nuclear translocation**

The first goal of this project was to determine whether Torsin A could respond to mechanical cues. To this end, we tested the effect of silencing Torsin A in U2OS cell line seeded on polyacrylamide gels of various rigidities. These gels served as a stimulus for MRTFA shuttling into the nucleus. On soft substrates MRTFA, due to its association with the monomers of G-Actin, is concentrated in the cytoplasm, on the contrary, the increase of the substrate stiffness induces actin polymerisation, liberating MRTF-A and allowing its translocation into the nucleus [47, 67]. We performed this experiment on U2OS cells expressing GFP - MRTFA.

Figures 2A, 2B and 2C show epifluorescence images of GFP- MRTFA localization on soft (4kPa) stiff (81kPa) gels and Glass in conditions of Torsin A knockdown. Figure 2D shows the nuclear/ cytoplasmic ratios of MRTFA fluorescence per unit area. MRTFA, on soft substrates, is more cytoplasmic under control conditions. Strikingly, depletion of Torsin A by using a specific siRNA significantly increased (p < 0.0001) the nuclear fraction of MRTFA. This effect is showed as an increase of nuclear fluorencence of MRTFA in siTorsin A conditions. As mentioned before, stiffness induces the translocation of MRTF-A into the nucleous, we therefore haven't observed a significant difference between the siControl and siTorsin-A on stiff substrates as the system seems already saturated.
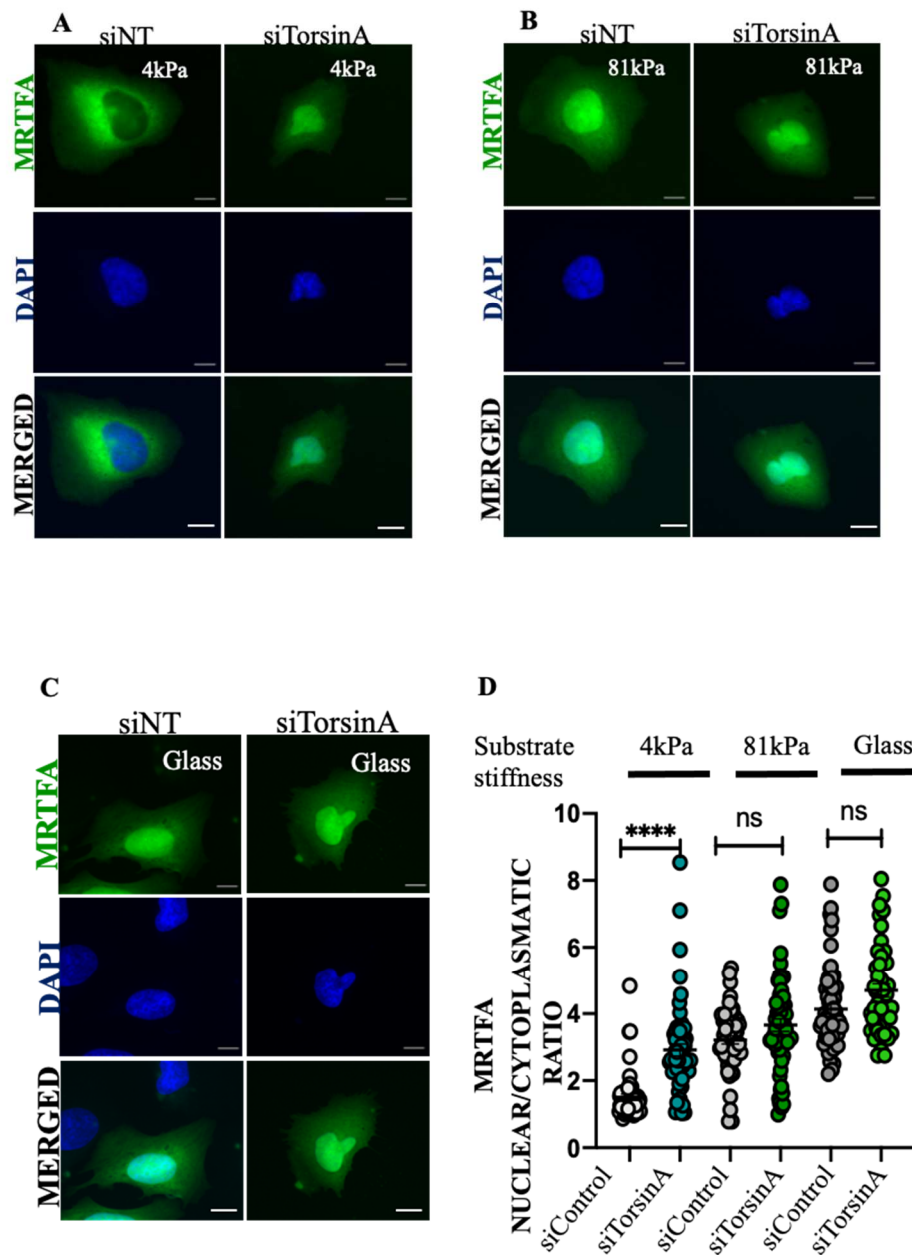
*Figure 2:(A) Epifluorescence images of MRTFA-GFP localization in control and Torsin A knockdown conditions on soft substrates in MRTFA-GFP U2OS cell line. (B) Epifluorescence images of MRTFA-GFP localization in control and Torsin A knockdown conditions on stiff substrates in MRTFA-GFP U2OS cell line. (C) Epifluorescence images of MRTFA-GFP localization in control and Torsin A knockdown conditions on Glass in MRTFA-GFP U2OS cell line. (D) Nuclear/cytoplasmic ratios of MRTFA-GFP on 4 kPa and 81 kPa gels and on glass in control and Torsin A knockdown conditions. All scale bars are 10 µm in length. All error bars are standard error measurements.*

## 3.3 Torsin A modulates YAP nuclear translocation

Then, aiming to evaluate if Torsin A effect in the nuclear translocation of transcription factors is MRTFA dependent, we performed similar experiments but analysing the nuclear translocation of Yes-associated protein (YAP) which is a "mechanotransducer" and a major downstream effector of the Hippo pathway [86]. The subcellular localization and activity of YAP are tightly regulated by cell substrate rigidity [66] and actin cytoskeleton remodelling [65]. These experiments were performed in U2OS cell lines. When the cells are plated on soft polyacrylamide gels YAP is usually distributed between nucleus and cytoplasm with a predominant cytoplasmic localization [66], while on stiff gels YAP is more concentrated into the nucleus. The experiments were performed also on glass, where YAP is completely concentrating into the nucleus. Upon knockdown of Torsin A, we observed a strong increase of YAP nuclear translocation both on soft and on stiff substrates.

Figures 3A, 3B and 3C show epifluorescence images of YAP localization on soft (4kPa) stiff (81kPa) gels and Glass in conditions of Torsin A knockdown. Figure 3D shows the nuclear/ cytoplasmic ratios YAP fluorescence per unit area. On soft substrates, YAP is more cytoplasmic under control conditions, but the nuclear fraction of YAP is significantly increased ($p < 0.0001$) when Torsin A is silenced. This effect is showed as an increase of nuclear fluorencence of YAP in siTorsin A conditions. On stiff substrates YAP is more nuclear in control conditions, but in soft substate the nuclear fraction of YAP is significantly increased ($p < 0.0001$) when Torsin A is silenced. On Glass, YAP is localized completely in the nucleus, and even in siTorsin A condition there is not an increase of YAP nuclear translocation because the system is saturated. This result suggest that Torsin A affects also YAP nuclear translocation.
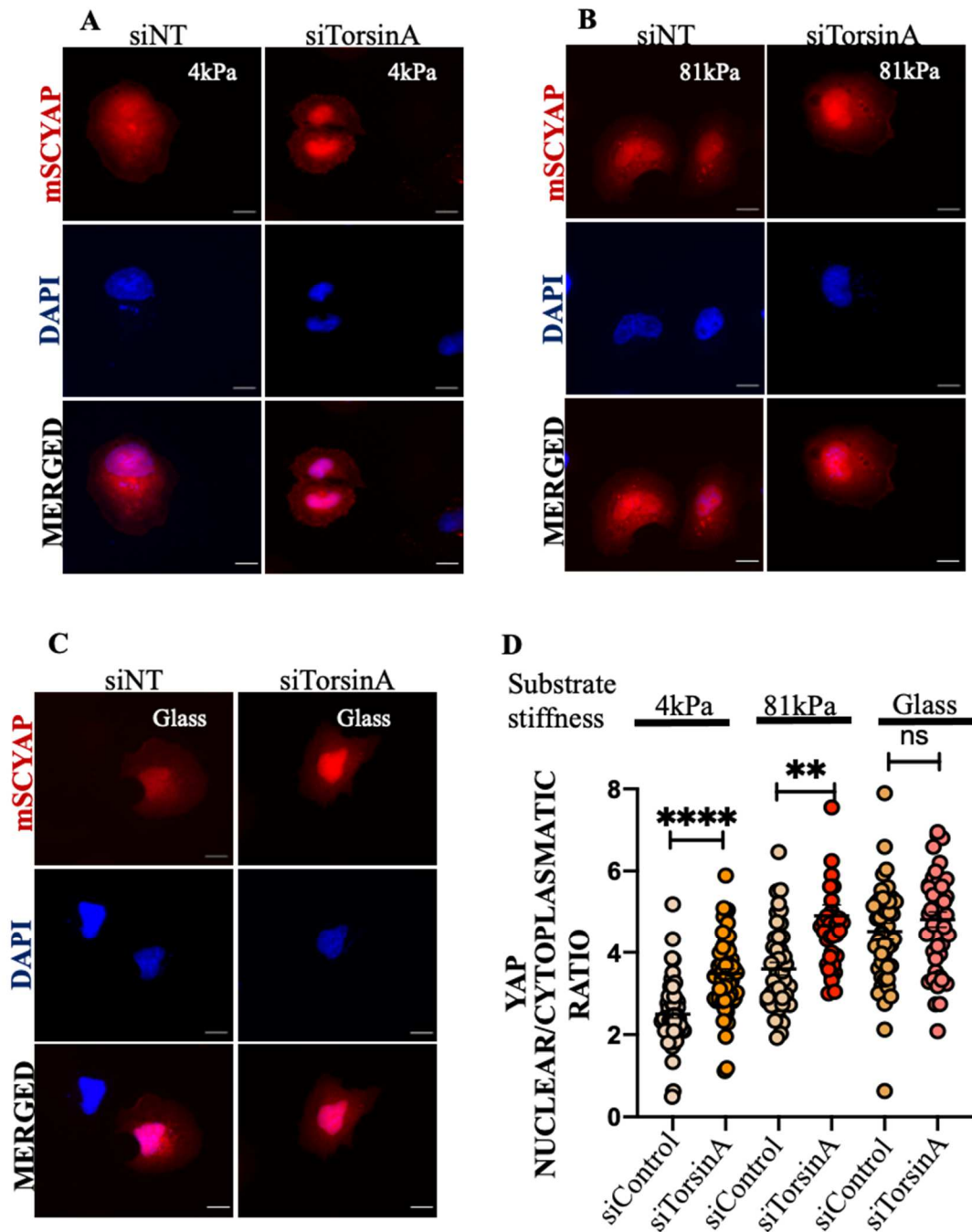
*Figure 3: (A) Epifluorescence images of pm_ScarlettYAP localization in control and Torsin A knockdown conditions on soft substrates in U2OS cells. (B) Epifluorescence images of pm_ScarlettYAP localization in control and Torsin A knockdown conditions on stiff substrates in U2OS cells. (C) Epifluorescence images of pm_ScarlettYAP localization in control and Torsin A knockdown conditions on Glass in U2OS cells. (D) Nuclear/cytoplasmic ratios of pm_ScarlettYAP on 4 kPa and 81 kPa gels and on Glass in control and Torsin A knockdown conditions. All scale bars are 10 µm in length. All error bars are standard error measurements.*

### 3.3.1 Torsin A overexpression blocks YAP nuclear translocation

To further confirm the Torsin A effect on nuclear translocation of transcription factors, we performed experiments of overexpression of Torsin A in U2OS cells line and we evaluated the YAP nuclear accumulation. Figures 4A, 4B and 4C show epifluorescence images of YAP localization on soft (4kPa) stiff (81kPa) gels and Glass in conditions of GFP-Torsin A overexpression. Figure 4D shows the nuclear/ cytoplasmic ratios YAP fluorescence per unit area. YAP, on soft substrates is more cytoplasmic under control conditions, while on stiff substrate YAP is localized into the nucleus. The overexpression of GFP-Torsin A determines a significantly reduction ($p < 0.0001$) of the nuclear fraction in all the cells plated on different substates rigidity. This effect is showed as reduction of nuclear of pm_Scarlett-YAP in GFP-Torsin A overexpression conditions. Our findings show that overexpressed Torsin A decreases the YAP nuclear translocation in cells plated both on soft and stiff substrates, suggesting that Torsin A plays a role as a mechanosensitive regulator of nuclear transport.
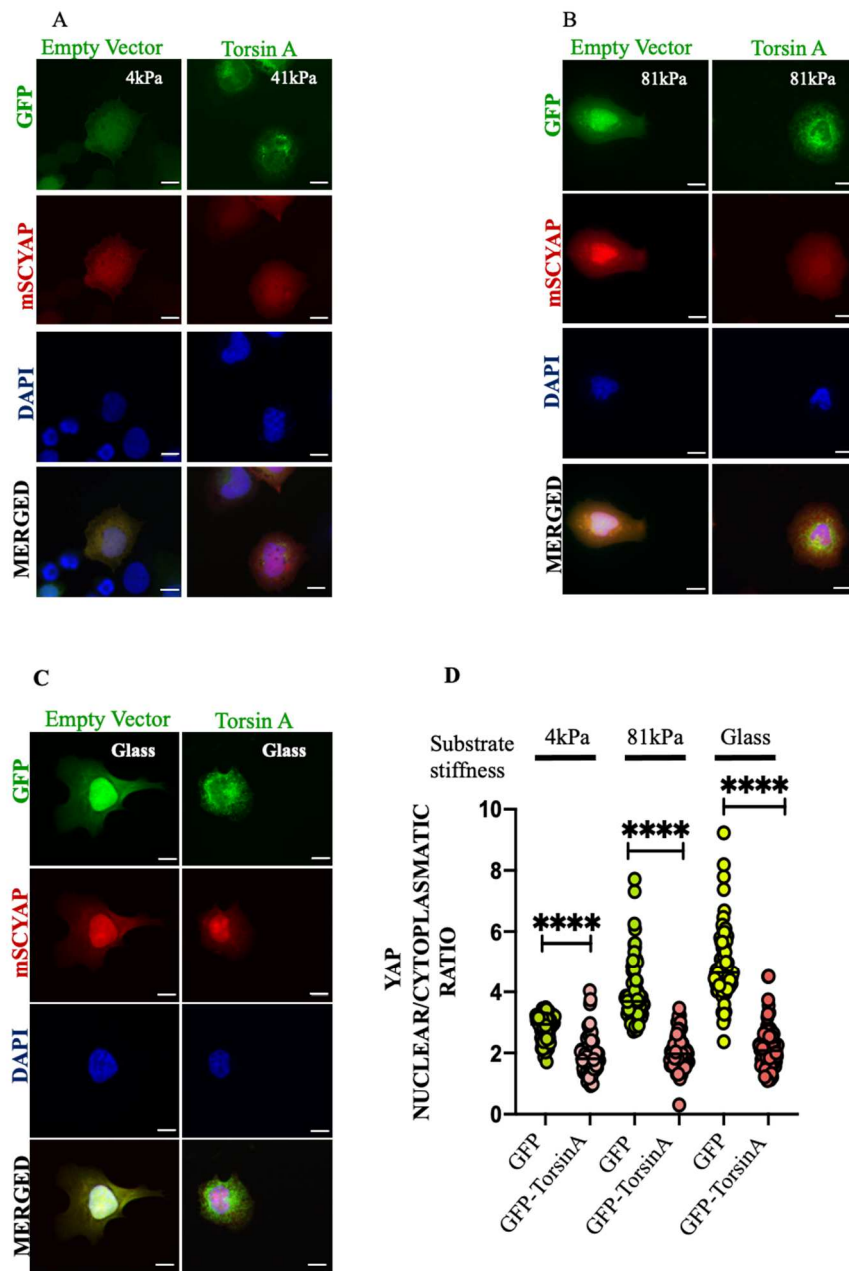
*Figure 4: (A) Epifluorescence images of pm_ScarlettYAP localization in control and GFP- Torsin A overexpression conditions on soft substrates in U2OS cells. (B) Epifluorescence images of pm_ScarlettYAP localization in control and GFP- Torsin A overexpression conditions on stiff substrates in U2OS cells. (C) Epifluorescence images of pm_ScarlettYAP localization in control and GFP- Torsin A overexpression conditions on Glass in U2OS cells. (D)Nuclear/cytoplasmic ratios of pm_ScarlettYAP on soft 4 kPa and stiff 81 kPa gels and on glass in control and GFP- Torsin A overexpression conditions. All scale bars are 10 µm in length. All error bars are standard error measurements.*

## 3.4 Which domain of Torsin A is important for its function?

Next, the domain of Torsin A involved in the nuclear translocation was investigated; beside we investigated whether the ATP- ase activity is required for the nuclear translocation of the protein. We performed overexpression of the Torsin A WT and three different mutants in U2OS cells:

- The first Torsin A - ΔE is responsible for the Dystonia disease. It contains a deletion of glutamic acid and it lies in C- terminal domain. This domain is the one involved in the NE localization of Torsin A [137].

- Torsin A E171Q has a point mutation in Walker B domain, and it is arrested in ATP bound state. It localises at NE [138].

- Torsin A K108A has a point mutation on Walker A domain, and it cannot bind ATP [139].

Figure 5 (A) shows immunofluorescence images of MRTFA localization on cells plated on Glass in conditions of GPF-Torsin A WT, GPF-Torsin A ΔE, GPF-Torsin A E171Q and Torsin A K108A overexpression in U2OS cells. The Overexpression of any variant of Torsin A led to lower nuclear accumulation of MRTFA $p < 0.0001$), compared to the control. This effect is showed as a reduction of nuclear fluorescence of MRTFA in GFP Torsin WT GFP-Torsin A ΔE and K108A are overexpressed. The only variant which does not have any effect on MRTFA nuclear is Torsin AE171Q. The results suggest that Torsin A does not require ATPase activity to influence nuclear translocat
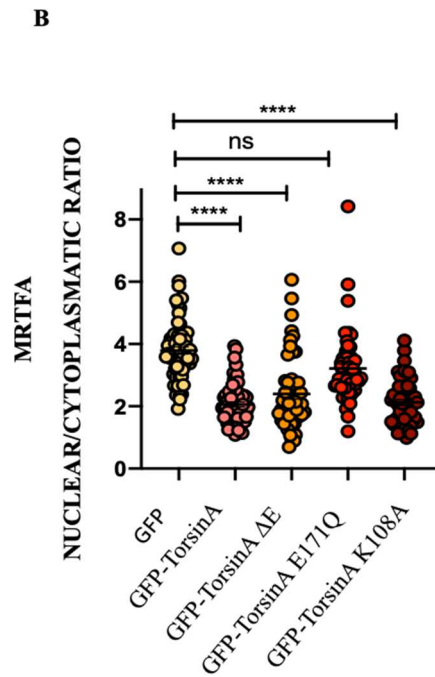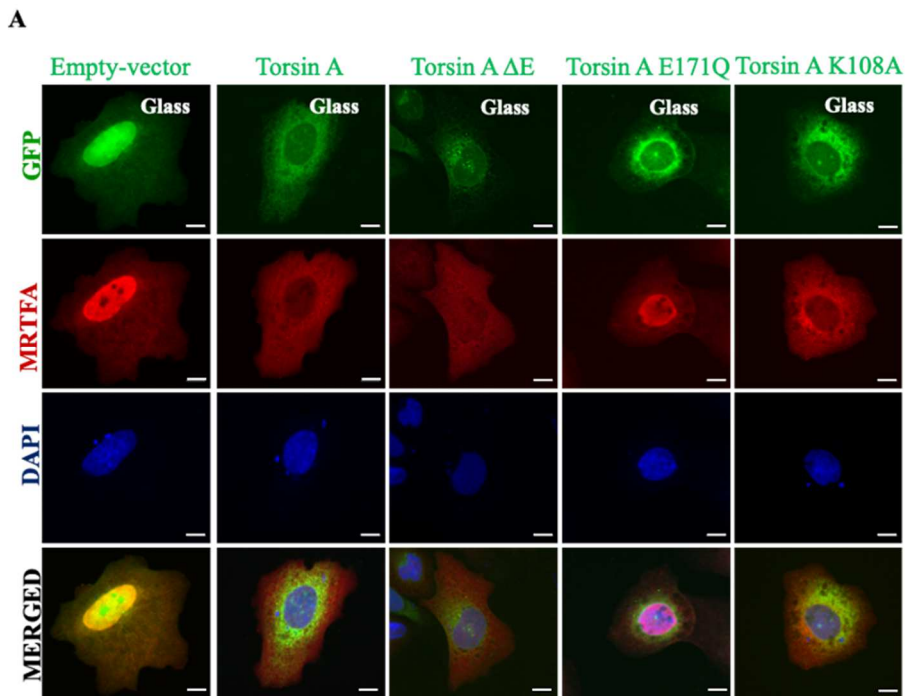
*Figure 5:(A) Immunofluorescent images taken from cells expressing GFP control vector, GFP- Torsin A wild-type, GFP Torsin A-ΔE, GFP Torsin A E171Q and GFP Torsin A K108A plated on Glass. 8(B) shows the nuclear/ cytoplasmic ratios of MRTFA fluorescence per unit area. All scale bars are 10 μm in length. All error bars are standard error measurements.*

## 3.5 Torsin A localizes on the nuclear envelope on soft substrates

We next investigated whether stiffness could impact on Torsin-A localisation. We performed epifluorescent experiments of U2OS expressing GFP-Torsin-A plated on gels with different stiffness. We found that on soft gels Torsin A localizes at NE, while on stiff substrates it loses this localization at the nuclear envelope and it is observed more on the ER. The strategic Torsin A's localization is in accordance with its role of modulator of nuclear translocation.

Knowing the relation between Torsin A localization and Lull1 [117 ,119] we investigated the role played by Lull1 in the change of localization by silencing Lull1 and then plaiting the cells on different substrates. As shown in Figure 6A and 6B when the expression of this cofactor is silenced Torsin A loses its localization at the NE even in cells plated on soft substrates restoring a phenotype more similar to the one observed when Torsin A is analysed on cells plated on a rigid support. This result suggests that the soft substate facilitate the binding between Torsin A and Lull 1.
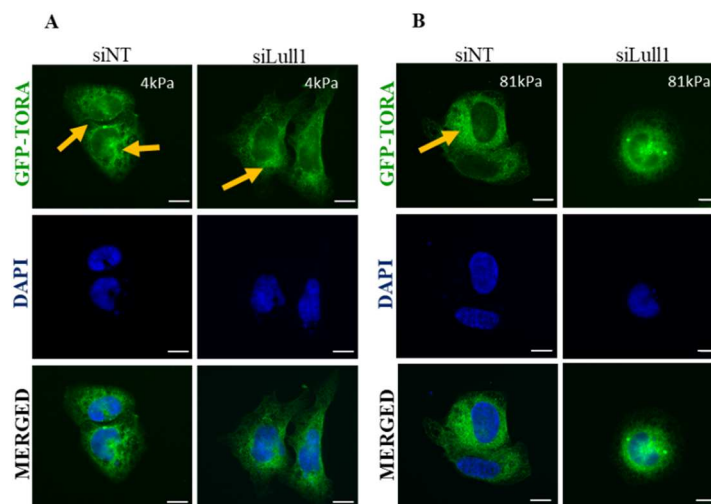
*Figure 6:(A) Epifluorescence images of GFP-Torsin A localization in control and after Lull1 knocked down using siRNA on soft substrates (4kPa) in U2OS cells. (B) Epifluorescence images of GFP-Torsin A localization in control and Lull1 knockdown conditions on stiff substrates(81kPa) in U2OS cells. All scale bars are 10 µm in length.*

## 3.6 Importin ß is involved in Torsin A localization

Then trying to understand if other proteins could be involved in Torsin A localization at the NE we focused on Importin ß. Importin ß is involved in the binding and in the transport of cargo into the nucleus and it mediates interactions with the nuclear pore complex [140 , 141]. In our experiment, we plated the cells on substrates with different stiffness and analysed the accumulation of Torsin A around the nucleus in each condition.

The epifluorescence images shown in Figure 7 (A) suggest that when the function of importin ß is inhibited by performing a 1-hour treatment with the drug Importazole, Torsin A loses its nuclear accumulation in cells plated on soft substrates. On the contrary, when the same experiment is repeated on stiff substrates (81kPa) and on Glass Figure 7 (B), (C) where Torsin A is already in the ER, no differences are noticed with when the importin ß function is inhibited.

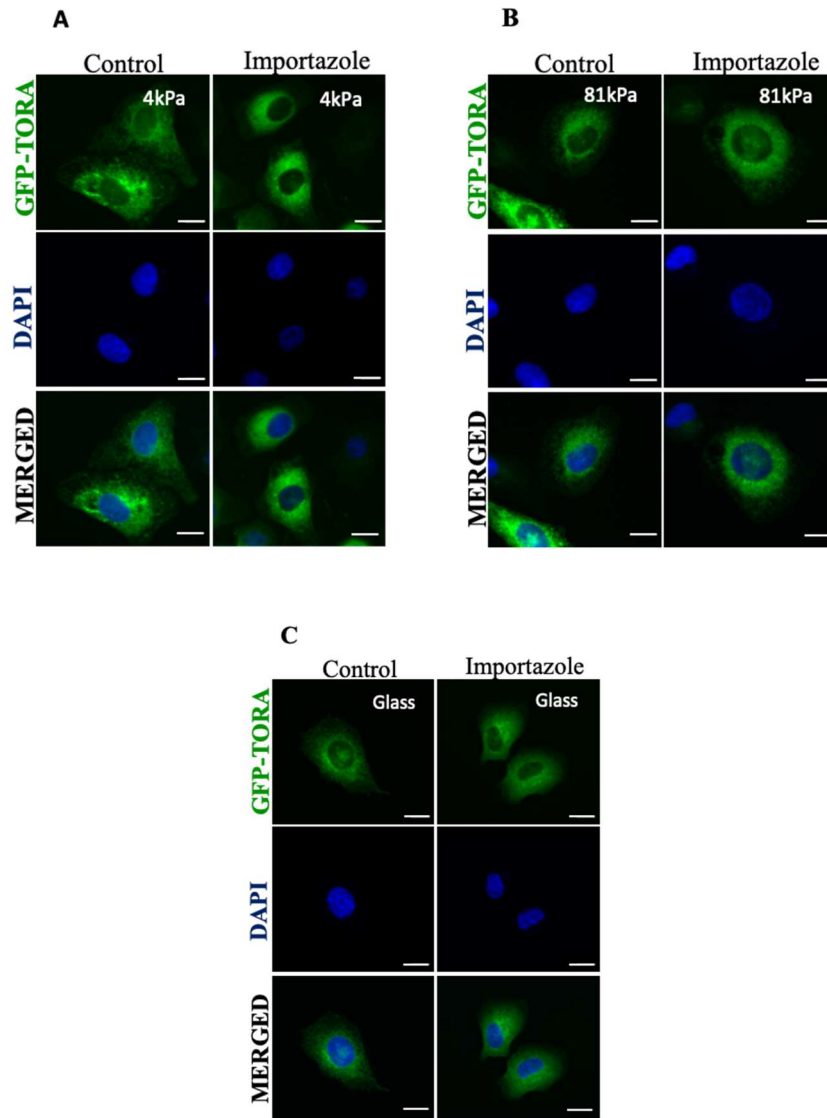This experiment reveals that Importin ß is required for nuclear envelope localization of Torsin A.



*Figure 7: (A) Epifluorescence images of GFP- Torsin A localization in control and under 1- hour treatment with Importazole (0.1 ug/ml) on soft substrates in U2OS cells. (B) Epifluorescence images of GFP- Torsin A localization in control and control and under 1- hour treatment with Importazole (0.1 ug/ml) on stiff substrates in U2OS cells. (C) Epifluorescence images of GFP- Torsin A localization in control and under 1- hour treatment with Importazole (0.1 ug/ml) on Glass in U2OS cells. All scale bars are 10 µm in length.*

**3.7 Can Torsin A localization be affected by cytoskeleton?**

Scientific evidences suggest that mechanical cues affect the increase of actin polymerization [142]. In particular on a soft substrate, we observe an increase of actin monomers and less actin filaments, on the contrary in cells plated on stiff substrates we have an enormous increase of actin filaments [143]. On the base of these evidences, we analysed a potential correlation between the actin polymerization and Torsin A localisation by using drugs that interfere with actin polymerization.

**3.7.1 Actin polymerization affects Torsin A localization**

We first performed these experiments plating the cells on soft substrates and treating them for 1hour with Latranculin B, a drug which binds actin monomers and prevents actin polymerization and with Jasplakinolide which stabilizes actin filaments. Cells with a reduction of actin polymerization due to the treatment with Latranculin B show Torsin A accumulation in the NE. On the contrary when actin polymerization is stabilized Torsin A does not accumulate in NE (Figure 8A). The same experiments were repeated in cells plated on stiff substrates (81kPa) and on Glass. Torsin A on stiff substrates does not localise on the nuclear envelope. By using Latranculin B and reducing the actin polymerization we noticed a Torsin A accumulation at the nuclear envelope. Conversely, we did not notice any differences in the Torsin A localization when we used Jasplakinolide and this suggests that actin polymerization impact Torsin A localization (Figure 8B, 8C). These results indicate that on soft substrates where the level of actin polymerisation is usually low, Torsin A localizes at NE and this blocks

the translocation of transcription factors while on stiff substrates it is observed mainly

in the ER and it allows the passages of the transcription factors in to nucleus.
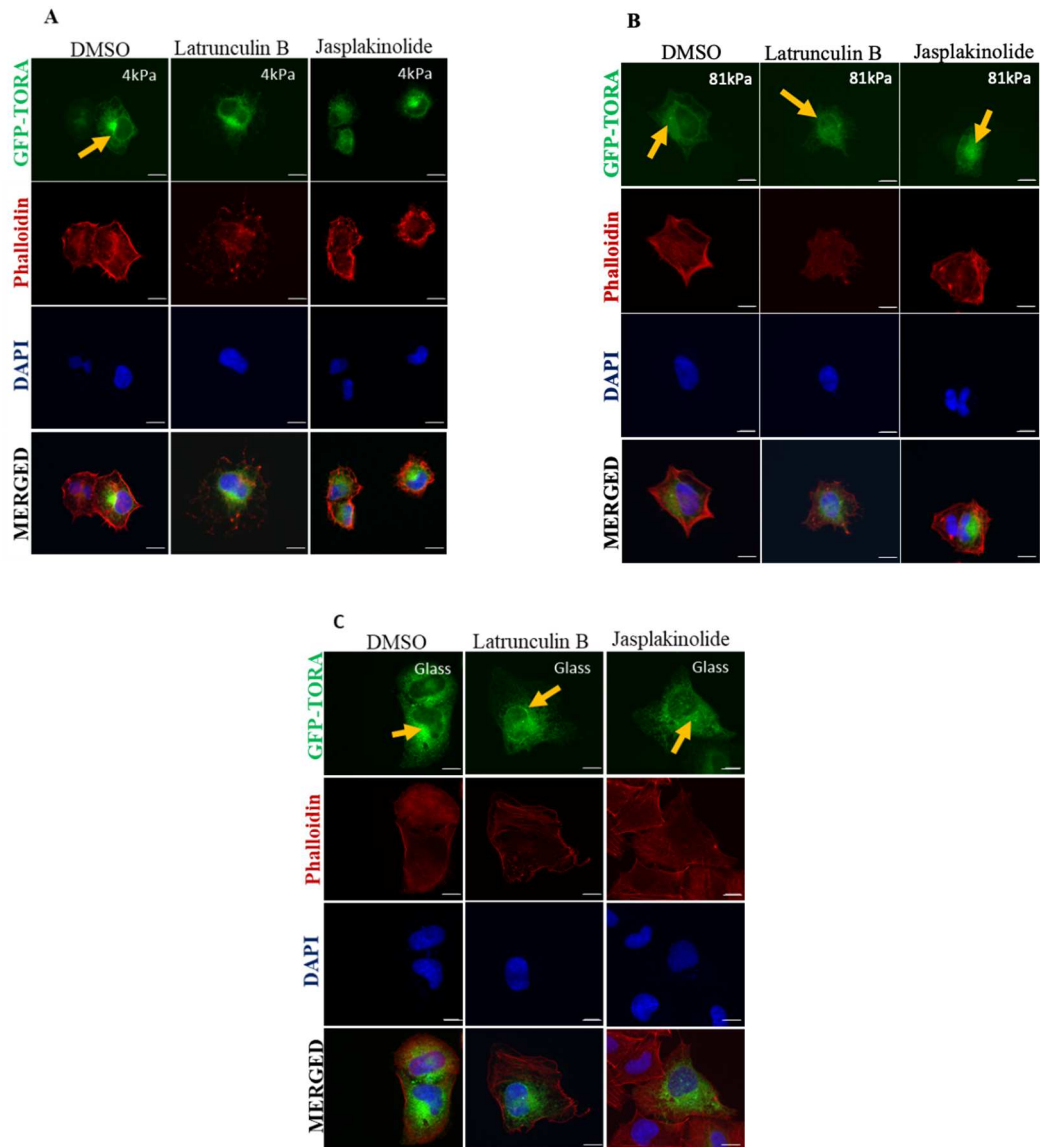


*Figure 8:(A) Epifluorescence images of GFP- Torsin A localization in control (DMSO) and under 1hour treatment with Latranculin B[0,1ug/ml] and Jasplakinolide [0,1ug/ml] on soft substrates in U2OS cells. (B)Epifluorescence images of GFP-Torsin A localization in control (DMSO) and control and under1hour treatment whit Latranculin B[0,1ug/ml] and Jasplakinolide [0,1ug/ml] on stiff substrates in U2OS cells. (C)Epifluorescence images of GFP- Torsin A localization in control (DMSO) and under treatment whit Latranculin B [0,1ug/ml] and Jasplakinolide [0,1ug/ml] on Glass in U2OS cells. All scale bars are 10 µm in length.*

### 3.7.2 Microtubules and Torsin A

Knowing that microtubules are one of the most important part of the cellular cytoskeleton [144, 145], we decided to interfere with their polymerization to assess whether this could affect the localisation of Torsin A. We performed these experiments plating the cells on soft substrates and doing a 1hour treatment with Nocodazole [0,1 un/ml] which is a drug that interfere with the polymerization of microtubules. Figure 9A shows how on soft cells, compared to the control, Torsin A loses its localization to the nuclear envelope when the cells are under Nocodazole treatment. The same experiments were performed in cells plated on stiff substrates and on Glass (Figure 9B, 9C). Torsin A does not localise on the Nuclear Envelope on stiff substrate. Here, the treatment with Nocodazole does not affect the Torsin A localisation at the ER. This experiment suggests on soft substrate where the cytoskeleton is less organised the reduction of microtubules polymerization modulates Torsin A localization [143] and the treatment with Nocodazole does not affect Torsin A localization.

*Figure 9: (A) Epifluorescence images of GFP- Torsin A localization in control (DMSO) and Nocodazole [0.1ug/ml] on soft substrates in U2OS cells. (B) Epifluorescence images of GFP- Torsin A localization in control (DMSO) and control and Nocodazole [0.1ug/ml] on stiff substrates in U2OS cells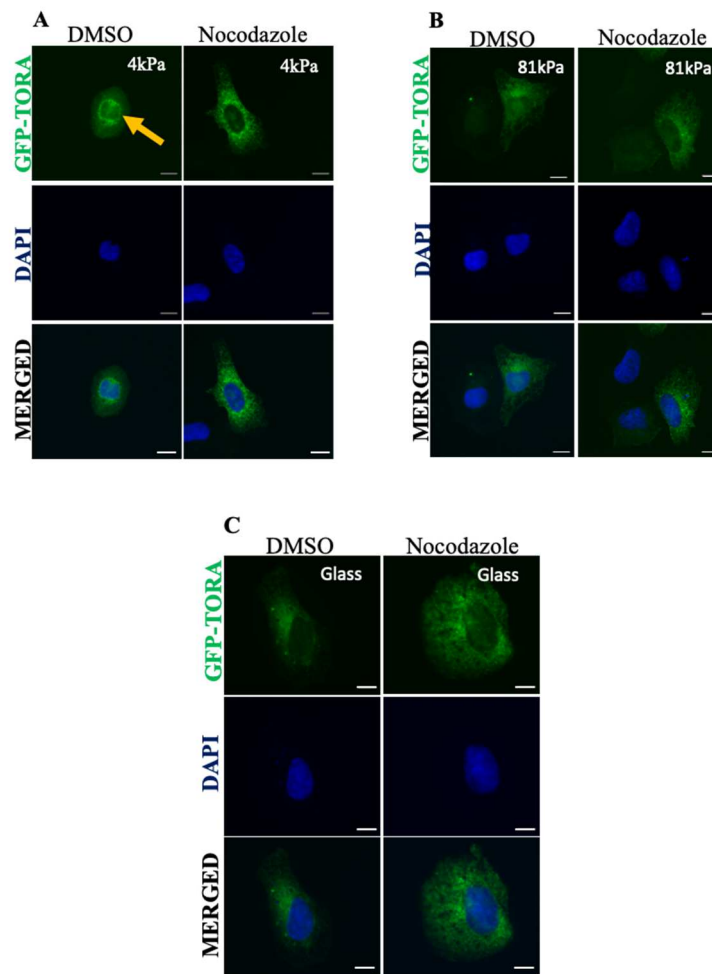. (C) Epifluorescence images of GFP- Torsin A localization in control (DMSO) and Nocodazole [0.1ug/ml] on Glass in U2OS cells. All scale bars are 10 µm in length.*

# Chapter 4

## 4. Discussion

In this research we investigated the role of Torsin A in protein nuclear transport. The trafficking of proteins within the nucleus is important for the maintenance of cell physiology, but it is also at the core of the origin of various pathologies with the aim of altering gene expression. The transport of molecules inside the nucleus is a process that requires the combination of chemical and mechanical signals from the external environment. Torsin A may play a crucial role in the control of nuclear transport, both because of its connection with the elements of the LINC complex and its association with the Nuclear Pore Complexes (NPCs) and because of its strategic localization. In order to study this function, MRTFA and YAP were used. They are mechanosensitive transcription factors that, by translocating into the nucleus, induce transcription not only of the cytoskeletal genes but also of the genes involved in cancerous metastases and invasion [146]. The findings of this study indicate that Torsin A strongly influences the translocation of molecules into the nucleus. In addition, Torsin A, as its structure suggests, could play the function of an holdase chaperone that binds molecules which control their nuclear translocation. In fact, with the silencing of Torsin A nuclear accumulation of MRTFA and YAP can be observed mainly on cells plated on soft substrates, while the overexpression of Torsin A wild type shows a cytoplasmic accumulation of YAP in cells plated both on soft and on rigid substrates. Through this result we provide valuable insights into the possible role of Torsin A in the modulation of gene transcription and hence its involvement in pathophysiological conditions such as cancer. Then investing which domain of Torsin A structure is

involved in the alteration of nuclear translocation of molecules, we tested different mutants, each presenting alteration in different residues. The increase of MRTFA nuclear translocation due to the stiffness of the substrate was always high. The only form that is not functional is the E171 Q, which remains blocked with the ATP bound without being hydrolysed [138]. This analysis concludes that the residues referred to above do not interfere with the blocking activity carried out by Torsin A. Through this analysis it is also possible to establish the connection between the position of Torsin A and its action on nuclear translocation and thus, as a controller of gene transcription. In fact, Torsin A exercises its function more on soft substrates, where it is located at the level of the nuclear envelope (NE), while on rigid substrates it appears to manifest itself more in the endoplasmic reticulum (ER).

Scientific studies have shown that the localization of Torsin A is strongly influenced by the presence of a cofactor Lull1 which carries Torsin A from the endoplasmic reticulum to the nuclear envelope (NE) [117]. Therefore, the silencing of this cofactor was performed in cells plated on soft substrates and it allowed to notice a reduced accumulation of Torsin A at the nuclear envelope level, while when this cofactor is silenced in cells plated on rigid substrates, Torsin A remains localized at the level of the ER, thus suggesting that the interaction between Lull1 and Torsin A is strongly dependent on the rigidity of the substrate. The soft substrates of 4kPa have a stiffness very close to that of the physiological tissues, and this leads to the hypothesis that the interaction between Lull1 and Torsin A, that brings Torsin A to the NE level, is intact and Torsin A reaches the NE where it exerts its function. The substrates of 81 kPa, on the other hand, mimic an environment much more similar to a pathological state. In

this context, the interaction between Lull1 and Torsin A is interrupted and therefore Torsin A, not being at the NE level, cannot control the passage of transcription factors involved in cancer progression such as MRTF-A and YAP.

Another protein responsible for transporting Torsin A at the level of the Nuclear Envelope,

Importin ß, was also identified. This protein, which is crucial for the transport of molecules

through the nuclear envelope and interacting with the nuclear pore complex [140, 141], emerged as an excellent candidate as a possible carrier of Torsin A at the level of the nuclear envelope. By using a specific inhibitor of Importin ß, Importazole we were able to block the localisation of Torsin A at the nuclear envelope, which is normally observed on soft substrates. This result indicates that localization of Torsin-A on the Nuclear envelope is mediated by an active process of translocation.

Subsequently, given the various scientific evidences between the rigidity of the substrate and the polymerization of cytoskeletal elements, we wondered if Torsin A depended on cytoskeletal elements such as actin and microtubules [143]. Actin polymerisation strongly increase when cells are plated on rigid substrates, while G actin monomers concentrations increase when cells are plated on soft substrates. The microtubules polymerization works the same way increasing on stiff substrate. Both allow the cell to adapt to changes in the surrounding environment by changing the shape and functions of the cell itself. Given the change in activity and localization of Torsin A due to changes in the rigidity of the substrate, compounds that selectively interfere with the polymerization of actin were used in order to evaluate its possible correlation with Torsin A.

# Bibliography

1- Ingber D.E., Cellular mechanotransduction: putting all the pieces together again. FASEB J, 2006.p.811– 27.

2- Orr A.W., Helmke B.P., Blackman B.R., Schwartz M.A,.Mechanisms of mechanotransduction. Dev Cell 2006, p.11– 20.

3- Vogel V., Sheetz M., Local force and geometry sensing regulate cell functions. Nat Rev Mol Cell Biol, 2006.p. 265 –75.

4- Eberl D.F., Hardy R.W., Kernan M.J., Genetically similar transduction mechanisms for touch and hearing in Drosophila. J Neurosci, 2000.p. 5981–8.

5- Syntichaki P., Tavernarakis N., Genetic models of mechanotransduction: the nematode

Caenorhabditis elegans. Physiol Rev 2004, p.1097–153.

6- Lammerding J., Kamm R.D., Lee R.T., Mechanotransduction in cardiac myocytes. Ann N Y Acad Sci 2004, p.53–70.

7- Garcia-Cardena, G., Biomechanical activation of vascular endothelium as a determinant of its functional phenotype. Proc Natl Acad Sci U S A 2001.p. 4478–85.

8- Gimbrone, M.A. et al., Endothelial Dysfunction, Hemodynamic Forces, and Atherogenesisa. Hemodynamics and atherogenesis.2000. p.230–9.

9- Haga J.H., Li Y.S., Chien S. Molecular basis of the effects of mechanical stretch on vascular smooth muscle cells. J Biomech, 2007.p.947–60.

10- Li Y.S., Haga J.H., Chien S., Molecular basis of the effects of shear stress on vascular endothelial cells. J Biomech, 2005.p.1949–71.

11-Ng C.P., Helm C.L., Swartz M.A., Interstitial flow differentially stimulates blood and lymphatic endothelial cell morphogenesis in vitro. Microvasc Res,2004. p.258–64.

12- Burger E.H., Klein-Nulend J., Mechanotransduction in bone-role of the lacuno-canalicular network. FASEB J ,1999.

13- Wirtz H.R., Dobbs L.G., The effects of mechanical forces on lung functions. Respir Physiol, 2000.p. 1– 17.

14- Serluca F.C., Drummond I.A., Fishman M.C., Endothelial signaling in kidney morphogenesis: a role for hemodynamic forces. Curr Biol, 2002.p.492–7.

15- Janmey P.A. and Miller R.T., Mechanisms of mechanical signalling in development and disease Journal of Cell Science, 2011. p. 9-18.

16- Levental, I., Georges, P. C. and Janmey, P. A. Soft biological materials and their impact on cell function. Soft Matter, 2007.p,299-306.

17- Georges, P.C. et al., Increased stiffness of the rat liver precedes matrix deposition: implications for fibrosis. Am. J. Physiol. Gastrointest. Liver Physiol, 2007. p1147-1154.

18- Assoian, R.K. and Klein, E.A., Growth control by intracellular tension and extracellular stiffness. Trends Cell. Biol, 2008. p.347-352.

19- Klein, E.A., et al., Cell-cycle control by physiological matrix elasticity and in vivo tissue stiffening. Curr. Biol, 2009. p.1511-1518.

20- Kumar, S. and Weaver, V. M., Mechanics, malignancy, and metastasis: the force journey of a tumor cell. Cancer Metastasis Rev, 2009. p. 113-127.

21-Levental, K. R., et al., Matrix crosslinking forces tumor progression by enhancing integrin signaling. Cell, 2009. p. 891-906.

22- Engler, A.J., et al., Embryonic cardiomyocytes beat best on a matrix with heart-like elasticity: scar-like rigidity inhibits beating. J. Cell Sci, 2008.p. 3794-3802.

23- Chaturvedi, R.R., Passive stiffness of myocardium from congenital heart disease and implications for diastole. Circulation, 2010. p. 979-988.

24- Cecelja, M. and Chowienczyk, P. Dissociation of aortic pulse wave velocity with risk factors for cardiovascular disease other than hypertension: a systematic review. Hypertension, 2009.p.1328-1336.

25- Mitchell, G., Arterial stiffness and cardiovascular events: the Framingham Heart Study. Circulation, 2010.p. 505-511.

26- DeLoach, S. S. and Townsend, R. R., Vascular stiffness: its measurement and significance for epidemiologic and outcome studies. Clin. J. Am. Soc. Nephrol, 2008.p. 184- 192.

27- Lacolley, P. et al., Genetics and pathophysiology of arterial stiffness. Cardiovasc, Res.2009. p.637-648.

28- Wells, R. G.,The role of matrix stiffness in regulating cell behavior. Hepatology, 2008. p.1394-1400.

29- Li, Z. et al., Transforming growth factor-beta and substrate stiffness regulate portal fibroblast activation in culture. Hepatology, 2007.p.1246-1256.

30- Tandon, R., et al., HIV infection changes glomerular podocyte cytoskeletal composition and results in distinct cellular mechanical properties. Am. J. Physiol. Renal. Physiol, 2006.

31- Weiss, P. and Garber, B., Shape and movement of mesenchyme cells as functions of the physical structure of the medium: contributions to a quantitative morphology. Proc. Natl. Acad. Sci, 1952. p.264-280.

32- McGrail, D. J. et al., Actomyosin tension as a determinant of metastatic cancer mechanical tropism. Phys. Biol.,2015.

33- Chaudhuri, P. K. et al., Topography induces differential sensitivity on cancer cell proliferation via Rho- ROCK-Myosin contractility. Sci. Rep, 2016.

34- Xi, W.; et al., Molecular insights into division of single human cancer cells in on-chip transparent microtubes. ACS Nano, 2016.p. 5835.

35- Chang, S.F. et al., Tumor cell cycle arrest induced by shear stress: Roles of integrins and Smad. Proc. Natl. Acad. Sci. U. S. A. 2008, p. 3927−3932.

36- Aragona, M. et al., A mechanical checkpoint controls multicellular growth through YAP/TAZ regulation by actin- processing factors. Cell 2013, p.1047−1059.

37- Liu, J.et al., Soft fibrin gels promote selection and growth of tumorigenic cells. Nat. Mater, 2012.p.734−741.

38- Paszek, M. J., et al., Tensional homeostasis and the malignant phenotype. Cancer Cell, 2005 p.241−254.

39- Jodele, S., Blavier, L., Yoon, J. M., DeClerck, Y. A., Modifying the soil to affect the seed: role of stromal-derived matrix metal- loproteinases in cancer progression. Cancer Metastasis, Rev. 2006 p. 35−43.

40- Provenzano P.P., Inman D.R., Keely P.J. Matrix density-induced mechanoregulation of breast cell phenotype, signaling, and gene expression through a FAK-ERK linkage. Oncogene,2009; p. 4326–4343.

41- Janmey, P. A. and Miller, R. T., Mechanisms of mechanical signaling in development and disease. J. Cell Sci, 2011.p. 9–18.

42- Hoyt, K. et al., Tissue elasticity properties as biomarkers for prostate cancer. Cancer Biomark, 2008.p.213–225.

43- Garra, B. S. et al., Elastography of breast lesions: initial clinical results. Radiology, 1997p. 79–86.

44- Baker, E. L., Bonnecaze, R. T. and Zaman, M. H., Extracellular matrix stiffness and architecture govern intracellular rheology in cancer. Biophys. 2009 p.1013-1021.

45- Paszek, M. J. et al., Tensional homeostasis and the malignant phenotype. Cancer Cell. 2005. p. 241-254

46- Finch-Edmondson, M. and Sudol M., Framework to function: mechanosensitive regulators of gene transcription. Cell Mol Biol Lett, 2016. p. 28.

47- Austen, K. et al., Extracellular rigidity sensing by talin isoform-specific mechanical linkages. Nat Cell Biol, 2015.p. 1597-606.

48- Humphries, J.D. et al., Vinculin controls focal adhesion formation by direct interactions with talin and actin. J Cell Biol, 2007. p. 1043-57.

49- Bays, J.L. and. DeMali K.A, Vinculin in cell-cell and cell-matrix adhesions. Cell Mol Life Sci, 2017.p. 2999-3009.

50- Courtemanche, N. et al., Tension modulates actin filament polymerization mediated by formin and profilin. Proc Natl Acad Sci U S A, 2013.p. 9752-7.

51- Gerace, L. and Burke B., Functional-Organization of the Nuclear-Envelope. Annual Review of Cell Biology, 1988. 4: p. 335-374.

52- Crisp, M. et al., Coupling of the nucleus and cytoplasm: role of the LINC complex. J Cell Biol, 2006. p. 41-53.

53- Mejat, A. and Misteli T., LINC complexes in health and disease. Nucleus, 2010.p.40-52.

54- Haque, F. et al., Mammalian SUN Protein Interaction Networks at the Inner Nuclear Membrane and Their Role in Laminopathy Disease Processes. Journal of Biological Chemistry, 2010. p. 3487-3498.

55- Dechat, T. et al., Nuclear lamins: major factors in the structural organization and function of the nucleus and chromatin. Genes & Development, 2008. p. 832-853.

56-Sosa, B.A., Kutay U., and Schwartz T.U., Structural insights into LINC complexes. Curr Opin Struct Biol, 2013. p. 285-91.

57- Alam, S.G. et al., The mammalian LINC complex regulates genome transcriptional responses to substrate rigidity. Sci Rep, 2016. p. 38063.

58- Aebi, U. et al., The Nuclear Lamina Is a Meshwork of Intermediate-Type Filaments. Nature, 1986.p. 560-564.

59- Raab, M., ESCRT III repairs nuclear envelope ruptures during cell migration to limit DNA damage and cell death. Science, 2016.p. 1507-1507.

60- Constantinescu, D. et al., Lamin A/C expression is a marker of mouse and human embryonic stem cell differentiation. Stem Cells, 2006. p. 177-85.

61- Spann, T.P. et al., Alteration of nuclear lamin organization inhibits RNA polymerase II-dependent transcription. J Cell Biol, 2002. p. 603-8.

62- Gruenbaum, Y. et al., The nuclear lamina comes of age. Nat Rev Mol Cell Biol, 200.: p. 21-31.

63-Van Steensel, B. and Belmont A.S., Lamina-Associated 27- Domains: Links with Chromosome Architecture, Heterochromatin, and Gene Repression. Cell, 2017. p. 780-791.

64- Pawlowski, R. et al., An actin-regulated importin alpha/beta-dependent extended bipartite NLS directs nuclear import of MRTF-A. EMBO J, 2010.p. 3448-58.

65- Furukawa, K.T. et al., The epithelial circumferential actin belt regulates YAP/TAZ through nucleocytoplasmic shuttling of merlin. Cell Rep, 2017p.1435–1447.

66- Elosegui-Artola, A. et al., Force triggers YAP nuclear entry by regulating transport across nuclear pores. Cell, 2017 p.1397–1410.

67- Infante, E. et al., The mechanical stability of proteins regulates their translocation rate into the cell nucleus. Nature Physics, 2019. p. 973-981.

68- Low, B.C. et al., YAP/TAZ as mechanosensors and mechanotransducers in regulating organ size and tumor growth. Febs Letters, 2014. p.2663-2670.

69- Olson, E. N. and Nordheim, A. Linking actin dynamics and gene transcription to drive cellular motile functions. Nat. Rev Moll cell Bio, 2010. p.353-365.

70- Zhao, B. et al., The Hippo-YAP pathway in organ size control and tumorigenesis: an updated version. Genes Dev, 2010 p.862–874.

71- Werner, S., MRTF-A controls myofibroblastic differentiation of human multipotent stromal cells and their tumour-supporting function in xenograft models. Scientific Reports, 2019.

72- Lian, I., Kim, J. and Guan K.L, The role of YAP transcription coactivator in regulating stem cell self-renewal and differentiation. Genes Dev, 2010.p.1006-1118.

73- Yanlei, M. et al., Hippo-YAP signaling pathway: A new paradigm for cancer therapy. Int J Cancer, 2014 p. 2275-228674.

74- Song, Z., The MRTF-A/B function as oncogenes in pancreatic cancer. Oncol Rep, 2016 p: 127-138.

75- Kim, T., MRTF potentiates TEAD-YAP transcriptional activity causing metastasis. The EMBO Journal, 2017. p.520–535.

76- Ma, Z., Fusion of two novel genes, RBM15 and MKL1, in the t (1;22) (p13;q13) of acute megakaryoblastic leukemia Nature Genetics, 2002. p.200–221.

77- Cen, B. et al., Megakaryoblastic Leukemia 1, a Potent Transcriptional Coactivator for Serum Response Factor (SRF), Is Required for Serum Induction of SRF Target Genes. Prywes R.Mol Cell Biol, 2003.p.6597–6608.

78- Clark, E. A. et al., Genomic analysis of metastasis reveals an essential role for RhoC. Nature, 2000. p.532–535.

79- Zhang, W.L. et al., miR-206 inhibits metastasis-relevant traits by degrading MRTF-A in anaplastic thyroid cancer, 2015 p.133-142

80- Evelyn C.R., Lisabeth E.M., Neubig R.R., Small-Molecule Inhibition of Rho/MKL/SRF Transcription in Prostate Cancer Cells: Modulation of Cell Cycle, ER Stress, and Metastasis Gene Networks. Microarrays, 2016. p.5-13.

81- Leal, A.S. et al., The Rho/MRTFpathwayinhibitorCCG-222740 reduces stellate cell activation and modulates immune cell populations in Kras (G12D); Pdx1-Cre (KC) mice. Sci. Rep, 2019.p.7072.

82- Kahl, D.J. et al., 5-Aryl-1,3,4-oxadiazol-2-ylthioalkanoic Acids: A Highly Potent New Class of Inhibitors of Rho/Myocardin-Related Transcription Factor (MRTF)/Serum Response Factor (SRF)-Mediated Gene Transcription as Potential Antifibrotic Agents for Scleroderma. J. Med. Chem, 2019.p. 4350–4369.

83-Lionarons, D.A. et al., RAC1(P29S) Induces a Mesenchymal Phenotypic Switch via Serum Response Factor to Promote Melanoma Development and Therapy Resistance. Cancer Cell. 2019 p.68–83.

84-Haak, A.J. et al., Pharmacological Inhibition of Myocardin-related Transcription Factor Pathway Blocks Lung Metastases of RhoC-Overexpressing Melanoma. Mol. Cancer Ther, 2017.p .193–204.

85- Meng, Z., Moroishi, T., Guan, K.L., Mechanisms of Hippo pathway regulation. Genes Dev, 2016.p. 1-17.

86- S. Dupont, L. et al., Role of YAP/TAZ in mechanotransduction. Nature, 2011.p.179-183.

87- Das, A. et al., YAP nuclear localization in the absence of cell-cell contact is mediated by a filamentous actin-dependent, Myosin IIand Phospho-YAP independent pathway during extracellular matrix mechanosensingJ. Biol. Chem, 2016. p. 6096-6110.

88- Lamar, J.M. et al., The Hippo pathway target, YAP, promotes metastasis through its TEAD-interaction domain. Proc. Natl. Acad. Sci, 2012.p. E2441–E2450.


89- Wang, X. Su, L. and Ou, Q. Yes-associated protein promotes tumour development in luminal epithelial derived breast cancer. Eur. J. Cancer, 2012.p. 1227–1234.

90- Kang, W. et al., Yes-associated protein 1 exhibits oncogenic property in gastric cancer and its nuclear accumulation associates with poor prognosis. Clin. Cancer Res, 2011.p. 2130–2139.

91- Slemmons, K.K. et al., Role of the YAP oncoprotein in priming RAS-driven rhabdomyosarcoma. PLoS ONE, 2015.

92- Pei, T. et al., YAP is a critical oncogene in human cholangiocarcinoma. Oncotarget 2015, p. 17206–17220.

93- Zender, L. et al., Identification and validation of oncogenes in liver cancer using an integrative oncogenomic approach. Cell, 2006.p. 1253–1267.

94- Butcher, D. T., Alliston, T. and Weaver, V. M. A tense situation: forcing tumour progression. Nat. Rev. Cancer, 2009.p. 108–122.

95- Erler, J. T. et al., Lysyl oxidase is essential for hypoxia-induced metastasis. Nature, 2006.p.1222 1226.

96- Hirata, E. et al., Intravital imaging reveals how BRAF inhibition generates drug-tolerant microenvironments with high integrin beta1/FAK signaling. Cancer Cell, 2015.p.574–588.

97- Kim, M. H. et al., Actin remodeling confers BRAF inhibitor resistance to melanoma cells through YAP/TAZ activation. EMBO J., 2016. p.462–478.

98- Calvo, F. et al., Mechanotransduction and YAP- dependent matrix remodelling is required for the generation and maintenance of cancer-associated fibroblasts. Nat. Cell Biol, 2013.p 637–646.

99- Noguchi, S., Saito,A. Nagase,T., YAP/TAZ Signaling as a Molecular Link between Fibrosis and Cancer .Int.J. Mol. Sci, 2018, p.3674.

100- Girard, C.A. et al., A feed-forward mechanosignaling loop confers resistance to therapies targeting the MAPK pathway in BRAF-mutant melanoma. Cancer Res, 2020. p.1927-1941.

101- Kirby, T.J. and. Lammerding, J., Emerging views of the nucleus as a cellular mechanosensor. Nature Cell Biology, 2018.p. 373-381.

102- Swift, J. et al., Nuclear Lamin-A Scales with Tissue Stiffness and Enhances Matrix-Directed Differentiation. Science, 2013.p. 341.

103- Sexton, T. et al., Gene regulation through nuclear organization. Nature Structural & Molecular Biology, 2007.p. 1049-1055.

104- Knockenhauer, K.E. and Schwartz T.U., The Nuclear Pore Complex as a Flexible and Dynamic Gate. Cell, 2016. p. 1162-1171.

105- Kowalczyk, S.W. et al., Single-molecule transport across an individual biomimetic nuclear pore complex. Nature Nanotechnology, 2011. p. 433-438.

106- Lim, R.Y.H. et al., Flexible phenylalanine-glycine nucleoporins as entropic barriers to nucleocytoplasmic transport. Proceedings of the National Academy of Sciences of the United States of America, 2006. p. 9512-9517.

107- Solmaz, S.R., Blobel G., and Melcak I., Ring cycle for dilating and constricting the nuclear pore. Proc Natl Acad Sci, 2013. p. 5858-63.

108- Frey, S. et al., Surface Properties Determining Passage Rates of Proteins through Nuclear Pores. Cell, 2018. p. 202.

109- Jungwirth, M. et al., Relative tissue expression of homologous torsinB correlates with the neuronal specific importance of DYT1 dystonia-associated torsinA. Hum Mol Genet, 2010. p. 888-900.

110- Chase, A.R. et al., Dynamic functional assembly of the Torsin AAA+ ATPase and its modulation by LAP1. Mol Biol Cell, 2017.p. 2765-2772.

111- McLean, P.J. et al., TorsinA and heat shock proteins act as molecular chaperones: suppression of alpha-synuclein aggregation. Journal of Neurochemistry, 2002. p. 846-854

112- Granata, A., Schiavo G, and Warner T.T., TorsinA and dystonia: from nuclear envelope to synapse. J Neurochem, 2009. p. 1596-609.

113- Nery, F.C., et al., TorsinA participates in endoplasmic reticulum-associated degradation. Nat Commun, 2011. p. 393.

114- McCullough, J. and W.I. Sundquist, Putting a finger in the ring. Nat Struct Mol Biol, 2014.p. 1025-7.

115- Naismith, T.V., Dalal. S., and Hanson, P.I., Interaction of torsinA with its major binding partners is impaired by the dystonia-associated DeltaGAG deletion. J Biol Chem, 2009.p. 27866-74.

116- Luxton, G.W., et al., TAN lines: a novel nuclear envelope structure involved in nuclear positioning. Nucleus, 2011.p. 173-81.

117- Zhao, C.G. et al., Regulation of Torsin ATPases by LAP1 and LULL1. Proceedings of the National Academy of Sciences of the United States of America, 2013.p. E1545-E1554.

118- Goodchild, R.E. et al., Access of torsinA to the inner nuclear membrane is activity dependent and regulated in the endoplasmic reticulum. J Cell Sci, 2015.p. 2854-65.

119- Laudermilch, E. et al., Dissecting Torsin/cofactor function at the nuclear envelope: a genetic study. Molecular Biology of the Cell, 2016. p. 3964-3971.

120- Nery, F.C. et al., TorsinA binds the KASH domain of nesprins and participates in linkage between nuclear envelope and cytoskeleton. Journal of Cell Science, 2008. p. 3476-3486.

121- Pappas, S.S. et al., TorsinA dysfunction causes persistent neuronal nuclear pore defects. Human Molecular Genetics, 2018. p. 407-420.

122- VanGompel, M.J. et al., A novel function for the Caenorhabditis elegans torsin OOC-5 in nucleoporin localization and nuclear import. Mol Biol Cell, 2015. p. 1752-63.

123- Mattoo, R.U. and Goloubinoff P., Molecular chaperones are nanomachines that catalytically unfold misfolded and alternatively folded proteins. Cell Mol Life Sci, 2014. p. 3311-25.

124- Hartl, F.U., Bracher A., and Hayer-Hartl, M., Molecular chaperones in protein folding and proteostasis. Nature, 2011. p. 324-32.

125- Sharma, S.K. et al., The kinetic parameters and energy cost of the Hsp70 chaperone as a polypeptide unfoldase. Nat Chem Biol, 2010. p. 914-20.

126- Diamant, S. et al., Size-dependent disaggregation of stable protein aggregates by the DnaK chaperone machinery. J Biol Chem, 2000. p. 21107-13.

127- Chase, A.R., Laudermilch, E. and C. Schlieker, Torsin ATPases: Harnessing Dynamic Instability for Function. Front Mol Biosci, 2017. p. 29.

128- Breakefield, X.O., Kamm, C. and Hanson P.I, TorsinA: Movement at many levels. Neuron, 2001. p. 9-12.

129- Ozelius, L.J.,The early-onset torsion dystonia gene (DYT1) encodes an ATP-binding protein. Nat Genet ,1997. p. 40-48.

130- Heiman, G.A. et al., Increased risk for recurrent major depression in DYT1 dystonia mutation carriers. Neurology ,2004. p.631-637.

131- Grundmann, K. et al., Overexpression of human wildtype tor- sinA and human DeltaGAG torsinA in a trans- genic mouse model causes phenotypic abnor- malities. Neurobiol Dis, 2007.p. 190-206.

132- Heining, F.A. et al., An examination of TOR1A variants in recurrent major depression. Int J Mol Epidemiol Genet ,2012. p. 91-95.

133- Forno, L.S., Pathology of Parkinson's disease, in: C.D. Marsden, S. Fahn (Eds.), Movement Disorders, Butterworth Scientific,1982. p 25–40.

134- Pollanen, M.S., Dickson, D.W., Bergeron, C., Pathology and biology of the Lewy body, J. Neuropathol. Exp. Neurol,1993. p.183–191.

135- Shashidharan, P. et al., TorsinA accumulation in Lewy bodies in sporadic Parkinson's disease. Brain Research, 2000.p. 379-38.

136- McGee, K.M., et al., Nuclear transport of the serum response factor coactivator MRTF-A is downregulated at tensional homeostasis. EMBO Rep, 2011. p. 963-70.

137- Goodchild, R.E. and Dauer, W.T., Mislocalization to the nuclear envelope: An effect of the dystonia-causing torsinA mutation. Proceedings of the National Academy of Sciences of the United States of America, 2004. p. 847-852.

138- Goodchild, R.E. et al., Access of torsinA to the inner nuclear membrane is activity dependent and regulated in the endoplasmic reticulum. J Cell Sci, 2015. p. 2854-65.

139- Naismith, T.V. et al., TorsinA in the nuclear envelope. Proceedings of the National Academy of Sciences of the United States of America, 2004. p.7612-7617.

140- Ström, A.C. and Weis, K., Importi- ß -like nuclear transport receptor. Genome Biology. 2001. p.3008.1–3008.9.

141- Lowe A.R.et al., Importin-β modulates the permeability of the nuclear pore complex in a Ran-dependent manner. Biophysics and structural biology, 2015.

142- Pollard, T.D. and Borisy, G.G., Cellular motility driven by assembly and disassembly of actin filaments. Cell, 2003. p. 453-65.

143- Jannatbabaei A. et al., Cytoskeletal remodeling induced by substrate rigidity regulates rheological behaviors in endothelial cells. Journal of Biomedical Materials Research, 2018.p.71-80.

144- Schliwa, M., The cytoskeleton. An introductory survey. Springer Wien. 1986.

145- Alberts, B., Molecular biology of the cell. Garland Science. 2015.p. 28123–28125.

146- Finch-Edmondson, M. and Sudol, M., Framework to function: mechanosensitive regulators of gene transcription. Cellular & Molecular Biology Letters. 2016. p. 21-26.

# Acknowledgements

# Pubblications

1. Vivacqua A., Sebastiani A., Miglietta A.M., Rigiracciolo D.C., Cirillo F., <u>Galli G.R.</u>, Talia M., Santolla M.F., Lappano R. Giordano F., Panno M.L., Maggiolini M. miR-338-3p Is Regulated by Estrogens through GPER in Breast Cancer Cells and Cancer-Associated Fibroblasts (CAFs).

2. Rigiracciolo DC, Santolla M.F., Lappano R, Vivacqua A, Cirillo F, <u>Galli G.R.</u>, Talia M., Muglia L, Pellegrino M, Nohata N, Di Martino MT, Maggiolini M. Focal adhesion Kinase (FAK) activaction by estrogens involves GPER in triple negative breast cancer cells.

3. Santolla M.F., Vivacqua A., Lappano R., Rigiracciolo DC, Cirillo F., <u>Galli G.R.</u>, Talia M. Brunetti G., Miglietta A.M. Belfiore A., Maggiolini M. GPER Mediates a Feedforward FGF2/FGFR1 Paracrine Activation Coupling CAFs to Cancer Cells toward Breast Tumor Progression.

4. Lappano R., Mallet C., Rizzuto B. Grande F., <u>Galli G.R.</u>, Byrne C., Broutine I., Boudieu L., Echalier A., Jacquot Y. and Maggiolini M. The Peptide ERα17p Is a GPER Inverse Agonist that Exerts Antiproliferative Effects in Breast Cancer Cells.

# miR-338-3p Is Regulated by Estrogens through GPER in Breast Cancer Cells and Cancer-Associated Fibroblasts (CAFs)

**Adele Vivacqua [1],\*, Anna Sebastiani [1], Anna Maria Miglietta [2], Damiano Cosimo Rigiracciolo [1], Francesca Cirillo [1], Giulia Raffaella Galli [1], Marianna Talia [1], Maria Francesca Santolla [1], Rosamaria Lappano [1], Francesca Giordano [1], Maria Luisa Panno [1] and Marcello Maggiolini [1],\***

[1]  Department of Pharmacy, Health and Nutritional Sciences, University of Calabria, 87036 Rende, Italy; annasebastiani86@gmail.com (A.S.); damianorigiracciolo@yahoo.it (D.C.R.); francesca89cirillo@libero.it (F.C.); giulia.r.galli@gmail.com (G.R.G.); mariannatalia11@gmail.com (M.T.); m.f.s@hotmail.it (M.F.S.); lappanorosamaria@yahoo.it (R.L.); francesca.giordano@unical.it (F.G.); mamissina@yahoo.it (M.L.P.)

[2]  Regional HospitalCosenza, 87100 Cosenza, Italy; annamariamiglietta@virgilio.it

\*  Correspondence: adele.vivacqua@unical.it (A.V.); marcellomaggiolini@yahoo.it (M.M.); Tel.: +39-0984-493-048 (A.V.); +39-0984-493-076 (M.M.)

**Abstract:** Estrogens acting through the classic estrogen receptors (ERs) and the G protein estrogen receptor (GPER) regulate the expression of diverse miRNAs, small sequences of non-coding RNA involved in several pathophysiological conditions, including breast cancer. In order to provide novel insights on miRNAs regulation by estrogens in breast tumor, we evaluated the expression of 754 miRNAs by TaqMan Array in ER-negative and GPER-positive SkBr3 breast cancer cells and cancer-associated fibroblasts (CAFs) upon 17β-estradiol (E2) treatment. Various miRNAs were regulated by E2 in a peculiar manner in SkBr3 cancer cells and CAFs, while miR-338-3p displayed a similar regulation in both cell types. By METABRIC database analysis we ascertained that miR-338-3p positively correlates with overall survival in breast cancer patients, according to previous studies showing that miR-338-3p may suppress the growth and invasion of different cancer cells. Well-fitting with these data, a miR-338-3p mimic sequence decreased and a miR-338-3p inhibitor sequence rescued the expression of genes and the proliferative effects induced by E2 through GPER in SkBr3 cancer cells and CAFs. Altogether, our results provide novel evidence on the molecular mechanisms by which E2 may regulate miR-338-3p toward breast cancer progression.

**Keywords:** breast cancer; CAFs; estrogens; GPER; miR-338-3p; c-Fos; Cyclin D1

## 1. Introduction

Estrogens play a crucial role in diverse pathophysiological conditions, including cancer [1]. The action of estrogens are mainly mediated by the classic estrogen receptors (ERs) [2], however several data have also indicated that the G protein estrogen receptor (GPER) may trigger a network of transduction pathways toward the progression of several types of tumors [3–8]. Among numerous biological targets, estrogens may modulate the expression of diverse microRNAs (miRNAs) [6], which are small non-coding RNA molecules of 22–25 nucleotides [9]. In particular, miRNAs inhibit the expression of certain genes at both transcriptional and post-transcriptional levels binding to complementary sequences located within the 3′ untranslated region (UTR) of target mRNAs [10,11]. Therefore, miRNAs may be involved in important biological processes, including cancer development [12–20]. The involvement of ERs in miRNA regulation by estrogens has been established [6]. Likewise, it has

been also reported that GPER may regulate the expression of certain miRNAs in normal and cancer cell contexts characterized by the presence or absence of ERs [21–25].

MiR-338-3p is a highly conserved gene located on the chromosome 17q25 and precisely on the 7th intron of the apoptosis-associated tyrosine kinase (AATK) [26,27]. MiR-338-3p, initially identified as a brain specifically expressed miRNA, has been involved in the formation of basolateral polarity and regulation of axonal respiration [28,29]. Various studies have also shown that miR-338-3p is downregulated in many types of malignancies, hence suggesting its potential role in tumor progression [30–34]. Nevertheless, the biological function of miR-338-3p and its prognostic significance remains to be fully understood.

In this present study we provide novel insights into the ability of estrogens to regulate miR-338-3p expression and function through GPER in ER-negative breast cancer cells and cancer associated fibroblasts (CAFs), which are main components of the tumor microenvironment [35,36]. On the basis of our findings miR-338-3p may be included among the miRNAs involved in breast tumor development.

## 2. Materials and Methods

### 2.1. Reagents

17β-estradiol (E2) was purchased from Sigma-Aldrich Corp. (Milan, Italy); rel-1-[4-(6-bromo-1,3-benzodioxol-5-yl)-3aR,4S,5,9bS-tetrahydro-3H-cyclopenta[c]quinolin-8-yl]-ethanone (G-1) was obtained from Tocris Bioscience (Space, Milan, Italy). All compounds were solubilized in dimethyl sulfoxide (DMSO).

### 2.2. Cell Cultures

Breast cancer cell line SkBr3 (ER-negative and GPER-positive) was obtained from ATCC (Manassas, VA, USA), used less than six months after revival and routinely tested and authenticated according to the ATCC suggestions. CAFs (ER-negative and GPER-positive) were extracted from invasive mammary ductal carcinomas obtained from mastectomies. Briefly, samples were cut into smaller pieces (1–2 mm diameter), placed in digestion solution (400 IU collagenase I, 100 IU hyaluronidase, and 10% FBS, containing antibiotic and antimycotic solution) and incubated overnight at 37 °C. The cells were then separated by differential centrifugation at $90\times g$ for 2 min. Supernatant containing fibroblasts was centrifuged at $485\times g$ for 8 min; the pellet obtained was suspended in fibroblasts growth medium (Medium 199 and Ham's F12 mixed 1:1 and supplemented with 10% FBS) and cultured at 37 °C in 5% $CO_2$. Primary cells cultures of breast fibroblasts were characterized by immunofluorescence. Briefly cells were incubated with human anti-vimentin (V9, sc-6260) and human anti-cytokeratin 14 (LL001 sc-53253), both from Santa Cruz Biotechnology (DBA, Milan, Italy) (data not shown). To characterize fibroblasts activation, we used anti-fibroblast activated protein α (FAPα) antibody (SS-13, sc-100528; Santa Cruz Biotechnology, DBA, Milan, Italy) (data not shown). Signed informed consent from all the patients was obtained and samples were collected, identified and used in accordance with approval by the Institutional Ethical Committee Board (Regional Hospital, Cosenza, Italy). Cell types were grown in a 37 °C incubator with 5% $CO_2$. SkBr3 breast cancer cells were maintained in RPMI-1640 without phenol red supplemented with 10% fetal bovine serum (FBS) and 100 µg/mL of penicillin/streptomycin (Gibco, Life Technologies, Milan, Italy). CAFs were cultured in a mixture of MEDIUM 199 and HAM'S F-12 (1:1) supplemented with 10% FBS and 100 µg/mL of penicillin/streptomycin (Gibco, Life Technologies, Milan, Italy). Cells were switched to medium without serum the day before experimental analysis.

### 2.3. RNA Extraction

Cells were maintained in regular growth medium and then switched to medium lacking serum before performing the indicated assays. Total RNA was extracted from cultured cells using miRVana Isolation Kit (Ambion, Life Technologies, Milan, Italy) according to the manufacturer's

recommendations. The RNA concentrations were determined using Gene5 2.01 Software in Synergy H1 Hybrid Multi-Mode Microplate Reader (BioTek, AHSI, Milan, Italy).

### 2.4. miRNA Expression Profiling

TaqMan™ Array Human MicroRNA A+B Cards Set v3.0 was used for global miRNA profiling. The panel includes two 384-well microfluidic cards (human miRNA pool A and pool B) that contain primers and probes for 754 different miRNAs in addition to small nucleolar RNAs that function as endogenous controls for data normalization. Equal quantity (100 ng) of RNA extracted from SkBr3 breast cancer cells and CAFs treated with vehicle or 100 nM E2 for 4 h was reverse-transcribed for cDNA synthesis using the Megaplex RT Primer Pool A or B and the TaqMan MicroRNA Reverse Transcription kit (Applied Biosystems).in a final volume of 7.5 μL (Applied Biosystems, Milan, Italy). The reverse transcription reaction was incubated for 2 min at 16 °C, 1 min at 42 °C and 1 s at 50 °C for 40 cycles, followed by 5 min at 85 °C to deactivate the enzyme. The cDNA obtained was pre-amplified using Megaplex Preamp primer pool A or B and TaqMan PreAmp Master Mix 2X in a final volume of 25 μL using the same temperature conditions above described. The product was diluted 1:4 in TE 0.1X, to which were added TaqMan Universal Master Mix no UNG 2X and nuclease free water. 100 μL of the sample/master mix for each multiplex pool were loaded into fill reservoirs on the microfluidic card. The array was then centrifuged, mechanically sealed with the Applied Biosystems sealer device and run on QuantStudio 6&7 Flex Real Time PCR System (Applied Biosystems, Life Technologies, Milan, Italy). The raw array data were analysed by DataAssist™. The baseline was set automatically, while the threshold was set manually at 0.2. Samples that had Ct values>32 were removed from the analysis. Each miRNA was normalized against the mean of the four RNU6B and its expression was then assessed in the E2 treated cells against the vehicle treated cells using the $2^{-\Delta\Delta CT}$ method [37]. miRNAs showing an increased value of 2-fold expression and a 50% reduction respect to vehicle-treated cells were selected. Venn diagram was obtained by http://bioinformatics.psb.ugent.be/cgibin/liste/Venn/calculate_venn.htpl.

### 2.5. Analysis of Public Data Set from METABRIC and Kaplan-Meier Plotter

Prognostic values of miR-338-3p levels, using METABRIC data set, were analyzed by Kaplan–Meier survival curves of breast cancer patients, using Kaplan-Meier Plotter (www.kmplot.com/analysis) [38]. Log-rank test was used for statistical analysis.

### 2.6. Real Time-PCR

cDNA for miRNA expression was synthesized from 100 ng of total RNA using the TaqMan microRNA Reverse Transcription Kit (Applied Biosystems, Life Technologies, Milan, Italy). The expression levels of miR-338-3p were quantified by TaqMan microRNA Assay Kit (Applied Biosystems, Milan, Italy), using the primers for the internal control RNU6B (assay ID 001093) and miR-338-3p (assay ID 002252). In order to measure the mRNA levels of c-Fos and Cyclin D1, 3μg of total RNA were reversely transcribed using the murine leukemia virus reverse transcriptase (Life Technologies, Milan, Italy), as indicated by the manufacturer. The quantitative PCR was performed using SYBR Green PCR Master Mix (Applied Biosystems, Life Technologies, Milan, Italy). Specific primers for Actin, which was used as internal control, c-Fos and Cyclin D1 genes were designed using Primer Express version 2.0 software (Applied Biosystems Inc, Milano, Italy). The sequences were as follows: Actin Fwd: 5′-AAGCCAACCCCACTTCTCTCTAA-3′ and Rev: 5′-CACCTCCCCTGTGTGGACTT-3′; c-Fos Fwd: 5′-CGAGCCCTTTGATGACTTCCT-3′ and Rev: 5′-GGAGCGGGCTGTCTCAGA-3′; Cyclin D1 Fwd: 5′-CCGTCCATGCGGAAGATC-3′ and Rev: 5′-ATGGCCAGCGGGAAGAC-3′. All experiments were performed in triplicate using QuantStudio 6&7 Flex Real Time PCR System (Applied Biosystems, Life Technologies, Milan, Italy). Data were normalized to the geometric mean of housekeeping gene to control the variability into expression levels and fold changes were calculated by relative quantification compared to respective scrambled controls [32].

### 2.7. Bioinformatic Tools

The sites miRNAbase (http://www.miRNAbase.org), Targetscan (http://www.targetscan.org) and miRDip (http://ophid.utoronto.ca/mirDIP/) were used to identified miR-338-3p target genes.

### 2.8. Constructs and Transfections

The negative control (miR-Ctrl), the miR-338-3p mimic (miR-338-3p m) (ID MC10716) and miR-338-3p inhibitor (miR-338-3p i) (ID MH10716) sequences were purchased from Ambion (Life Technologies, Milan, Italy) and transfected into the cells 48 h before the treatments, using X-treme GENE 9 DNA Transfection Reagent (Roche Diagnostics, Sigma-Adrich, Milan, Italy). Silencing of GPER expression was obtained by using the construct previously described [39]. The plasmid DN-Fos, which encodes a c-Fos mutant that heterodimerizes with c-Fos dimerization partners but does not allow DNA binding, was a kind gift from Dr. C. Vinson (NIH, Bethesda, MD, USA).

### 2.9. Western Blotting

Cells were maintained in complete medium before the transfection assays, which are performed in medium without serum for 48 h and then treated as indicated. Cells were lysed in RIPA buffer containing a mixture of protease inhibitors. Equal amounts of protein extract were resolved on SDS-polyacrylamide gel, transferred to a nitrocellulose membrane (Amersham Biosciences, Italy), probed overnight at 4 °C with antibodies against: c-Fos (E-8, sc-166940) and β-Actin (AC-15, sc-69879) (Santa Cruz Biotechnology, DBA, Italy), GPER (AB137479) (Abcam, Euroclone, Milan, Italy) and Cyclin D1 (Origene, DBA, Milan, Italy). Proteins were detected by horseradish peroxidase-linked secondary antibodies (Biorad, Milan, Italy) and revealed using the chemiluminescent substrate for western blotting Westar Nova 2.0 (Cyanagen, Biogenerica, Catania, Italy).

### 2.10. Luciferase Assays

Cells were seeded in regular growth medium into 24-well plates. The next day the growth medium was replaced with medium lacking serum and the transfection was performed using X-tremeGene9 reagent, as recommended by the manufacturer (Roche Diagnostics), with a mixture containing Cyclin-D1-luc, the internal control pRL-TK and miR-Ctrl, miR-338-3p m, alone or in presence of miR-338-3p i, shGPER, DN-Fos as indicated. The cells were treated overnight with 100 nM of E2 or G1. Luciferase activity was measured using the Dual Luciferase kit (Promega, Milan, Italy) according to the manufacturer's instructions. Firefly luciferase values were normalized to the internal transfection control provided by the Renilla luciferase activity. The normalized relative light unit (RLU) values obtained from cells transfected with respective scrambled controls were set as 1-fold induction upon which the activity induced by the treatment was calculated.

### 2.11. Cell Proliferation Assays

For quantitative proliferation assay, cells ($1 \times 10^4$) were seeded in 24-well plates in regular growth medium. Cells were washed, once they had attached, and then incubated in medium containing 2.5% charcoal stripped fetal bovine serum, before the transfection with 25 nM miR-338-p m and 50 nM miR-338-3p i, as indicated. Transfection was renewed every 2 day, while the cells were treated every day. Evaluation of cell growth was performed on day 6 using automatic counter (Countess™-Invitrogen).

### 2.12. Cell Cycle Analysis

To analyze cell cycle distribution, CAFs were cultured in regular medium and shifted in medium containing 2.5% charcoal-stripped FBS at the 70% confluence. Next, miRNA sequences as indicated were added to cells using X-treamGene9 reagent (Roche Diagnostics, Milan, Italy). After 24 h, 100 nM E2 or 100 nM G-1 were put in the medium for additional 24 h. Cells were pelleted, once washed with phosphate buffered saline and stained with a solution containing 50 μg/mL propidium iodide in 1 x

PBS (PI), 20 U/mL RNAse-A and 0.1% Triton (Sigma-Aldrich, Milan, Italy). The DNA content was measured using a FACScan flow cytometer (Becton Dickinson, Mountain View, CA, USA) and the data acquired using CellQuest software. Cell cycle profiles were determined using ModFit LT. The proportion of the cells in G0/G1, S and G2/M phases was each estimated as a percentage of the total events (10,000 cells).

*2.13. Statistical Analysis*

Data were analyzed by one-way ANOVA with Dunnett's multiple comparisons where applicable, using GraphPad Prism version 6.01 (GraphPad Software, Inc., San Diego, CA, USA). $p < 0.05$ (*) was considered statistically significant.

## 3. Results

*3.1. miRNAs Expression by E2 in SkBr3 Cancer Cells and CAFs*

In order to provide novel insights on the action of estrogens toward miRNAs modulation in breast cancer, the ER-negative SkBr3 breast cancer cells and CAFs were treated with 100 nM E2 for 4 h and then analyzed by TaqMan™ Array Human MicroRNA. A total amount of 754 miRNAs involved in diverse pathophysiological conditions (www.thermofisher.com/order/catalog/product/4444913) were evaluated, thereafter we focused our attention on miRNAs displaying a Ct< 32 along with at least 2 fold increase or 50% reduction upon E2 exposure respect to vehicle-treated cells. On the basis of these criteria, we identified 25 and 29 E2-regulated miRNAs in SkBr3 cancer cells (Figure 1A) and CAFs (Figure 2A), respectively. In particular, in SkBr3 cancer cells 23 miRNAs were up-regulated and 2 miRNAs were down-regulated by E2 treatment (Figure 1B). As it concerns CAFs, among the 29 E2-regulated miRNAs, 7 showed an increase and 22 a reduction upon E2 stimulation (Figure 2B). To identify unique and shared E2-regulated miRNAs in both cell types, we then calculated a Venn diagram. SkBr3s cancer cells and CAFs shared only the expression of 2 miRNAs (Figure 3A), namely miR-144 and miR-338-3p, which exhibited a similar response (Figure 3B). Considering that in our previous studies we evaluated the role of miR-144 in tumor cell growth [25], in the present investigation we aimed to determine the mechanisms leading to the estrogen regulation of miR-338-3p and its action in breast cancer. Hence, we began our study ascertaining that miR-338-3p expression correlates positively with the overall survival in 1283 breast tumor patients, as reported in the Molecular Taxonomy of Breast Cancer International Consortium (METABRIC) database [40] (Figure 3C). Nicely fitting with these findings, previous evidence has suggested that miR-338-3p may function as a tumor suppressor in certain malignancies including breast cancer [30–34].
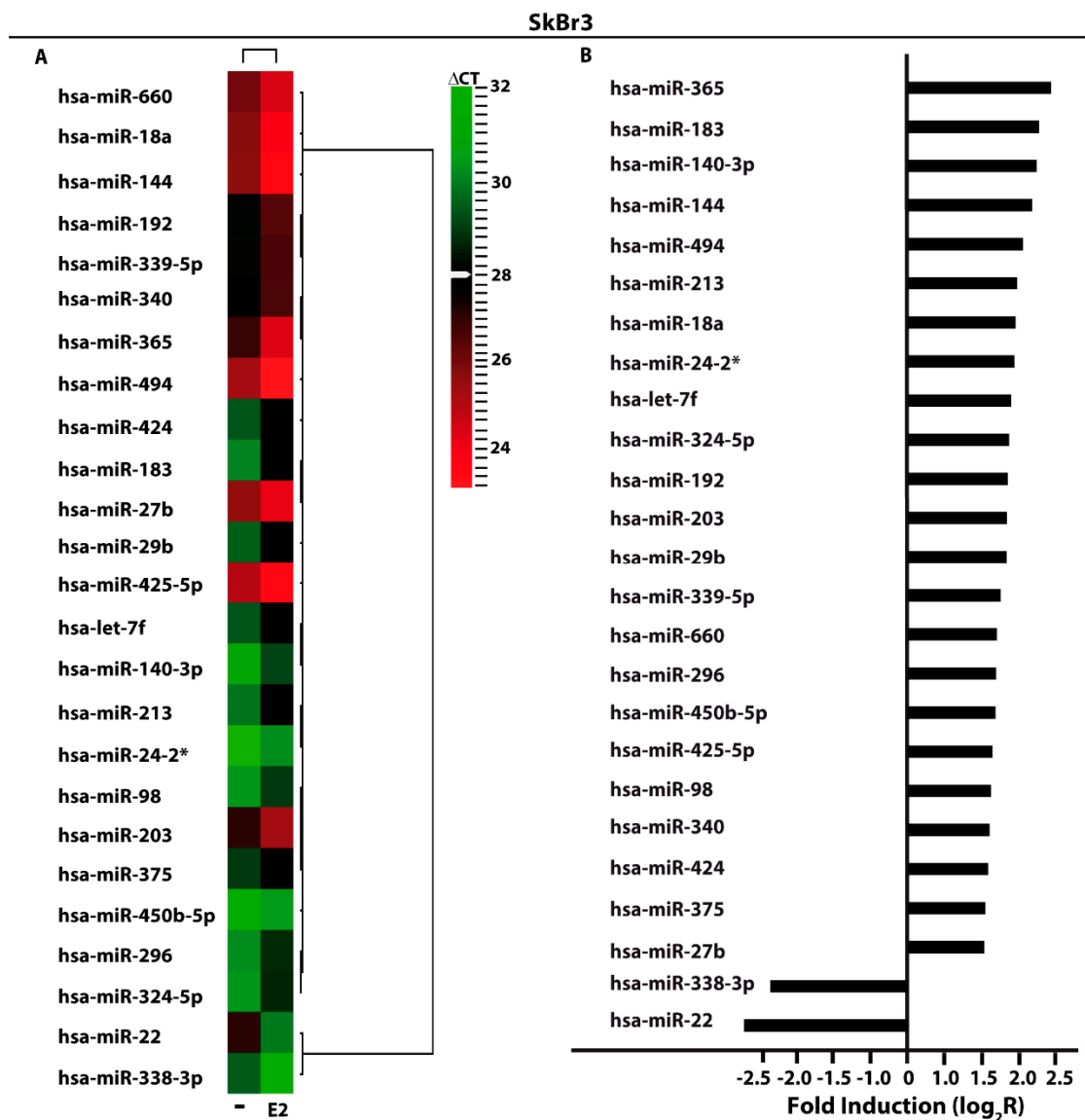
**Figure 1.** E2-modulated miRNAs expression in SkBr3 breast cancer cells. (**A**) Heat Map representation of E2-modulated miRNAs in SkBr3 cancer cells treated with 100 nM E2 for 4 h and analyzed by TaqMan Low-Density Array Human miRNA. Row represents a miRNA and column represents the treatment used. Each column is illustrated according to a color scale from green (low expression) to red (high expression). The distance measured is Euclidean Distance and the clustering method is complete linkage. Dendrograms of clustering analysis for miRNAs and samples are displayed on the top and right, respectively. (**B**) Up- and down-regulated miRNAs in SkBr3 breast cancer cells upon E2 stimulation. The values are indicated as log2 fold change (R) calculated respect to vehicle (-).
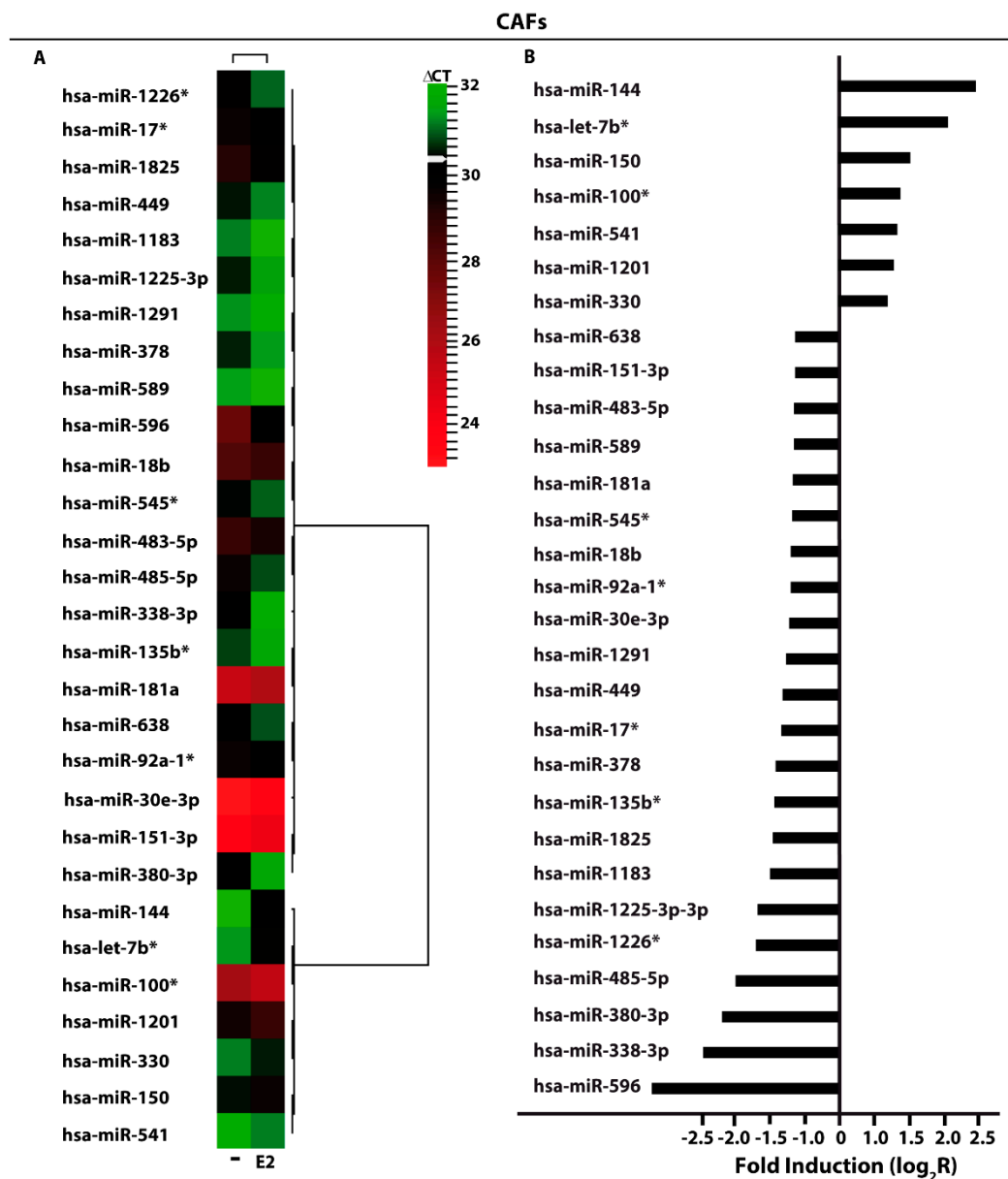
**Figure 2.** E2-modulated miRNAs expression in CAFs. (**A**) Heat Map representation of E2-modulated miRNAs in CAFs treated with 100 nM E2 for 4 h and analyzed by TaqMan Low-Density Array Human miRNA. Row represents a miRNA and column represents the treatment used. Each column is illustrated according to a color scale from green (low expression) to red (high expression). The distance measured is Euclidean Distance and the clustering method is complete linkage. Dendrograms of clustering analysis for miRNAs and samples are displayed on the top and right, respectively. (**B**) Up- and down-regulated miRNAs in CAFs upon E2 stimulation. The values are indicated as log2 fold change (R) calculated respect to vehicle (-).
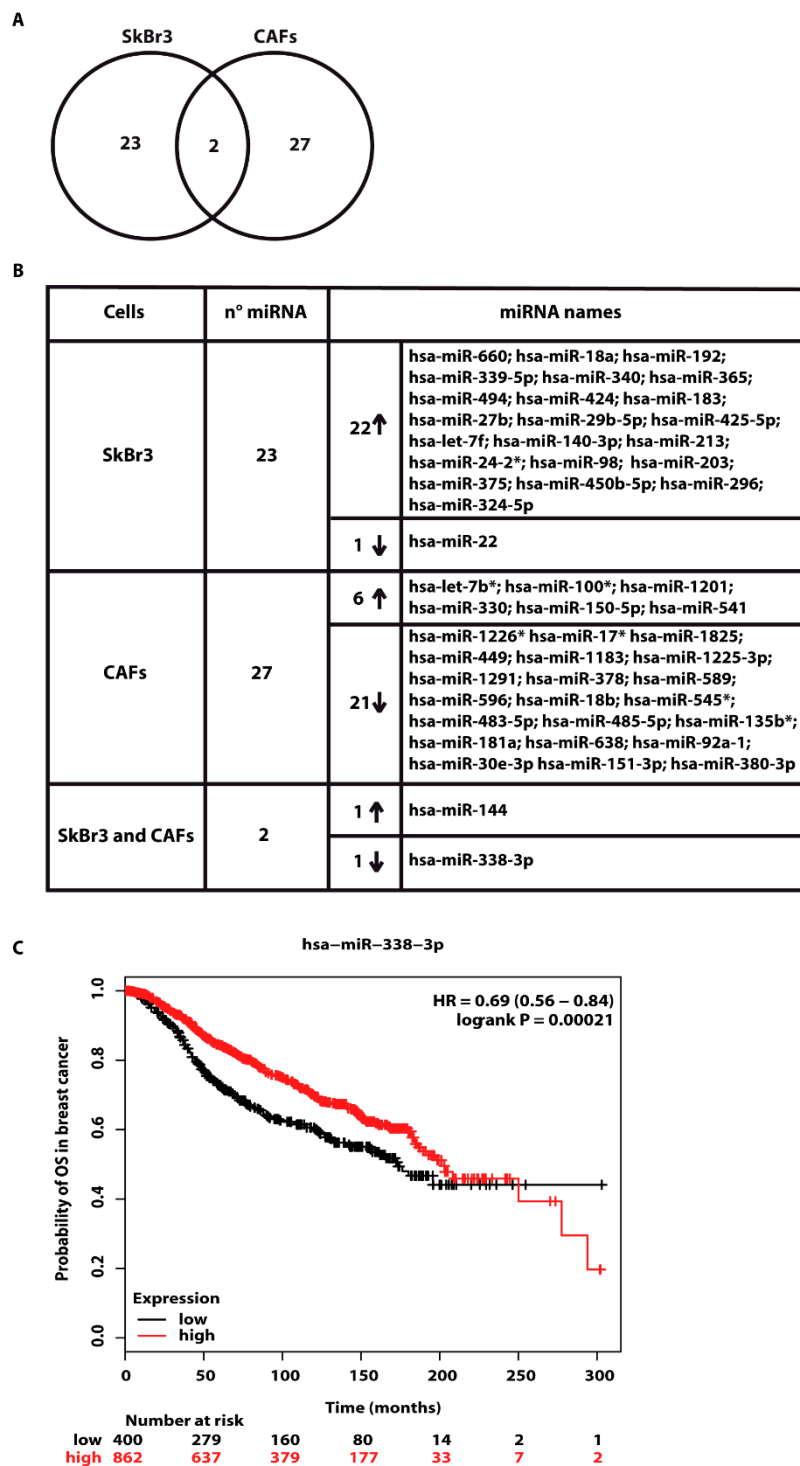
**Figure 3.** Exclusive and shared expression of miRNAs between SkBr3 and CAFs. (**A**) Venn Diagram of E2-modulated miRNAs in SkBr3 cancer cells and CAFs. (**B**) Up and down-regulated miRNAs by 100 nM E2 treatment for 4 h in SkBr3 cancer cells and CAFs. (**C**) The expression of miR-338-3p is associated with higher overall survival in breast cancer patients. The evaluation was performed by Kaplan–Meier Plotter (http://www.kmplot.com). Statistical analysis was made using the log-rank test.

*3.2. GPER Is Involved in the Regulation of miR-338-3p by E2 and G-1 in SkBr3 Cancer Cells and CAFs*

On the basis of the aforementioned results, we then attempted to define the molecular mechanisms involved in the estrogenic regulation of miR-338-3p performing a time-course study upon 100 nM of E2

and 100 nM of the selective GPER ligand G-1. Worthy, the inhibitory effects of E2 and G-1 on miR-338-3p expression were no longer evident silencing GPER in SkBr3 cancer cells (Figure 4A–C) and in CAFs (Figure 4D–F). Thereafter, we aimed to identify putative target genes of miR-338-3p by a bioinformatic analysis of available algorithms (http://ophid.utoronto.ca/mirDIP; http://www.microrna.org;http://www.targetscan.org). Among others, two putative target sequences of miR-338-3p located within the 3′-UTR of the oncogene c-Fos were found (Figure 5A). According to our previous studies showing that estrogens regulate c-Fos levels in diverse cancer cell types [41–44], the induction of c-Fos mRNA and protein expression upon a 4 h treatment with 100 nM E2 and 100 nM G-1 was abolished silencing GPER in SkBr3 cancer cells (Figure 5B,C) and CAFs (Figure 5D,E). Next, we found that in SkBr3 cells and CAFs transfected for 48 h with a miR-338-3p mimic sequence, the treatment for 4 h with 100 nM E2 and 100 nM G-1 is no longer able to induce c-Fos mRNA and protein levels, a response rescued transfecting the miR-338-3p mimic sequence in combination with a miR-338-3p inhibitor sequence (Figure 6A–F).
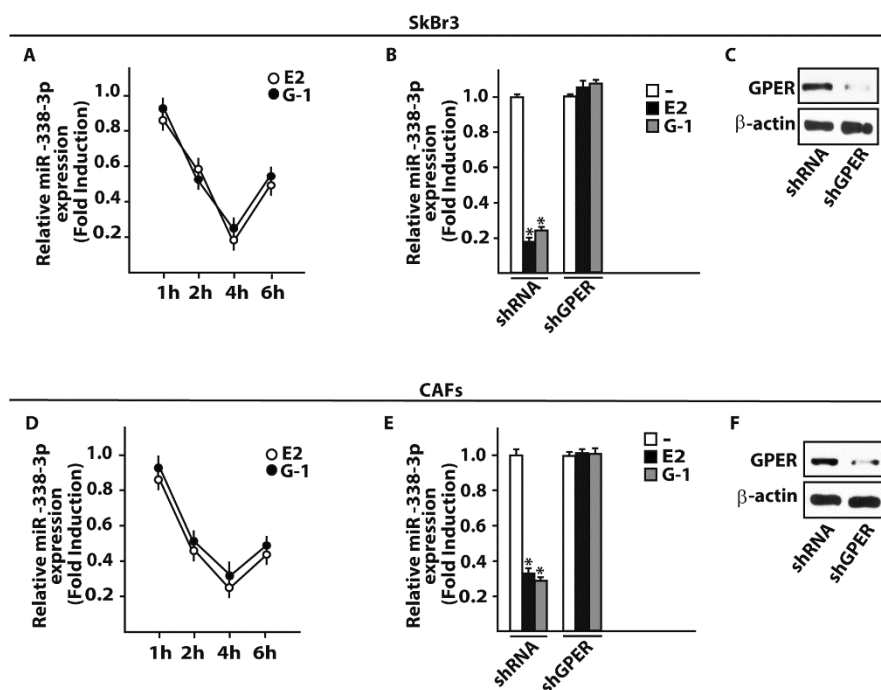


**Figure 4.** E2 and G-1 down-regulate miR-338-3p levels in SkBr3 cancer cells and CAFs. SkBr3 breast cancer cells (**A**) and CAFs (**D**) were stimulated with 100 nM E2 or 100 nM G-1 as indicated and analyzed by RT-PCR. Each point is plotted as fold changes of cells receiving treatments respect to cells treated with vehicle (-) and represents the mean ± SD of three independent experiments performed in triplicate. MiR-338-3p expression upon a 4 h treatment with 100 nM E2 or 100 nM G-1 in SkBr3 cells (**B**) and CAFs (**E**) previously transfected with shRNA or shGPER for 48 h. Each column represents the mean ± SD of three independent experiments performed in triplicate. Efficacy of GPER silencing in SkBr3 cells (**C**) and CAFs (**F**). β-actin serves as a loading control. (*) indicates $p < 0.05$, for cells receiving treatments vs cells treated with vehicle.
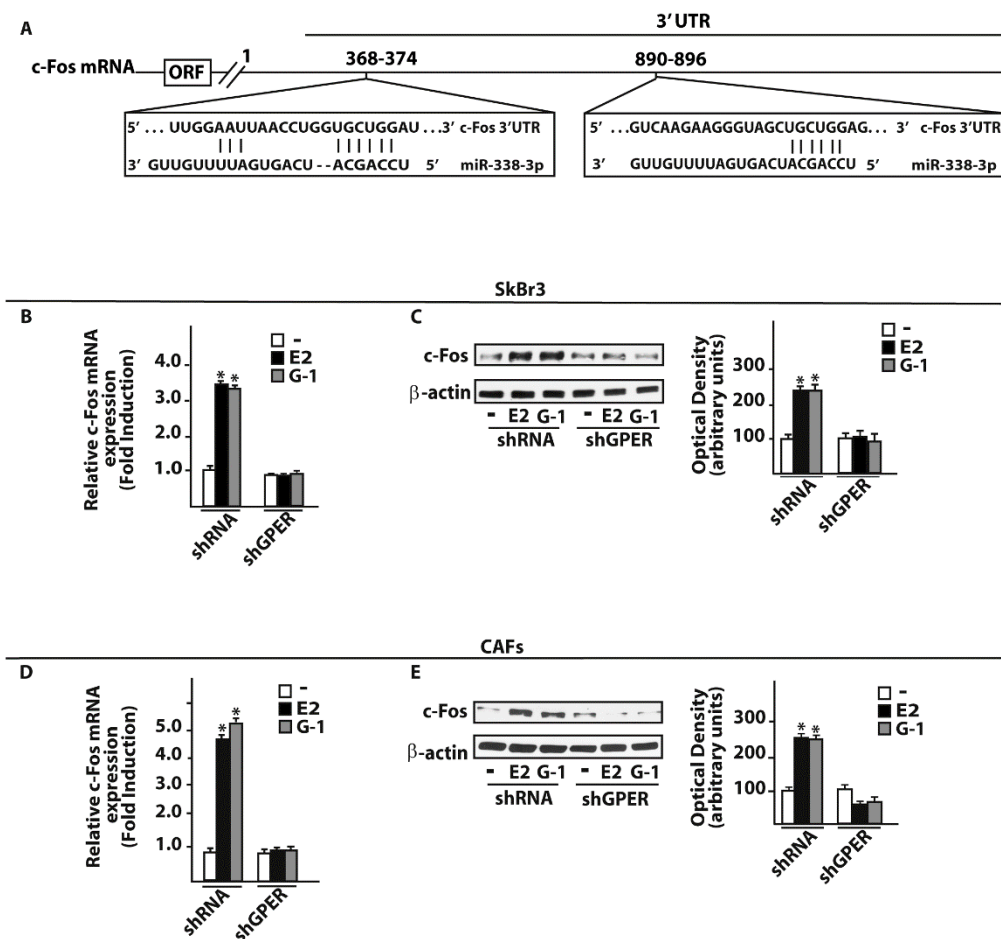
**Figure 5.** c-Fos is a target gene of miR-338-3p. (**A**) Schematic alignment between the miR-338-3p sequence and the 3′-UTR mRNA region of c-Fos. mRNA expression of c-Fos in SkBr3 cancer cells (**B**) and CAFs (**D**) transfected with shRNA or shGPER for 48 h and then treated for 4 h with 100 nM E2 or 100 nM G-1. Each column represents the mean ± SD of three independent experiments performed in triplicate. c-Fos protein expression in SkBr3 cancer cells (**C**) and CAFs (**E**) transfected with shRNA or shGPER for 48 h and then treated for 4 h with 100 nM E2 or 100 nM G-1. Side panels show densitometry analysis of the blots normalized to the loading control β-actin.
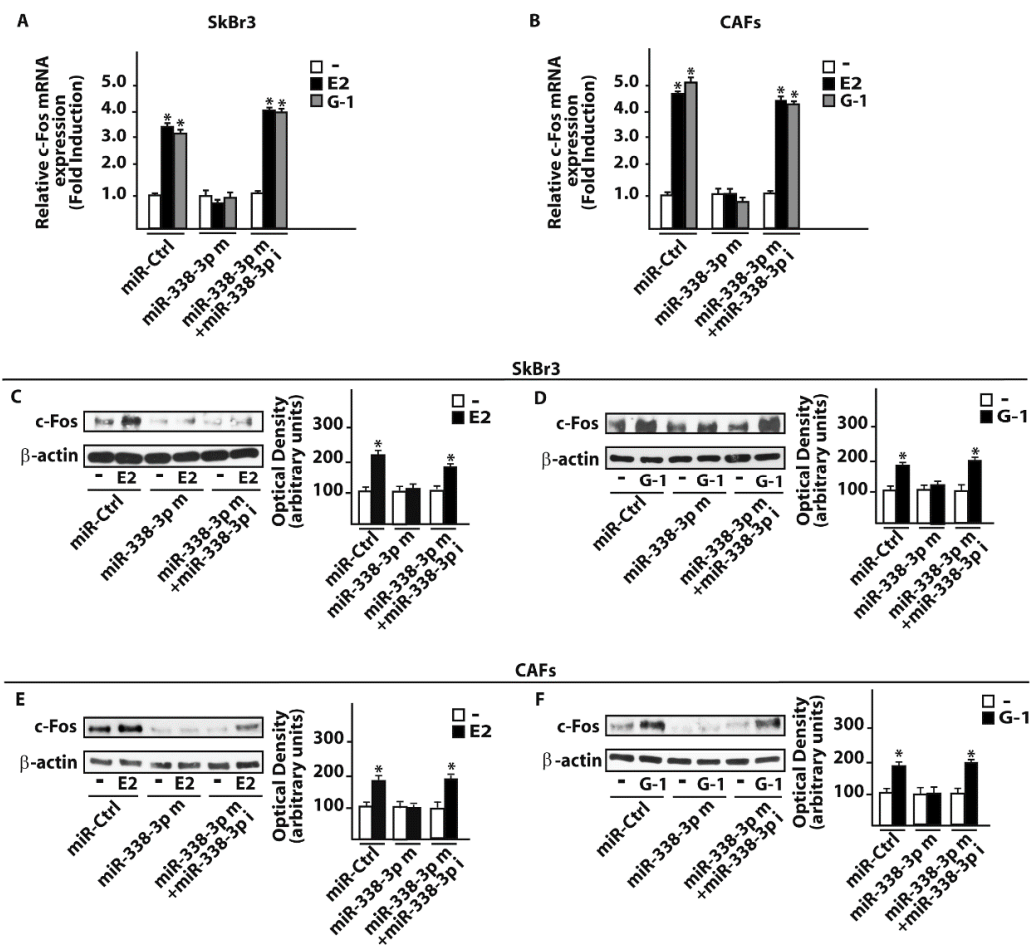
**Figure 6.** miR-338-3p prevents c-fos induction by E2 and G-1 in SkBr3 cancer cells and CAFs. mRNA levels of c-Fos in SkBr3 cancer cells (**A**) and CAFs (**B**) transfected for 48 h with 25 nM miR-Ctrl or miR-338-3p mimic (miR-338-3p m) in combination or not with 50 nM miR-338-3p inhibitor (miR-338-3p i) and then treated for 4 h with 100 nM E2 or 100 nM G-1. Each column represents the mean ± SD of three independent experiments performed in triplicate. c-Fos protein levels in SkBr3 cancer cells (**C, D**) and CAFs (**E, F**) transfected for 48 h with 25 nM miR-Ctrl or miR-338-3p mimic (miR-338-3p m) in combination or not with 50 nM miR-338-3p inhibitor (miR-338-3p i) and then stimulated for 4 h with 100 nM E2 or 100 nM G-1. Side panels show densitometry analysis of the blots normalized to the loading control β-actin. (*) indicates $p < 0.05$, for cells receiving treatments vs cells treated with vehicle (-).

### 3.3. miR-338-3p Triggers Inhibitory Effects on the Proliferation Induced by E2 and G-1

As in our previous investigations c-Fos was involved in the regulation of cyclins [43,45], we assessed that the transactivation of the Cyclin D1 promoter sequence by 100 nM E2 and 100 nM G-1 was prevented co-transfecting a dominant negative c-Fos expression construct (DN-Fos) in SkBr3 and CAFs (Figure 7A,B). Nicely recapitulating the aforementioned results, the Cyclin D1 promoter luciferase activity induced by 100 nM E2 and 100 nM G-1 was inhibited using the miR-338-3p mimic, an effect rescued by the miR-338-3p inhibitor sequence (Figure 7C,D). In addition, similar findings were observed evaluating the regulation of Cyclin D1 at both mRNA (Figure 7E,F) and protein levels (Figure 8A–D). As biological counterpart, the proliferative responses elicited by 100 nM E2 and 100 nM G-1 in SkBr3 cancer cells and CAFs were prevented silencing GPER or transfecting the DN-Fos construct (Figure 9A,B). Furthermore, the miR-338-3p mimic sequence decreased the proliferation induced by 100 nM E2 and 100 nM G-1 (Figure 9A,B), however this effect was rescued co-transfecting the miR-338-3p inhibitor (Figure 9A,B). Further supporting the aforementioned findings, the treatment for

24 h with 100 nM E2 and 100 nM G-1 triggered inhibitory effects on cell cycle progression transfecting CAFs with the miR-338-3p mimic sequence, however this response was rescued in the presence of the miR-338-3p inhibitor sequence (Figure 9C). Overall, these results suggest that estrogenic GPER signaling regulates miR-338-3p expression and function in SkBr3 cancer cells and CAFs.
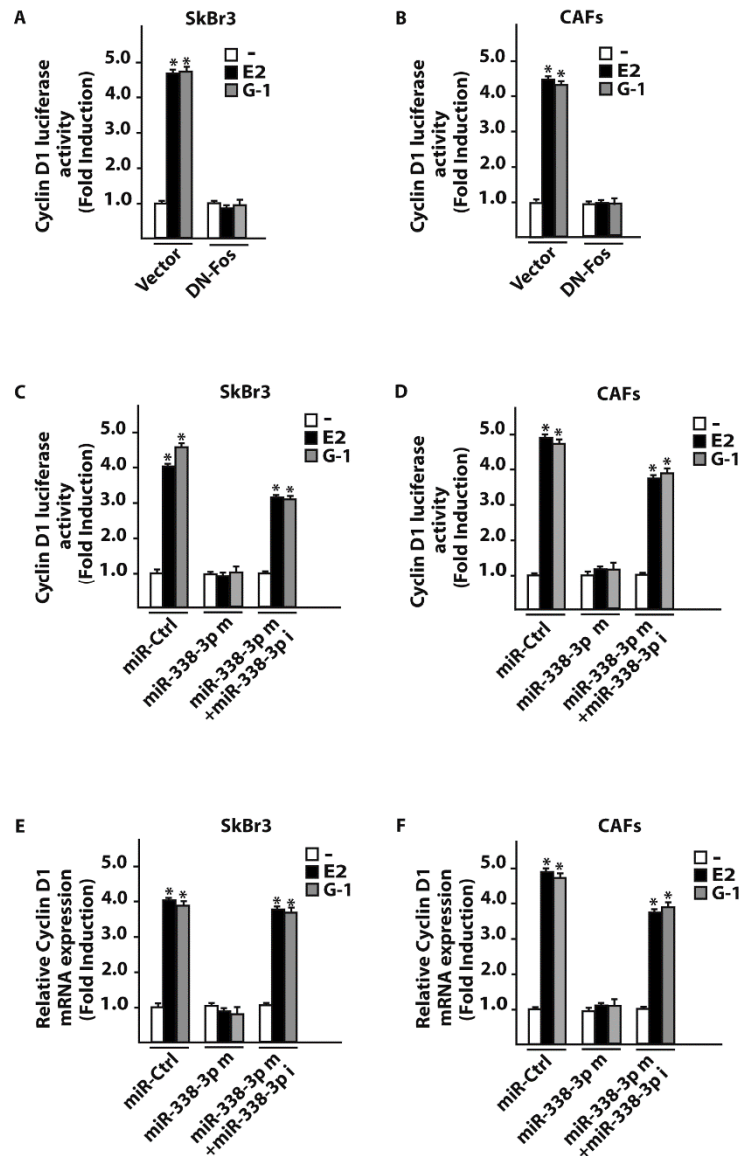


**Figure 7.** c-Fos and miR-338-3p are involved in Cyclin D1 regulation in SkBr3 cancer cells and CAFs. Luciferase activity of Cyclin D1 reporter gene in SkBr3 cancer cells (**A**) and CAFs (**B**) transfected for 8 h with a vector or a dominant-negative c-Fos construct (DN-Fos) before treatment with 100 nM of E2 and 100 nM G-1 for 18 h. Luciferase activity of Cyclin D1 reporter gene in SkBr3 cancer cells (**C**) and CAFs (**D**) transfected for 24 h with 25 nM miR-Ctrl or miR-338-3p mimic (miR-338-3p m) in combination or not with 50 nM miR-338-3p inhibitor (miR-338-3p i) before treatment for 18 h with 100 nM E2 or 100 nM G-1. The luciferase activity was normalized to the internal transfection control, values of cells receiving vehicle (-) were set as 1-fold induction upon which the activity obtained upon the indicated treatments was calculated. mRNA expression of Cyclin D1 in SkBr3 cells (**E**) and CAFs (**F**) transfected for 48 h with 25 nM miR-Ctrl or miR-338-3p mimic (miR-338-3p m) in combination or not with 50 nM miR-338-3p inhibitor (miR-338-3p i) before treatment for 8 h with 100 nM E2 or 100 nM G-1. Each column represents the mean ± SD of three independent experiments performed in triplicate. (*) indicates $p < 0.05$ for cells receiving treatments vs cells treated with vehicle (-).
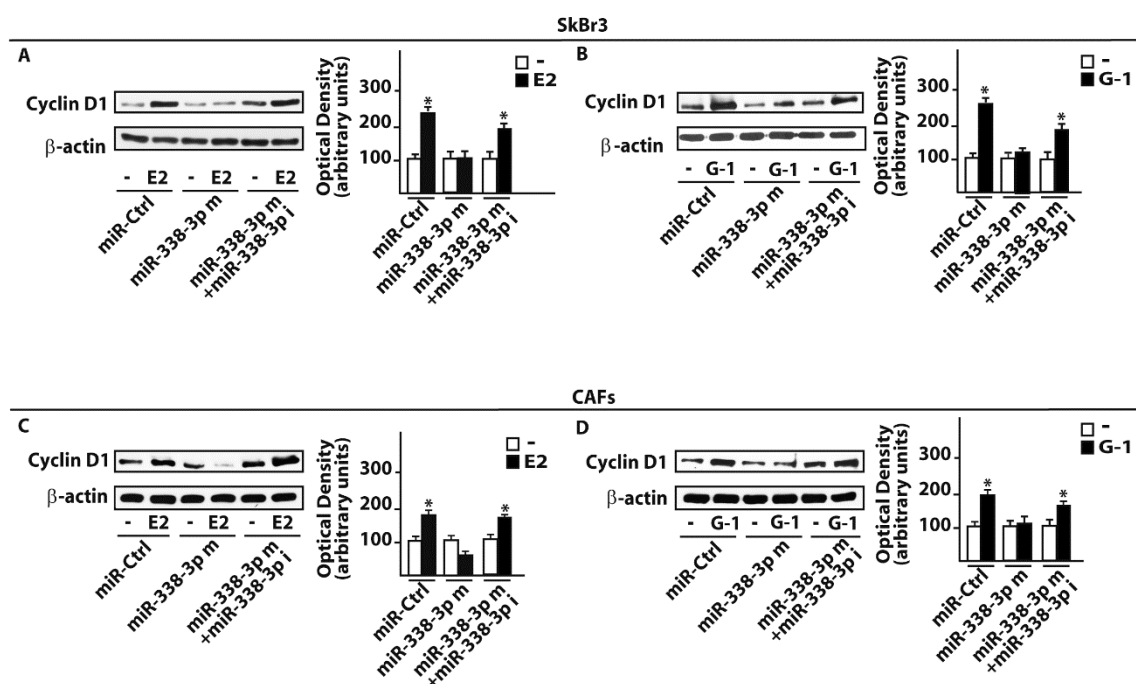
**Figure 8.** miR-338-3p prevents Cyclin D1 protein induction by E2 and G1 in SkBr3 cancer cells and CAFs. Cyclin D1 protein expression in SkBr3 cancer cells (**A**,**B**) and CAFs (**C**,**D**) transfected for 48 h with 25 nM miR-Ctrl or miR-338-3p mimic (miR-338-3p m) in combination or not with 50 nM miR-338-3p inhibitor (miR-338-3p i) before treatment for 12h with 100 nM E2 or 100 nM G-1. Side panels show densitometry analysis of the blots normalized to the loading control β-actin. (*) indicates $p < 0.05$ for cells receiving treatments vs cells treated with vehicle (-).
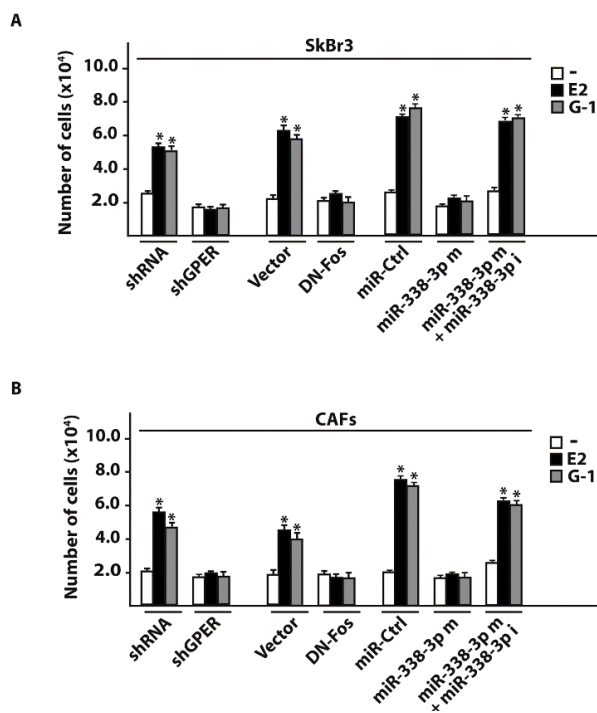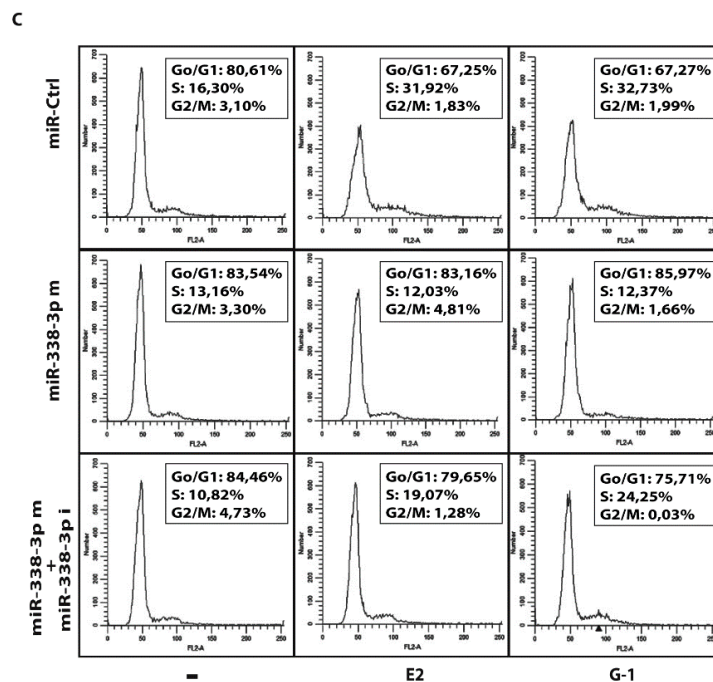


**Figure 9.** *Cont.*

**Figure 9.** miR-338-3p decreases the proliferation of SkBr3 cancer cells and CAFs induced by E2 and G-1. Cell proliferation in SkBr3 cancer cells (**A**) and CAFs (**B**) transfected every 2 days with 100ng shRNA or shGPER, 100ng vector or a dominant-negative c-Fos construct (DN-Fos) and 25 nM miR-Ctrl or miR-338-3p mimic (miR-338-3p m) in combination or not with 50 nM miR-338-3p inhibitor (miR-338-3p i). Cells were treated every day with 100 nM E2 or 100 nM G-1 and counted on day 6. Each column represents the mean $\pm$ SD of three independent experiments performed in triplicate. (*) indicates $p <$ 0.05 for cells receiving treatments vs cells treated with vehicle (-). (**C**) Representative pictures of cell cycle analysis in CAFs transfected for 48 h with 25 nM miR-Ctrl or miR-338-3p mimic (miR-338-3p m) in combination or not with 50 nM miR-338-3p inhibitor (miR-338-3p i) before the treatment for 24 h with 100 nM E2 and 100 nM G-1. In each panel, the percentages of cells in G0/G1, S and G2/M phases of the cell cycle are indicated. Values represent the mean $\pm$ SD of three independent experiments.

## 4. Discussion

Performing a microarray analysis of 754 miRNAs involved in diverse diseases, in the present study we determined that diverse miRNAs are regulated by E2 in both SkBr3 breast cancer cells and CAFs. In particular, we assessed that E2 increases 23 miRNAs and lowers 2 miRNAs in SkBr3 cells, while E2 triggers the up-regulation of 7 miRNAs and the down-regulation of 22 miRNAs in CAFs. In addition, in both cell types E2 induced the expression of miR-144 and repressed the levels of miR-338-3p, which is known as an inhibitor of cancer progression [30–34]. Considering that miR-144 was investigated in our previous study [25], we attempted to provide novel insights into the estrogen regulation of miR-338-3p. First, we performed a METABRIC analysis that revealed a positive correlation of miR-338-3p with the overall survival in breast cancer patients. Then, we evidenced that a miR-338-3p mimic sequence prevents the expression of c-Fos, Cyclin-D1 and the growth effects induced by E2 and G-1 through GPER in SkBr3 cells and CAFs. Worthy, these effects triggered by E2 and G-1 were rescued using a miR-338-3p inhibitor sequence. Altogether, the aforementioned results provide new insights on the molecular mechanisms involved in the expression and function of certain miRNAs upon estrogen exposure in both breast cancer cells and CAFs.

Breast tumor is the most common malignancy in females and its incidence is increasing worldwide [46]. Several studies are ongoing in order to identify novels biological targets that may be considered toward innovative therapeutic approaches. To date, few markers like the estrogen receptor (ER), the progesterone receptor (PR) and the human epidermal growth factor receptor 2 (HER2), have been identified as predictors of clinical responses to breast cancer treatments [47]. None of these

markers, however, well evaluates tumor invasion or provides early detection of cancer progression [48]. In this context, GPER has been suggested as a further predictor of breast cancer aggressiveness as its expression was found positively associated with clinic-pathological features of cancer progression and poor survival rates [49,50]. Moreover, GPER has been also indicated as an independent factor to predict a reduced disease-free survival in patients treated with tamoxifen [49]. The lack of GPER in the plasma membrane was also related to excellent long-term prognosis in ER-positive breast tumors treated with tamoxifen, an observation that highlighted the potential importance of GPER expression in different cancer cell types [51].

Despite the stimulatory effects elicited by GPER on the growth of diverse cancer cells [3–6], high doses of the GPER agonist G-1 ($\geq$1 μM) have been shown to exert an inhibitory action on the proliferation of certain cancer cell lines [52–56]. Therefore, the different biological responses mediated by GPER in distinct tumor cell contexts may depend on the receptor expression repertoire, the signaling pathways activated and other factors that remain to be fully elucidated.

The involvement of diverse miRNAs in breast cancer progression has been well established [6]. For instance, it has been reported that let-7d, miR-210 and miR-221 are down-regulated in the breast ductal carcinoma in situ and up-regulated following the invasive transition. Moreover, miR-9, miR-10b, miR-21, miR-29a, miR-155 and miR-373-520 family were found to promote the metastatic tumor dissemination [57]. Next, member of the let-7, miR-200, miR-34 and miR-125b families, were able to regulate the epithelial-mesenchymal transition in breast cancer [57]. According to the results obtained in the present investigation, previous studies have indicated that in diverse pathophysiological conditions, including breast cancer, the regulation of certain miRNAs by E2 may involve GPER activation [21,25,58,59]. It has been shown that GPER activation by estrogens stimulates a network of transduction pathways, which triggers key factors involved in cell growth, differentiation and transformation, like c-Fos [5,44,60,61]. The proto-oncogene c-Fos represents a prototypical "immediate early" gene since its expression is rapidly induced by different extracellular stimuli through the activation of the serine-threonine kinases of mitogen-activated protein kinase (MAPK) family [62,63]. The nuclear protein encoded by c-Fos interacts with Jun family members to form the heterodimeric activating protein-1 transcription factor complex (AP-1), which binds to TGAC/GTC/AA sequences (AP-1 responsive elements) located within the promoter sequences of target genes [62,64]. Many studies focusing on the oncogenic functions of c-Fos have demonstrated its involvement in tumor growth through the modulation of Cyclin D1, which is a nuclear regulatory subunit of the cyclin-dependent kinases (CDK)-4 and CDK-6 [65–67]. Nicely fitting with these data, we determined that in SkBr3 cancer cells and CAFs E2 and G-1 induce c-Fos and Cyclin D1 expression toward cell proliferation. According to the inhibitory function of miR-338-3p in certain cancer types [30–34], we also found that miR-338-3p abrogates the abovementioned effects triggered by E2 and G-1 in SkBr3 cells and in important components of the tumor microenvironment as CAFs [35,36]. In this regard, our data highlight additional mechanisms by which tumor cells and CAFs cooperate toward worse cancer features. Well-fitting with the present findings, it has been established that cancer development involves the functional interaction of malignant cells with the tumor microenvironment [68,69]. For instance, stromal cells like CAFs generate a dynamic signaling network through the secretion of growth factors and cytokines that stimulate the proliferation and dissemination of cancer cells [70,71]. In this context, the regulation of miR-338-3p shared by breast cancer cells and CAFs may be a further mechanism linking the estrogen stimulation of both the tumor microenvironment and tumor cells.

## 5. Conclusions

miRNAs target numerous genes involved in the cell growth and survival of diverse types of tumors, including breast cancer [72]. Therefore, changes in miRNAs expression may have a prognostic role along with a therapeutic perspective in cancer patients. Here, we have provided novel insights on the molecular mechanisms through which estrogenic GPER signaling in both breast cancer cells and CAFs lowers the expression of miR-338-3p, which has been reported to act as an inhibitor of cancer cell

growth and invasion [30–34]. Further studies are needed to better define the functions of miR-338-3p and its usefulness in innovative therapeutic approaches in breast cancer patients.

## References

1. Burns, K.A.; Korach, K.S. Estrogen receptors and human disease: An update. *Arch. Toxicol.* **2012**, *86*, 1491–1504. [CrossRef] [PubMed]

2. Nilsson, S.; Gustafsson, J. Estrogen receptors: Therapies targeted to receptor subtypes. *Clin. Pharmacol. Ther.* **2011**, *89*, 44–55. [CrossRef] [PubMed]

3. Cirillo, F.; Pellegrino, M.; Malivindi, R.; Rago, V.; Avino, S.; Muto, L.; Dolce, V.; Vivacqua, A.; Rigiracciolo, D.C.; De Marco, P.; et al. GPER is involved in the regulation of the estrogen-metabolizing CYP1B1 enzyme in breast cancer. *Oncotarget* **2017**, *8*, 106608–106624. [CrossRef] [PubMed]

4. Santolla, M.F.; Avino, S.; Pellegrino, M.; De Francesco, E.M.; De Marco, P.; Lappano, R.; Vivacqua, A.; Cirillo, F.; Rigiracciolo, D.C.; Scarpelli, A.; et al. SIRT1 is involved in oncogenic signaling mediated by GPER in breast cancer. *Cell Death Dis.* **2015**, *6*, e1834. [CrossRef] [PubMed]

5. Prossnitz, E.R.; Barton, M. Estrogen biology: New insights into GPER function and clinical opportunities. *Mol. Cell. Endocrinol.* **2014**, *389*, 71–83. [CrossRef] [PubMed]

6. Vrtačnik, P.; Ostanek, B.; Mencej-Bedrač, S.; Marc, J. The many faces of estrogen signaling. *Biochem. Med.* **2014**, *24*, 329–342. [CrossRef] [PubMed]

7. Santolla, M.F.; Lappano, R.; De Marco, P.; Pupo, M.; Vivacqua, A.; Sisci, D.; Abonante, S.; Iacopetta, D.; Cappello, A.R.; Dolce, V.; et al. G protein-coupled estrogen receptor mediates the up-regulation of fatty acid synthase induced by 17β-estradiol in cancer cells and cancer-associated fibroblasts. *J. Biol. Chem.* **2012**, *287*, 43234–43245. [CrossRef] [PubMed]

8. Vivacqua, A.; Romeo, E.; De Marco, P.; De Francesco, E.M.; Abonante, S.; Maggiolini, M. GPER mediates the Egr-1 expression induced by 17β-estradiol and 4-hydroxitamoxifen in breast and endometrial cancer cells. *Breast Cancer Res. Treat.* **2012**, *133*, 1025–1035. [CrossRef] [PubMed]

9. Bartel, D.P. MicroRNAs: Genomics, biogenesis, mechanism, and function. *Cell* **2004**, *116*, 281–297. [CrossRef]

10. Bartel, D.P. MicroRNAs: Target recognition and regulatory functions. *Cell* **2009**, *136*, 215–233. [CrossRef] [PubMed]

11. Fabian, M.R.; Sonenberg, N.; Filipowicz, W. Regulation of mRNA translation and stability by microRNAs. *Annu. Rev. Biochem.* **2010**, *79*, 351–379. [CrossRef] [PubMed]

12. Ben-Hamo, R.; Efroni, S. MicroRNA regulation of molecular pathways as a generic mechanism and as a core disease phenotype. *Oncotarget* **2015**, *6*, 1594–1604. [CrossRef] [PubMed]

13. Gross, N.; Kropp, J.; Khatib, H. MicroRNA signaling in embryo development. *Biology* **2017**, *6*, 34. [CrossRef] [PubMed]

14. Montagner, S.; Dehó, L.; Monticelli, S. MicroRNAs in hematopoietic development. *BMC Immunol.* **2014**, *15*, 14. [CrossRef] [PubMed]

15. Singh, R.P.; Massachi, I.; Manickavel, S.; Singh, S.; Rao, N.P.; Hasan, S.; Mc Curdy, D.K.; Sharma, S.; Wong, D.; Hahn, B.H.; et al. The role of miRNA in inflammation and autoimmunity. *Autoimmun. Rev.* **2013**, *12*, 1160–1165. [CrossRef] [PubMed]

16. Malemud, C.J. MicroRNAs and osteoarthritis. *Cells* **2018**, *7*, 92. [CrossRef] [PubMed]

17. Vannini, I.; Fanini, F.; Fabbri, M. Emerging roles of microRNAs in cancer. *Curr. Opin. Genet. Dev.* **2018**, *48*, 128–133. [CrossRef] [PubMed]

18. Santolla, M.F.; Lappano, R.; Cirillo, F.; Rigiracciolo, D.C.; Sebastiani, A.; Abonante, S.; Tassone, P.; Tagliaferri, P.; Di Martino, M.T.; Maggiolini, M.; et al. miR-221 stimulates breast cancer cells and cancer-associated fibroblasts (CAFs) through selective interference with the A20/c-Rel/CTGF signaling. *J. Exp. Clin. Cancer Res.* **2018**, *37*, 94. [CrossRef] [PubMed]

19. Inamura, K. Major tumor suppressor and oncogenic non-coding RNAs: Clinical relevance in lung cancer. *Cells* **2017**, *6*, 12. [CrossRef] [PubMed]

20. Vivacqua, A.; De Marco, P.; Belfiore, A.; Maggiolini, M. Recent advances on the role of microRNAs in both insulin resistance and cancer. *Curr. Pharm. Des.* **2017**, *23*, 3658–3666. [CrossRef] [PubMed]

21. Jacovetti, C.; Abderrahmani, A.; Parnaud, G.; Jonas, J.C.; Peyot, M.L.; Cornu, M.; Laybutt, R.; Meugnier, E.; Rome, S.; Thorens, B.; et al. MicroRNAs contribute to compensatory β cell expansion during pregnancy and obesity. *J. Clin. Investig.* **2012**, *122*, 3541–3551. [CrossRef] [PubMed]

22. Wang, Y.; Liu, Z.; Shen, J. MicroRNA-421-targeted PDCD4 regulates breast cancer cell proliferation. *Int. J. Mol. Med.* **2018**. [CrossRef] [PubMed]

23. Tao, S.; He, H.; Chen, Q.; Yue, W. GPER mediated estradiol reduces miR-148a to promote HLA-G expression in breast cancer. *Biochem. Biophys. Res. Commun.* **2014**, *451*, 74–78. [CrossRef] [PubMed]

24. Zhang, Y.; Fang, J.; Zhao, H.; Yu, Y.; Cao, X.; Zhang, B. Downregulation of microRNA-1469 promotes the development of breast cancer via targeting HOXA1 and activating PTEN/PI3K/AKT and Wnt/β-catenin pathways. *J. Cell. Biochem.* **2018**. [CrossRef] [PubMed]

25. Vivacqua, A.; De Marco, P.; Santolla, M.F.; Cirillo, F.; Pellegrino, M.; Panno, M.L.; Abonante, S.; Maggiolini, M. Estrogenic gper signaling regulates mir144 expression in cancer cells and cancer-associated fibroblasts (cafs). *Oncotarget* **2015**, *6*, 16573–16587. [CrossRef] [PubMed]

26. Rodriguez, A.; Griffiths-Jones, S.; Ashurst, J.L.; Bradley, A. Identification of mammalian microRNA host genes and transcription units. *Genome Res.* **2004**, *14*, 1902–1910. [CrossRef] [PubMed]

27. Raghunath, M.; Patti, R.; Bannerman, P.; Lee, C.M.; Baker, S.; Sutton, L.N.; Phillips, P.C.; Damodar Reddya, C. A novel kinase, AATYK induces and promotes neuronal differentiation in a human neuroblastoma (SH-SY5Y) cell line. *Mol. Brain Res.* **2000**, *77*, 151–162. [CrossRef]

28. Tsuchiya, S.; Oku, M.; Imanaka, Y.; Kunimoto, R.; Okuno, Y.; Terasawa, K.; Sato, F.; Tsujimoto, G.; Shimizu, K. MicroRNA-338-3p and microRNA-451 contribute to the formation of basolateral polarity in epithelial cells. *Nucleic Acids Res.* **2009**, *37*, 3821–3827. [CrossRef] [PubMed]

29. Aschrafi, A.; Schwechter, A.D.; Mameza, M.G.; Natera-Naranjo, O.; Gioio, A.E.; Kaplan, B.B. MicroRNA-338 regulates local cytochrome c oxidase IV mRNA levels and oxidative phosphorylation in the axons of sympathetic neurons. *J. Neurosci.* **2008**, *28*, 12581–12590. [CrossRef] [PubMed]

30. Cao, R.; Shao, J.; Hu, Y.; Wang, L.; Li, Z.; Sun, G.; Gao, X. microRNA-338-3p inhibits proliferation, migration, invasion, and EMT in osteosarcoma cells by targeting activator of 90 kDa heat shock protein ATPase homolog 1. *Cancer Cell Int.* **2018**, *18*, 49. [CrossRef] [PubMed]

31. Li, Y.; Chen, P.; Zu, L.; Liu, B.; Wang, M.; Zhou, Q. MicroRNA-338-3p suppresses metastasis of lung cancer cells by targeting the EMT regulator Sox4. *Am. J. Cancer Res.* **2016**, *6*, 127–140. [PubMed]

32. Jin, Y.; Zhao, M.; Xie, Q.; Zhang, H.; Wang, Q.; Ma, Q. MicroRNA-338-3p functions as tumor suppressor in breast cancer by targeting SOX4. *Int. J. Oncol.* **2015**, *47*, 1594–1602. [CrossRef] [PubMed]

33. Wen, C.; Liu, X.; Ma, H.; Zhang, W.; Li, H. miR-338-3p suppresses tumor growth of ovarian epithelial carcinoma by targeting Runx2. *Int. J. Oncol.* **2015**, *46*, 2277–2285. [CrossRef] [PubMed]

34. Huang, X.H.; Chen, J.S.; Wang, Q.; Chen, X.L.; Wen, L.; Chen, L.Z.; Bi, J.; Zhang, L.J.; Su, Q.; Zeng, W.T. miR-338-3p suppresses invasion of liver cancer cell by targeting smoothened. *J. Pathol.* **2011**, *225*, 463–472. [CrossRef] [PubMed]

35. Farhood, B.; Najafi, M.; Mortezaee, K. Cancer-associated fibroblasts: Secretions, interactions, and therapy. *J. Cell. Biochem.* **2018**. [CrossRef] [PubMed]

36. Kalluri, R.; Zeisberg, M. Fibroblasts in cancer. *Nat. Rev. Cancer* **2006**, *6*, 392–401. [CrossRef] [PubMed]

37. Pfaffl, M.W. A new mathematical model for relative quantification in real-time RT-PCR. *Nucleic Acids Res.* **2001**, *29*, e45. [CrossRef] [PubMed]

38. Lanczky, A.; Nagy, A.; Bottai, G.; Munkacsy, G.; Paladini, L.; Szabo, A.; Santarpia, L.; Gyorffy, B. miRpower: A web-tool to validate survival-associated miRNAs utilizing expression data from 2178 breast cancer patients. *Breast Cancer Res Treat.* **2016**, *160*, 439–446. [CrossRef] [PubMed]

39. Vivacqua, A.; Lappano, R.; De Marco, P.; Sisci, D.; Aquila, S.; De Amicis, F.; Fuqua, S.A.; Andò, S.; Maggiolini, M. G protein-coupled receptor 30 expression is up-regulated by EGF and TGF alpha in estrogen receptor alpha-positive cancer cells. *Mol. Endocrinol.* **2009**, *23*, 1815–1826. [CrossRef] [PubMed]

40. Curtis, C.; Shah, S.P.; Chin, S.F.; Turashvili, G.; Rueda, O.M.; Dunning, M.J.; Speed, D.; Lynch, A.G.; Samarajiwa, S.; Yuan, Y.; et al. The genomic and transcriptomic architecture of 2,000 breast tumours reveals novel subgroups. *Nature* **2012**, *486*, 346–352. [CrossRef] [PubMed]

41. Albanito, L.; Madeo, A.; Lappano, R.; Vivacqua, A.; Rago, V.; Carpino, A.; Oprea, T.I.; Prossnitz, E.R.; Musti, A.M.; Andò, S.; et al. G protein-coupled receptor 30 (GPR30) mediates gene expression changes and growth response to 17β-estradiol and selective GPR30 ligand G-1 in ovarian cancer cells. *Cancer Res.* **2007**, *67*, 1859–1866. [CrossRef] [PubMed]

42. Vivacqua, A.; Bonofiglio, D.; Recchia, A.G.; Musti, A.M.; Picard, D.; Andò, S.; Maggiolini, M. The G protein-coupled receptor GPR30 mediates the proliferative effects induced by 17β-estradiol and hydroxytamoxifen in endometrial cancer cells. *Mol. Endocrinol.* **2006**, *20*, 631–646. [CrossRef] [PubMed]

43. Vivacqua, A.; Bonofiglio, D.; Albanito, L.; Madeo, A.; Rago, V.; Carpino, A.; Musti, A.M.; Picard, D.; Andò, S.; Maggiolini, M. 17β-estradiol, genistein, and 4-hydroxytamoxifen induce the proliferation of thyroid cancer cells through the G protein-coupled receptor GPR30. *Mol. Pharmacol.* **2006**, *70*, 1414–1423. [CrossRef] [PubMed]

44. Maggiolini, M.; Vivacqua, A.; Fasanella, G.; Recchia, A.G.; Sisci, D.; Pezzi, V.; Montanaro, D.; Musti, A.M.; Picard, D.; Andò, S. The G protein-coupled receptor GPR30 mediates c-fos up-regulation by 17β-estradiol and phytoestrogens in breast cancer cells. *J. Biol. Chem.* **2004**, *279*, 27008–27016. [CrossRef] [PubMed]

45. Madeo, A.; Maggiolini, M. Nuclear alternate estrogen receptor GPR30 mediates 17β-estradiol-induced gene expression and migration in breast cancer-associated fibroblasts. *Cancer Res.* **2010**, *70*, 6036–6046. [CrossRef] [PubMed]

46. Siegel, R.; Naishadham, D.; Jemal, A. Cancer statistics, 2013. *Cancer J. Clin.* **2013**, *63*, 11–30. [CrossRef] [PubMed]

47. Schettini, F.; Buono, G.; Cardalesi, C.; Desideri, I.; De Placido, S.; Del Mastro, L. Hormone receptor/human epidermal growth factor receptor 2-positive breast cancer: Where we are now and where we are going. *Cancer Treat. Rev.* **2016**, *46*, 20–26. [CrossRef] [PubMed]

48. Jiang, W.G.; Sanders, A.J.; Katoh, M.; Ungefroren, H.; Gieseler, F.; Prince, M.; Thompson, S.K.; Zollo, M.; Spano, D.; Dhawan, P.; et al. Tissue invasion and metastasis: Molecular, biological and clinical perspectives. *Semin. Cancer Biol.* **2015**, *35*, S244–S275. [CrossRef] [PubMed]

49. Molina, L.; Figueroa, C.D.; Bhoola, K.D.; Ehrenfeld, P. GPER-1/GPR30 a novel estrogen receptor sited in the cell membrane: Therapeutic coupling to breast cancer. *Expert Opin. Ther. Targets* **2017**, *21*, 755–766. [CrossRef] [PubMed]

50. Filardo, E.J. A role for G-protein coupled estrogen receptor (GPER) in estrogen-induced carcinogenesis: Dysregulated glandular homeostasis, survival and metastasis. *J. Steroid Biochem. Mol. Biol.* **2018**, *176*, 38–48. [CrossRef] [PubMed]

51. Sjöström, M.; Hartman, L.; Grabau, D.; Fornander, T.; Malmström, P.; Nordenskjöld, B.; Sgroi, D.C.; Skoog, L.; Stål, O.; Fredrik Leeb-Lundberg, L.M.; et al. Lack of G protein-coupled estrogen receptor (GPER) in the plasma membrane is associated with excellent long- term prognosis in breast cancer. *Breast Cancer Res. Treat.* **2014**, *145*, 61–71. [CrossRef] [PubMed]

52. Ariazi, E.A.; Brailoiu, E.; Yerrum, S.; Shupp, H.A.; Slifker, M.J.; Cunliffe, H.E.; Black, M.A.; Donato, A.L.; Arterburn, J.B.; Oprea, T.I.; et al. The G protein-coupled receptor GPR30 inhibits proliferation of estrogen receptor-positive breast cancer cells. *Cancer Res.* **2014**, *70*, 1184–1194. [CrossRef] [PubMed]

53. Chimento, A.; Casaburi, I.; Rosano, C.; Avena, P.; De Luca, A.; Campana, C.; Martire, E.; Santolla, M.F.; Maggiolini, M.; Pezzi, V.; et al. Oleuropein and hydroxytyrosol activate GPER/GPR30-dependent pathways leading to apoptosis of ERnegative SKBR3 breast cancer cells. *Mol. Nutr. Food Res.* **2014**, *58*, 478–489. [CrossRef] [PubMed]

54. Weißenborn, C.; Ignatov, T.; Ochel, H.J.; Costa, S.D.; Zenclussen, A.C.; Ignatov, Z.; Ignatov, A. GPER functions as a tumor suppressor in triple-negative breast cancer cells. *J. Cancer Res. Clin. Oncol.* **2014**, *140*, 713–723. [CrossRef] [PubMed]

55. Weißenborn, C.; Ignatov, T.; Poehlmann, A.; Wege, A.K.; Costa, S.D.; Zenclussen, A.C.; Ignatov, A. GPER functions as a tumor suppressor in MCF-7 and SKBR-3 breast cancer cells. *J. Cancer Res. Clin. Oncol.* **2014**, *140*, 663–671. [CrossRef] [PubMed]

56. Chan, Q.K.; Lam, H.M.; Ng, C.F.; Lee, A.Y.; Chan, E.S.; Ng, H.K.; Ho, S.M.; Lau, K.M. Activation of GPR30 inhibits the growth of prostate cancer cells through sustained activation of Erk1/2, c-jun/c-fos-dependent upregulation of p21, and induction of $G_2$ cell-cycle arrest. *Cell Death Differ.* **2010**, *7*, 1511–1523. [CrossRef] [PubMed]

57. Volinia, S.; Galasso, M.; Sana, M.E.; Wise, T.F.; Palatini, J.; Huebner, K.; Croce, C.M. Breast cancer signatures for invasiveness and prognosis defined by deep sequencing of microRNA. *Proc. Natl. Acad. Sci. USA* **2012**, *109*, 3024–3029. [CrossRef] [PubMed]

58. Vidal-Gómez, X.; Pérez-Cremades, D.; Mompeón, A.; Dantas, A.P.; Novella, S.; Hermenegildo, C. MicroRNA as crucial regulators of gene expression in estradiol-treated human endothelial cells. *Cell. Physiol. Biochem.* **2018**, *45*, 1878–1892. [CrossRef] [PubMed]

59. Zhang, H.; Wang, X.; Chen, Z.; Wang, W. MicroRNA-424 suppresses estradiol-induced cell proliferation via targeting GPER in endometrial cancer cells. *Cell. Mol. Biol.* **2015**, *61*, 96–101. [PubMed]

60. Prossnitz, E.R.; Maggiolini, M. Mechanisms of estrogen signaling and gene expression via GPR30. *Mol. Cell. Endocrinol.* **2009**, *308*, 32–38. [CrossRef] [PubMed]

61. Pandey, D.P.; Lappano, R.; Albanito, L.; Madeo, A.; Maggiolini, M.; Picard, D. Estrogenic GPR30 signalling induces proliferation and migration of breast cancer cells through CTGF. *EMBO J.* **2009**, *28*, 523–532. [CrossRef] [PubMed]

62. Durchdewald, M.; Angel, P.; Hess, J. The transcription factor Fos: A Janus-type regulator in health and disease. *Histol. Histopathol.* **2009**, *11*, 1451–1461. [CrossRef]

63. Hess, J.; Angel, P.; Schorpp-Kistner, M. AP-1 subunits: Quarrel and harmony among siblings. *J. Cell Sci.* **2004**, *117*, 5965–5973. [CrossRef] [PubMed]

64. Milde-Langosch, K. The Fos family of transcription factors and their role in tumourigenesis. *Eur. J. Cancer* **2005**, *41*, 2449–2461. [CrossRef] [PubMed]

65. Bancroft, C.C.; Chen, Z.; Yeh, J.; Sunwoo, J.B.; Yeh, N.T.; Jackson, S.; Jackson, C.; Van Waes, C. Effects of pharmacologic antagonists of epidermal growth factor receptor, PI3K and. MEK signal kinases on NF-κB and AP-1 activation and IL-8 and VEGF expression in human head and neck squamous cell carcinoma lines. *Int. J. Cancer* **2002**, *99*, 538–548. [CrossRef] [PubMed]

66. Mishra, A.; Bharti, A.C.; Saluja, D.; Das, B.C. Transactivation and expression patterns of Jun and Fos/AP-1 super-family proteins in human oral cancer. *Int. J. Cancer* **2010**, *126*, 819–829. [CrossRef] [PubMed]

67. Qie, S.; Diehl, J.A. Cyclin D1, cancer progression, and opportunities in cancer treatment. *J. Mol. Med.* **2016**, *94*, 1313–1326. [CrossRef] [PubMed]

68. Han, Y.; Zhang, Y.; Jia, T.; Sun, Y. Molecular mechanism underlying the tumor-promoting functions of carcinoma-associated fibroblasts. *Tumor Biol.* **2015**, *36*, 1385–1394. [CrossRef] [PubMed]

69. Bhowmick, N.A.; Neilson, E.G.; Moses, H.L. Stromal fibroblasts in cancer initiation and progression. *Nature* **2004**, *432*, 332–337. [CrossRef] [PubMed]

70. Cheng, N.; Chytil, A.; Shyr, Y.; Joly, A.; Moses, H.L. Transforming growth factor-beta signaling-deficient fibroblasts enhance hepatocyte growth factor signaling in mammary carcinoma cells to promote scattering and invasion. *Mol. Cancer Res.* **2008**, *6*, 1521–1533. [CrossRef] [PubMed]

71. Zhi, K.; Shen, X.; Zhang, H.; Bi, J. Cancer-associated fibroblasts are positively correlated with metastatic potential of human gastric cancers. *J. Exp. Clin. Cancer Res.* **2010**, *29*, 66. [CrossRef] [PubMed]

72. Di Leva, G.; Cheung, D.G.; Croce, C.M. miRNA clusters as therapeutic targets for hormone-resistant breast cancer. *Expert Rev. Endocrinol. Metab.* **2015**, *10*, 607–617. [CrossRef] [PubMed]

# Focal adhesion kinase (FAK) activation by estrogens involves GPER in triple-negative breast cancer cells

Damiano Cosimo Rigiracciolo[1], Maria Francesca Santolla[1], Rosamaria Lappano[1], Adele Vivacqua[1], Francesca Cirillo[1], Giulia Raffaella Galli[1], Marianna Talia[1], Lucia Muglia[1], Michele Pellegrino[1], Nijiro Nohata[2], Maria Teresa Di Martino[3*] and Marcello Maggiolini[1*]

## Abstract

**Background:** Focal adhesion kinase (FAK) is a cytoplasmatic protein tyrosine kinase that associates with both integrins and growth factor receptors toward the adhesion, migration and invasion of cancer cells. The G-protein coupled estrogen receptor (GPER) has been involved in the stimulatory action of estrogens in breast tumor. In this study, we have investigated the engagement of FAK by GPER signaling in triple negative breast cancer (TNBC) cells.

**Methods:** Publicly available large-scale database and patient data sets derived from "The Cancer Genome Atlas" (TCGA; www.cbioportal.org) were used to assess FAK expression in TNBC, non-TNBC tumors and normal breast tissues. MDA-MB 231 and SUM159 TNBC cells were used as model system. The levels of phosphorylated FAK, other transduction mediators and target genes were detected by western blotting analysis. Focal adhesion assay was carried out in order to determine the focal adhesion points and the formation of focal adhesions (FAs). Luciferase assays were performed to evaluate the promoters activity of c-FOS, EGR1 and CTGF upon GPER activation. The mRNA expression of the aforementioned genes was measured by real time-PCR. Boyden chamber and wound healing assays were used in order to evaluate cell migration. The statistical analysis was performed by ANOVA.

**Results:** We first determined by bioinformatic analysis that the mRNA expression levels of the gene encoding FAK, namely PTK2, is higher in TNBC respect to non-TNBC and normal breast tissues. Next, we found that estrogenic GPER signaling triggers Y397 FAK phosphorylation as well as the increase of focal adhesion points (FAs) in TNBC cells. Besides, we ascertained that GPER and FAK activation are involved in the STAT3 nuclear accumulation and gene expression changes. As biological counterpart, we show that FAK inhibition prevents the migration of TNBC cells upon GPER activation.

**Conclusions:** The present data provide novel insights regarding the action of FAK in TNBC. Moreover, on the basis of our findings estrogenic GPER signaling may be considered among the transduction mechanisms engaging FAK toward breast cancer progression.

**Keywords:** TNBC, MDA-MB 231, SUM159, GPER, G-15, FAK, VS-4718, STAT3, STA21

* Correspondence: teresadm@unicz.it; marcellomaggiolini@yahoo.it
[3]Department of Experimental and Clinical Medicine, Magna Graecia University, 88100 Catanzaro, Italy
[1]Department of Pharmacy, Health and Nutritional Sciences, University of Calabria, 87036 Rende, Italy
Full list of author information is available at the end of the article

## Background

Significant progresses have been reached in the diagnosis and therapy of breast cancer, nevertheless this malignancy still represents the most common leading cause of cancer-related deaths among women worldwide [1]. One of the major challenges for the treatment of breast cancer is its heterogeneous nature, which reflects the different responses to the therapy [2]. Commonly, breast cancer is classified into four major molecular subtypes and each of these has different risk factors for incidence, therapeutic responses, disease progression and preferential organ sites of metastasis [3]. For instance, the triple negative breast cancer (TNBC) exhibits the resistance to different chemotherapies and represents the most aggressive tumor characterized by a low 5-year survival rate (approximately < 30%) [4]. To date, the rate of relapse and the mortality of patients affected by TNBC results at least in part from tumor cell spreading and the consequent development of metastasis [5]. Signals generated from the interaction between cancer cells and the tumor extracellular matrix (ECM) are considered the most common molecular drivers required for cancer cell migration and invasion [6]. In particular, integrin receptors, G-protein coupled receptors, cytokine receptors and tyrosine kinases receptors, sense changes in ECM composition leading to the activation of numerous subcellular biomechanic structures [7, 8]. Among these, the focal adhesion kinase (FAK, also known as PTK2), has been shown to exert a main role in facilitating and promoting the invasiveness of tumor cells [9–11]. Upon activation by integrin-ECM engagment [8] or GPCR agonists [12], FAK can be phosphorylated at the Y397 residue, which allows the formation of a binding site for many SH2 domain containing molecules like Src [13], PI3K [14], Grb7 [15] and PLCγ [16]. In addition to its function as tyrosine kinase, FAK serves as a scaffolding protein triggering the recruitment of diverse molecules to its tyrosine sites [17, 18]. The multifaceted interactions of FAK with various signal transduction mediators may contribute to the FAK-dependent processes involved in cancer development [19]. Indeed, FAK action has been associated to aggressive cancer features as the cell adhesion and spreading [20–22], the enhancement of cell proliferation and survival [23, 24] and the facilitation of invasive cell phenotypes [25–27]. In this context, it is worth mentioning that FAK was shown to be over-expressed in a wide variety of human malignancies, including invasive and metastatic breast tumors [28–30]. Indeed, increased FAK expression and activity has been correlated with different poor prognostic indicators in breast cancer patients [31, 32]. In this regard, it has been observed that the inhibition of FAK may reduce the metastatic potential of breast cancer cells [33–35], indicating FAK as a promising therapeutic target for the treatment of

aggressive malignancies [36]. Nevertheless, a better understanding on the molecular mechanisms through which FAK activation may contribute to breast cancer progression is still needed.

In recent years, several studies have characterized the role of the G-protein coupled estrogen receptor (GPER, also known as GPR30) in the context of the rapid actions exerted by estrogens [37–39]. Our and other previous investigations have demonstrated that estrogenic GPER signaling mediates stimulatory effects in both breast cancer cells and the tumor microenvironment [40–44]. In this vein, it has been reported that GPER activation triggers different transduction cascades including the epidermal growth factor receptor (EGFR), the mitogen-activated protein kinase (MAPK), the phosphatidylinositol 3-kinase/protein kinase B (PI3K/AKT), intracellular $Ca^{2+}$ mobilization and cyclic AMP (cAMP) production [38]. GPER was also shown to mediate gene expression changes, important biological responses like cell proliferation and migration and it was found negatively correlated with relapse free survival in breast cancer patients [45, 46].

In the framework of the aforementioned findings, in the current study we have focused on the role of GPER in the regulation of FAK signaling by estrogens using the invasive and metastatic TNBC MDA-MB 231 and SUM159 cells as experimental model. Taking advantage of publicly available large-scale genomics and patient data sets as The Cancer Genome Atlas (TCGA), we have found a higher expression of PTK2 gene encoding FAK in TNBC respect to non-TNBC and normal breast tissues. Next, we have observed that estrogens through GPER triggers Y397 FAK phosphorylation, increase FAs and induce gene expression changes. Corroborating these findings, FAK inhibition prevented the migration skill of MDA-MB 231 and SUM159 cells induced by estrogens via GPER. On the basis of the aforementioned results, GPER contributes to the estrogen-activated FAK signaling. Moreover, our data suggest that the GPER-FAK transduction pathway may be considered in more comprehensive targeted therapies in TNBC.

## Methods

### Publicly database and bioinformatics analysis

The clinical significance of PTK2 (FAK coding gene) in TNBC was assessed by microarray data of NCBI Gene Expression Omnibus (GEO) archive (GSE38959) [pubmed: 23254957] and RNA sequencing data in Invasive Breast Cancer Cohort of TCGA project (The Cancer Genome Atlas: https://cancergenome.nih.gov/) [pubmed: 23000897]. The gene expression data of GEO and TCGA were retrieved on August 2nd, 2018 from GEO (https://www.ncbi.nlm.nih.gov/geo/), cBioportal (http://www.cbioportal.org/) or UCSC Xena (https://xena.ucsc.edu/)

[pubmed:23550210 and bioRxiv:326470]. The normalized mRNA expression values in the RNA sequencing data were processed and distributed in $log_2$ transformed RSEM (RNA-Seq by Expectation Maximization) values (cBioportal) or $log_2$ transformed (RSEM+ 1) (UCSC Xena). The Z-scores of PTK2 mRNA expression data and clinical sample information corresponding to breast cancer patients were collected from cBioportal. The status of ER, PR and HER2 IHCs were used for classification of breast cancer subtypes. The PTK2 High group (mRNA Z-score more than 1) and the PTK2 Low group (mRNA Z-score equal or less than 1) were analyzed by Kaplan–Meier survival curves and log-rank statistics.

### Cell cultures

TNBC cell lines MDA-MB 231 were obtained from ATCC (Manassas, VA, USA). TNBC cell lines SUM159 were kindly provided by Dr. W.T. Khaled, University of Cambridge, UK. Cells were used less than 6 months after resuscitation and routinely tested and authenticated according to the ATCC suggestions. MDA-MB 231 cells were maintained in DMEM/F12 (Dulbecco's modified Eagle's medium) (Life Technologies, Milan, Italy) with phenol red, supplemented with 5% FBS and 100 μg/ml of penicillin/streptomycin. SUM159 cells were maintained in DMEM/F12 (Dulbecco's modified Eagle's medium) (Life Technologies, Milan, Italy) with phenol red, supplemented with 1 μg/ml of insulin, 1 μg/ml of hydrocortisone, 5% FBS and 100 μg/ml of penicillin/ streptomycin. MDA-MB 231 and SUM159 cells were grown in a 37 °C incubator with 5% $CO_2$. Cells to be processed for immunoblot and RT-PCR assays were switched to medium without serum and phenol red the day before treatments.

### Reagents and drugs

17β-Estradiol (E2) and PI3K inhibitor Wortmannin (WM) were purchased from Sigma-Aldrich (Milan, Italy). G-1 (1-[4-(– 6-bromobenzol [1,3]diodo-5-yl)-3a,4,5,9b-tetrahidro3H5cyclopenta[c]quinolin-8yl]-ethanone) and G-15 (3aS, 4R, 9bR)-4-(6-bromo-1, 3-benzodioxol-5-yl)-3a,4, 5,9b-3H-cyclopenta [c] quinolone were obtained from Tocris Bioscience (Space, Milan, Italy). Src kinase inhibitor PP2 was bought from Selleckchem (DBA, Milan, Italy). MEK inhibitor PD98059 (PD) was purchased from Calbiochem (DBA, Milan, Italy). STAT3 transcription factor signaling inhibitor STA21 and Focal Adhesion Kinase selective inhibitor VS-4718 were bought from Santa Cruz Biotechnology (DBA, Milan, Italy). All the aforementioned compounds were dissolved in dimethyl-sulfoxide (DMSO).

### RNA extraction and real-time PCR

Total RNA was extracted from cell cultures using the TRIzol commercial kit (Life Technologies, Milan, Italy) according to the manufacturer's protocol. RNA was quantified spectrophotometrically and quality was checked by electrophoresis through agarose gels stained with ethidium bromide. Only samples that were not degraded and showed clear 18 S and 28 S bands under UV light were used for RT-PCR. Total cDNA was synthesized from the RNA by reverse transcription using the murine leukemia virus reverse transcriptase (Life Technologies, Milan, Italy), following the protocol provided by the manufacturer. The expression of selected genes was quantified by real-time PCR using Step One (™) sequence detection system (Applied Biosystems Inc., Milan, Italy), following the manufacturer's instructions. Gene-specific primers were designed using Primer Express version 2.0 software (Applied Biosystems. Inc., Milan, Italy) and are as follows: human c-FOS Fwd: 5′-CGAG CCCTTTGATGACTTCCT-3′ and Rev.: 5′-GGAGCGG GCTGTCTCAGA-3′; human EGR1 Fwd: 5′-GCCT GCGACATCTGTGGAA-3′ and Rev.: 5′-CGCAAGTGG ATCTTGGTATGC-3′; human CTGF Fwd: 5′-ACCT GTGGGATGGGCATCT-3′ and Rev.: 5′-CAGGCGGCT CTGCTTCTCTA-3′; 18S Fwd: 5′-GGCGTCCCCCAACT TCTTA-3 and Rev.: 5′-GGGCATCACAGACCTGTTA TT-3′. Assays were performed in triplicate and the RNA expression values were normalized using 18S expression and then calculated as fold induction.

### Plasmids, transfections and luciferase assays

The luciferase reporter plasmid for c-fos encoding a 2. 2-kb 5'upstream fragment of human c-fos was a gift from Dr. K. Nose (Hatanodai, Shinagawa-ku, Tokyo). EGR1-luc plasmid, containing the – 600 to + 12 5′- flanking sequence from the human EGR1 gene, was kindly provided by Dr. Safe (Texas A&M University). The CTGF luciferase reporter plasmid p (– 1999/+ 36)-Luc (CTGF-luc), based on the backbone of vector pGL3-basic (Promega) was a gift from Dr. B. Chaqour [47]. The Renilla luciferase expression vector pRL-TK (Promega, Milan, Italy) was used as internal transfection control. MDA-MB 231 TNBC cells ($1 \times 10^5$) were plated into 24-well dishes with 500 μl/ well culture medium containing 5% FBS. Cell medium was replaced on the day of transfection with serum-free medium and transfection was performed using X-tremeGENE 9 DNA Transfection Reagent as recommended by the manufacture (Sigma–Aldrich) and a mixture containing 0.5 μg of each reporter plasmid and 5 ng of pRL-TK. After 6 h, cells were treated with E2 and G1 alone or in combination with GPER antagonist GA15 or STAT3 inhibitor STA21 and incubated for 18 h. Luciferase activity was measured using the Dual Luciferase Kit (Promega, Milan, Italy) according

to the manufacturer's recommendations. Firefly luciferase activity was normalized to the internal transfection control provided by the Renilla luciferase activity. Normalized relative light unit values obtained from cells treated with vehicle (DMSO) were set as 1-fold induction upon which the activity induced by treatments was calculated.

### Western blotting analysis

MDA-MB 231 and SUM159 cells were grown in 10 cm dishes, exposed to the treatments and then lysed as previously described [48]. Equal amounts of whole protein extract were electrophoresed through a reducing SDS/8 and 10% (w/n) polyacrylamide gels, electroblotted onto a nitrocellulose membrane (Amersham Biosciences, GE Healthcare, Milan, Italy), and probed with primary antibodies against Y397-FAK (Cell Signaling Technology, Milan, Italy), FAK (H-1) (Santa Cruz Biotechnology, DBA, Milan, Italy), phosphorylated ERK1/2 (E-4) (Santa Cruz Biotechnology, DBA, Milan, Italy), ERK2 (C-14) (Santa Cruz Biotechnology, DBA, Milan, Italy), p-AKT1/2/3 (Ser 473)-R (Santa Cruz Biotechnology, DBA, Milan, Italy), AKT/1/2/3 (H-136) (Santa Cruz Biotechnology, DBA, Milan, Italy), c-FOS (H-125) (Santa Cruz Biotechnology, DBA, Milan, Italy), EGR1 (C19) (Santa Cruz Biotechnology, DBA, Milan, Italy), CTGF (Origene, DBA, Milan, Italy) and β-actin (C2) (Santa Cruz Biotechnology, DBA, Milan, Italy). Proteins were detected by horseradish peroxidase-linked secondary antibodies (Santa Cruz Biotechnology, DBA, Milan, Italy) and then revealed using the ECL™ Western Blotting Analysis System (GE Healthcare, Milan, Italy).

### Focal adhesion assay

MDA-MB 231 cells cultured on fibronectin-coated 6 well plates were serum deprived and then treated for 30 min with E2 and G1 alone or in combination with G15, as indicated. Then cells were washed three times with PBS, fixed in 4% paraformaldehyde for 15 min, permeabilized with 0.2% Triton X-100, washed three times with PBS and incubated overnight with or without (negative control) a rabbit primary antibody anti p-FAK (Y397) (Cell Signaling Technology, Milan, Italy). After incubation, the wells were extensively washed with PBS and incubated with donkey anti-rabbit IgG-FITC (1:300; purchased from Alexa Fluor, Life Technologies, Milan, Italy) for 1 h at room temperature. Finally, cells were washed with PBS and incubated in PBS buffer containing 4′, 6-diamidino-2-phenylindole dihydrochloride (DAPI), (1:1000), (Sigma-Aldrich, Milan, Italy) 10 min at room temperature for nuclear staining. FAs images were acquired on the Cytation 3

Cell Imaging Multimode Reader (BioTek, Winooski, VT) and analysed using the software Gen5 (BioTek, Winooski, VT).

### STAT3 nuclear immunofluorescence staining

50% confluent MDA-MB 231 cells grown on 6 well plates were serum-deprived and then treated for 1 h with E2 and G1 alone or in the presence of GPER antagonist G-15 or VS-4718 FAK inhibitor, as indicated. Next, cells were fixed in 4% paraformaldehyde for 15 min at room temperature, permeabilized with 0.2% Triton X-100, washed three times with PBS and incubated overnight with or without (negative control) a rabbit primary antibody against STAT3 (Cell Signaling Technology, Milan, Italy). After incubation, the wells were extensively washed with PBS and incubated with donkey anti-rabbit IgG-FITC (1:400; purchased from Alexa Fluor, Life Technologies, Milan, Italy) for 1 h at room temperature. Finally, cells were washed with PBS and incubated in PBS buffer containing 4′, 6-diamidino-2-phenylindole dihydrochloride (DAPI), (1:1000), (Sigma-Aldrich, Milan, Italy) 10 min at room temperature for nuclear staining. Imaging showing nuclear STAT3 accumulation were acquired on the Cytation 3 Cell Imaging Multimode Reader (BioTek, Winooski, VT) and analysed using the software Gen5 (BioTek, Winooski, VT).

### Transwell migration assay

Migration assay was performed in triplicate using boyden chambers (Costar Transwell, 8 mm polycarbonate membrane, Sigma Aldrich, Milan, Italy). Briefly, MDA-MB 231 and SUM159 cells were seeded onto the upper membrane of the chamber at a density of $2,5 \times 10^5$ cells/ml. Next, the cells were exposed to the treatment with E2 or G1 used alone or in combination with GPER antagonist G-15, VS4718 FAK inhibitor or STA21 STAT3 inhibitor. 4 h after seeding, the cells on the bottom side of the membrane, were fixed with paraformaldehyde, permeabilized with methanol and finally stained with GIEMSA for 15 min at room temperature. Cell migrated were counted by using Cytation 3 Cell Imaging Multimode Reader (BioTek, Winooski, VT).

### Scratch wound healing assay

MDA-MB 231 cells were allowed to grow in 6 well/plates in regular medium supplemented with 5% FBS until they reached a 70 to 80% confluence. To create a scratch of the cell monolayer, a p200 pipette tip was used. Cells were then washed twice with PBS to remove the detached cells and treated with the various compounds, as indicated. The migration ability of the cells was evaluated after 24 h of treatments.

## Statistical analysis

The statistical analysis was performed using ANOVA followed by Newman–Keuls' testing to determine differences in means. $p < 0.05$ was considered as statistically significant.

## Results

### Database analysis of the PTK2 gene encoding FAK in TNBC

Previous studies have shown the potential role of FAK toward the breast tumorigenesis and aggressive breast tumor phenotypes [28, 49–51]. On the basis of these findings, we began our study exploring the clinical significance of the FAK encoding gene PTK2 in TNBC by the TCGA database (http://cbioportal.org). The analysis

of the RNA sequencing data derived from Invasive Breast Cancer Cohort of TCGA project (The Cancer Genome Atlas: https://cancergenome.nih.gov/), revealed that the PTK2 mRNA expression levels are significantly higher in TNBC compared with normal breast tissues in two independent cohort datasets (Fig. 1a-b). In addition, we found that the PTK2 mRNA expression levels are significantly higher also in ER+/PR +/HER2- and ER-/PR-/HER2+ breast tumors respect to normal breast tissues, however the TNBC samples displayed the highest expression levels among the different breast cancer phenotypes (Fig. 1c). Next, we also assessed the Kaplan–Meier univariate survival of patients groups, comparing those with high PTK2 (mRNA Z-score more than 1) with those exhibiting low PTK2 (mRNA Z-score
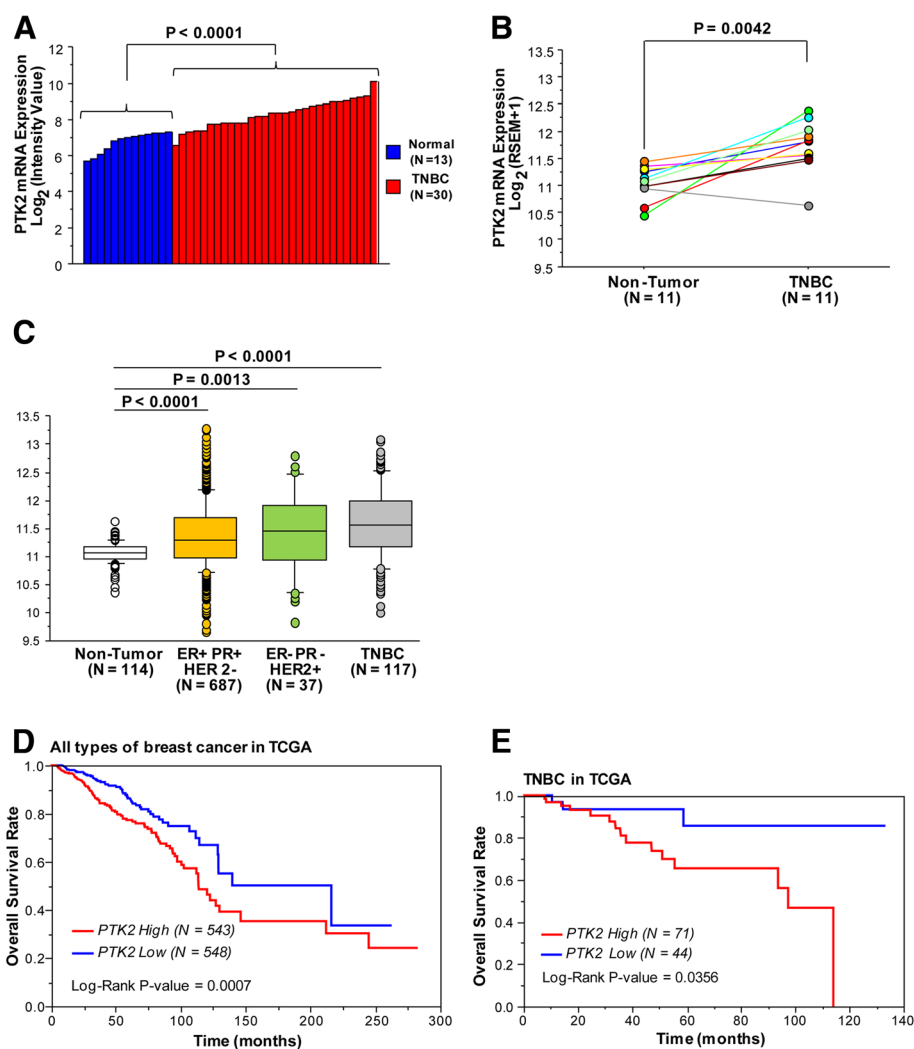


**Fig. 1** The PTK2 gene encoding FAK is over-expressed in TNBC. **a** Comparison of PTK2 mRNA expression between laser-microbeam microdissected TNBC and normal breast cells. **b** Comparison of PTK2 mRNA expression between matched TNBC and non-tumor breast tissues. **c** Comparison of PTK2 mRNA expression among non-tumor breast tissues, ER+/PR+/HER2-, ER-/PR-/HER2+ and TNBC as reported in TCGA. **d** Clinical outcome in all types of breast cancer with high PTK2 (mRNA Z-score > 1) or low PTK2 (mRNA Z-score ≤ 1) displayed by Kaplan-Meier plots with log-rank tests. **e** Clinical outcome in TNBC patients with high PTK2 (mRNA Z-score > 1) or low PTK2 (mRNA Z-score ≤ 1) displayed by Kaplan-Meier plots with log-rank tests

equal or less than 1). In this regard, we ascertained that the PTK2 high group has a significant poorer overall survival respect to the PTK2 low group in all types of breast cancer as well as in TNBC (Fig. 1d-e). Overall, these data highlight the role of FAK in breast cancer toward the malignant aggressiveness as in TNBC patients.

### GPER mediates FAK activation and the induction of FAs by E2 and G1

FAK represents a main component in the integrins-mediated transduction pathway and contributes to diverse signaling cascades triggered by a wide range of stimuli as

growth factors, cytokines and G-protein coupled receptor agonists [52, 53]. As previous studies have revealed that estrogens may regulate the focal adhesion complexes not only through the classical estrogen receptor α (ERα) in breast tumor and endothelial cells [54–56] but also via GPER in human dermal fibroblasts [57], we aimed to investigate whether GPER is involved in the activation of FAK in TNBC MDA-MB 231 and SUM159 cells [58]. Both E2 and the GPER selective agonist G1 triggered the Y397 FAK phosphorylation along with the activation of ERK1/2 and AKT in MDA-MB 231 cells (Fig. 2a-b), however these responses were no longer
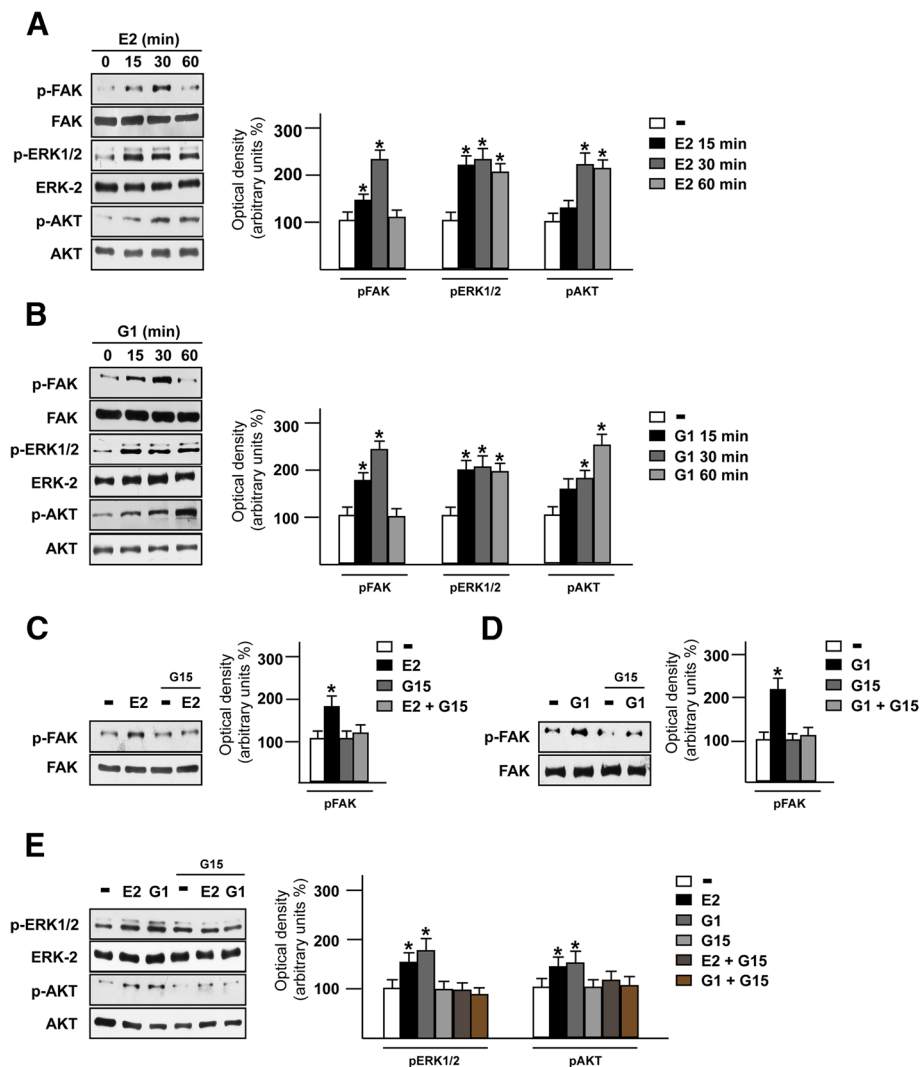


**Fig. 2** E2 and G1 trigger FAK Y397 activation in TNBC cells. Immunoblots showing FAK, ERK1/2 and AKT phosphorylation upon exposure with 100 nM E2 (**a**) or 100 nM G1 (**b**) in MDA-MB 231 cells, as indicated. Side panels show densitometric analysis of the immunoblots normalized to the loading control. Immunoblots showing FAK phosphorylation in MDA-MB 231 cells treated for 30 min with 100 nM E2 (**c**) or 100 nM G1 (**d**) alone and in combination with 100 nM GPER antagonist G15. Side panels show densitometric analysis of the immunoblots normalized to the loading control. **e** Immunoblots showing ERK1/2 and AKT phosphorylation in MDA-MB 231 cells treated for 30 min with 100 nM E2 or 100 nM G1 alone and in combination with 100 nM GPER antagonist G15. Side panels show densitometric analysis of the immunoblots normalized to the loading control. FAK, ERK-2 and AKT expression levels were used as loading controls for pFAK, pERK1/2 and pAKT, respectively. Results shown are representative of at least three independent experiments. (**\***) indicates $p < 0.05$

evident in the presence of the GPER antagonist G-15 (Fig. 2c-e) or using the FAK inhibitor namely VS-4718 (also known as PND-1186) [34] (Fig. 3a-d). Likewise, we ascertained that both the GPER antagonist G-15 and the FAK kinase inhibitor VS-4718 prevent the Y397 FAK phosphorylation induced by E2 and G1 in

SUM159 TNBC cells (Additional file 1: Figure S1A-D). Next, we assessed that the c-Src kinase inhibitor PP2 and the MEK inhibitor PD98059, but not the PI3K inhibitor wortmannin, abolish the Y397 FAK phosphorylation upon E2 and G1 exposure (Fig. 3e-j). As expected, the MEK inhibitor PD98059 and the PI3K
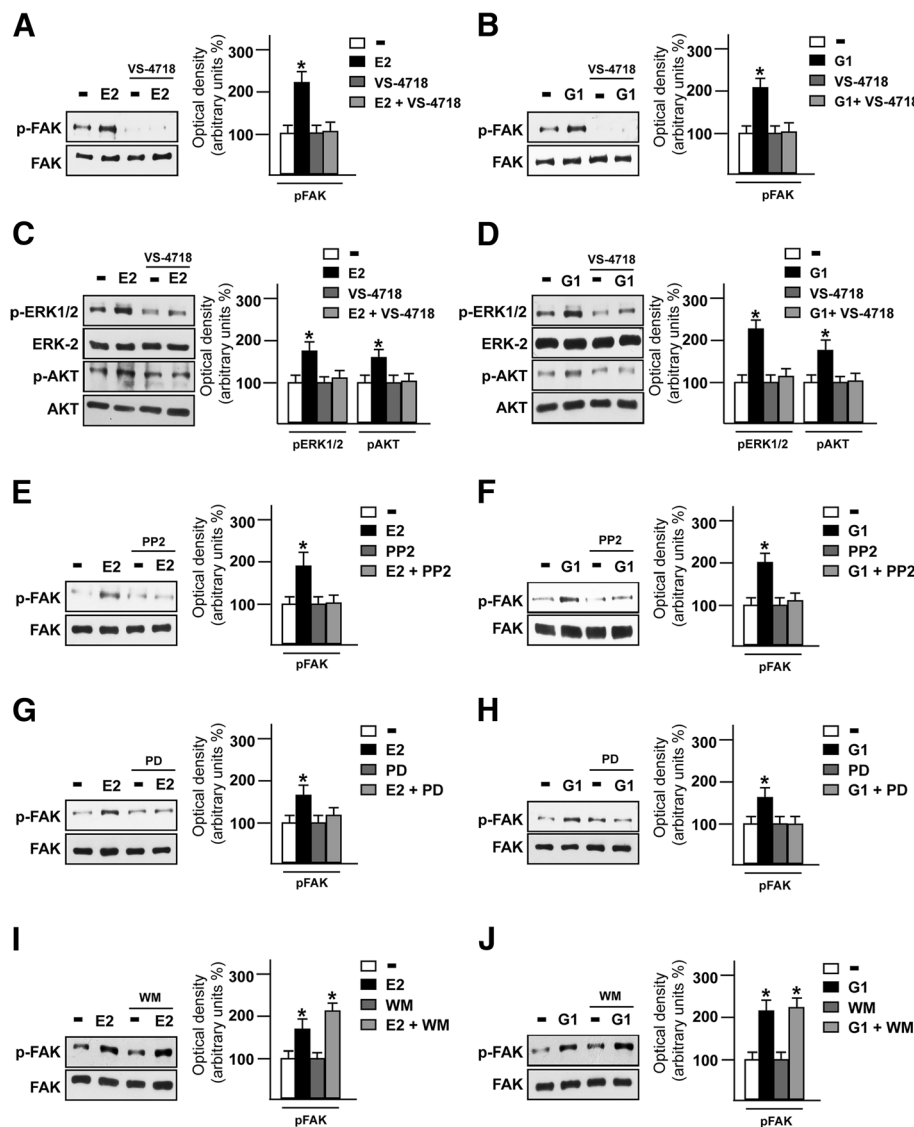


**Fig. 3** Transduction signaling mediating FAK Y397 phosphorylation. Immunoblots showing FAK phosphorylation in MDA-MB 231 cells treated for 30 min with 100 nM E2 (**a**) and 100 nM G1 (**b**) alone or in combination with 1 μM FAK kinase inhibitor VS-4718. Side panels show densitometric analysis of the immunoblots normalized to the loading control. Immunoblots showing ERK1/2 and AKT phosphorylation in MDA-MB 231 cells treated for 30 min with 100 nM E2 (**c**) and 100 nM G1 (**d**) alone or in combination with 1 μM FAK kinase inhibitor VS-4718. Side panels show densitometric analysis of the immunoblots normalized to the loading control. Immunoblots showing FAK phosphorylation in MDA-MB 231 cells treated for 30 min with 100 nM E2 (**e**) and 100 nM G1 (**f**) alone or in combination with 1 μM c-Src inhibitor PP2. Side panels show densitometric analysis of the immunoblots normalized to the loading control. Immunoblots showing FAK phosphorylation in MDA-MB 231 cells treated for 30 min with 100 nM E2 (**g**) and 100 nM G1 (**h**) alone or in combination with 10 μM MEK inhibitor PD98059 (PD). Side panels show densitometric analysis of the immunoblots normalized to the loading control. Immunoblots showing FAK phosphorylation in MDA-MB 231 cells treated for 30 min with 100 nM E2 (**i**) and 100 nM G1 (**j**) alone or in combination with 10 μM PI3K inhibitor Wortmannin. Side panels show densitometric analysis of the immunoblots normalized to the loading control. FAK, ERK-2 and AKT expression were used as loading controls for pFAK, pERK and pAKT, respectively. Results shown are representative of at least three independent experiments. (**\***) indicates $p < 0.05$

inhibitor wortmannin, inhibited respectively the phosphorylation of ERK and AKT induced by E2 and G1 (Additional file 2: Figure S2A-D). Overall, these findings point out that FAK activation by estrogenic signaling may occur through the GPER/c-Src/MEK transduction pathway. As FAs are important sub-cellular structure mediating cell adhesion to ECM in tumor spreading [59, 60], we then determined by immunofluorescence assays that FAs formation prompted by E2 and G1 is prevented using the GPER antagonist G-15 (Fig. 4a-c), thus suggesting the involvement of GPER in the above mentioned response observed in MDA-MB 231 cells.

## FAK is involved in the STAT3 nuclear accumulation and gene expression changes induced by E2 and G1 through GPER

It has been reported that FAK knockdown may affect the activation of the signal transducer and activator of transcription 3 (STAT3), which is a point of convergence for numerous oncogenic pathways [61–65]. As GPER was also involved in the activation of STAT3 [66, 67], we aimed to evaluate the role of FAK in the STAT3 nuclear accumulation triggered by estrogenic GPER signaling. Of note, we found that E2 and G1 induce the nuclear shuttle of STAT3, however this effect
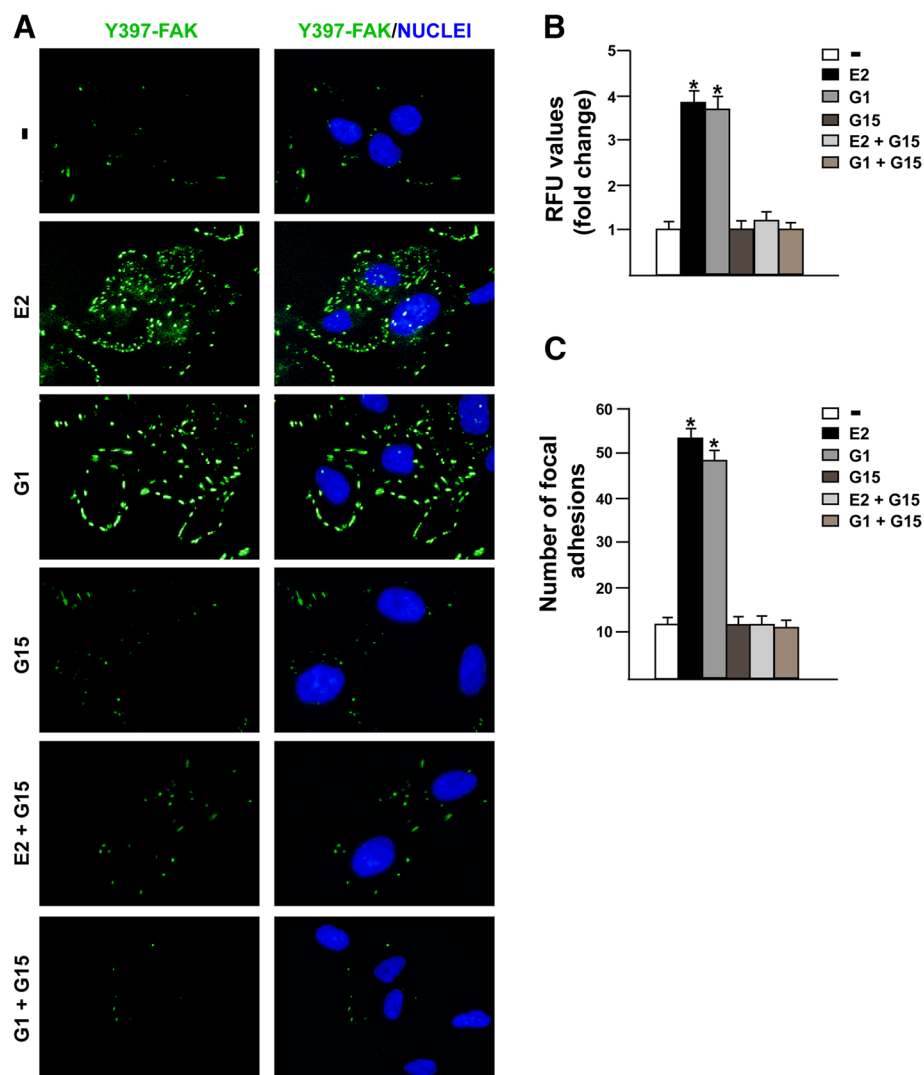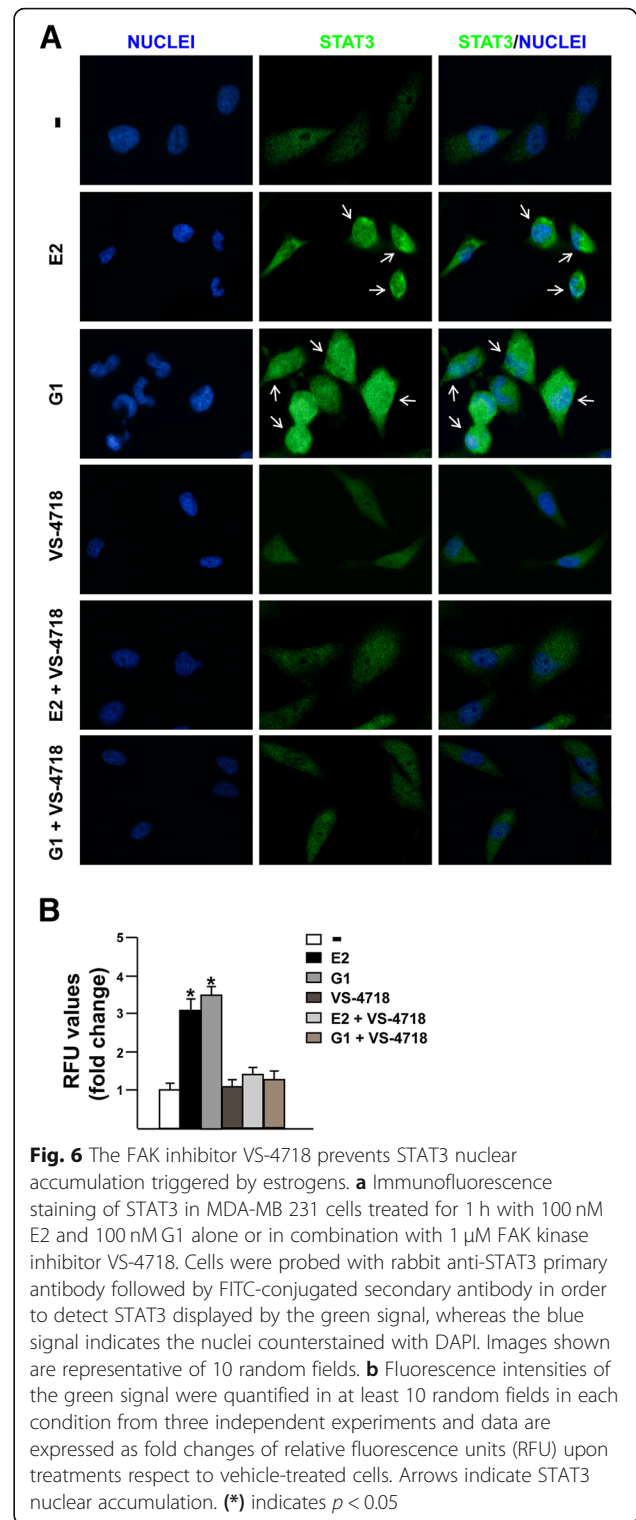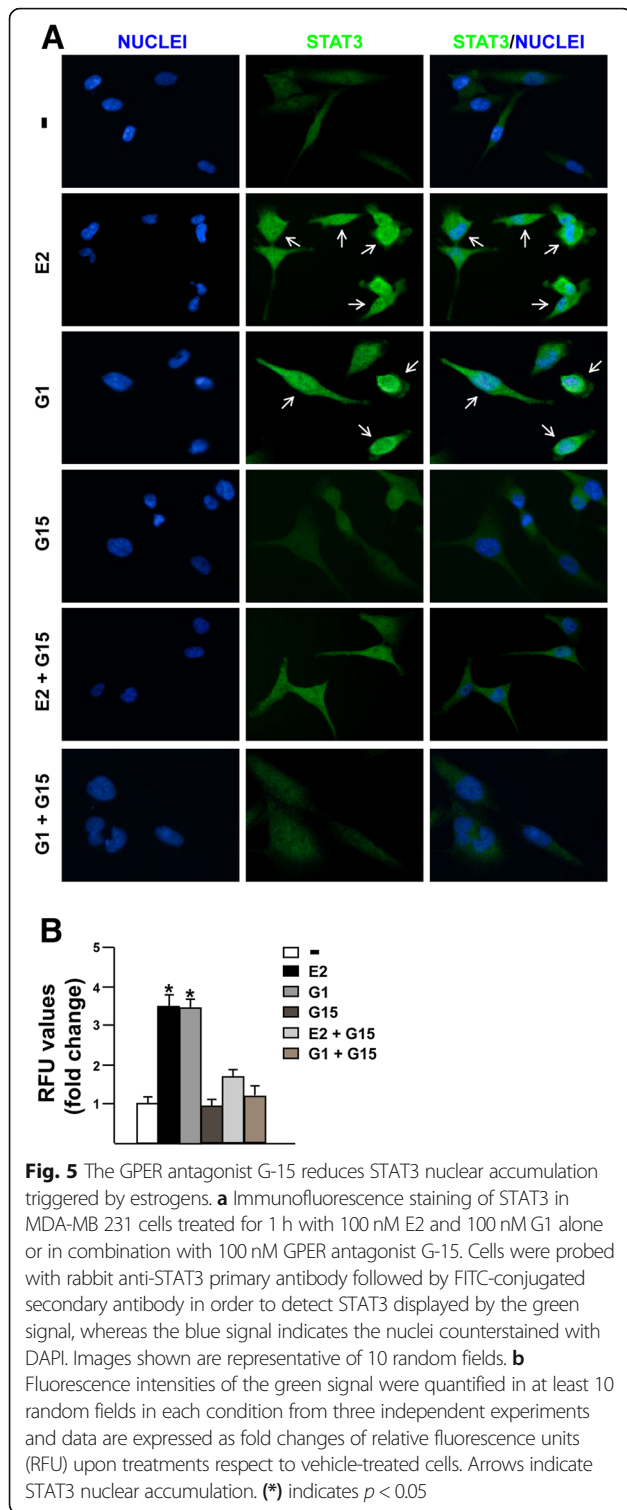


**Fig. 4** GPER mediates focal adhesions (FAs) in TNBC. **a** Immuofluorescence staining of Focal Adhesions (FAs) in MDA-MB 231 cells treated for 30 min with 100 nM E2 and 100 nM G1 alone or in combination with 100 nM GPER antagonist G15. Cells were probed with anti-phosphotyrosine primary antibody and FITC-conjugated secondary antibody in order to visualize FAs displayed by the green signal, whereas the blue signal indicates the nuclei counterstained with DAPI. Images shown are representative of 10 random fields from three independent experiments. **b** Fluorescence intensities of the green signal were quantified in at least 10 random fields in each condition and results are expressed as fold changes of relative fluorescence units (RFU) upon treatments respect to vehicle-treated cells. **c** FAs number was quantified in at least 10 random fields in each condition and results are expressed as mean focal adhesions ± SD from three independent experiments upon treatments respect to vehicle-treated cells. (*) indicates $p < 0.05$

**Fig. 5** The GPER antagonist G-15 reduces STAT3 nuclear accumulation triggered by estrogens. **a** Immunofluorescence staining of STAT3 in MDA-MB 231 cells treated for 1 h with 100 nM E2 and 100 nM G1 alone or in combination with 100 nM GPER antagonist G-15. Cells were probed with rabbit anti-STAT3 primary antibody followed by FITC-conjugated secondary antibody in order to detect STAT3 displayed by the green signal, whereas the blue signal indicates the nuclei counterstained with DAPI. Images shown are representative of 10 random fields. **b** Fluorescence intensities of the green signal were quantified in at least 10 random fields in each condition from three independent experiments and data are expressed as fold changes of relative fluorescence units (RFU) upon treatments respect to vehicle-treated cells. Arrows indicate STAT3 nuclear accumulation. **(*)** indicates $p < 0.05$



**Fig. 6** The FAK inhibitor VS-4718 prevents STAT3 nuclear accumulation triggered by estrogens. **a** Immunofluorescence staining of STAT3 in MDA-MB 231 cells treated for 1 h with 100 nM E2 and 100 nM G1 alone or in combination with 1 μM FAK kinase inhibitor VS-4718. Cells were probed with rabbit anti-STAT3 primary antibody followed by FITC-conjugated secondary antibody in order to detect STAT3 displayed by the green signal, whereas the blue signal indicates the nuclei counterstained with DAPI. Images shown are representative of 10 random fields. **b** Fluorescence intensities of the green signal were quantified in at least 10 random fields in each condition from three independent experiments and data are expressed as fold changes of relative fluorescence units (RFU) upon treatments respect to vehicle-treated cells. Arrows indicate STAT3 nuclear accumulation. **(*)** indicates $p < 0.05$

was no longer evident in the presence of the GPER antagonist G-15 (Fig. 5a-b) or using the FAK inhibitor VS-4718 (Fig. 6a-b), as assessed by immunofluorescence assay in MDA-MB 231 cells. As our and other previous studies have evidenced that GPER triggers a

specific gene signature in breast cancer cells toward relevant biological effects [45, 68, 69], we then sought to investigate whether STAT3 may contribute to gene expression changes mediated by GPER in MDA-MB 231 cells. First, we assessed that the GPER antagonist
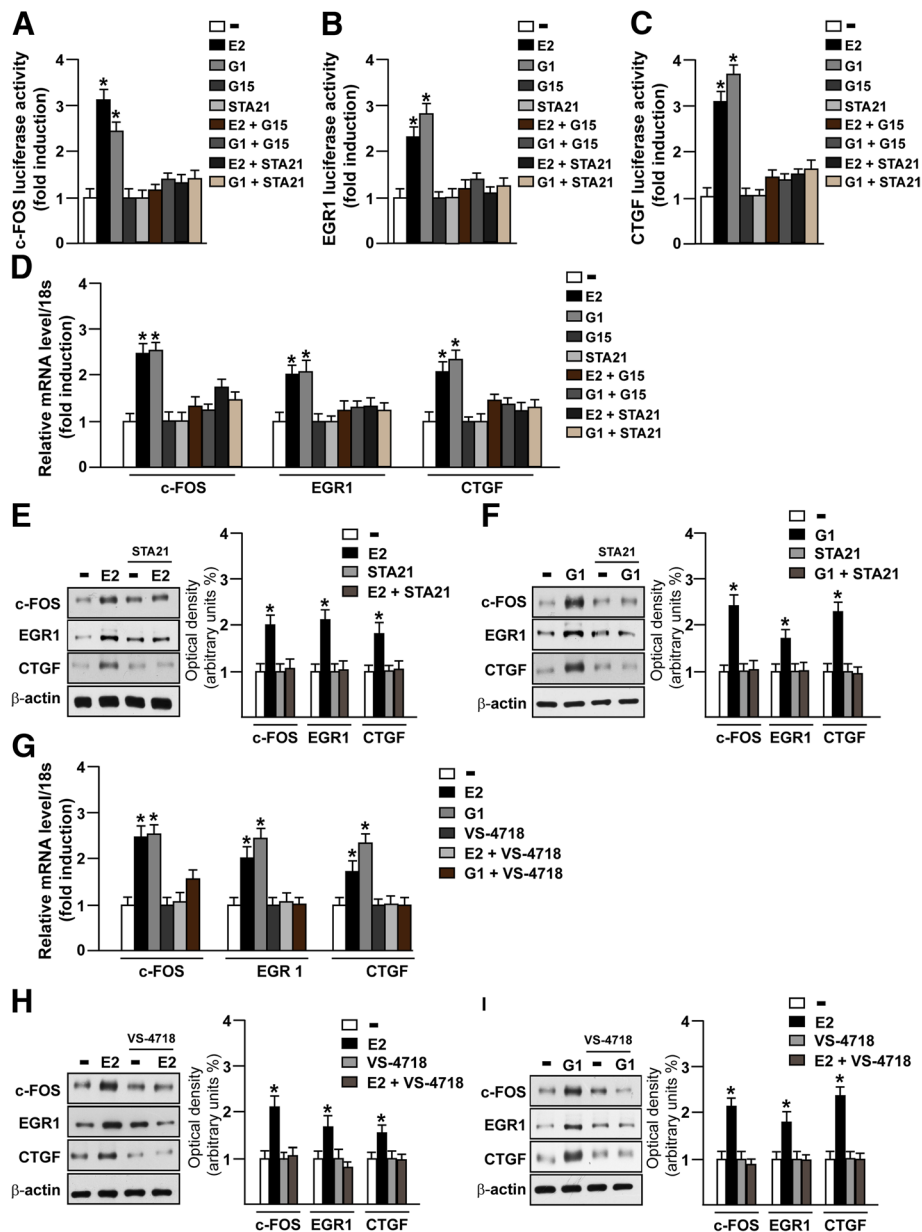
**Fig. 7** c-FOS, EGR1 and CTGF regulation by FAK and STAT3. c-FOS (**a**), EGR1 (**b**) and CTGF (**c**) luciferase promoter activity in MDA-MB 231 cells treated for 18 h with 100 nM E2 and 100 nM G1 alone or in combination with 100 nM GPER antagonist G15 or 20 μM STAT3 inhibitor STA21. The luciferase activities were normalized to the internal transfection control and values of cells receiving vehicle were set as 1-fold induction upon which the activities induced by treatments were calculated. Each data point represents the mean ± SD of three independent experiments performed in triplicate. **d** c-FOS, EGR1 and CTGF mRNA expression measured by real time-PCR in MDA-MB 231 cells treated for 4 h with 100 nM E2 and 100 nM G1 alone or in combination with 100 nM GPER antagonist G15 or 20 μM STAT3 inhibitor STA21. Values normalized to the 18 s expression are shown as fold changes of the mRNA expression induced by treatments compared to cells treated with vehicle (−). **e-f** Immunoblots showing c-FOS, EGR1 and CTGF protein expression in MDA-MB 231 cells treated for 4 h with 100 nM E2 (**e**) and 100 nM G1 (**f**) alone or in combination with 20 μM STAT3 inhibitor STA21. Side panels show densitometric analysis of the immunoblots normalized to β-actin. **g** c-FOS, EGR1 and CTGF mRNA expression measured by real time-PCR in MDA-MB 231 cells treated for 4 h with 100 nM E2 and 100 nM G1 alone or in combination with 1 μM FAK kinase inhibitor VS-4718. Values normalized to the 18 s expression are shown as fold changes of the mRNA expression induced by treatments compared to cells treated with vehicle (−). Immunoblots showing c-FOS, EGR1 and CTGF protein expression in MDA-MB 231 cells treated for 4 h with 100 nM E2 (**h**) and 100 nM G1 (**i**) alone or in combination with 1 μM FAK kinase inhibitor VS-4718. Side panels show densitometric analysis of the immunoblots normalized to β-actin. Results shown are representative of three independent experiments. (*) indicates $p < 0.05$
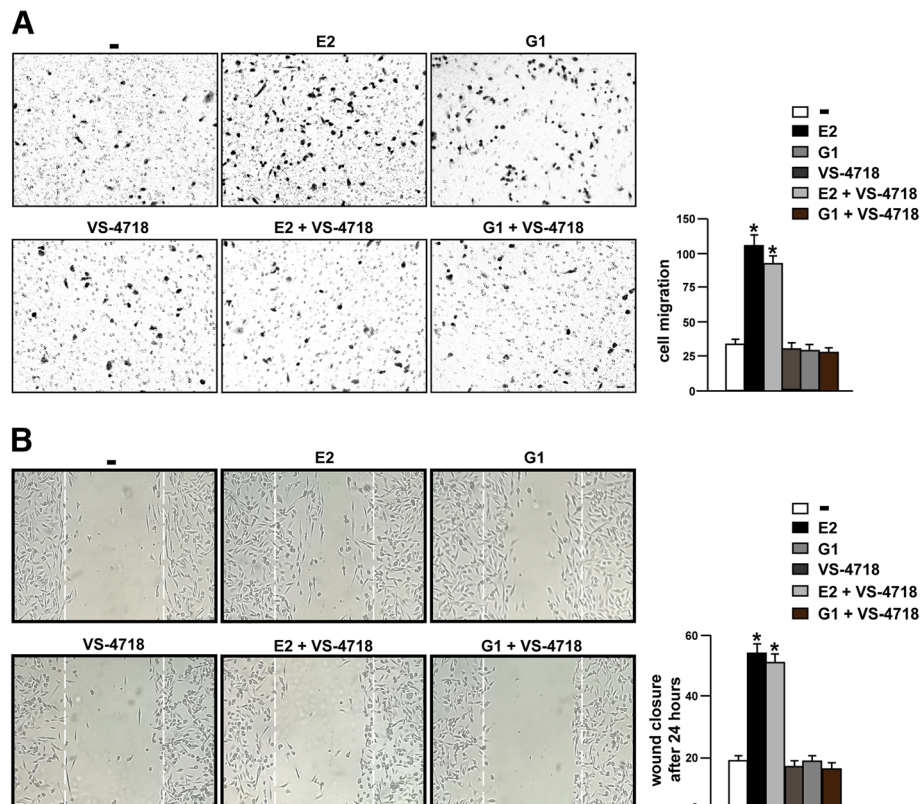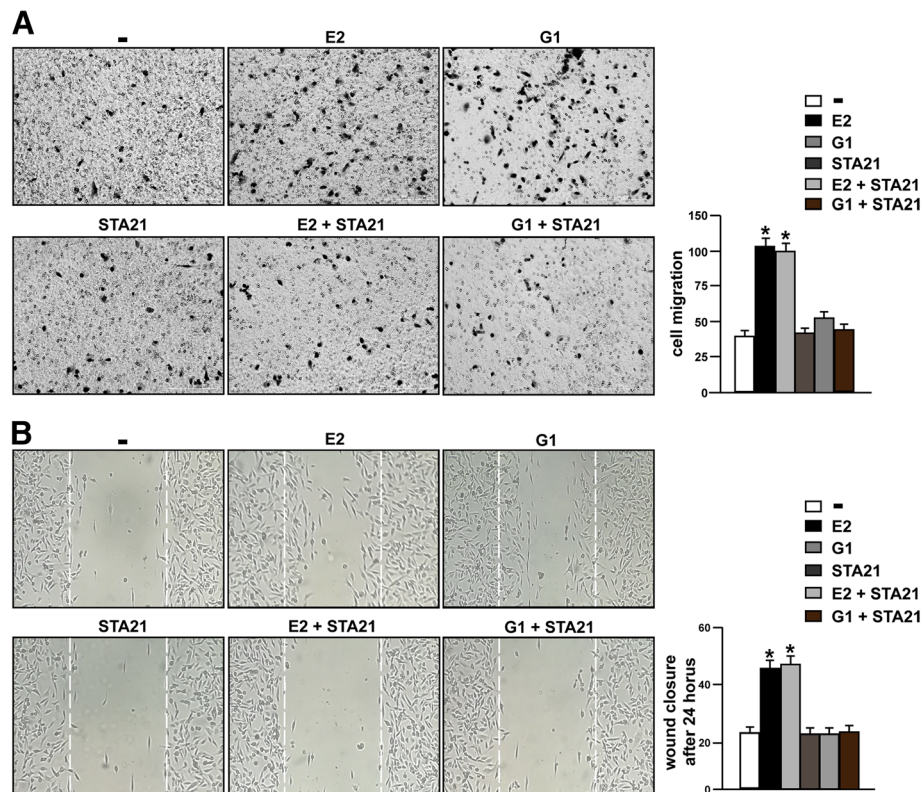
**Fig. 8** The FAK inhibitor VS-4718 inhibits the migration of TNBC cells induced by E2 and G1. **a** Boyden Chamber assays showing the migration of MDA-MB 231 cells treated for 4 h with 100 nM E2 and 100 nM G1 alone or in combination with 1 μM FAK kinase inhibitor VS-4718. The results are shown as cells migrating through the membrane at the bottom of the well upon treatments respect to vehicle (−). Results shown are representative of three independent experiments. **b** Cell migration was evaluated by wound-healing assay in MDA-MB 231 cells treated for 24 h with 100 nM E2 and 100 nM G1 alone or in combination with 1 μM FAK kinase inhibitor VS-4718. White dotted lines indicate the wound borders at the beginning of the assay and recorded 24 h post- scratching. Results shown are representative of three independent experiments. **(\*)** indicates $p < 0.05$

G-15 and the STAT3 inhibitor namely STA21 repress the transactivation of c-FOS (Fig. 7a), EGR1 (Fig. 7b) and CTGF (Fig. 7c) promoter activity triggered by E2 and G1 treatments. In accordance with these results, G-15 and STA21 reduced the mRNA expression levels of c-FOS, EGR1 and CTGF induced by E2 and G1 (Fig. 7d). Interestingly, c-FOS, EGR1 and CTGF protein levels induced by E2 and G1 were abrogated using STA21 (Fig. 7e-f) and both the mRNA and protein levels of c-FOS, EGR1 and CTGF triggered by E2 and G1 were prevented using the FAK inhibitor VS-4718 (Fig. 7g-i). Altogether, these results reveal that STAT3 along with FAK may contribute to the regulation of GPER target genes in TNBC cells.

## FAK and STAT3 inhibition prevents the migration of TNBC cells

Several reports have highlighted the role of FAK in the migration of cancer cells [70]. Accordingly, we assessed that the migratory effects induced by E2 and G1 were abolished not only in the presence of the GPER antagonist G-15 (Additional file 3: Figure S3A) but also using the FAK inhibitor VS-4718, as evaluated by boyden chamber assay performed in MDA-MB 231 cells (Fig. 8a). In addition, scratch monolayer experiments evidenced that G-15 (Additional file 3: Figure S3B) and VS-4718 (Fig. 8b) lessen the wound closure triggered by E2 and G1. In order to further corroborate these results, we assessed that both the GPER antagonist G-15 and the FAK inhibitor VS-4718 reduce the migration of SUM159 cells stimulated by E2 and G1 (Additional file 4: Figure S4A). As STAT3 may contribute to the migration of breast cancer cells [71], we aimed to ascertain its involvement in the migratory features of TNBC cells mediated by GPER. Boyden chamber and wound healing assays revealed that the migration of MDA-MB 231 cells stimulated by E2 and G1 is abolished using the STAT3 inhibitor STA21 (Fig. 9a-b). Overall, both FAK and STAT3 may contribute to the invasive skills of TNBC cells prompted by estrogenic GPER signaling.

**Fig. 9** The STAT3 inhibitor STA21 suppresses the migration of TNBC cells induced by E2 and G1. **a** Boyden Chamber assays showing the migration of MDA-MB 231 cells treated for 4 h with 100 nM E2 and 100 nM G1 alone or in combination with 20 μM STAT3 inhibitor STA21. The results are shown as cells migrating through the membrane at the bottom of the well upon treatments respect to vehicle (–). Results shown are representative of three independent experiments. **b** Cell migration was evaluated by wound-healing assay in MDA-MB 231 cells treated for 24 h with 100 nM E2 and 100 nM G1 alone or in combination with 20 μM STAT3 inhibitor STA21. White dotted lines indicate the wound borders at the beginning of the assay and recorded 24 h post- scratching. Results shown are representative of three independent experiments. **(\*)** indicates $p < 0.05$

## Discussion

In the present study, we first assessed that the mRNA expression of PTK2/FAK is associated with worse survival rates and up-regulated in the aggressive TNBC respect to non-TNBC and normal breast samples, as determined by a bioinformatic analysis of cancer genomics TCGA datasets (www.cbioportal.org). Next, to provide novel insights on the molecular mechanisms through which FAK may be involved in the TNBC progression, we ascertained its role in gene expression changes and the migratory skills of TNBC cells triggered by estrogenic GPER signaling. In particular, we found that GPER stimulation induces Y397 FAK phosphorylation and increases the number of FAs in TNBC cells. In addition, we demonstrated the role exerted by FAK in the GPER-mediated nuclear accumulation of STAT3 and the involvement of both FAK and STAT3 toward the regulation of GPER target genes and the migratory responses of TNBC cells.

Several studies have correlated FAK expression and activity with different types of primary and metastatic cancers, including breast malignancy [36, 72]. In this regard, FAK expression was shown not only associated

with invasive and metastatic breast cancer [73], but also as an early event occurring in breast tumorigenesis [51, 74]. In accordance with these studies, the expression of FAK was linked to a poor clinical outcome [31], therefore further highlighting the contribution of FAK in the development of breast tumor.

It has been established that FAK plays a main action in the formation of focal adhesion complexes, hence acting as a key regulator of important processes in both normal and cancer cells [75, 76]. A well characterized mechanism promoting FAK activation involves the integrin-ECM engagment and the subsequent co-clustering of proteins (i.e. talin and paxillin) with the cytoplasmic tail of integrin [77]. In addition, FAK may be activated by various extracellular stimuli such as steroids like estrogens [56], growth factors [78], cytokines [79], phospholipids, lipid mediators [80] and GPCRs initiated pathways [12, 81].

Estrogens may be involved in the regulation of several cytoskeletal and membrane remodeling components as the focal adhesion complexes [54, 55]. In particular, estrogens regulate cell morphology and the interaction with ECM, thus driving the cell movement under the control of the

actin organization [54, 55]. In this regard, it has been reported that estrogens through ERα induce the phosphorylation of FAK and its subsequent translocation within the membrane sites where focal adhesion complexes are assembled [56]. Besides, estrogens-induced cytoskeleton re-organization and focal adhesion strengthening may also occur via GPER [57], which mediates estrogenic signaling in diverse types of tumors [44, 68, 82–84]. Further extending the aforementioned findings, in the present study we have documented that estrogens through GPER triggers the activation of FAK in TNBC cells, in accordance with previous data obtained in different cancer cell contexts [85].

Estrogenic GPER signaling may contribute to the regulation of several genes in tumor cells via diverse transcription factors [45] as well as the involvement of STAT3 [66, 67]. Upon activation STAT3 forms homo- or heterodimers through the SH2 and the C-terminal domains, then translocates into the nucleus where it binds specific sequences located in the promoter sequences of target genes [61, 86]. In this scenario, our immunofluorescence studies revealed that GPER mediates an enhanced nuclear accumulation of STAT3 in TNBC cells. Interestingly, this effect was prevented not only in the presence of the GPER antagonist G-15, but also using the FAK inhibitor VS-4718, in accordance with previous studies suggesting that FAK is involved in the STAT3 activation and transcriptional activity [62–65]. Of note, not only the GPER antagonist G15 but also the DNA-binding STAT3 inhibitor STA21 reduced the promoter activity and the expression of the GPER target genes c-FOS, EGR1 and CTGF [45], further corroborating the involvement of STAT3 in the regulation of these genes [87–89]. Likewise, the expression levels of c-FOS, EGR1 and CTGF were reduced using the FAK inhibitor VS-4718, thus suggesting that FAK is also involved in the GPER-mediated regulation of the aforementioned genes.

FAK signaling has long been linked to the cell migration process, which represents a crucial skill toward cancer cell invasion and metastasis [90]. Indeed, several FAK-downstream pathways have been implicated in cell migration as Src and PI3K transduction cascades [91–95]. In addition, FAK-mediated cell migration was shown to require diverse key factors involved in the cytoskeleton remodeling as the Rho subfamily of small GTPases [96], N-WASP [97], and Arp2/3 complex [98]. On the basis of these observations, FAK inhibitors are currently considered promising chemoterapeutic agents [8]. In this respect, our data further highlight the use of FAK inhibitors given that the treatments with VS-4718 prevented the migration of TNBC cells upon the agonist activation of GPER. Overall, our findings suggest that FAK is involved in the stimulatory action of GPER in TNBC cells, however further

investigations are needed to better define this functional cooperation toward the aggressive features of breast malignancy.

## Conclusion

In the present study we have provided new evidence regarding the engagement of FAK in the estrogenic GPER signaling in TNBC cells. In particular, we have assessed that FAK contributes to the GPER mediated STAT3 activation, the gene expression changes and the invasiveness of TNBC cells. Together, these findings suggest that the action of GPER through FAK may be considered toward combination treatments targeting TNBC.

## Additional files

**Additional file 1: Figure S1.** GPER stimulation triggers FAK Y397 activation in SUM159 TNBC cells. Immunoblots showing FAK phosphorylation in SUM159 cells treated for 30 min with 100 nM E2 (A) or 100 nM G1 (B) alone or in combination with 100 nM GPER antagonist G-15. Side panels show densitometric analysis of the immunoblots normalized to the loading control. Immunoblots showing FAK phosphorylation in SUM159 cells treated for 30 min with 100 nM E2 (C) or 100 nM G1 (D) alone and in combination with 1 μM FAK kinase inhibitor VS-4718. Side panels show densitometric analysis of the immunoblots normalized to the loading control. FAK expression was used as loading control for pFAK. Results shown are representative of at least three independent experiments. **(*)** indicates *p* < 0.05 (TIF 1732 kb)

**Additional file 2: Figure S2.** The MEK inhibitor PD98059 and the PI3K inhibitor Wortmannin prevent respectively the activation of ERK and AKT induced by E2 and G1 in MDA-MB 231 TNBC cells. Immunoblots showing ERK phosphorylation in MDA-MB 231 cells treated for 30 min with 100 nM E2 (A) or 100 nM G1 (B) alone or in combination with 10 μM MEK inhibitor PD98059 (PD). Side panels show densitometric analysis of the immunoblots normalized to the loading control. Immunoblots showing AKT phosphorylation in MDA-MB 231 cells treated for 30 min with 100 nM E2 (C) or 100 nM G1 (D) alone and in combination with 10 μM PI3K inhibitor Wortmannin. Side panels show densitometric analysis of the immunoblots normalized to the loading control. ERK and AKT expression levels were used as loading controls for pERK and pAKT. Results shown are representative of at least three independent experiments. **(*)** indicates *p* < 0.05 (TIF 1738 kb)

**Additional file 3: Figure S3.** The GPER antagonist G-15 reduces the migration of MDA-MB 231 TNBC cells induced by E2 and G1. (A) Boyden Chamber assays showing the migration of MDA-MB 231 cells treated for 4 h with 100 nM E2 and 100 nM G1 alone or in combination with 100 nM GPER antagonist G-15. The results are shown as cells migrating through the membrane at the bottom of the well upon treatments respect to vehicle (−). Results shown are representative of three independent experiments. (B) Cell migration was evaluated by wound-healing assay in MDA-MB 231 cells treated for 24 h with 100 nM E2 and 100 nM G1 alone or in combination with 100 nM GPER antagonist G-15. White dotted lines indicate the wound borders at the beginning of the assay and recorded 24 h post-scratching. Results shown are representative of three independent experiments. **(*)** indicates *p* < 0.05

**Additional file 4: Figure S4.** The GPER antagonist G-15 and the FAK inhibitor VS-4718 inhibit the migration of SUM159 TNBC cells induced by E2 and G1. (A) Boyden Chamber assays showing the migration of SUM159 cells treated for 4 h with 100 nM E2 and 100 nM G1 alone or in combination with 100 nM GPER antagonist G-15 and 1 μM FAK kinase inhibitor VS-4718. The results are shown as cells migrating through the membrane at the bottom of the well upon treatments respect to vehicle (−). Results shown are representative of three independent experiments. **(*)** indicates *p* < 0.05

## Publisher's Note
Springer Nature remains neutral with regard to jurisdictional claims in published maps and institutional affiliations.

## Author details
[1]Department of Pharmacy, Health and Nutritional Sciences, University of Calabria, 87036 Rende, Italy. [2]MSD K.K, Tokyo 102-8667, Japan. [3]Department of Experimental and Clinical Medicine, Magna Graecia University, 88100 Catanzaro, Italy.

## References
1. Siegel RL, Miller KD, Jemal A. Cancer statistics. CA Cancer J Clin. 2018;68:7–30.
2. Polyak K. Heterogeneity in breast cancer. J Clin Invest. 2011;121:3786–8.
3. Tong CWS, Wu M, Cho WCS, KKW T. Recent Advances in the Treatment of Breast Cancer. Front Oncol. 2018;8:227.
4. He Y, Jiang Z, Chen C, Wang X. Classification of triple-negative breast cancers based on Immunogenomic profiling. J Exp Clin Cancer Res. 2018;37:327.
5. Weigelt B, Peterse JL, Van't veer LJ. Breast cancer metastasis: markers and models. Nat Rev Cancer. 2005;5:591–602.
6. Desgrosellier JS, Cheresh DA. Integrins in cancer: biological implications and therapeutic opportunities. Nat Rev Cancer. 2010;10:9–22.
7. He X, Lee B, Jiang Y. Cell-ECM interactions in tumour invasion. Adv Exp Med Biol. 2016;936:73–91.
8. Sulzmaier FJ, Jean C, Schlaepfer DD. FAK in cancer: mechanistic findings and clinical applications. Nat Rev Cancer. 2014;14:598–610.
9. Taliaferro-Smith L, Oberlick E, Liu T, McGlothen T, Alcaide T, Tobin R, et al. FAK activation is required for IGF1R-mediated regulation of EMT, migration, and invasion in mesenchymal triple negative breast cancer cells. Oncotarget. 2015;6:4757–72.
10. Shen J, Cao B, Wang Y, Ma C, Zeng Z, Liu L, et al. Hippo component YAP promotes focal adhesion and tumour aggressiveness via transcriptionally activating THBS1/FAK signalling in breast cancer. J Exp Clin Cancer Res. 2018;37:175.
11. Jean C, Chen XL, Nam JO, Tancioni I, Uryu S, Lawson C, et al. Inhibition of endothelial FAK activity prevents tumor metastasis by enhancing barrier function. J Cell Biol. 2014;204:247–63.
12. Fan RS, Jacamo RO, Jiang X, Sinnett-Smith J, Rozengurt E. G protein-coupled receptor activation rapidly stimulates focal adhesion kinase phosphorylation at Ser-843. Mediation by Ca2+, calmodulin and Ca2+/calmodulin-dependent kinase II. J Biol Chem. 2005;280:24212–20.
13. Wu JC, Chen YC, Kuo CT, Wenshin Yu H, Chen YQ, Chiou A, et al. Focal adhesion kinase-dependent focal adhesion recruitment of SH2 domains directs SRC into focal adhesions to regulate cell adhesion and migration. Sci Rep. 2015;5:18476.
14. Chen HC, Guan JL. Association of focal adhesion kinase with its potential substrate phosphatidylinositol 3-kinase. Proc Natl Acad Sci U S A. 1994;91:10148–52.
15. Shen TL, Han DC, Guan JL. Association of Grb7 with phosphoinositides and its role in the regulation of cell migration. J Biol Chem. 2002;277:29069–77.
16. Carloni V, Romanelli RG, Pinzani M, Laffi G, Gentilini P. Focal adhesion kinase and phospholipase C gamma involvement in adhesion and migration of human hepatic stellate cells. Gastroenterology. 1997;112:522–31.
17. Fan H, Zhao X, Sun S, Luo M, Guan JL. Function of focal adhesion kinase scaffolding to mediate endophilin A2 phosphorylation promotes epithelial-mesenchymal transition and mammary cancer stem cell activities in vivo. J Biol Chem. 2013;288:3322–33.
18. Béraud C, Dormoy V, Danilin S, Lindner V, Béthry A, Hochane M, et al. Targeting FAK scaffold functions inhibits human renal cell carcinoma growth. Int J Cancer. 2015;137:1549–59.
19. Parsons JT. Focal adhesion kinase: the first ten years. J Cell Sci. 2003;116:1409–16.
20. Li D, Zhang Y, Zhang H, Zhan C, Li X, Ba T, et al. CADM2, as a new target of miR-10b, promotes tumor metastasis through FAK/AKT pathway in hepatocellular carcinoma. J Exp Clin Cancer Res. 2018;37:46.
21. Thamilselvan V, Craig DH, Basson MD. FAK association with multiple signal proteins mediates pressure-induced colon cancer cell adhesion via a Src-dependent PI3K/Akt pathway. FASEB J. 2007;21:1730–41.
22. von Sengbusch A, Gassmann P, Fisch KM, Enns A, Nicolson GL, Haier J. Focal adhesion kinase regulates metastatic adhesion of carcinoma cells within liver sinusoids. Am J Pathol. 2005;166:585–96.
23. Lai H, Zhao X, Qin Y, Ding Y, Chen R, Li G, et al. FAK-ERK activation in cell/matrix adhesion induced by the loss of apolipoprotein E stimulates the malignant progression of ovarian cancer. J Exp Clin Cancer Res. 2018;37:32.
24. Lim ST, Chen XL, Lim Y, Hanson DA, Vo TT, Howerton K, et al. Nuclear FAK promotes cell proliferation and survival through FERM-enhanced p53 degradation. Mol Cell. 2008;29:1–22.
25. Luo J, Yao JF, Deng XF, Zheng XD, Jia M, Wang YQ, et al. 14, 15 EET induces breast cancer cell EMT and cisplatin resistance by up-regulating integrinαvβ3 and activating FAK/PI3K/AKT signaling. J Exp Clin Cancer Res. 2018;37:23.
26. Schlaepfer DD, Mitra SK. Multiple connections link FAK to cell motility and invasion. Curr Opin Genet Dev. 2004;14:92–101.
27. Liu C, Qu L, Zhao C, Shou C. Extracellular gamma-synuclein promotes tumor cell motility by activating β1 integrin focal adhesion kinase signaling pathway and increasing matrix metalloproteinase-24, −2 protein secretion. J Exp Clin Cancer Res. 2018;37:117.
28. Golubovskaya VM, Ylagan L, Miller A, Hughes M, Wilson J, Wang D, et al. High focal adhesion kinase expression in breast carcinoma is associated with lymphovascular invasion and triple-negative phenotype. BMC Cancer. 2014;14:769.
29. Cance WG, Harris JE, Iacocca MV, Roche E, Yang X, Chang J, et al. Immunohistochemical analyses of focal adhesion kinase expression in benign and malignant human breast and colon tissues: correlation with preinvasive and invasive phenotypes. Clin Cancer Res. 2000;6:2417–23.
30. Agochiya M, Brunton VG, Owens DW, Parkinson EK, Paraskeva C, Keith WN, et al. Increased dosage and amplification of the focal adhesion kinase gene in human cancer cells. Oncogene. 1999;18:5646–53.
31. Lark AL, Livasy CA, Dressler L, Moore DT, Millikan RC, Geradts J, et al. High focal adhesion kinase expression in invasive breast carcinomas is associated with an aggressive phenotype. Mod Pathol. 2005;18:1289–94.
32. Golubovskaya VM. Focal adhesion kinase as a cancer therapy target. Anti Cancer Agents Med Chem. 2010;10:735–41.
33. Qiang YY, Li CZ, Sun R, Zheng LS, Peng LX, Yang JP, et al. Along with its favorable prognostic role, CLCA2 inhibits growth and metastasis of

nasopharyngeal carcinoma cells via inhibition of FAK/ERK signaling. J Exp Clin Cancer Res. 2018;37:34.

34. Walsh C, Tanjoni I, Uryu S, Tomar A, Nam JO, Luo H, et al. Oral delivery of PND-1186 FAK inhibitor decreases tumor growth and spontaneous breast to lung metastasis in pre-clinical models. Cancer Biol Ther. 2010;9:778–90.

35. Provenzano PP, Inman DR, Eliceiri KW, Beggs HE, Keely PJ. Mammary epithelial-specific disruption of focal adhesion kinase retards tumor formation and metastasis in a transgenic mouse model of human breast cancer. Am J Pathol. 2008;173:1551–65.

36. Lee BY, Timpson P, Horvath LG, Daly RJ. FAK signaling in human cancer as a target for therapeutics. Pharmacol Ther. 2015;146:132–49.

37. Prossnitz ER, Arterburn JB, Smith HO, Oprea TI, Sklar LA, Hathaway HJ. Estrogen signaling through the transmembrane G protein-coupled receptor GPR30. Annu Rev Physiol. 2008;70:165–90.

38. Prossnitz ER, Maggiolini M. Mechanisms of estrogen signaling and gene expression via GPR30. Mol Cell Endocrinol. 2009;308:32–8.

39. Prossnitz ER, Barton M. The G-protein-coupled estrogen receptor GPER in health and disease. Nat Rev Endocrinol. 2011;7:715–26.

40. Maggiolini M, Picard D. The unfolding stories of GPR30, a new membrane-bound estrogen receptor. J Endocrinol. 2010;204:105–14.

41. Cirillo F, Pellegrino M, Malivindi R, Rago V, Avino S, Muto L, et al. GPER is involved in the regulation of the estrogen-metabolizing CYP1B1 enzyme in breast cancer. Oncotarget. 2017;8:106608–24.

42. Lappano R, Maggiolini M. GPER is involved in the functional liaison between breast tumor cells and cancer-associated fibroblasts (CAFs). J Steroid Biochem Mol Biol. 2018;176:49–156.

43. De Marco P, Lappano R, De Francesco EM, Cirillo F, Pupo M, Avino S, et al. GPER signalling in both cancer-associated fibroblasts and breast cancer cells mediates a feedforward IL1β/IL1R1 response. Sci Rep. 2016;6:24354.

44. Rigiracciolo DC, Scarpelli A, Lappano R, Pisano A, Santolla MF, Avino S, et al. GPER is involved in the stimulatory effects of aldosterone in breast cancer cells and breast tumor-derived endothelial cells. Oncotarget. 2016;7:94–111.

45. Pandey DP, Lappano R, Albanito L, Madeo A, Maggiolini M, Picard D. Estrogenic GPR30 signalling induces proliferation and migration of breast cancer cells through CTGF. EMBO J. 2009;28:523–32.

46. Filardo EJ, Graeber CT, Quinn JA, Resnick MB, Giri D, DeLellis RA, et al. Distribution of GPR30, a seven membrane-spanning estrogen receptor, in primary breast cancer and its association with clinicopathologic determinants of tumor progression. Clin Cancer Res. 2006;12:6359–66.

47. Chaqour B, Yang R, Sha Q. Mechanical stretch modulates the promoter activity of the profibrotic factor CCN2 through increased actin polymerization and NF-kappaB activation. J Biol Chem. 2006;281:20608–222.

48. Lappano R, Rosano C, Santolla MF, Pupo M, De Francesco EM, De Marco P, et al. Two novel GPER agonists induce gene expression changes and growth effects in cancer cells. Curr Cancer Drug Targets. 2012;12:531–42.

49. Luo M, Guan JL. Focal adhesion kinase: a prominent determinant in breast cancer initiation, progression and metastasis. Cancer Lett. 2010; 289:127–39.

50. Yom CK, Noh DY, Kim WH, Kim HS. Clinical significance of high focal adhesion kinase gene copy number and overexpression in invasive breast cancer. Breast Cancer Res Treat. 2011;128:647–55.

51. Lightfoot HM Jr, Lark A, Livasy CA, Moore DT, Cowan D, Dressler L, et al. Upregulation of focal adhesion kinase (FAK) expression in ductal carcinoma in situ (DCIS) is an early event in breast tumorigenesis. Breast Cancer Res Treat. 2004;88:109–16.

52. Lim ST, Chen XL, Tomar A, Miller NL, Yoo J, Schlaepfer DD. Knock-in mutation reveals an essential role for focal adhesion kinase activity in blood vessel morphogenesis and cell motility-polarity but not cell proliferation. J Biol Chem. 2010;285:21526–36.

53. Mitra SK, Hanson DA, Schlaepfer DD. Focal adhesion kinase: in command and control of cell motility. Nat Rev Mol Cell Biol. 2005;6:56–68.

54. Giretti MS, Fu XD, De Rosa G, Sarotto I, Baldacci C, Garibaldi S, et al. Extra-nuclear signalling of estrogen receptor to breast cancer cytoskeletal remodelling, migration and invasion. PLoS One. 2008;3:e22–38.

55. Simoncini T, Scorticati C, Mannella P, Fadiel A, Giretti MS, Fu XD, et al. Estrogen receptor alpha interacts with Galpha13 to drive actin remodeling and endothelial cell migration via the RhoA/rho kinase/moesin pathway. Mol Endocrinol. 2006;20:1756–71.

56. Sanchez AM, Flamini MI, Zullino S, Gopal S, Genazzani AR, Simoncini T. Estrogen receptor-alpha promotes endothelial cell motility through focal adhesion kinase. Mol Hum Reprod. 2011;17:219–26.

57. Carnesecchi J, Malbouyres M, de Mets R, Balland M, Beauchef G, Vié K, et al. Estrogens induce rapid cytoskeleton re-organization in human dermal fibroblasts via the non-classical receptor GPR30. PLoS One. 2015;10: e0120672.

58. Jovanović B, Beeler JS, Pickup MW, Chytil A, Gorska AE, Ashby WJ, et al. Transforming growth factor beta receptor type III is a tumor promoter in mesenchymal-stem like triple negative breast cancer. Breast Cancer Res. 2014;16:R69.

59. Huang R, Rofstad EK. Integrins as therapeutic targets in the organ-specific metastasis of human malignant melanoma. J Exp Clin Cancer Res. 2018;37:92.

60. Sood AK, Coffin JE, Schneider GB, Fletcher MS, De Young BR, Gruman LM, et al. Biological significance of focal adhesion kinase in ovarian cancer: role in migration and invasion. Am J Pathol. 2004;165:1087–95.

61. Huang C, Yang G, Jiang T, Huang K, Cao J, Qiu Z. Effects of IL-6 and AG490 on regulation of Stat3 signaling pathway and invasion of human pancreatic cancer cells in vitro. J Exp Clin Cancer Res. 2010;29:51.

62. Pei G, Lan Y, Chen D, Ji L, Hua ZC. FAK regulates E-cadherin expression via p-SrcY416/p-ERK1/2/p-Stat3Y705 and PPARγ/miR-125b/Stat3 signaling pathway in B16F10 melanoma cells. Oncotarget. 2017;8:13898–908.

63. Xiao F, Connolly DC. FAK mediates STAT3 activation, migration and invasion in ovarian carcinoma cells. Cancer Res. 2014. https://doi.org/10.1158/1538-7445.

64. Visavadiya NP, Keasey MP, Razskazovskiy V, Banerjee K, Jia C, Lovins C, et al. Integrin-FAK signaling rapidly and potently promotes mitochondrial function through STAT3. Cell Commun Signal. 2016;14:32.

65. Hamilton DW, Jamshidi F, Brunette DM. Focal adhesion mediated intracellular signaling, Stat3 translocation and osteoblast differentiation: regulation by substratum topography. Mater Sci Eng Technol. 2009. https://doi.org/10.1002/mawe.200800370.

66. Li S, Wang B, Tang Q, Liu J, Yang X. Bisphenol A triggers proliferation and migration of laryngeal squamous cell carcinoma via GPER mediated upregulation of IL-6. Cell Biochem Funct. 2017;35:209–16.

67. Wang J, Xu J, An X, Lyu J. Estrogen activates GPER mediated IL-6/ STAT3 signaling pathway to enhance proliferation in breast cancer SKBR-3 cells. Journal of Third Military Medical University. 2015;4:340–5.

68. Madeo A, Maggiolini M. Nuclear alternate estrogen receptor GPR30 mediates 17β-estradiol - induced gene expression and migration in breast cancer–associated fibroblasts. Cancer Res. 2010;70:6036–46.

69. Vivacqua A, Romeo E, De Marco P, De Francesco EM, Abonante S, Maggiolini M. GPER mediates the Egr-1 expression induced by 17β-estradiol and 4-hydroxitamoxifen in breast and endometrial cancer cells. Breast Cancer Res Treat. 2012;133:1025–35.

70. Hauck CR, Hsia DA, Schlaepfer DD. The focal adhesion kinase-a regulator of cell migration and invasion. IUBMB Life. 2002;53:115–9.

71. Barbieri I, Pensa S, Pannellini T, Quaglino E, Maritano D, Demaria M, et al. Constitutively active Stat3 enhances neu-mediated migration and metastasis in mammary tumors via upregulation of Cten. Cancer Res. 2010; 70:2558–67.

72. Golubovskaya VM, Kweh FA, Cance WG. Focal adhesion kinase and cancer. Histol Histopathol. 2009;24:503–10.

73. Owens LV, Xu L, Craven RJ, Dent GA, Weiner TM, Kornberg L, et al. Overexpression of the focal adhesion kinase (p125FAK) in invasive human tumors. Cancer Res. 1995;55:2752–5.

74. Oktay MH, Oktay K, Hamele-Bena D, Buyuk A, Koss LG. Focal adhesion kinase as a marker of malignant phenotype in breast and cervical carcinomas. Hum Pathol. 2003;34:240–5.

75. Yoon H, Dehart JP, Murphy JM, Lim ST. Understanding the roles of FAK in cancer: inhibitors, genetic models, and new insights. J Histochem Cytochem. 2015;63:114–28.

76. Tai YL, Chen LC, Shen TL. Emerging roles of focal adhesion kinase in cancer. Biomed Res Int. 2015;2015:690690.

77. Mitra SK, Schlaepfer DD. Integrin-regulated FAK-Src signaling in normal and cancer cells. Curr Opin Cell Biol. 2006;18:516–23.

78. Sieg DJ, Hauck CR, Ilic D, Klingbeil CK, Schaefer E, Damsky CH, et al. FAK integrates growth-factor and integrin signals to promote cell migration. Nat Cell Biol. 2000;2:249–56.

79. Schlaepfer DD, Hou S, Lim ST, Tomar A, Yu H, Lim Y, et al. Tumor necrosis factor-alpha stimulates focal adhesion kinase activity required for mitogen-activated kinase-associated interleukin 6 expression. J Biol Chem. 2007;282:17450–9.

80.  Navarro-Tito N, Robledo T, Salazar EP. Arachidonic acid promotes FAK activation and migration in MDA-MB-231 breast cancer cells. Exp Cell Res. 2008;314:3340–55.

81.  Cohen-Hillel E, Mintz R, Meshel T, Garty BZ, Ben-Baruch A. Cell migration to the chemokine CXCL8: paxillin is activated and regulates adhesion and cell motility. Cell Mol Life Sci. 2009;66:884–99.

82.  Lappano R, Maggiolini M. G protein-coupled receptors: novel targets for drug discovery in cancer. Nat Rev Drug Discov. 2011;10:47–60.

83.  Pupo M, Pisano A, Abonante S, Maggiolini M, Musti AM. GPER activates notch signalling in breast cancer cells and cancer-associated fibroblasts (CAFs). Int J Biochem Cell Biol. 2014;46:56–67.

84.  De Francesco EM, Angelone T, Pasqua T, Pupo M, Cerra MC, Maggiolini M. GPER mediates cardiotropic effects in spontaneously hypertensive rat hearts. PLoS One. 2013;8:e69322.

85.  Tsai CL, Wu HM, Lin CY, Lin YJ, Chao A, Wang TH, et al. Estradiol and tamoxifen induce cell migration through GPR30 and activation of focal adhesion kinase (FAK) in endometrial cancers with low or without nuclear estrogen receptor α (ERα). PLoS One. 2013;8:e72999.

86.  Carpenter RL, Lo HW. STAT3 target genes relevant to human cancers. Cancers (Basel). 2014;6:897–925.

87.  Joo A, Aburatani H, Morii E, Iba H, Yoshimura A. STAT3 and MITF cooperatively induce cellular transformation through upregulation of c-fos expression. Oncogene. 2004;23:726–34.

88.  Alvarez JV, Febbo PG, Ramaswamy S, Loda M, Richardson A, Frank DA. Identification of a genetic signature of activated signal transducer and activator of transcription 3in human tumors. Cancer Res. 2005;65:5054–62.

89.  Gressner OA, Peredniene I, Gressner AM. Connective tissue growth factor reacts a san IL-6/STAT3-regulated hepatic negative acute phase protein. World J Gastroenterol. 2011;17:151–63.

90.  van Nimwegen MJ, van de Water B. Focal adhesion kinase: a potential target in cancer therapy. Biochem Pharmacol. 2007;73:597–609.

91.  Zhao X, Guan JL. Focal adhesion kinase and its signaling pathways in cell migration and angiogenesis. Adv Drug Deliv Rev. 2011;63:610–5.

92.  Hiscox S, Jordan NJ, Morgan L, Green TP, Nicholson RI. Src kinase promotes adhesion-independent activation of FAK and enhances cellular migration in tamoxifen-resistant breast cancer cells. Clin Exp Metastasis. 2007;24:157–67.

93.  Reiske HR, Kao SC, Cary LA, Guan JL, Lai JF, Chen HC. Requirement of phosphatidylinositol 3- kinase in focal adhesion kinase-promoted cell migration. J Biol Chem. 1999;274:12361–6.

94.  Sawhney RS, Liu W, Brattain MG. A novel role of ERK5 in integrin-mediated cell adhesion and motility in cancer cells via Fak signaling. J Cell Physiol. 2009;219:152–61.

95.  Carragher NO, Westhoff MA, Fincham VJ, Schaller MD, Frame MC. A novel role for FAK as a protease-targeting adaptor protein: regulation by p42 ERK and Src. Curr Biol. 2003;13:1442–50.

96.  Chen BH, Tzen JT, Bresnick AR, Chen HC. Roles of rho-associated kinase and myosin light chain kinase in morphological and migratory defects of focal adhesion kinase-null cells. J Biol Chem. 2002;277:33857–63.

97.  Wu X, Suetsugu S, Cooper LA, Takenawa T, Guan JL. Focal adhesion kinase regulation of N-WASP subcellular localization and function. J Biol Chem. 2004;279:9565–76.

98.  Serrels B, Serrels A, Brunton VG, Holt M, McLean GW, Gray CH, et al. Focal adhesion kinase controls actin assembly via a FERM-mediated interaction with the Arp2/3 complex. Nat Cell Biol. 2007;9:1046–56.

# GPER Mediates a Feedforward FGF2/FGFR1 Paracrine Activation Coupling CAFs to Cancer Cells toward Breast Tumor Progression

**Maria Francesca Santolla** [1] , **Adele Vivacqua** [1], **Rosamaria Lappano** [1],
**Damiano Cosimo Rigiracciolo** [1], **Francesca Cirillo** [1], **Giulia Raffaella Galli** [1], **Marianna Talia** [1],
**Giuseppe Brunetti** [2] , **Anna Maria Miglietta** [3], **Antonino Belfiore** [4] **and Marcello Maggiolini** [1,*]

[1]   Department of Pharmacy, Health and Nutritional Sciences, University of Calabria, 87036 Rende, Italy;
      mariafrancesca.santolla@unical.it (M.F.S.); adele.vivacqua@unical.it (A.V.);
      rosamaria.lappano@unical.it (R.L.); damianorigiracciolo@yahoo.it (D.C.R.); francesca.cirillo@unical.it (F.C.);
      giulia.r.galli@gmail.com (G.R.G.); mariannatalia11@gmail.com (M.T.)
[2]   University of Natural Resources and Life Sciences, 1180 Vienna, Austria; giusep.bru@gmail.com
[3]   Regional Hospital, 87100 Cosenza, Italy; annamariamiglietta@virgilio.it
[4]   Endocrinology, Department of Clinical and Experimental Medicine, University of Catania, Garibaldi-Nesima
      Hospital, 95122 Catania, Italy; antonino.belfiore@unict.it
[*]   Correspondence: marcellomaggiolini@yahoo.it or marcello.maggiolini@unical.it

**Abstract:** The FGF2/FGFR1 paracrine loop is involved in the cross-talk between breast cancer cells and components of the tumor stroma as cancer-associated fibroblasts (CAFs). By quantitative PCR (qPCR), western blot, immunofluorescence analysis, ELISA and ChIP assays, we demonstrated that 17β-estradiol (E2) and the G protein estrogen receptor (GPER) agonist G-1 induce the up-regulation and secretion of FGF2 via GPER together with the EGFR/ERK/c-fos/AP-1 signaling cascade in (ER)-negative primary CAFs. Evaluating the genetic alterations from METABRIC and TCGA datasets, we then assessed that FGFR1 is the most frequently amplified FGFRs family member and its amplification/expression associates with shorter survival rates in breast cancer patients. Therefore, in order to assess the functional FGF2/FGFR1 interplay between CAFs and breast cancer cells, we generated the FGFR1-knockout MDA-MB-231 cells using CRISPR/Cas9 genome editing strategy. Using conditioned medium from estrogen-stimulated CAFs, we established that the activation of FGF2/FGFR1 paracrine signaling triggers the expression of the connective tissue growth factor (CTGF), leading to the migration and invasion of MDA-MB-231 cells. Our findings shed new light on the role elicited by estrogens through GPER in the activation of the FGF2/FGFR1 signaling. Moreover, our findings may identify further biological targets that could be considered in innovative combination strategies halting breast cancer progression.

**Keywords:** cancer-associated fibroblasts; GPER; breast cancer; estrogen; FGFR1; FGF2

## 1. Introduction

Cross-talk between stromal and epithelial cells plays an important role in diverse pathophysiological conditions, including malignant diseases [1–3]. In this regard, it has been largely reported that the acquisition of an aggressive phenotype does not depend exclusively on the intrinsic cancer cell properties, but also on stromal features [4]. For instance, cancer-associated fibroblasts (CAFs), one of the most abundant cell types within the tumor microenvironment, coordinate a multifaceted biochemical program that promotes cancer cell proliferation, migration, invasion, epithelial-mesenchymal transition (EMT), and angiogenesis [5]. Indeed, it has been shown that paracrine

mediators secreted by CAFs, such as cytokines and growth factors, exert an important role in the acquisition of malignant features [6,7].

The fibroblast growth factor (FGF)-FGF receptor (FGFR) axis is one of the major signal transduction pathways mediating the interaction between tumor stroma and cancer cells [8,9]. FGFRs family includes four highly conserved transmembrane receptor tyrosine kinases (FGFR1-4) and one receptor that binds to FGF ligands, although it lacks the intracellular kinase domain (FGFR5, also known as FGFRL1) [10]. FGFRs can be activated either in an autocrine fashion by FGFs produced by the tumor cells or in a paracrine manner by FGFs secreted by the stromal components [11]. The activation of FGFRs triggers the phosphorylation of extracellular signal-regulated kinase (ERK), phosphatidylinositol 3-kinase (PI3K), and other transduction pathways, regulating many physiological processes including embryogenesis, tissue homeostasis, and angiogenesis [12,13]. Abnormal activation of the FGFR1-mediated signaling pathway can be caused by translocation, point mutation and amplification of the FGFR1 gene, hence leading to malignant transformation and cancer progression [9,14,15]. Likewise, increased FGF2 levels have been observed in plasma samples of patients affected by diverse malignancies, such as leukemia and lung and breast cancers, especially when metastases are present [16,17]. Among diverse stimuli, FGF2 expression and secretion can be regulated by estrogens [18,19], which act mainly through the classical estrogen receptors (ER)$\alpha$ and ER$\beta$ leading to the proliferation, migration and survival of breast cancer cells [20]. The G protein estrogen receptor (GPER, also called GPR30) has been identified as a further receptor able to mediate the action of estrogens in numerous pathophysiological conditions [21,22]. GPER activation induces a network of signal transduction pathways including activation of the epidermal growth factor receptor (EGFR), intracellular cyclic adenosine monophosphate (AMP) accumulation, calcium mobilization, activation of ERK1/2 and PI3K [23]. Moreover, GPER triggers the expression of various genes involved in the growth and migration of diverse estrogen-responsive tumors [24–27]. Of note, the stimulatory action mediated by estrogenic GPER signaling has been also evidenced in breast primary CAFs revealing the existence of a functional cooperation between these important components of the tumor stroma and cancer cells [28–31]. Recent studies have shown that a functional interaction between ER and FGFR-mediated pathways may occur toward breast cancer progression, indicating that the simultaneous inhibition of both receptors could be considered in more comprehensive treatments [11,32,33]. GPER was also involved in the estrogen-induced regulation of FGF2 toward the autocrine stimulation of the cognate receptor FGFR1 in astroglial cells [19].

Here, we provided novel insights into the ability of estrogens to regulate a feedforward FGF2/FGFR1 activation between the ER-negative CAFs and breast cancer cells. On the basis of our findings, GPER may be included among the factors facilitating the estrogen-activated cross-talk within the tumor microenvironment toward breast tumor progression.

## 2. Materials and Methods

### 2.1. Reagents

We purchased (1-[4-(-6-bromobenzol [1,3] diodo-5-yl)-3a,4,5,9b-tetrahidro3H5cyclopenta[c] quinolin-8yl]-ethanone) (G-1), (3aS,4R,9bR)-4-(6-Bromo-1, 3-benzodioxol-5-yl)-3a,4,5,9b-3H-cyclopenta [c]quinolone (G15) from Tocris Bioscience (Space, Milan, Italy); 17$\beta$-Estradiol (E2), Wortmannin (WM) from Sigma-Aldrich (Milan, Italy); PD173074 from Selleckchem (DBA, Milan, Italy); PD98059 from Calbiochem (DBA, Milan, Italy); tyrphostin AG1478 from Biomol Research Laboratories (Milan, Italy) and recombinant human Fibroblast Growth Factor (FGF2) 100-18B, from PEPROTECH (SIAL, Rome, Italy). All compounds were solubilized in dimethyl sulfoxide (DMSO), except for FGF2, which was dissolved in aqueous buffer (0.1% BSA).

## 2.2. Cell Cultures

MDA-MB-231, MCF-7, and SkBr3 breast cancer cells were obtained from the ATCC (Manassas, USA). MDA-MB-231 and MCF-7 cells were maintained in DMEM/F12 (Life Technologies, Milan, Italy), 10% fetal bovine serum (FBS) and 1% of penicillin/streptomycin, while SkBr3 cells were maintained in RPMI-1640 (Life Technologies, Milan, Italy), 10% fetal bovine serum (FBS), and 1% of penicillin/streptomycin (Life Technologies, Milan, Italy). Cells were used less than six months after resuscitation and mycoplasma negativity was tested monthly. CAFs were extracted from invasive mammary ductal carcinomas obtained from mastectomies, while normal fibroblasts (NFs) were isolated from a non-cancerous breast tissue at least 2 cm from the outer tumor margin, as previously described [25,28,34]. Primary cells cultures of breast fibroblasts were characterized by immunofluorescence. Cells were incubated with anti-vimentin (V9, sc-6260), anti-cytokeratin 14 (LL001 sc-53,253) and anti-fibroblast activated protein $\alpha$ (FAP$\alpha$) (H-56) antibodies that were obtained from Santa Cruz Biotechnology (DBA, Milan, Italy) (Supplementary Figure S1). All cells were grown in a 37 °C incubator with 5% $CO_2$ and switched to medium without serum and phenol red the day before treatments to be processed for immunoblot and quantitative PCR (qPCR) assays.

## 2.3. Gene Expression Studies

Total RNA was extracted and complementary DNA (cDNA) was synthesized by reverse transcription as described in our previous work [35]. Quantitative PCR (qPCR) assays were performed using platform Quant Studio7 Flex Real-Time PCR System (Life Technologies, Milan, Italy). Gene-specific primers were designed using Primer Express version 2.0 software (Applied Biosystems). For FGF2, FGFR1, c-fos, CTGF and the ribosomal protein 18S, which was used as a control gene to obtain normalized values, the primers were: 5′-AGTGTGTGCTAACCGTTACCT-3′ (FGF2 forward) and 5′-ACTGCCCAGTTCGTTTCAGTG-3′ (FGF2 reverse); 5′- CCCGTAGCTCCATATTGGACA-3′ (FGFR1 forward) and 5′- TTTGCCATTTTTCAACCAGCG-3′ (FGFR1 reverse); 5′-CGAGCCCTTTGATGACT TCCT-3′ (c-fos forward) and 5′-GGAGCGGGCTGTCTCAGA-3′ (c-fos reverse); 5′-ACCTGTGGGATG GGCATCT-3′ (CTGF forward) and 5′-CAGGCGGCTCTGCTTCTCTA-3′ (CTGF reverse); 5′- GGCGT CCCCCAACTTCTTA-3′ (18S forward) and 5′-GGGCATCACAGACCTGTTATT-3′ (18S reverse). Assays were performed in triplicate and the results were normalized with control mRNA levels of 18S. Relative mRNA levels were calculated using the $^{\Delta\Delta}$Ct method comparing to control group.

## 2.4. Gene silencing Experiments and Plasmids

Cells were transfected by X-treme GENE 9 DNA Transfection Reagent (Roche Diagnostics, Sigma-Aldrich, Milan, Italy) for 24 h before treatments with a control vector and a specific shRNA sequence for each target gene. The short hairpin (sh)RNA constructs to knock down the expression of GPER and CTGF, and the unrelated shRNA control constructs have been described previously [24,30,36]. The plasmid DN/c-fos, which encodes for c-fos mutant that heterodimerizes with c-fos dimerization partners but does not allow DNA binding, was a kind gift from Dr C. Vinson (NIH, Bethesda, MD, USA).

## 2.5. CRISPR/Cas9-Mediated FGFR1 Knockout

Short guide RNA (sgRNA) sequence targeting human FGFR1 was designed using the E-CRISP sgRNA Designer (http://www.e-crisp.org/E-CRISP/) and cloned into the pSpCas9 (BB)-2A-Puro (PX459) vector (kindly provided by Dr. W.T. Khaled, University of Cambridge, UK) according to the protocol described in Ran et al. [37]. The *FGFR1* sgRNA sequence is as follows: *sgFGFR1*: 5′-CGGCCTAGCGGTGCAGAGTG-3′. Then, the plasmid with sgRNA was transiently transfected into MDA-MB-231 cells using Lipofectamine LTX (Life Technologies, Milan Italy). Two days after transfection the cells were selected via growth in a medium contained 1 μg/mL puromycin dihydrochloride (Sigma-Aldrich, Milan, Italy). After puromycin selection, the puromycin-resistant

colonies were picked and expanded in regular medium. Then, immunoblots for FGFR1 protein were performed to evaluate the efficiency of the FGFR1 knockout.

### 2.6. Immunofluorescence Microscopy

50% percent confluent cultured grown on coverslips were serum deprived for 24 h and then treated for 6 h with E2 and G-1 alone and in combination with G15, as indicated. Where required, cells were previously transfected for 24 h with shRNA or shGPER (as described above) and then treated for 6 h with E2 and G-1. Next, cells were fixed in 4% paraformaldehyde in PBS, permeabilized with 0.2% Triton X-100, washed 3 times with PBS and incubated at 4 °C overnight with a mouse primary antibody against FGF2 (C-2) (Santa Cruz Biotechnology, DBA, Milan, Italy). After incubation, the slides were extensively washed with PBS, probed with donkey anti-mouse IgG-FITC (1:300; purchased from Alexa Fluor, Life Technologies, Milan Italy) and 4, 6-diamidino-2-phenylindole dihydrochloride (DAPI) (1:1000; Sigma-Aldrich, Milan, Italy). Then, the images were obtained using the Cytation 3 Cell Imaging Multimode reader (BioTek, AHSI, Milan Italy) and analyzed by the Gen5 software (BioTek, AHSI, Milan Italy).

### 2.7. Conditioned Medium Derived from CAFs

CAFs were cultured in regular growth medium, then washed twice with PBS and transferred in medium without serum for 24 h. Next, CAFs were treated for 6 h with E2 and G-1 alone and in combination with G15, as indicated; then, cells were washed twice with PBS and cultured for additional 12 h with fresh serum-free medium. Thereafter, the supernatants were collected, centrifuged at 3500 rpm for 5 min to remove cell debris and used as conditioned medium in the appropriate experiments.

### 2.8. Western Blot Analysis

CAFs and MDA-MB-231 cells were processed to obtain protein lysates for western blot analysis as previously described [29]. Primary antibodies were as follows: GPER (AB137479) (Abcam, Euroclone Milan, Italy); CTGF (TA806803) (OriGene Technologies, DBA, Milan, Italy); FGFR1 (#9740) and p-FGFR1 (#3476) (CST, Euroclone Milan, Italy); c-fos (E8), phosphorylated extracellular signal-regulated kinase (ERK) (E-4), ERK2 (C-14), p-AKT1/2/3 (Ser 473)-R, AKT/1/2/3 (H-136) and β-actin (AC-15) (Santa Cruz Biotechnology, DBA, Milan, Italy). Proteins were detected by horseradish peroxidase-linked secondary antibodies (Biorad, Milan, Italy) and revealed using the chemiluminescent substrate for western blotting Westar Nova 2.0 (Cyanagen, Biogenerica, Catania, Italy).

### 2.9. Enzyme-Linked Immunosorbent Assay

The concentrations of FGF2 in conditioned medium collected from CAFs were measured using human FGF2 ELISA Kit (Thermo Fisher Scientific, Monza Italy), according to the manufacturer's instructions. Briefly, after incubation with conditioned media for 2 h at room temperature (RT), the plates were washed four times using 1X wash buffer, then 100 μL Hu FGF2 Biotin conjugate solution were added into each well, except the chromogen blanks, for 1 h at RT. Next, the plates were washed four times using 1X wash buffer and then 100 μL 1X Streptavidin-HPR solution were added into each well for 30 min at RT. Following incubation, plates were washed four times using 1X wash buffer and a colour-substrate solution was added to each well. After incubation in the dark for 30 min at RT, 100 μL of stop solution was used to stop reaction. Then, the plates were read at 450 nm on a Microplate Spectrophotometer Epoch™ (BioTek, AHSI, Milan Italy).

### 2.10. Chromatin Immunoprecipitation (ChIP) Assay

Chip experiments were performed as previously described [29]. The primers used to amplify a region containing an AP-1 site located into the FGF2 promoter sequence were: 5′-GTTTCTA CAAGGAGGCACGTC-3′ (Fw) and 5′-GAGATGCCAAATCTGATGCCA-3′ (Rv). qPCR data were normalized respect to unprocessed lysates (Input DNA) and the results were reported as fold changes respect to nonspecific IgG.

### 2.11. Analysis of Public Datasets from METABRIC and TCGA and Kaplan-Meier Plotter

Images of genomic alterations in Molecular Taxonomy of Breast Cancer International Consortium (METABRIC) and The Cancer Genome Atlas (TCGA) databases were captured from cBioPortal (http://www.cbioportal.org) [38,39]. Prognostic values of mRNA expression or copy-number (CN) gains of FGFR1 from METABRIC [40,41] breast cancer samples were analyzed by Kaplan-Meier survival curves. Long-rank test was used for statistical analysis. The mRNA expression z-Scores of FGFR1 and CTGF were retrieved from METABRIC [40,41] breast cancer samples analyzed for gene expression using Illumina Human v3 microarray. Data were processed using the Python programming language to identify correlation patterns among different genes. In particular, pairwise linear regressions of mRNA levels between FGFR1 and CTGF were calculated. The Pearson correlation coefficients measured the magnitude of the linear relationship between genes.

### 2.12. Polarization Assay

FGFR1 (WT) and FGFR1 (KO) MDA-MB-231 cells were serum deprived for 24 h and then exposed for 8 h to conditioned media collected from CAFs or to FGF2, as indicated. Then cells were processed as previously described [28,42].

### 2.13. Scratch Assay

FGFR1 (WT) and FGFR1 (KO) MDA-MB-231 cells were seeded into 12-well plates and they were allowed to grow in regular growth medium until they were 70–80% confluent. Next, cells were switched in medium without serum and after 24 h a p200 pipette tip was used to create a scratch of the cell monolayer. Cells were washed twice with PBS and then incubated at 37 °C with conditioned media collected from CAFs or with FGF2 for 24 h, as indicated. Pictures were photographed at 0 h and 24 h after scratching using inverted phase contrast microscope (5×magnification). The rate of cell migration was calculated by quantifying the % of wound closure area using the WCIF ImageJ software, according to the formula:

$$\% \text{ of wound closure} = [(At = 0 \text{ h}) - (At = \Delta \text{ h}) / (At = 0 \text{ h})] \times 100\%$$

### 2.14. Transwell Migration and Invasion Assays

Transwell 8 μm polycarbonate membrane (Costar, Sigma-Aldrich, Milan, Italy) was used to evaluate in vitro migration and invasion of FGFR1 (WT) and FGFR1 (KO) MDA-MB-231 cells. $5 \times 10^4$ cells in 300 μL serum-free medium were seeded in the upper chamber, coated with (invasion assay) or without (migration assay) Corning® Matrigel® Growth Factor Reduced (GFR) Basement Membrane Matrix (Biogenerica, Catania, Italy) at a 1:3 dilution. Medium containing 10% FBS was then added into the lower chamber as a chemoattractant. 4 h after seeding, cells on the upper surface of the membrane were removed by wiping with Q-tip, and invaded or migrated cells were fixed with 100% methanol, stained with Giemsa (Sigma-Aldrich, Milan, Italy), photographed using Cytation 3 Cell Imaging Multimode Reader (BioTek, AHSI, Milan Italy) and counted using the WCIF ImageJ software.

### 2.15. Statistical Analysis

Data were analyzed by one-way ANOVA with Dunnett's multiple comparisons, where applicable, using GraphPad Prism, 6.01 (GraphPad Software, Inc., San Diego, CA, USA). (*) $p < 0.05$ and (**) $p < 0.01$ were considered statistically significant.

### 2.16. Ethics Approval and Consent to Participate

All procedures are conformed to the Helsinki Declaration for the research on humans. Signed informed consent was obtained from all patients and the experimental research has been performed with the ethical approval provided by the "Comitato Etico Regione Calabria, Cosenza, Italy" (approval code: 166, 2 December 2016).

## 3. Results

### 3.1. GPER Mediates the Induction of FGF2 Expression by E2 and G-1 in Breast Cancer-Associated Fibroblasts (CAFs)

Previous studies have shown that estrogens acting either through ER or GPER up-regulate FGF2 expression and secretion in both normal and cancer cells [19,32,43]. In order to provide novel insights into the FGF2 regulation by estrogens within the tumor microenvironment, we sought to address whether estrogens may regulate FGF2 levels in ER-negative/ GPER-positive CAFs isolated from breast tumor patients (see material and methods section). Worthy of note, both E2 and G-1 induced the expression of FGF2 at the mRNA (Figure 1a,b) and protein levels (Figure 1c) in CAFs. However, the response to E2 and G-1 was no longer observed after GPER silencing (Figure 1d, Supplementary Figure S2) or using the GPER antagonist G15 (Figure 2a,b). In contrast, E2 and G-1 were not able to elicit FGF2 up-regulation in fibroblasts derived from noncancerous breast tissue (data not shown). By performing ELISA experiments, we then observed that the secretion of FGF2 in CAFs medium upon treatments with E2 and G-1 is abrogated treating cells with the GPER antagonist G15 (Figure 2c). As GPER activation induces the stimulation of diverse transduction pathways [23], we also found that FGF2 up-regulation prompted by E2 and G-1 was prevented either by the EGFR tyrosine kinase inhibitor AG1478 (AG) or the MEK inhibitor PD98059 (PD), but not by the PI3K inhibitor Wortmannin (WM) (Supplementary Figure S3a,b). Taken together, these findings indicate that, in CAFs, both E2 and G-1 induce FGF2 expression through the GPER-EGFR-ERK1/2 signaling cascade.
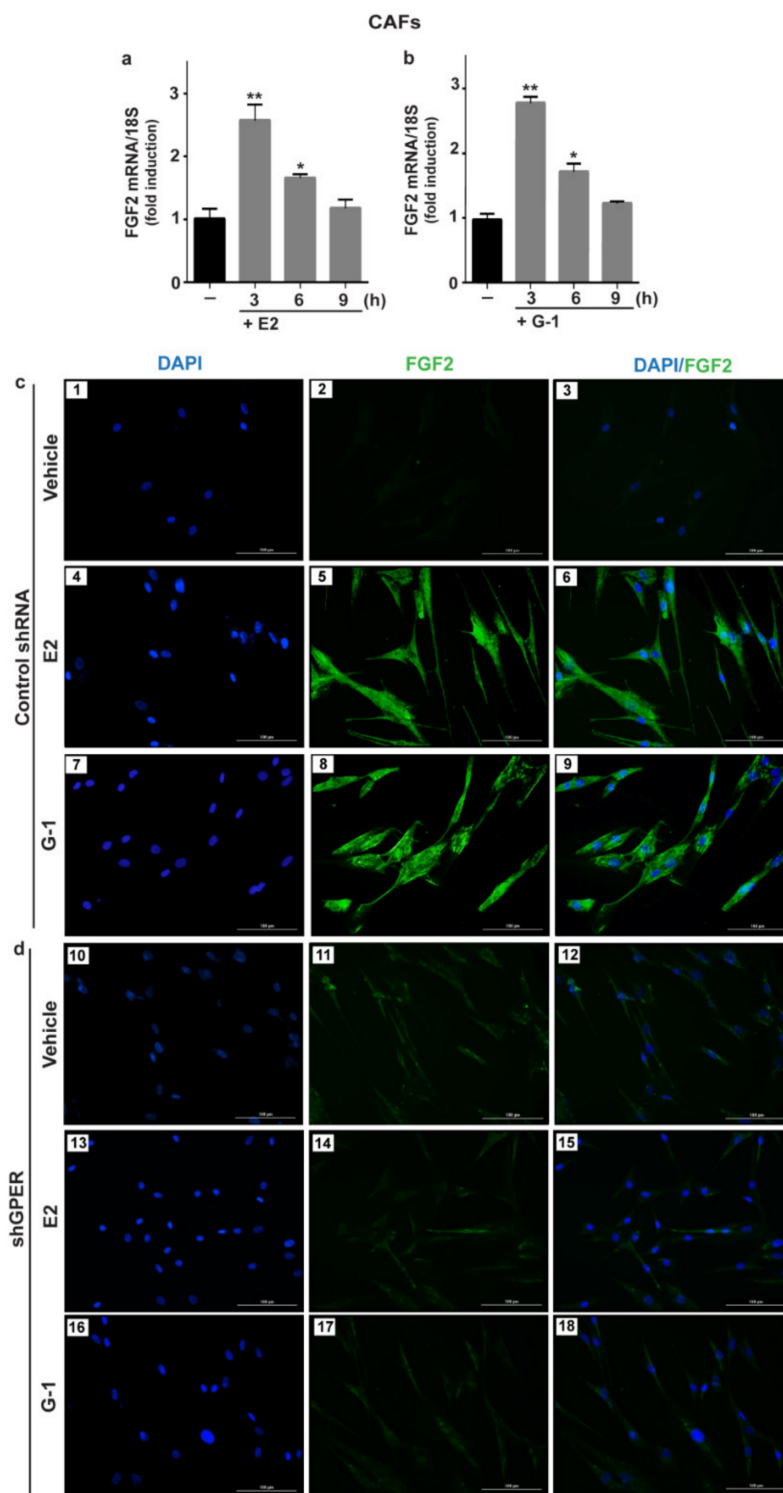
**Figure 1.** E2 and G-1 induce FGF2 expression through GPER in CAFs. 10 nM E2 (**a**) and 100 nM G-1 (**b**) induced FGF2 mRNA expression, as evaluated by quantitative PCR (qPCR). Values were normalized to 18S expression and shown as fold changes of FGF2 mRNA expression upon E2 and G-1 treatments respect to cells exposed to vehicle (). Each column represents the mean ± standard deviation (SD) of three independent experiments performed in triplicate. (**) indicates $p < 0.01$ and (*) indicates $p < 0.05$. (**c,d**) FGF2 protein expression by immunofluorescence in CAFs transfected for 24 h with control shRNA (panels 1–9) or sh G protein estrogen receptor (shGPER) (panels 10–18) and then treated for 6 h with vehicle, 10 nM E2 and 100 nM G-1, as indicated. FGF2 accumulation is shown by the green signal, nuclei are stained by 4, 6-diamidino-2-phenylindole dihydrochloride (DAPI) (blue signal), scale bar = 100 μm. Images shown are representative of two independent experiments.
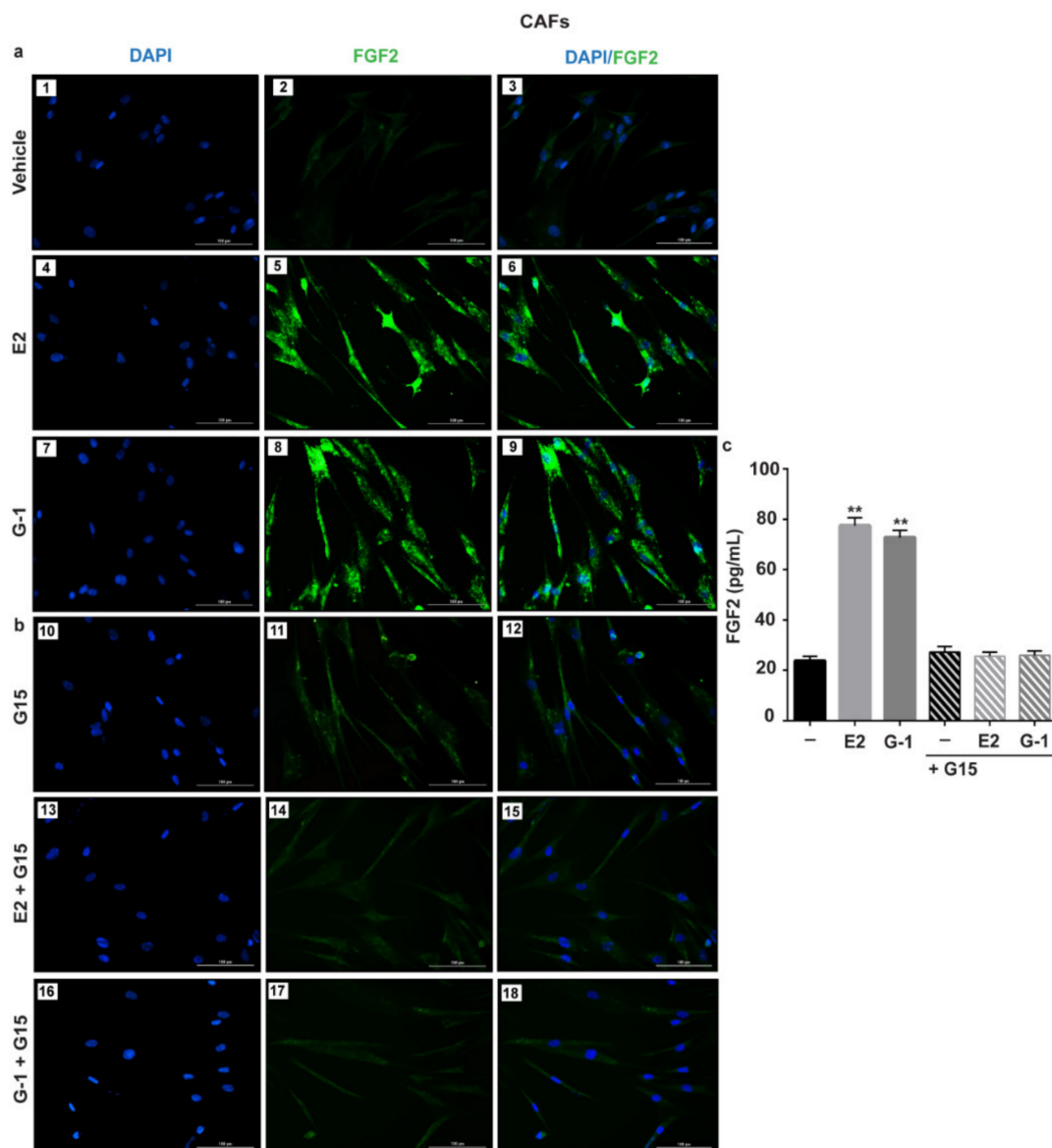
**Figure 2.** GPER mediates the up-regulation and the secretion of FGF2 by E2 and G-1 in CAFs. FGF2 protein expression by immunofluorescence in CAFs treated for 6 h with vehicle, 10 nM E2 and 100 nM G-1, alone (panels 1–9) (**a**) and in combination with 100 nM GPER antagonist G15 (panels 10–18) (**b**). FGF2 accumulation is shown by the green signal, nuclei are stained by DAPI (blue signal), scale bar = 100 μm. Images shown are representative of two independent experiments. (**c**) ELISA of FGF2 levels in supernatants collected from CAFs treated for 18 h with vehicle (-), 10 nM E2 and 100 nM G-1 alone and in combination with 100 nM GPER antagonist G15. Each column represents the mean ±SD of three independent experiments performed in triplicate. (**\*\***) indicates $p < 0.01$.

### 3.2. c-fos is Involved in the FGF2 up-Regulation Induced by Estrogenic GPER Signaling in CAFs

As the activation of GPER-EGFR-ERK1/2 transduction pathway leads to c-fos expression [22,29], we determined c-fos response at both mRNA and protein levels upon E2 and G-1 exposure in CAFs (Figure 3a–c). Then, we established that both ligands trigger the recruitment of c-fos to the AP-1 site located within the FGF2 promoter region (Figure 3d,e). Further supporting these results, the up-regulation of FGF2 protein expression induced by E2 and G-1 was prevented transfecting CAFs with a dominant negative form of c-fos (DN/c-fos) (Figure 3f,g). Collectively, the abovementioned findings suggest that, in CAFs, GPER along with the EGFR-ERK1/2-c-fos-AP-1 signaling pathway mediates FGF2 expression in response to E2 or G-1.
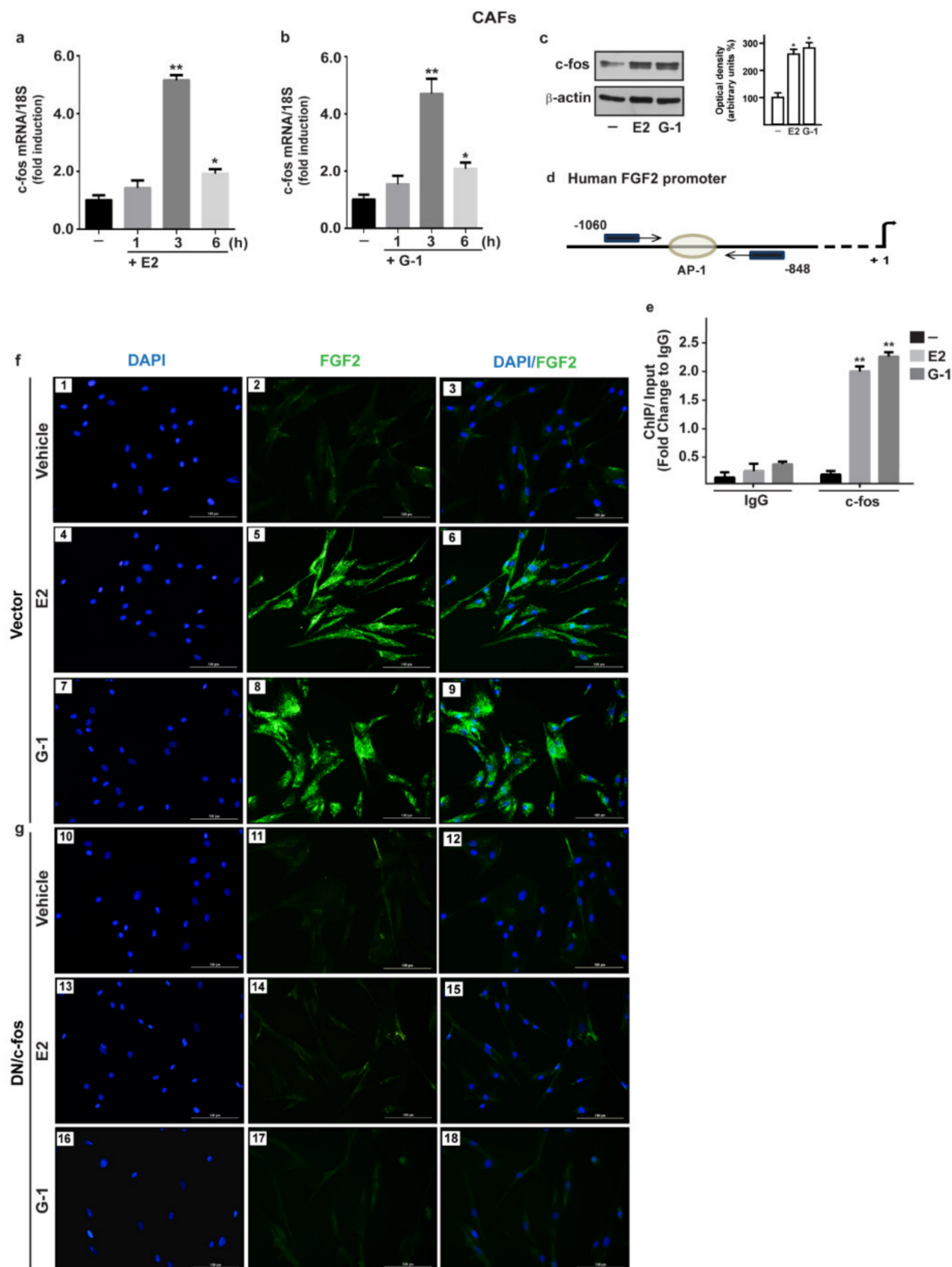
**Figure 3.** The oncogene fos (c-fos) is involved in the up-regulation of FGF2 by E2 and G-1 in CAFs. 10 nM E2 (**a**) and 100 nM G-1 (**b**) induced c-fos mRNA expression, as evaluated by qPCR. Values were normalized to 18S expression and shown as fold changes of c-fos mRNA expression upon E2 and G-1 treatments respect to cells exposed to vehicle (-). (**c**) The treatment for 3 h with 10 nM E2 and 100 nM G-1 up-regulated c-fos protein, which is recruited to the AP-1 site located within the FGF2 promoter region (-1060/-848; the transcriptional start site is indicated as + 1), as ascertained by Chromatin Immunoprecipitation (ChIP)-qPCR assay (**d**,**e**). Data were normalized to the input and reported as fold changes respect to Immunoblobulin G (IgG). Each column represents the mean ±SD of three independent experiments performed in triplicate. In immunoblot experiments β-actin served

as a loading control, side panels show densitometric analysis of the blot normalized to the loading control. (*) indicates $p < 0.05$ and (**) indicates $p < 0.01$. (**f**) FGF2 protein expression by immunofluorescence in CAFs transfected for 18 h with a vector (panels 1–9), or (**g**) with a construct encoding for a dominant negative form of c-fos (DN/c-fos) (panels 10–18) and then treated for 6 h with vehicle, 10 nM E2 and 100 nM G-1, as indicated. FGF2 accumulation is evidenced by the green signal, nuclei are stained by DAPI (blue signal), scale bar = 100 μm. Images shown are representative of two independent experiments.

## 3.3. Conditioned Medium (CM) from Estrogens-Stimulated CAFs Activates the FGFR1-ERK1/2-AKT Transduction Pathway in MDA-MB-231 Cells

Previous studies have shown that the activation of the FGF2-FGFR1 autocrine and/or paracrine loop plays an important role toward the migration and invasion of cancer cells [44–46]. Moreover, FGFR1 has been found highly amplified in breast cancer patients and associated with endocrine resistance [11,14]. In accordance with these observations, a large-scale genomic analysis of METABRIC and TCGA databases allowed us to assess not only that FGFR1 represents the most amplified receptor of the FGFRs family members but also that FGFR1 amplification occurs in nearly 14% of breast cancer patients (Figure 4a,b) [38,39]. Of note, breast cancer patients with either higher expression or copy number (CN) gains of FGFR1 are associated with shorter overall survival rates respect to the rest of the cohort (Figure 4c,d). Taken into account the aforementioned results, we focused on FGF2-FGFR1 signaling in the context of paracrine communication between CAFs and breast cancer cells. In this vein, we used MDA-MB-231 cells as model system because these cells did not express FGF2 [47], but rather displayed high expression levels of FGFR1 (Supplementary Figure S4). In order to better investigate the role of FGFR1 in our experimental model, we used CRISPR/Cas9 genome editing technology to generate FGFR1 knockout (KO) MDA-MB-231 cell line (Figure 4e,f). Given that both E2 and G-1 stimulate the expression and the secretion of FGF2 in CAFs (see Figure 1; Figure 2), we then ascertained that CM from E2 and G-1 treated-CAFs induces FGFR1 phosphorylation in MDA-MB-231 cells, as well as the stimulation of the two main pathways downstream FGFR1 activation, such as ERK1/2 and AKT [11,48] (Figure 5a–c). Next, in parallel experiments, the FGFR1 inhibitor PD173074 was found to abolish both ERK1/2 and AKT phosphorylation (Figure 5a–c). Accordingly, CM obtained from E2 and G-1 treated-CAFs did not induce ERK1/2 and AKT activation in FGFR1 (KO) MDA-MB-231 cells (Figure 5d–g).
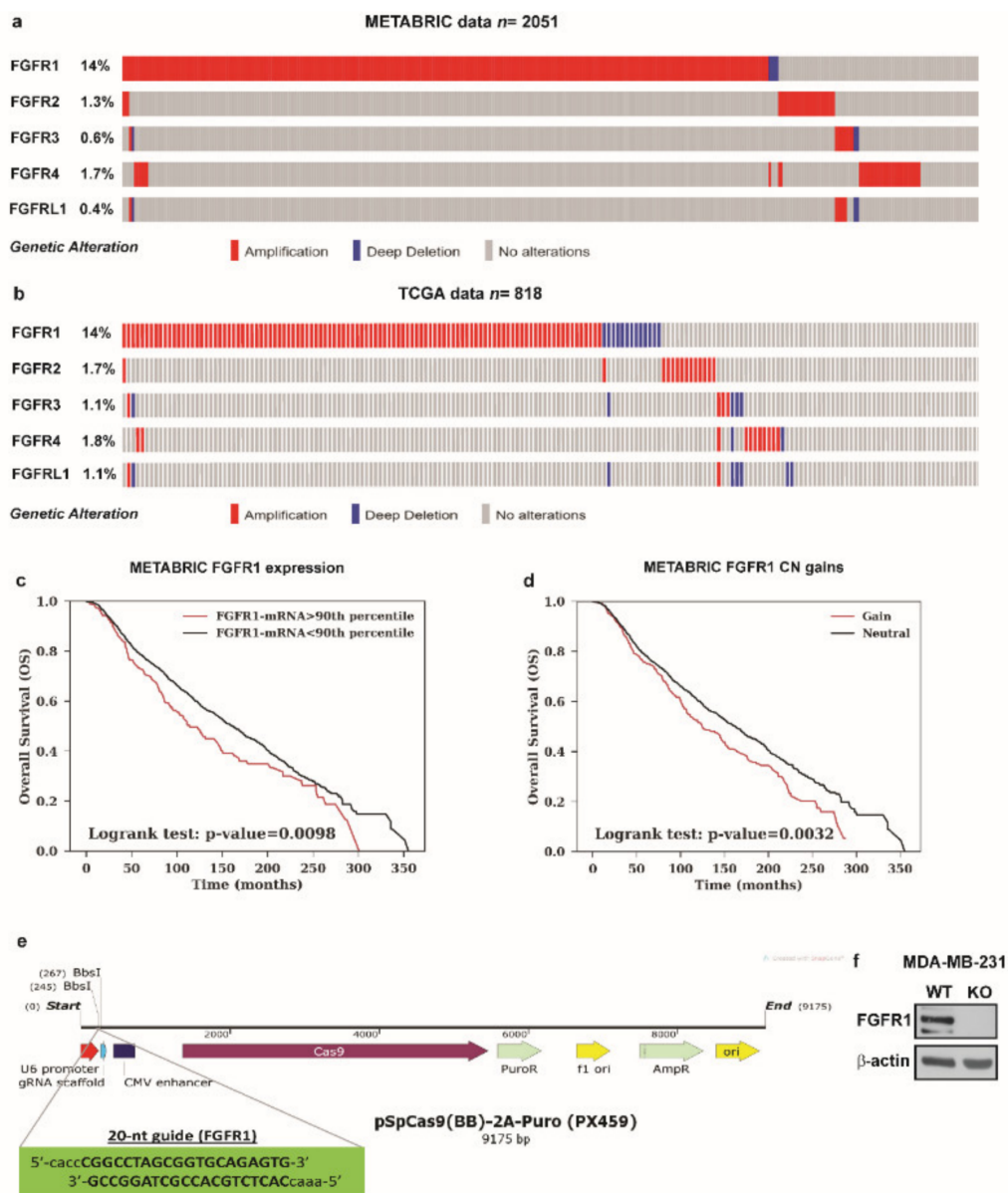
**Figure 4.** Analysis of METABRIC and TCGA datasets and CRISPR/Cas9-mediated FGFR1 knockout (KO) in MDA-MB-231 cells. (**a**,**b**) The OncoPrint of genomic alteration of FGFRs members showed that FGFR1 is the most amplified receptor of the family in human breast cancer patients. Each row represents a gene and each column represents a tumor sample. Red bars indicate gene amplifications, blue bars deep deletions and grey bars no alterations. (**c**,**d**) Kaplan-Meir plots show the overall survival (OS) from METABRIC dataset between patients with normal or high FGFR1 mRNA expression or between patients with copy number (CN) gains or without (neutral). Statistical analysis was performed using the long-rank test. (**e**) Schematic representation of the pX459 plasmid and the sgRNA sequence used to generate FGFR1 (KO) MDA-MB-231 cells. (**f**) Immunoblots of lysates generated from FGFR1 (WT) and FGFR1 (KO) MDA-MB-231 cells. β-actin served as loading control. Immunoblots shown are representative of three independent experiments.
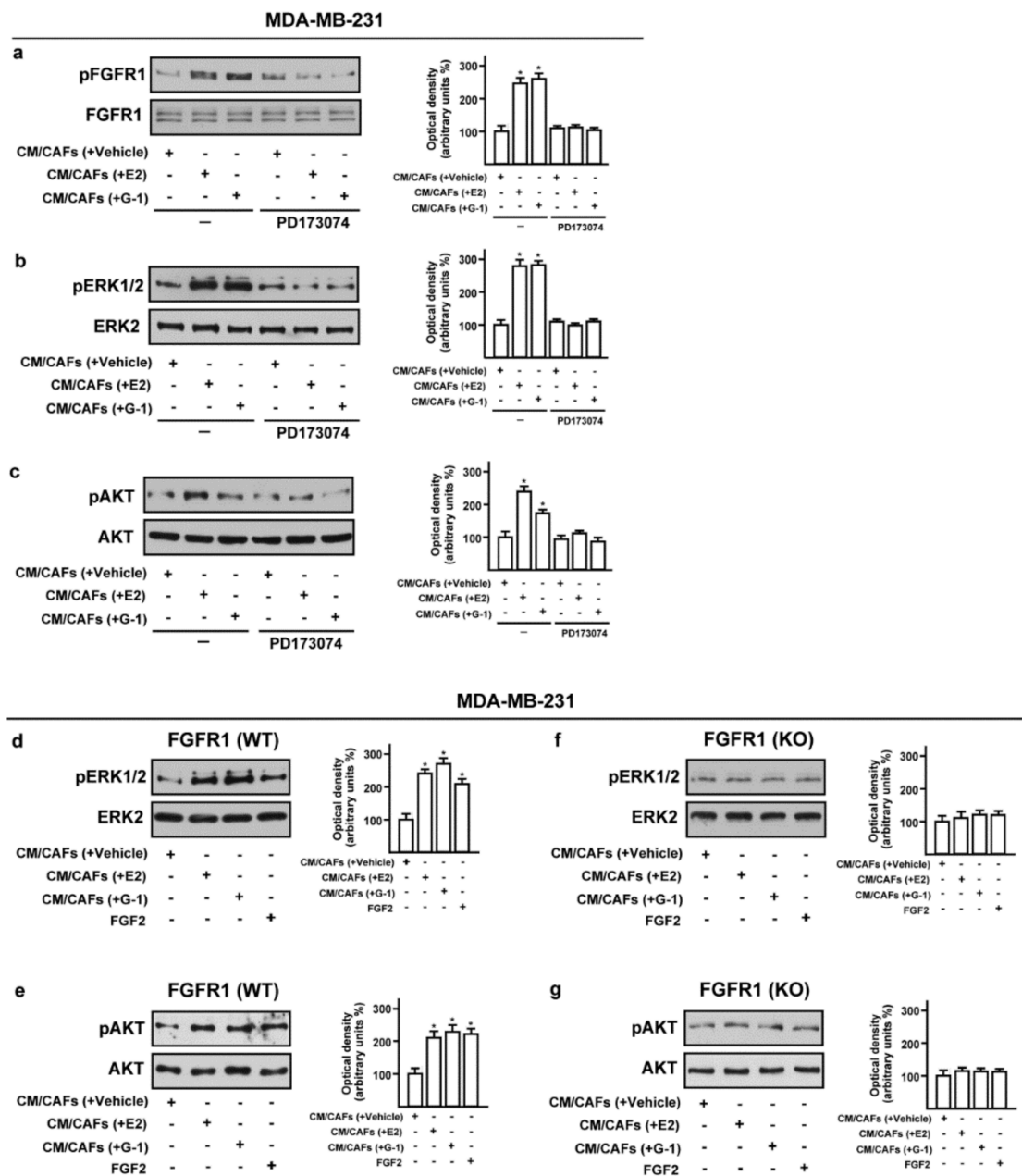
**Figure 5.** Conditioned medium (CM) from estrogen-stimulated CAFs induces the activation of FGFR1- signaling pathway in MDA-MB-231 cells. (**a–c**) Phosphorylation of FGFR1, ERK1/2, AKT in MDA-MB-231 cells exposed for 1 h to CM from CAFs treated for 18 h with vehicle [CM/CAFs (+vehicle)], 10 nM E2 [CM/CAFs (+E2)] or 100 nM G-1 [CM/CAFs (+G-1)], alone and in the presence of 1 μM FGFR1 inhibitor PD173074. (**d,e**) Activation of ERK1/2 and AKT in FGFR1 (WT) MDA-MB-231 cells upon exposure for 1 h to CM from CAFs treated for 18 h with 10 nM E2 [CM/CAFs (+E2)], 100 nM G-1 [CM/CAFs (+G-1)]; (**f,g**) In FGFR1 (KO) MDA-MB-231 cells cultured in the same conditions as described above, the activation of ERK1/2 and AKT was no longer observed. FGF2 at 25 nM was used as positive control. FGFR1, ERK2, AKT and β-actin served as loading control, as indicated. Side panels show densitometric analysis of the blots normalized to the loading controls. Immunoblots shown are representative of three independent experiments. (*) indicates $p < 0.05$.

*3.4. FGF2/FGFR1 Paracrine Activation Up-Regulates CTGF Expression in MDA-MB-231 Cells*

A synergic action between FGF2 and connective tissue growth factor (CTGF) may occur in diverse pathophysiological conditions [49–51]. Hence, we analyzed the mRNA levels of FGFR1 and CTGF

in METABRIC breast cancer patients database [40,41] and we found a positive correlation between FGFR1 and CTGF expression (Figure 6a). Therefore, we investigated the involvement of FGF2/FGFR1 paracrine activation by estrogen-stimulated CAFs on CTGF expression in MDA-MB-231 cells. Worthy of note, CM collected from E2 and G-1 treated-CAFs triggered CTGF expression at both mRNA (Figure 6b) and protein levels (Figure 6c,d) in FGFR1 (WT) MDA-MB-231 cells but not in FGFR1 (KO) MDA-MB-231 cells. Next, the up-regulation of CTGF protein levels observed in the aforementioned conditions was also abrogated in the presence of the FGFR1 inhibitor PD173074, the MEK inhibitor PD98059 as well as the PI3K inhibitor Wortmannin (WM) (Figure 6e–g). Altogether, these findings suggest that FGF2/FGFR1 paracrine activation induced by estrogen-stimulated CAFs prompts CTGF expression through the involvement of ERK1/2 and AKT signaling cascades in MDA-MB-231 cells.
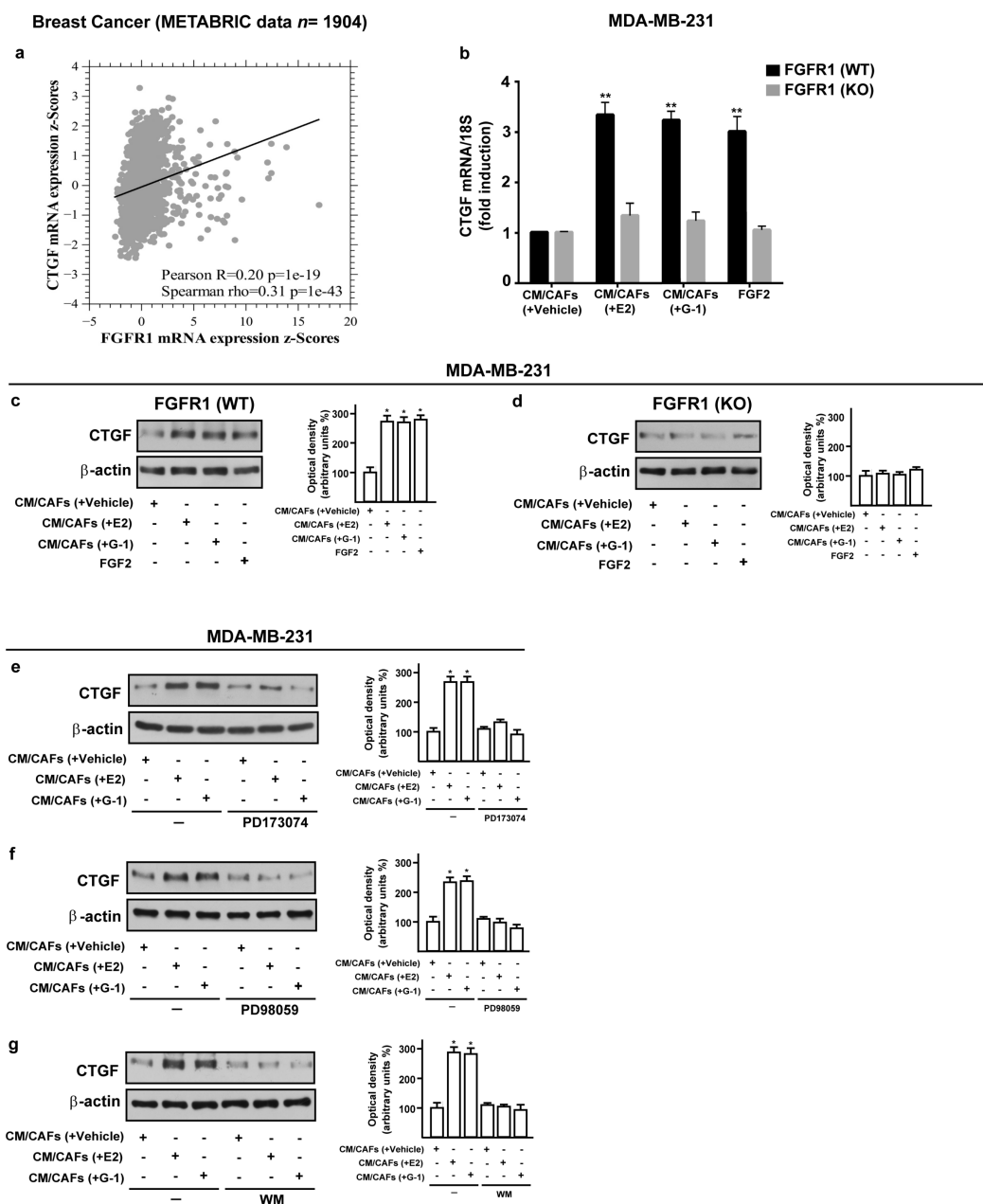


**Figure 6.** Conditioned medium (CM) from estrogen-stimulated CAFs up-regulates CTGF levels through FGFR1 signaling pathway in MDA-MB-231 cells. (**a**) Pairwise linear regressions of FGFR1 versus CTGF mRNA levels were performed on METABRIC dataset of 1904 breast tumor samples. Scatter plot shows

positive correlation between FGFR1 and CTGF expression. (**b**–**d**) CTGF mRNA and protein levels in FGFR1 (WT) and FGFR1 (KO) MDA-MB-231 cells exposed for 3 h to CM from CAFs treated for 18 h with vehicle [CM/CAFs (+vehicle)], 10 nM E2 [CM/CAFs (+E2)] or 100 nM G-1 [CM/CAFs (+G-1)], or exposed to 25 nM FGF2, as positive control, evaluated by qPCR and western blot. In RNA experiments, values were normalized to the expression of 18S and shown as fold changes of CTGF mRNA expression upon CM from CAFs treated with E2 and G-1 respect to cells exposed to CM from CAFs treated with vehicle. Each column represents the mean ±SD of three independent experiments performed in triplicate. (**e**–**g**) Up-regulation of CTGF protein expression in MDA-MB-231 cells exposed for 3 h to CM from CAFs treated for 18 h with vehicle [CM/CAFs (+vehicle)], 10 nM E2 [CM/CAFs (+E2)], or 100 nM G-1 [CM/CAFs (+G-1)] was no longer observed in the presence of 1 μM FGFR1 inhibitor PD173074, 10 μM MEK inhibitor PD98059 or 100 nM PI3K inhibitor Wortmannin (WM). β-actin served as loading control. Side panels show densitometric analysis of the blots normalized to the loading controls. Immunoblots shown are representative of three independent experiments. (**) indicates $p < 0.01$ and (*) indicates $p < 0.05$.

### 3.5. FGF2/FGFR1 Paracrine Activation Induces Cell Migration and Invasion Through CTGF in MDA-MB-231 Cells

Upon FGF2/FGFR1 activation, breast cancer cells may acquire invasive phenotype features modulating the expression of cell junction proteins, promoting a spindle-like morphology and increasing cell motility [52–54]. Recapitulating the abovementioned results, CM collected from E2 and G-1 treated-CAFs increased spindle-like morphology in FGFR1 (WT) MDA-MB-231 cells, but not in FGFR1 (KO) MDA-MB-231 cells as evaluated by the polarity index (Figure 7a,b). Performing scratch (Supplementary Figure S5a,b) and transwell assays (Figure 7c,d), we then observed that the migration and invasion of FGFR1 (WT) MDA-MB-231 cells promoted by CM from E2 and G-1 treated-CAFs were no longer evident in FGFR1 (KO) MDA-MB-231 cells as well as using the FGFR1 inhibitor PD173074 (data not shown). Next, we found that, in MDA-MB-231 cells, CTGF silencing prevents the migratory and invasive effects triggered by CM obtained from E2 and G-1 treated-CAFs (Figure 8a,b). Taken together, these results suggest that CTGF is involved by FGF2/FGFR1 paracrine activation toward important biological features elicited in MDA-MB-231 cells.
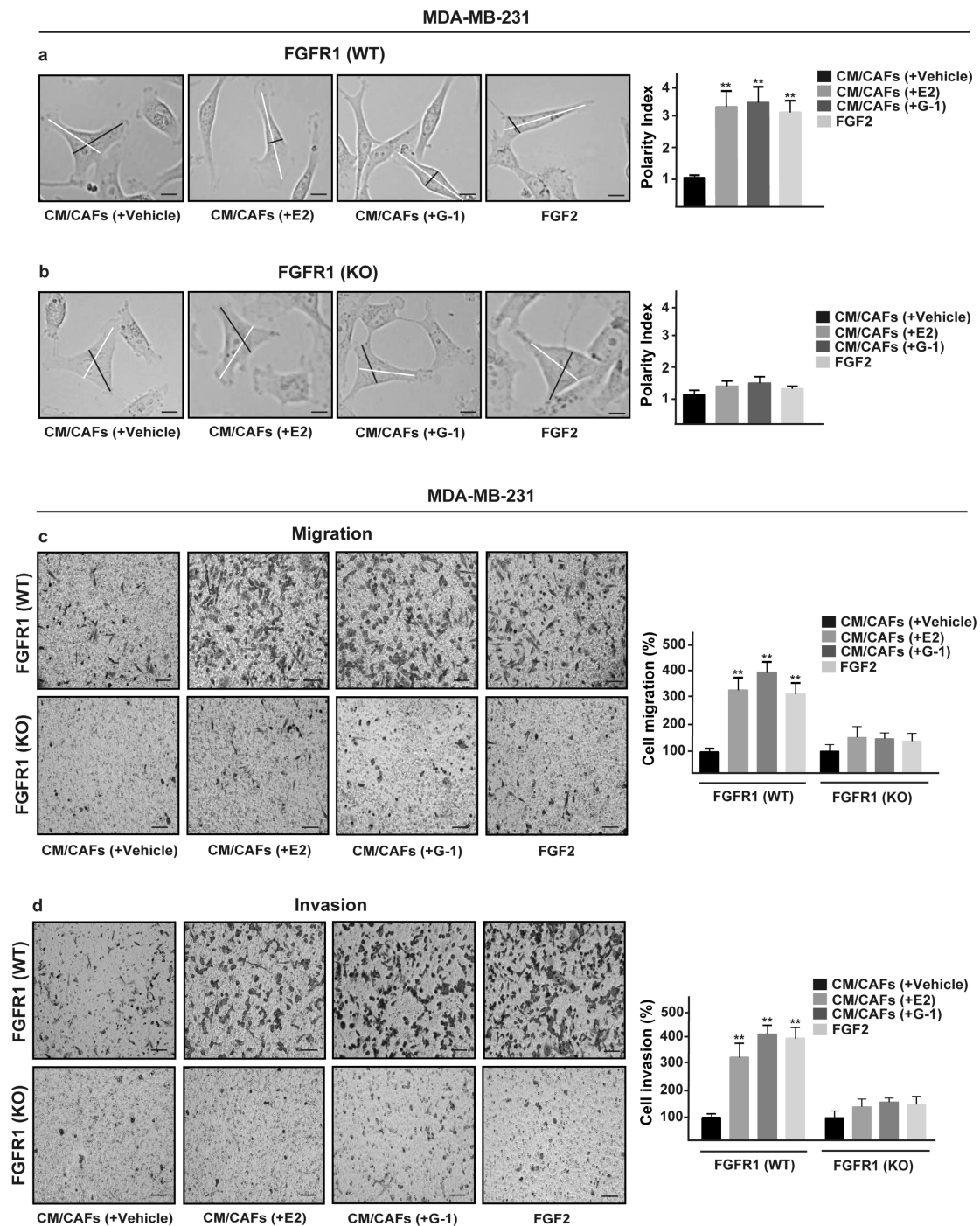
**Figure 7.** FGFR1 paracrine activation promotes migration and invasion in MDA-MB-231 cells. (**a**) FGFR1 (WT) and (**b**) FGFR1 (KO) MDA-MB-231 cells were cultured for 8 h in CM from CAFs treated for 18 h with vehicle [CM/CAFs (+vehicle)], 10 nM E2 [CM/CAFs (+E2)] or 100 nM G-1 [CM/CAFs (+G-1)], or exposed to 25 nM FGF2, as positive control. Lines traced on cells were used to calculate the Polarity Index (PI). White lines define the migratory axis and black lines the transversal axis. PI = 1.0 indicates a polygonal shape, whereas a value > 1.0 defines ranges of migratory shapes. Scale bar = 30 μm. Images shown are representative of 30 random fields acquired in three independent experiments. Transwell assays were used to assess cell migration (**c**) and invasion (**d**) in FGFR1 (WT) and FGFR1 (KO) MDA-MB-231 cells cultured for 8 h in CM from CAFs treated for 18 h with vehicle [CM/CAFs (+vehicle)], 10 nM E2 [CM/CAFs (+E2)] or 100 nM G-1 [CM/CAFs (+G-1)], or exposed to 25 nM FGF2, as positive control. Cells were counted in at least 10 random fields at 10× magnification, in three independent experiments performed in triplicate. Scale bar = 200 μm, (**) indicates $p < 0.01$.
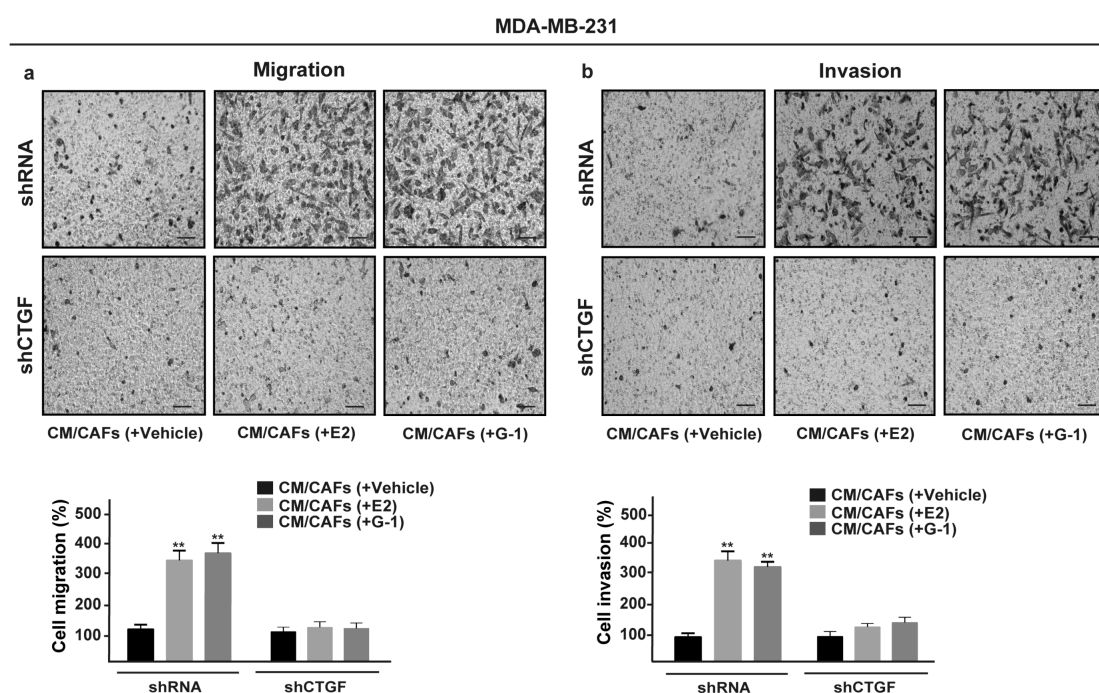
**Figure 8.** CTGF is required for migration and invasion induced by FGFR1 paracrine activation in MDA-MB-231 cells. Transwell assays were used to assess cell migration (**a**) and invasion (**b**) in MDA-MB-231 cells transfected for 24 h with control shRNA or shCTGF and then cultured for 8 h in CM from CAFs treated for 18 h with vehicle [CM/CAFs (+vehicle)], 10 nM E2 [CM/CAFs (+E2)] or 100 nM G-1 [CM/CAFs (+G-1)]. Cells were counted in at least 10 random fields at 10× magnification, in three independent experiments performed in triplicate. Scale bar = 200 μm, (**\*\***) indicates $p < 0.01$.

## 4. Discussion

In the current study, we provide novel evidence regarding the role of GPER in the regulation of FGF2 expression triggered by estrogens within the tumor microenvironment. In particular, using primary patient-derived breast CAFs, we ascertained that both E2 and the selective GPER agonist G-1 induce the expression and secretion of FGF2 activating the GPER/EGFR/ERK/c-fos/AP-1 signaling cascade. Analyzing publicly available databases, we then showed that FGFR1 is the most frequently amplified receptor of the FGFRs family along with its association with shorter survival rates in breast cancer patients [38–41]. In addition, focusing on the FGF2/FGFR1 functional interaction that occurs between CAFs and breast cancer cells, we determined that FGF2 secretion by estrogens-treated CAFs prompts the up-regulation of CTGF expression through the FGFR1-ERK1/2-AKT signaling cascade in MDA-MB-231 cells. As biological counterpart, we found that cell motility and invasiveness triggered by the FGF2/FGFR1 paracrine activation are abrogated by CTGF silencing.

In recent years, considerable attention has been deserved to the involvement of the tumor stroma toward cancer development [55]. In this regard, it has been shown that the interactions between tumor cells and the associated stroma represent a solid relationship that impacts disease initiation, progression, and patient prognosis [56]. For instance, CAFs acting as main players within the tumor stroma, provide a supportive microenvironment for aggressive features of cancer cells [57–60]. Indeed, CAFs are able to sustain cancer cell growth together with the invasion and metastasis via paracrine actions elicited by cytokines and growth factors released in the tumor microenvironment [6,61]. To date, in breast malignancies ~80% of stromal fibroblasts acquire the activated landscapes of CAFs that boost the proliferation of cancer cells at both the primary and the metastatic sites [62]. Additionally, CAFs may increase the in situ estrogen production, which contributes to the development of breast carcinomas through a multifaceted interactions among different transduction pathways [18,63]. In this vein, several lines of evidence have shown that cancer cells may acquire aberrant growth and invasion

properties through the dysregulation of the FGF/FGFR signaling [8,64], as highlighted in large-scale analyses of human cancer genomes [65–68]. Moreover, the up-regulation and secretion of FGF2 toward the stimulation of FGFR1 signaling in breast cancers was reported to occur upon estrogen stimulation through the classical ER [32,43]. GPER has been also involved in the stimulatory effects exerted by estrogens and its expression was associated with the tumor size, the distant metastasis, and the recurrence of breast malignancies [21–23]. Likewise, the role of GPER has been ascertained in CAFs toward the proliferation, migration, and spreading of breast tumor cells [22]. In accordance with these findings, our current results provide new data showing that GPER mediates the expression and secretion of FGF2 in breast CAFs leading to the paracrine activation of the FGFR1-ERK1/2-AKT transduction signaling along with important biological responses in MDA-MB-231 cells.

Metastasis, the leading cause of mortality for breast cancer patients, is a complex and multi-stage process that comprise cellular transformation and tumor growth, angiogenesis, and invasion of target organs [69,70]. In this context, it has been reported that EMT may prompt diverse processes of the metastatic cascade [71,72]. Accordingly, recent studies have shown that FGFR1 activation promotes EMT and metastasis through different signaling pathways in various tumors as prostate, breast, and lung cancers [17,46,73]. High FGF2 expression and secretion have been found in triple-negative breast cancer cell lines, in particular in those showing a mesenchymal phenotype [47,74]. In addition, several factors including vascular endothelial growth factor (VEGF), PC-cell-derived growth factor (PCDGF), epidermal growth factor (EGF), and CTGF were demonstrated to confer migratory and metastatic properties to breast cancer cells [75,76]. As CTGF is concerned, mechanical stresses, cytokines, and growth factors stimulations have been reported to be able to alter its expression levels toward the cytoskeletal reorganization and migratory features in breast cancer cells [24,75,77,78]. Previous studies have also suggested a correlation between FGF2 levels and CTGF-activated signaling in different pathophysiological conditions [49–51]. Further corroborating these findings, in the present study a positive correlation between FGFR1 and CTGF expression was assessed by a bioinformatic analysis on 1904 breast tumor samples retrieved from METABRIC dataset. Next, we demonstrated that the paracrine activation of the FGF2/FGFR1 transduction pathway prompts the expression of CTGF, which was involved in the migratory and invasive responses observed in MDA-MB-231 cells.

## 5. Conclusions

Our findings indicate that GPER mediates a feed-forward FGF2/FGFR1 engagement within the tumor microenvironment linking CAFs to breast cancer cells toward tumor progression. Moreover, on the basis of the present data GPER may be included among the transduction mechanisms involved in the FGF2/FGFR1 paracrine activation that may contribute to breast cancer development.

**Author Contributions:** M.F.S., A.B., and M.M. conceived the study and carried out its design. M.F.S., A.V., R.L., D.C.R., F.C., G.R.G., and M.T. performed the experiments. M.F.S., A.V., and R.L. analyzed the data. G.B. conducted the bioinformatics analyses. A.M.M. provided breast tumor samples. M.F.S., A.B., and M.M. wrote the paper. All authors read and approved the final manuscript.

**Conflicts of Interest:** The authors declare no conflict of interest.

## Abbreviations

| | |
|---|---|
| CAFs | cancer associated fibroblasts |
| FGFR1 | fibroblast growth factor receptor 1 |
| FGF2 | fibroblast growth factor 2 |
| GPER | G protein estrogen receptor |
| CRISPR | Clustered Regularly Interspaced Short Palindromic Repeats |
| sgRNA | single guide RNA |
| WT | Wild type |
| KO | Knockout ERK, extracellular signal-regulated kinase |
| AP-1 | activator protein 1 |
| PI3K | phosphatidylinositol 3-kinase |
| CTGF/CCN2 | connective tissue growth factor |

## References

1. Hanahan, D.; Coussens, L.M. Accessories to the crime: Functions of cells recruited to the tumor microenvironment. *Cancer Cell* **2012**, *21*, 309–322. [CrossRef] [PubMed]
2. Hayward, S.W.; Wang, Y.; Cao, M.; Hom, Y.K.; Zhang, B.; Grossfeld, G.D.; Sudilovsky, D.; Cunha, G.R. Malignant transformation in a nontumorigenic human prostatic epithelial cell line. *Cancer Res.* **2001**, *61*, 8135–8142. [PubMed]
3. Procacci, P.; Moscheni, C.; Sartori, P.; Sommariva, M.; Gagliano, N. Tumor–stroma cross-talk in human pancreatic ductal adenocarcinoma: A focus on the effect of the extracellular matrix on tumor cell phenotype and invasive potential. *Cells* **2018**, *7*, 158. [CrossRef] [PubMed]
4. Marsh, T.; Pietras, K.; McAllister, S.S. Fibroblasts as architects of cancer pathogenesis. *Biochim. Biophys. Acta Mol. Basis Dis.* **2013**, *1832*, 1070–1078. [CrossRef] [PubMed]
5. Kalluri, R. The biology and function of fibroblasts in cancer. *Nat. Rev. Cancer* **2016**, *16*, 582–598. [CrossRef] [PubMed]
6. Han, Y.; Zhang, Y.; Jia, T.; Sun, Y. Molecular mechanism underlying the tumor-promoting functions of carcinoma-associated fibroblasts. *Tumor Biol.* **2015**, *36*, 1385–1394. [CrossRef] [PubMed]
7. Augsten, M. Cancer-associated fibroblasts as another polarized cell type of the tumor microenvironment. *Front. Oncol.* **2014**, *4*, 62. [CrossRef] [PubMed]
8. Carter, E.P.; Fearon, A.E.; Grose, R.P. Careless talk costs lives: Fibroblast growth factor receptor signalling and the consequences of pathway malfunction. *Trends Cell Biol.* **2015**, *25*, 221–233. [CrossRef] [PubMed]
9. Katoh, M. FGFR inhibitors: Effects on cancer cells, tumor microenvironment and whole-body homeostasis (Review). *Int. J. Mol. Med.* **2016**, *38*, 3–15. [CrossRef] [PubMed]
10. Sleeman, M.; Fraser, J.; McDonald, M.; Yuan, S.; White, D.; Grandison, P.; Kumble, K.; Watson, J.D.; Murison, J.G. Identification of a new fibroblast growth factor receptor, FGFR5. *Gene* **2001**, *271*, 171–182. [CrossRef]
11. Babina, I.S.; Turner, N.C. Advances and challenges in targeting FGFR signalling in cancer. *Nat. Rev. Cancer* **2017**, *17*, 318–332. [CrossRef] [PubMed]
12. Dieci, M.V.; Arnedos, M.; Andre, F.; Soria, J.C. Fibroblast growth factor receptor inhibitors as a cancer treatment: From a biologic rationale to medical perspectives. *Cancer Discov.* **2013**, *3*, 264–279. [CrossRef] [PubMed]
13. Englinger, B.; Kallus, S.; Senkiv, J.; Laemmerer, A.; Moser, P.; Gabler, L.; Groza, D.; Kowol, C.; Heffeter, P.; Grusch, M.; et al. Lysosomal sequestration impairs the activity of the preclinical FGFR inhibitor PD173074. *Cells* **2018**, *7*, 259. [CrossRef] [PubMed]
14. Formisano, L.; Young, C.D.; Bhola, N.; Giltnane, J.M.; Estrada, M.V.; Arteaga, C.L. FGFR1 is associated with resistance to interaction with estrogen receptor (ER) α endocrine therapy in ER+/FGFR1-amplified breast cancer. *Cancer Res.* **2015**, *75*, 2435. [CrossRef]
15. Wynes, M.W.; Hinz, T.K.; Gao, D.; Martini, M.; Marek, L.A.; Ware, K.E.; Edwards, M.G.; Böhm, D.; Perner, S.; Helfrich, B.A.; et al. FGFR1 mRNA and protein expression, not gene copy number, predict FGFR TKI sensitivity across all lung cancer histologies. *Clin. Cancer Res.* **2014**, *20*, 3299–3309. [CrossRef] [PubMed]

16.　Ruotsalainen, T.; Joensuu, H.; Mattson, K.; Salven, P. High pretreatment serum concentration of basic fibroblast growth factor is a predictor of poor prognosis in small cell lung cancer. *Cancer Epidemiol. Biomarkers Prev.* **2002**, *11*, 1492–1495. [PubMed]

17.　Brown, W.S.; Tan, L.; Smith, A.; Gray, N.S.; Wendt, M.K.; Wendt, M.; Taylor, M.; Schiemann, B.; Sossey-Alaoui, K.; Schiemann, W.; et al. Covalent targeting of fibroblast growth factor receptor inhibits metastatic breast cancer. *Mol. Cancer Ther.* **2016**, *15*, 2096–2106. [CrossRef] [PubMed]

18.　Ren, Y.; Jia, H.H.; Xu, Y.Q.; Zhou, X.; Zhao, X.H.; Wang, Y.F.; Song, X.; Zhu, Z.Y.; Sun, T.; Dou, Y.; et al. Paracrine and epigenetic control of CAF-induced metastasis: The role of HOTAIR stimulated by TGF-β1 secretion. *Mol. Cancer* **2018**, *17*, 5. [CrossRef] [PubMed]

19.　Huang, C.; Yuan, P.; Wu, J.; Huang, J. Estrogen regulates excitatory amino acid carrier 1 (EAAC1) expression through sphingosine kinase 1 (SphK1) transacting FGFR-mediated ERK signaling in rat C6 astroglial cells. *Neuroscience* **2016**, *319*, 9–22. [CrossRef] [PubMed]

20.　Jia, M.; Dahlman-Wright, K.; Gustafsson, J.A. Estrogen receptor alpha and beta in health and disease. *Best Pract. Res. Clin. Endocrinol. Metab.* **2015**, *29*, 557–568. [CrossRef] [PubMed]

21.　Prossnitz, E.R.; Maggiolini, M. Mechanisms of estrogen signaling and gene expression via GPR30. *Mol. Cell. Endocrinol.* **2009**, *308*, 32–38. [CrossRef] [PubMed]

22.　Lappano, R.; Maggiolini, M. G protein-coupled receptors: Novel targets for drug discovery in cancer. *Nat. Rev. Drug Discov.* **2011**, *10*, 47–60. [CrossRef] [PubMed]

23.　Maggiolini, M.; Picard, D. The unfolding stories of GPR30, a new membrane-bound estrogen receptor. *J. Endocrinol.* **2010**, *204*, 105–114. [CrossRef] [PubMed]

24.　Pandey, D.P.; Lappano, R.; Albanito, L.; Madeo, A.; Maggiolini, M.; Picard, D. Estrogenic GPR30 signalling induces proliferation and migration of breast cancer cells through CTGF. *EMBO J.* **2009**, *28*, 523–532. [CrossRef] [PubMed]

25.　De Francesco, E.M.; Pellegrino, M.; Santolla, M.F.; Lappano, R.; Ricchio, E.; Abonante, S.; Maggiolini, M. GPER mediates activation of HIF1α/VEGF signaling by estrogens. *Cancer Res.* **2014**, *74*, 4053–4064. [CrossRef] [PubMed]

26.　Lappano, R.; Santolla, M.F.; Pupo, M.; Sinicropi, M.S.; Caruso, A.; Rosano, C.; Maggiolini, M. MIBE acts as antagonist ligand of both estrogen receptor α and GPER in breast cancer cells. *Breast Cancer Res.* **2012**, *14*, R12. [CrossRef] [PubMed]

27.　Lappano, R.; Rosano, C.; Santolla, M.F.; Pupo, M.; de Francesco, E.M.; de Marco, P.; Ponassi, M.; Spallarossa, A.; Ranise, A.; Maggiolini, M. Two novel GPER agonists induce gene expression changes and growth effects in cancer cells. *Curr. Cancer Drug Targets* **2012**, *12*, 531–542. [CrossRef] [PubMed]

28.　De Marco, P.; Lappano, R.; De Francesco, E.M.; Cirillo, F.; Pupo, M.; Avino, S.; Vivacqua, A.; Abonante, S.; Picard, D.; Maggiolini, M. GPER signalling in both cancer-associated fibroblasts and breast cancer cells mediates a feedforward IL1β/IL1R1 response. *Sci. Rep.* **2016**, *6*, 24354. [CrossRef] [PubMed]

29.　Santolla, M.F.; Avino, S.; Pellegrino, M.; De Francesco, E.M.; De Marco, P.; Lappano, R.; Vivacqua, A.; Cirillo, F.; Rigiracciolo, D.C.; Scarpelli, A.; et al. SIRT1 is involved in oncogenic signaling mediated by GPER in breast cancer. *Cell Death Dis.* **2015**, *6*, e1834. [CrossRef] [PubMed]

30.　De Marco, P.; Bartella, V.; Vivacqua, A.; Lappano, R.; Santolla, M.F.; Morcavallo, A.; Pezzi, V.; Belfiore, A.; Maggiolini, M. Insulin-like growth factor-I regulates GPER expression and function in cancer cells. *Oncogene* **2012**, *32*, 678–688. [CrossRef] [PubMed]

31.　Vivacqua, A.; Sebastiani, A.; Miglietta, A.; Rigiracciolo, D.; Cirillo, F.; Galli, G.; Talia, M.; Santolla, M.; Lappano, R.; Giordano, F.; et al. miR-338-3p is regulated by estrogens through GPER in breast cancer cells and cancer-associated fibroblasts (CAFs). *Cells* **2018**, *7*, 203. [CrossRef] [PubMed]

32.　Fillmore, C.M.; Gupta, P.B.; Rudnick, J.A.; Caballero, S.; Keller, P.J.; Lander, E.S.; Kuperwasser, C. Estrogen expands breast cancer stem-like cells through paracrine FGF/Tbx3 signaling. *Proc. Natl. Acad. Sci. USA* **2010**, *107*, 21737–21742. [CrossRef] [PubMed]

33.　Balko, J.M.; Mayer, I.A.; Sanders, M.E.; Miller, T.W.; Kuba, M.G.; Meszoely, I.M.; Wagle, N.; Garraway, L.A.; Arteaga, C.L. Discordant cellular response to presurgical letrozole in bilateral synchronous ER+ breast cancers with a KRAS mutation or FGFR1 gene amplification. *Mol. Cancer Ther.* **2012**, *11*, 2301–2305. [CrossRef] [PubMed]

34. De Francesco, E.M.; Lappano, R.; Santolla, M.F.; Marsico, S.; Caruso, A.; Maggiolini, M. HIF-1alpha/GPER signaling mediates the expression of VEGF induced by hypoxia in breast cancer associated fibroblasts (CAFs). *Breast Cancer Res.* **2013**, *15*, R64. [CrossRef] [PubMed]

35. Santolla, M.F.; De Francesco, E.M.; Lappano, R.; Rosano, C.; Abonante, S.; Maggiolini, M. Niacin activates the G protein estrogen receptor (GPER)-mediated signalling. *Cell. Signal.* **2014**, *26*, 1466–1475. [CrossRef] [PubMed]

36. Pisano, A.; Santolla, M.F.; De Francesco, E.M.; De Marco, P.; Rigiracciolo, D.C.; Perri, M.G.; Vivacqua, A.; Abonante, S.; Cappello, A.R.; Dolce, V.; et al. GPER, IGF-IR, and EGFR transduction signaling are involved in stimulatory effects of zinc in breast cancer cells and cancer-associated fibroblasts. *Mol. Carcinog.* **2017**, *56*, 580–593. [CrossRef] [PubMed]

37. Ran, F.A.; Hsu, P.D.P.; Wright, J.; Agarwala, V.; Scott, D.A.; Zhang, F. Genome engineering using the CRISPR-Cas9 system. *Nat. Protoc.* **2013**, *8*, 2281–2308. [CrossRef] [PubMed]

38. Cerami, E.; Gao, J.; Dogrusoz, U.; Gross, B.E.; Sumer, S.O.S.; Aksoy, B.A.B.; Jacobsen, A.; Byrne, C.J.; Heuer, M.L.; Larsson, E.; et al. The cBio cancer genomics portal: An open platform for exploring multidimensional cancer genomics data. *Cancer Discov.* **2012**, *2*, 401–404. [CrossRef] [PubMed]

39. Gao, J.; Aksoy, B.A.; Dogrusoz, U.; Dresdner, G.; Gross, B.; Sumer, S.O.; Sun, Y.; Jacobsen, A.; Sinha, R.; Larsson, E.; et al. Integrative analysis of complex cancer genomics and clinical profiles using the cBioPortal. *Sci.Signal.* **2013**, *6*, 1–19. [CrossRef] [PubMed]

40. Curtis, C.; Shah, S.P.; Chin, S.F.; Turashvili, G.; Rueda, O.M.; Dunning, M.J.; Speed, D.; Lynch, A.G.; Samarajiwa, S.; Yuan, Y.; et al. The genomic and transcriptomic architecture of 2000 breast tumours reveals novel subgroups. *Nature* **2012**, *486*, 346–352. [CrossRef] [PubMed]

41. Pereira, B.; Chin, S.F.; Rueda, O.M.; Vollan, H.K.M.; Provenzano, E.; Bardwell, H.A.; Pugh, M.; Jones, L.; Russell, R.; Sammut, S.J.; et al. The somatic mutation profiles of 2433 breast cancers refines their genomic and transcriptomic landscapes. *Nat. Commun.* **2016**, *7*, 11479. [CrossRef] [PubMed]

42. Vicente-Manzanares, M.; Koach, M.A.; Whitmore, L.; Lamers, M.L.; Horwitz, A.F. Segregation and activation of myosin IIB creates a rear in migrating cells. *J. Cell Biol.* **2008**, *183*, 543–554. [CrossRef] [PubMed]

43. Siegfried, J.M.; Farooqui, M.; Rothenberger, N.J.; Dacic, S.; Stabile, L.P. Interaction between the estrogen receptor and fibroblast growth factor receptor pathways in non-small cell lung cancer. *Oncotarget* **2017**, *8*, 24063–24076. [CrossRef] [PubMed]

44. Coleman, S.J.; Chioni, A.-M.; Ghallab, M.; Anderson, R.K.; Lemoine, N.R.; Kocher, H.M.; Grose, R.P. Nuclear translocation of FGFR1 and FGF2 in pancreatic stellate cells facilitates pancreatic cancer cell invasion. *EMBO Mol. Med.* **2014**, *6*, 467–481. [CrossRef] [PubMed]

45. Tanner, Y.; Grose, R.P. Dysregulated FGF signalling in neoplastic disorders. *Semin. Cell Dev. Biol.* **2016**, *53*, 126–135. [CrossRef] [PubMed]

46. Wang, K.; Ji, W.; Yu, Y.; Li, Z.; Niu, X.; Xia, W.; Lu, S. FGFR1-ERK1/2-SOX2 axis promotes cell proliferation, epithelial–mesenchymal transition, and metastasis in FGFR1-amplified lung cancer. *Oncogene* **2018**, *37*, 5340–5354. [CrossRef] [PubMed]

47. Sharpe, R.; Pearson, A.; Herrera-Abreu, M.T.; Johnson, D.; Mackay, A.; Welti, J.C.; Natrajan, R.; Reynolds, A.R.; Reis-Filho, J.S.; Ashworth, A.; et al. FGFR signaling promotes the growth of triple-negative and basal-like breast cancer cell lines both in vitro and in vivo. *Clin. Cancer Res.* **2011**, *17*, 5275–5286. [CrossRef] [PubMed]

48. Lundin, L.; Rönnstrand, L.; Cross, M.; Hellberg, C.; Lindahl, U.; Claesson-Welsh, L. Differential tyrosine phosphorylation of fibroblast growth factor (FGF) receptor-1 and receptor proximal signal transduction in response to FGF-2 and heparin. *Exp. Cell Res.* **2003**, *287*, 190–198. [CrossRef]

49. Xu, R.; Zhao, H.; Muhammad, H.; Dong, M.; Besenbacher, F.; Chen, M. Dual-delivery of FGF-2/CTGF from silk fibroin/PLCL-PEO coaxial fibers enhances MSC proliferation and fibrogenesis. *Sci. Rep.* **2017**, *7*, 8509. [CrossRef] [PubMed]

50. Aoyama, E.; Kubota, S.; Takigawa, M. CCN2/CTGF binds to fibroblast growth factor receptor 2 and modulates its signaling. *FEBS Lett.* **2012**, *586*, 4270–4275. [CrossRef] [PubMed]

51. Chujo, S.; Shirasaki, F.; Kondo-Miyazaki, M.; Ikawa, Y.; Takehara, K. Role of connective tissue growth factor and its interaction with basic fibroblast growth factor and macrophage chemoattractant protein-1 in skin fibrosis. *J. Cell. Physiol.* **2009**, *220*, 189–195. [CrossRef] [PubMed]

52. Yang, M.; Yu, X.; Li, X.; Luo, B.; Yang, W.; Lin, Y.; Li, D.; Gan, Z. TNFAIP3 is required for FGFR1 activation-promoted proliferation and tumorigenesis of premalignant DCIS. COM human mammary epithelial cells. *Breast Cancer Res.* **2018**, *20*, 1–14. [CrossRef] [PubMed]

53. Compagni, A.; Wilgenbus, P.; Impagnatiello, M.A.; Cotten, M.; Christofori, G. Fibroblast growth factors are required for efficient tumor angiogenesis. *Cancer Res.* **2000**, *60*, 7163–7169. [PubMed]

54. Ronca, R.; Giacomini, A.; Rusnati, M.; Presta, M. The potential of fibroblast growth factor/fibroblast growth factor receptor signaling as a therapeutic target in tumor angiogenesis. *Expert Opin. Ther. Targets* **2015**, *19*, 1361–1377. [CrossRef] [PubMed]

55. Liotta, L.A.; Kohn, E.C. The microenvironment of the tumour-host interface. *Nature* **2001**, *411*, 375–379. [CrossRef] [PubMed]

56. Quail, D.F.; Joyce, J.A. Microenvironmental regulation of tumor progression and metastasis. *Nat. Med.* **2013**, *19*, 1423–1437. [CrossRef] [PubMed]

57. Bhowmick, N.A.; Neilson, E.G.; Moses, H.L. Stromal fibroblasts in cancer initiation and progression. *Nature* **2004**, *432*, 332–337. [CrossRef] [PubMed]

58. De Wever, O.; Mareel, M. Role of tissue stroma in cancer cell invasion. *J. Pathol.* **2003**, *200*, 429–447. [CrossRef] [PubMed]

59. De Wever, O.; Demetter, P.; Mareel, M.; Bracke, M. Stromal myofibroblasts are drivers of invasive cancer growth. *Int. J. Cancer* **2008**, *123*, 2229–2238. [CrossRef] [PubMed]

60. Van der Horst, G.; Bos, L.; van der Pluijm, G. Epithelial plasticity, cancer stem cells, and the tumor-supportive stroma in bladder carcinoma. *Mol. Cancer Res.* **2012**, *10*, 995–1009. [CrossRef] [PubMed]

61. Karagiannis, G.S.; Poutahidis, T.; Erdman, S.E.; Kirsch, R.; Riddell, R.H.; Diamandis, E.P. Cancer-associated fibroblasts drive the progression of metastasis through both paracrine and mechanical pressure on cancer tissue. *Mol. Cancer Res.* **2012**, *10*, 1403–1418. [CrossRef] [PubMed]

62. Orimo, A.; Gupta, P.B.; Sgroi, D.C.; Arenzana-Seisdedos, F.; Delaunay, T.; Naeem, R.; Carey, V.J.; Richardson, A.L.; Weinberg, R.A. Stromal fibroblasts present in invasive human breast carcinomas promote tumor growth and angiogenesis through elevated SDF-1/CXCL12 secretion. *Cell* **2005**, *121*, 335–348. [CrossRef] [PubMed]

63. Yamaguchi, Y.; Hayashi, S. Estrogen-related cancer microenvironment of breast carcinoma. *Endocr. J.* **2009**, *56*, 1–7. [CrossRef] [PubMed]

64. Sobhani, N.; Ianza, A.; D'Angelo, A.; Roviello, G.; Giudici, F.; Bortul, M.; Zanconati, F.; Bottin, C.; Generali, D. Current status of fibroblast growth factor receptor-targeted therapies in breast cancer. *Cells* **2018**, *7*, 76. [CrossRef] [PubMed]

65. Campbell, J.; Ryan, C.J.; Brough, R.; Bajrami, I.; Pemberton, H.N.; Chong, I.Y.; Costa-Cabral, S.; Frankum, J.; Gulati, A.; Holme, H.; et al. Large-scale profiling of kinase dependencies in cancer cell lines. *Cell Rep.* **2016**, *14*, 2490–2501. [CrossRef] [PubMed]

66. Touat, M.; Ileana, E.; Postel-Vinay, S.; André, F.; Soria, J.C. Targeting FGFR signaling in cancer. *Clin. Cancer Res.* **2015**, *21*, 2684–2694. [CrossRef] [PubMed]

67. Mohammadi, M.; Froum, S.; Hamby, J.M.; Schroeder, M.C.; Panek, R.L.; Lu, G.H.; Eliseenkova, A.V.; Green, D.; Schlessinger, J.; Hubbard, S.R. Crystal structure of an angiogenesis inhibitor bound to the FGF receptor tyrosine kinase domain. *EMBO J.* **1998**, *17*, 5896–5904. [CrossRef] [PubMed]

68. Dutt, A.; Salvesen, H.B.; Chen, T.-H.; Ramos, A.H.; Onofrio, R.C.; Hatton, C.; Nicoletti, R.; Winckler, W.; Grewal, R.; Hanna, M.; et al. Drug-sensitive FGFR2 mutations in endometrial carcinoma. *Proc. Natl. Acad. Sci. USA* **2008**, *105*, 8713–8717. [CrossRef] [PubMed]

69. Van't Veer, L.J.; Weigelt, B. Road map to metastasis. *Nat. Med.* **2003**, *9*, 999–1000. [CrossRef] [PubMed]

70. Kraljevic, S.P.; Sedic, M.; Bosnjak, H.; Spaventi, S.; Pavelic, K. Metastasis: New perspectives on an old problem. *Mol. Cancer* **2011**, *11*, 22. [CrossRef] [PubMed]

71. Lamouille, S.; Xu, J.; Derynck, R. Molecular mechanisms of epithelial-mesenchymal transition. *Nat. Rev. Mol. Cell Biol.* **2014**, *15*, 178. [CrossRef] [PubMed]

72. De Craene, B.; Berx, G. Regulatory networks defining EMT during cancer initiation and progression. *Nat. Rev. Cancer* **2013**, *13*, 97. [CrossRef] [PubMed]

73. Acevedo, V.D.; Gangula, R.D.; Freeman, K.W.; Li, R.; Zhang, Y.; Wang, F.; Ayala, G.E.; Peterson, L.E.; Ittmann, M.; Spencer, D.M. Inducible FGFR-1 activation leads to irreversible prostate adenocarcinoma and an epithelial-to-mesenchymal transition. *Cancer Cell* **2007**, *12*, 559–571. [CrossRef] [PubMed]

74. Abramson, V.G.; Lehmann, B.D.; Ballinger, T.J.; Pietenpol, J.A. Subtyping of triple-negative breast cancer: Implications for therapy. *Cancer* **2015**, *121*, 8–16. [CrossRef] [PubMed]

75. Chen, P.-S.; Wang, M.-Y.; Wu, S.-N.; Su, J.-L.; Hong, C.-C.; Chuang, S.-E.; Chen, M.-W.; Hua, K.-T.; Wu, Y.-L.; Cha, S.-T.; et al. CTGF enhances the motility of breast cancer cells via an integrin-αvβ3-ERK1/2-dependent S100A4-upregulated pathway. *J. Cell Sci.* **2007**, *120*, 2053–2065. [CrossRef] [PubMed]

76. Goltsov, A.; Deeni, Y.; Khalil, H.; Soininen, T.; Kyriakidis, S.; Hu, H.; Langdon, S.; Harrison, D.; Bown, J. Systems analysis of drug-induced receptor tyrosine kinase reprogramming following targeted mono- and combination anti-cancer therapy. *Cells* **2014**, *3*, 563–591. [CrossRef] [PubMed]

77. Cicha, I.; Goppelt-Struebe, M. Connective tissue growth factor: Context-dependent functions and mechanisms of regulation. *BioFactors* **2009**, *35*, 200–208. [CrossRef] [PubMed]

78. Kang, Y.; Siegel, P.M.; Shu, W.; Drobnjak, M.; Kakonen, S.M.; Cordón-Cardo, C.; Guise, T.A.; Massagué, J. A multigenic program mediating breast cancer metastasis to bone. *Cancer Cell* **2003**, *3*, 537–549. [CrossRef]

# The Peptide ERα17p Is a GPER Inverse Agonist that Exerts Antiproliferative Effects in Breast Cancer Cells

**Rosamaria Lappano [1], Christophe Mallet [2,3], Bruno Rizzuti [4], Fedora Grande [1], Giulia Raffaella Galli [1], Cillian Byrne [5], Isabelle Broutin [6], Ludivine Boudieu [2,3], Alain Eschalier [2,3], Yves Jacquot [5,*,†] and Marcello Maggiolini [1,*]**

[1] Department of Pharmacy, Health and Nutritional Sciences, University of Calabria, 87036 Rende, Italy; rosamaria.lappano@unical.it (R.L.); fedora.grande@unical.it (F.G.); giulia.r.galli@gmail.com (G.R.G.)

[2] NEURO-DOL Basics & Clinical Pharmacology of Pain, INSERM, CHU, Université Clermont Auvergne, F-63000 Clermont-Ferrand, France; christophe.mallet@uca.fr (C.M.); ludivine.boudieu@uca.fr (L.B.); alain.eschalier@uca.fr (A.E.)

[3] ANALGESIA Institute, Université Clermont Auvergne, F-63000 Clermont-Ferrand, France

[4] CNR-NANOTEC, Licryl-UOS Cosenza and CEMIF.Cal, Department of Physics, University of Calabria, 87036 Rende, Italy; bruno.rizzuti@fis.unical.it

[5] Laboratoire des Biomolécules (LBM), CNRS-UMR 7203, Sorbonne University, Ecole Normale Supérieure, 75252 Paris Cedex 05, France; cillian.byrne@upmc.fr

[6] Cibles Thérapeutiques et Conception de Médicaments (CiTCoM), CNRS–UMR 8038, Faculté des Sciences Pharmaceutiques et Biologiques, Université Paris Descartes, 75270 Paris Cedex 06, France; isabelle.broutin@parisdescartes.fr

**\*** Correspondence: yves.jacquot@sorbonne-universite.fr (Y.J.); marcellomaggiolini@yahoo.it or marcello.maggiolini@unical.it (M.M.); Tel.: +33-(0)1 44 27 44 44 (Y.J.); +39 0984 493076 (M.M.)

**†** Future Affiliation: Cibles Thérapeutiques et Conception de Médicaments (CiTCoM), CNRS–UMR 8038, Faculté des Sciences Pharmaceutiques et Biologiques, Université Paris Descartes, 75270 Paris Cedex 06, France.

**Abstract:** The inhibition of the G protein-coupled estrogen receptor (GPER) offers promising perspectives for the treatment of breast tumors. A peptide corresponding to part of the hinge region/AF2 domain of the human estrogen receptor α (ERα17p, residues 295–311) exerts anti-proliferative effects in various breast cancer cells including those used as triple negative breast cancer (TNBC) models. As preliminary investigations have evoked a role for the GPER in the mechanism of action of this peptide, we focused our studies on this protein using SkBr3 breast cancer cells, which are ideal for GPER evaluation. ERα17p inhibits cell growth by targeting membrane signaling. Identified as a GPER inverse agonist, it co-localizes with GPER and induces the proteasome-dependent downregulation of GPER. It also decreases the level of pEGFR (phosphorylation of epidermal growth factor receptor), pERK1/2 (phosphorylation of extracellular signal-regulated kinase), and c-fos. ERα17p is rapidly distributed in mice after intra-peritoneal injection and is found primarily in the mammary glands. The N-terminal PLMI motif, which presents analogies with the GPER antagonist PBX1, reproduces the effect of the whole ERα17p. Thus, this motif seems to direct the action of the entire peptide, as highlighted by docking and molecular dynamics studies. Consequently, the tetrapeptide PLMI, which can be claimed as the first peptidic GPER disruptor, could open new avenues for specific GPER modulators.

**Keywords:** peptide; anti-proliferation; inverse agonist; desensitizer; GPER; SkBr3; breast cancer

## 1. Introduction

The 66 kDa human estrogen receptor α (ERα) is a transcription factor belonging to the superfamily of steroid hormone receptors [1]. This ubiquitous protein is widely distributed in the uterus, ovaries, breast tissue, and bones, as well as in the central nervous and cardiovascular systems. At the cellular scale, it is located in the nucleus, within membranes including the caveolae [2] and the mitochondria [3] where it displays distinct effects.

In addition to the palmitoylated ERα [4], two truncated ERα isoforms (i.e., 36 kDa [5] and 46 kDa [6]) have been identified at the cell membrane. An additional estrogen-interacting hepta-transmembrane G protein-coupled estrogen receptor 1 (GPER1 or GPER), also called G protein-coupled receptor 30 (GPR30), has been described [7]. GPER participates in the action of estrogens through growth factor receptors including the epidermal growth factor receptor (EGFR) to activate mitogen-activated protein kinases (MAPK) such as the extracellular signal-regulated kinase (ERK1/2) [8]. Thus, GPER is a real target for the treatment of breast tumors [9].

In the ERα, the hinge region, delimited by the residues 263 and 302, spatially links the C and E/F domains and participates, as such, in the control of transcription [10]. Besides the $K^{303}NSLALSLT^{311}$ N-terminal sequence of the ERα E domain, amino acids located at the C-terminal region of the D domain (sequence: $P^{293}SPLMIKRSK^{303}$) are particularly subjected to post-translational modifications. The 295–311 sequence is prone to acetylation [11–13], phosphorylation [14,15], methylation [16], ubiquitination [12,17], and SUMOylation [18], suggesting that this region of the receptor is important for transcription. Accordingly, the 295–311 deleted protein (ERαΔ295-311) is constitutively active [19]. As such, the sequence 302–339 is considered as a part of the ERα autonomous transactivation function AF2a [20]. In the same context, the motif $K^{299}RSKK^{303}$, which corresponds to the third nuclear receptor localization signal [21], is sensitive to proteolysis [22,23]. The close proximity of this cationic motif to the cysteine 447 palmitoylation site (~15 Å) and its ability to associate with anionic phospholipids suggests that it could participate in the stabilization of the protein at the membrane [24]. The K303R mutation, which seems to participate in tamoxifen resistance, has been found in invasive breast tumors, highlighting the importance of this part of the protein in malignancy onset [25,26]. In the context of the whole receptor, the 295–311 sequence is located at the surface of the ERα and belongs to a larger flexible helix (residues 295–330) partially folded in an extended left-handed polyproline II (PPII) conformation [27]. This observation implies that some interactions with protein partners could occur [28]. Apart from its association with $Ca^{2+}$-calmodulin [19,29,30] and DNA-bond c-jun [31], the 395–311 part of the ERα interacts intramolecularly with the sole ERα type II β turn of the ligand-binding domain (LBD, sequence: $V^{364}PGF^{367}$ [27]), which can associate with the proline-rich nuclear receptor co-activator (PNRC) [32] and possibly with the protein FKBP52 [33,34]. In the light of the aforementioned observations, this part of the ERα, albeit small in size, poses more questions than it provides answers. Consequently, the short D domain has garnered considerable interest during the last decade.

We have thus synthesized the human ERα-derived peptide PLMIKRSKKNSLALSLT (ERα17p, residues 295 to 311) and tested its effects in different experimental conditions and in various ERα-positive (ERα+) and -negative (ERα−) breast cancer cell lines. Under physiological conditions, it elicits apoptosis and necrosis independently from the ERα status [35]. After intraperitoneal injections at low concentration (1.5 mg/kg, three times a week for four weeks), this peptide decreases by ~50% the size of ERα-related human breast tumors (MDA-MB-231 breast cancer cells) xenografted in nude mice [35]. In the light of these substantial results, the peptide ERα17p could be a putative anticancer drug active on triple negative breast tumors (TNBC) for which no specific treatment currently exists.

We have attempted to probe the mechanism of action of ERα17p in physiological conditions (i.e., in complete serum) by focusing on membrane-initiated signaling pathways. We show that the peptide co-localizes with the GPER in ERα-negative SKBR3 breast cancer cells. Identified as an inverse agonist, it decreases the basal activity of GPER and triggers anti-proliferative activity. These effects are concurrent with a proteasome-dependent GPER downregulation, a decreased phosphorylation of EGFR and ERK1/2, and a decrease of the level of c-fos. It also targets the ovaries, the uterus and, seemingly,

the mammary glands. Following docking and molecular dynamics studies, the N-terminal PLMI tetrapeptide motif, which presents structural similarities with the GPER ligand PBX1 [36] and which most likely supports the action of ERα17p, is predicted to interact within the GPER ligand-binding site.

## 2. Materials and Methods

### 2.1. Peptide Synthesis

All chemicals were purchased from Sigma Aldrich (Saint-Quentin-Fallavier, France). The peptides were manually synthesized via Fmoc solid phase peptide synthesis (SPPS) using a preloaded Fmoc-Thr-Novasyn TGA resin (Merck, Fontenay sous Bois, France), as previously described [24,37]. Peptide cleavage and side-chain deprotection was carried out prior to lyophilization, purification, and characterization. The crude products were purified by semi-preparative reverse-phase high performance liquid chromatography RP-HPLC (Waters, Saint-Quentin en Yveline, France) using a Waters 600 pump and controller and a 2487 UV–Vis detector ($\lambda$ = 220 nm, flow rate = 5 mL/min). Solvents used for elution: A (milliQ water with 0.1% of trifluoroacetic acid (TFA)) and B (acetonitrile:milliQ water (90:10) with 0.1% TFA). Analytical RP-HPLC conditions: $\lambda$ = 220 nm, flow rate = 1 mL/min. The purified peptides were then characterized by matrix assisted laser desorption ionization time of flight (MALDI-TOF) mass spectrometry using a 4700 Proteomic Analyzer (Applied Biosystems, Foster City, CA, USA). α cyano-4-hydroxycinnamic acid (HCCA) was used as a matrix. Characterization data of the peptide ERα17p (PLMIKRSKKNSLALSLT) as well as of its fragments (PLMI) are reported elsewhere [24,37]. The scrambled peptide (KLSKNKRLMTISPLSLA) was purchased from the Plateforme d'Ingénierie des Protéines (Christophe Piesse, Institut de Biologie Paris-Seine, IBPS, FR 3631, Paris, France).

N-terminal ERα17p labeling was carried out by using 5(6)-carboxyfluorescein (fluorescein-Ahx-ERα17p-COOH, where Ahx corresponds to aminohexanoic acid), following the standard Fmoc peptide synthesis protocol [24,37]. A SymetriPrep $C_8$ column (7.8 mm × 300 mm, 7 μm particle size, 300 Å pore size, Waters, Saint-Quentin en Yveline, France) and appropriate eluent gradient (30% to 60% of solvent B over 20 min) were used for semi-preparative RP-HPLC. $R_t$ = 10.4 min. Analytical RP-HPLC was carried out using an ACE 5 $C_{18}$ 300 Å. RP-HPLC conditions: 5% to 60% of solvent B over 20 min; $R_t$ = 17.13 min. Calculated isotopic $m/z$ = 2369.29 (found: 2369.21).

The sequence $H_2N$-ERα17p-Pra-COOH, where Pra corresponds to propargyl glycine, was obtained by standard Fmoc peptide synthesis [24,37]. The Pra was used for the synthesis of the "click" Cy5-labeled version of ERα17p. Briefly, the purified peptide $H_2N$-ERα17p-Pra-COOH (3 mg, 1.16 μmol) and Cy5 azide (1 mg, 0.97 μmol) were dissolved in water (1 mL). To this was added, with stirring, 1.2 mg of $CuSO_4.5H_2O$ (4.83 μmol) in 100 μL water:DMF (95:5). Sodium ascorbate (4.8 mg, 24.1 μmol) was then added to this solution. The mixture was stirred for 30 min and purified directly by RP-HPLC. The recovered fractions were freeze-dried to yield a deep red powder (1.5 mg, yield = 33%). An Xbridge RP $C_{18}$ column (30 × 100 mm) was used for purification. Semi-preparative RP-HPLC conditions: 20–40% of solvent B over 10 min. $R_t$ = 7.6 min. Analytical RP-HPLC was carried using an Agilent technologies Ultimate 3000 pump, autosampler and RS UV–Vis variable wavelength detector with a Higgins Analytical Proto 300 C18 column (4.6 × 100 mm). Analytical RP-HPLC conditions: 15–80% of solvent B over 10 min. $R_t$ = 6.28 min. Calculated isotopic $m/z$ = 2827.44 (found: 2826.31).

### 2.2. Fluorescence Spectroscopy

The recombinant Grb2 protein was obtained and purified following a previously published protocol [38]. The interaction of ERα17p with Grb2 SH3 domains was estimated using a fluorescence-based titration assay, which was performed at 18 °C in a 1 cm pathlength cell with stirring using a Jasco FP-6200 spectrofluorimeter (Jasco, Essex, United Kingdom). Excitation and emission wavelengths were fixed at 280 and 350 nm, respectively. A Grb2 concentration of 1 μM in 50 mM Tris buffer adjusted to pH 8.0 was initially used. Fluorescence changes were recorded upon

the addition of 5 μL of a peptide solution at $10^{-3}$ M. The experimental curve was analyzed with the software Prism™ (version 5.0a, GraphPad Software, San Diego, California, USA). The experiment was performed twice.

### 2.3. Cell Growth Assays

17β-Estradiol (E$_2$) and MG-132 were purchased from Sigma-Aldrich (Milan, Italy) and solubilized in ethanol and DMSO, respectively. G-1 and G-36 were bought from Tocris Bioscience (Bristol, UK) and dissolved in DMSO. SkBr3 breast cancer cells were obtained by ATCC and used less than 6 months after resuscitation. The cells were maintained in RPMI 1640 without phenol red but supplemented with 5% fetal bovine serum (FBS) and 100 mg/mL penicillin/streptomycin (Life Technologies, Milan, Italy). Cells were grown in a 37 °C incubator with 5% CO$_2$.

Cells were seeded in 24-well plates in regular growth medium. After cells attached, they were incubated in medium containing 2.5% charcoal-stripped fetal bovine serum (FBS) and treated for 72 h either in the presence or absence of the tested molecules. Treatments were renewed every day. Cells were counted on day 4 using an automated cell counter (Life Technologies, Milan, Italy), following the manufacturer's recommendations.

### 2.4. TUNEL Experiments

Cell apoptosis was determined by TdT-mediated dUTP Nick-End Labeling (TUNEL) assay [39] conducted using a DeadEnd Fluorometric TUNEL System (Promega, Milan, Italy) and performed according to the manufacturer's instructions. Briefly, cells were treated for 72 h under various conditions (see figure legends), then were fixed in freshly prepared 4% paraformaldehyde solution in PBS (pH 7.4) for 25 min at 4 °C. After fixation, they were permeabilized in 0.2% Triton X-100 solution in PBS for 5 min. After washing twice with washing buffer for 5 min, the cells were covered with equilibration buffer at room temperature for 5 to 10 min. The labeling reaction was performed using terminal deoxynucleotidyl transferase end-labeling TdT and fluorescein-dUTP cocktail for each sample and incubated for 1 h at 37 °C, where TdT catalyzes the binding of fluorescein-dUTP to free 3′OH ends of the nicked DNA. After rinsing, the cells were washed with 2× saline-sodium citrate (SSC) solution buffer and subsequently incubated with 4′,6-diamidino-2-phenylindole (DAPI; Sigma-Aldrich, Milan, Italy) to stain nuclei and then analyzed using the Cytation 3 Cell Imaging Multimode Reader (BioTek, Winooski, VT, USA).

### 2.5. Fluorescence Microscopy

Cells were seeded in Lab-Tek II chamber slides at a density of $1 \times 10^5$ per well and incubated for 24 h in the maintenance medium. Cells were then treated as specified (see the legends of the figures), fixed in 4% paraformaldehyde, permeabilized with 0.1% TWEEN three times for 5 min and were then blocked for 30 min at room temperature with PBS containing 10% normal donkey serum (Santa Cruz Biotechnology, DBA, Milan, Italy), 0.1% Triton X-100, and 0.05% TWEEN (3 × 5 min). Thereafter, the cells were incubated overnight at 4 °C with a primary antibody against GPER (TA35133, 1:250, purchased from Origene, DBA, Milan, Italy) in PBS containing 0.05% TWEEN. After incubation, the slides were extensively washed with PBS and incubated with Alexa Fluor™ 594 goat anti-rabbit IgG (H + L) (1:250, purchased from Life Technologies, Milan, Italy). The slides were imaged on the Cytation 3 Cell Imaging Multimode reader (BioTek, Winooski, VT, USA).

### 2.6. Immunoblotting

Cells were grown in 10-cm dishes exposed to treatments, and then lysed in 500 μL of 50 mmol/L NaCl, 1.5 mmol/L MgCl$_2$, 1 mmol/L EGTA, 10% glycerol, 1% Triton X-100, 1% sodium dodecyl sulfate (SDS), and a mixture of protease inhibitors containing 1 mmol/L aprotinin, 20 mmol/L phenylmethylsulfonyl fluoride and 200 mmol/L sodium orthovanadate. Equal amounts of whole protein extracts were resolved on a 10% SDS-polyacrylamide gel and transferred to a nitrocellulose membrane (Amersham Biosciences, GE Healthcare, Milan, Italy), which were probed with primary antibodies against GPER (TA 35133, OriGene, Herford, Germany), pEGFR Tyr-1173 (sc-12351), EGFR (1005), phosphorylated ERK1/2 (E-4), ERK2 (C-14), c-fos (E-8), and β-actin (C2) (Santa Cruz Biotechnology, DBA, Milan, Italy) and then revealed using the ECL™ system from GE Healthcare (Milan, Italy).

### 2.7. Gene Expression Studies

Total RNA was extracted, and cDNA was synthesized by reverse transcription as previously described [40]. The expression of selected genes was quantified by real-time PCR using a Quant Studio7 Flex Real-Time PCR System platform (Applied Biosystems Inc, Milan, Italy). Gene-specific primers were designed using Primer Express version 2.0 software (Applied Biosystems Inc, Milan, Italy). For GPER and actin, whose genes were used as controls to obtain normalized values, the primers were 5′-ACACACCTGGGTGGACACAA-3′ (GPER forward) and 5′-GGAGCCAGAAGCCACATCTG-3′ (GPER reverse) as well as 5′-AAGCCACCCCACTTCTCTCTAA-3′ (actin forward) and 5′-CACCTCCCCTGTGTGGACTT-3′ (actin reverse), respectively. The assays were performed in triplicate and the results were normalized for actin expression and then calculated as fold induction of RNA expression.

### 2.8. In Vivo and Ex Vivo Fluorescence Imaging

Female mice RjOrl:SWISS (30 g, Janvier, France) were acclimatized for a week before testing. They were housed under controlled environmental conditions (between 21 and 22 °C; 55% humidity, 12 h light/dark cycles, food and water ad libitum). All experiments were approved by the local ethics committees (#18022) and performed according to the European legislation (Directive 2010/63/EU) concerning the protection of animals used for scientific purposes. In vivo and ex vivo fluorescence imaging was realized using the IVIS Spectrum system (Perkin Elmer, Waltham, MA) and a Cy5 filter set (excitation 640 nm; emission 680 nm). Female mice were injected intra-peritoneally with H$_2$N-ERα17p-Pra(Cy5)-COOH 2 mg/kg. For in vivo imaging, mice were anesthetized with 2% isoflurane (Aerrane, Baxter, Mississauga, CA) in air/O$_2$ (80/20). Acquisitions were realized 15 min and 30 min post-injection. Then, they were sacrificed and uterine horns, ovaries, and skin with abdominal mammary glands were removed to perform ex vivo fluorescence imaging of isolated organs. All images were acquired and analyzed using Living Image 4.7.2 software (PerkinElmer, Waltham, MA). Experiments were realized in the multimodal imaging platform IVIA (Clermont-Ferrand, France).

### 2.9. Docking Studies

In the absence of any experimentally solved structure, the GPER conformation was modeled using the GPCR-I-TASSER server [41], which is expressly dedicated to modeling G protein-coupled receptors. The protein structure was refined in its unliganded form in simulations performed with the GROMACS package [42] and complexed with the ligands using AutoDock Vina for initial prediction of their binding locations [43]. Finally, all-atom molecular dynamics (MDs) simulations in explicit water and in the presence of charge-neutralizing counter-ions were carried out to refine the protein–ligand complexes and to evaluate the effects of the ligand dynamics in GPER binding.

The peptide ERα17p was built from the N-terminal region of the human ERα ligand-binding domain in complex with E$_2$ and the E2#23FN3 monobody and deposited in the Protein Data Bank as entry 2OCF [44]. Missing regions including the tetrapeptidic sequence PLMI were reconstructed in

silico. Complete conformational freedom was given to all the missing residues of the ligand during the docking procedure and the whole structure was free to rearrange during the MD simulation step.

Molecular docking was carried out with high exhaustiveness of search according to a previously reported procedure [45]. AMBER ff99SB-ILDN [46] and GAFF [47] force fields were used for protein and ligand MD simulations, respectively. After an initial period of equilibration, conformational sampling was performed in the isobaric-isothermal ensemble for 20 ns. Reference values and coupling times used for the barostat and thermostat and other simulation conditions including the modeling of electrostatic and van der Waals forces and treatment of long-range corrections to London dispersion interactions, were as previously reported for other analogous protein–ligand complexes [48,49]. At the end of the MD simulations, the binding modes and the affinity of the ligands were estimated from the structures of the protein–ligand complexes obtained every nanosecond. The binding energy was evaluated by using the AutoDock Vina energy evaluation function [43] in score-only mode.

### 2.10. Statistical Analysis

Statistical analysis was done using ANOVA followed by the Newman–Keuls' method to determine differences in means. $p < 0.05$ was considered as statistically significant.

## 3. Results

### 3.1. ERα17p Elicits Anti-Proliferative Activity through GPER

We began our study by evaluating the proliferation of SkBr3 cells in the presence of the peptide ERα17p. After 72 h of treatment with 10 μM ERα17p, we noticed a roughly 25% decrease in the growth of SkBr3 cells (Figure 1A). No effect was observed with the scramble peptide. However, TUNEL assays failed to reveal apoptosis (Figure 2A,B).
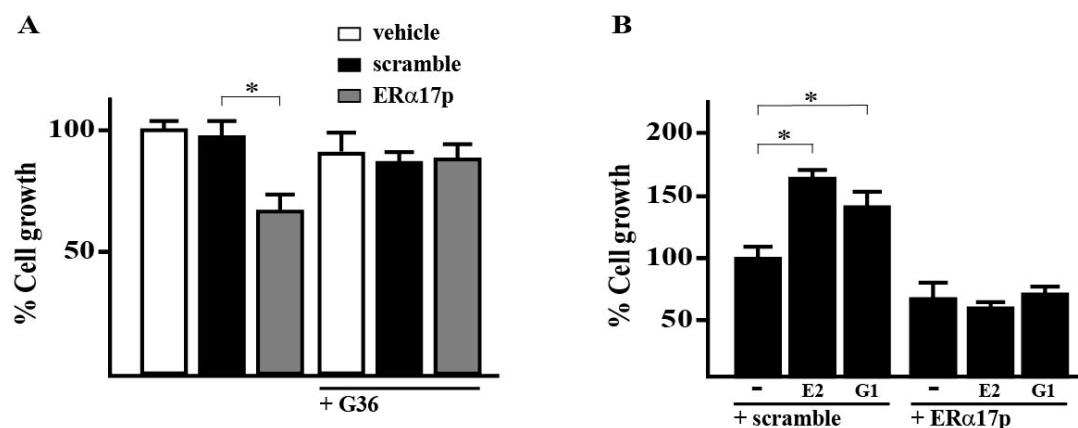


**Figure 1.** The peptide estrogen receptor $\alpha$ (ERα17p) inhibits the growth of SkBr3 breast cancer cells through the G protein-coupled estrogen receptor (GPER). (**A**) Effects of vehicle, 10 μM scramble peptide (control) and 10 μM ERα17p on SkBr3 cell growth in the presence or absence of the GPER antagonist G-36 (100 nM). (**B**) The proliferation of the SkBr3 breast cancer cells upon treatment with 100 nM $E_2$ or 100 nM G-1 is inhibited by 10 μM ERα17p. Cells were treated for three days with the indicated treatments and counted on day four. Proliferation of cells receiving vehicle was set as 100%, upon which cell growth induced by treatments was calculated. Each data point is the average ± SD of three independent experiments performed in triplicate. (∗) indicates $p < 0.05$.

Next, we tested the anti-proliferative action of ERα17p in the presence of the GPER antagonist G-36, [50], the GPER agonists G-1 [51] and $E_2$ [52], each at a concentration of 100 nM. The antagonist G-36 decreases the anti-proliferative action of ERα17p by ~50% (Figure 1A). The cell growth percentages obtained with G-36, alone, or after a pre-incubation of 72 h with 10 μM ERα17p were identical. We also observed that ERα17p at the same concentration prevents the growth effects induced by 100 nM $E_2$ or

G-1 (Figure 1B). No effect was observed with the scramble peptide. In any case, no additive effects were observed between ERα17p and the tested GPER ligands. Importantly, a negative cell growth value can be assigned to ERα17p when referred to the GPER in the absence of ligand (normalized reference with the scramble peptide: 100%).
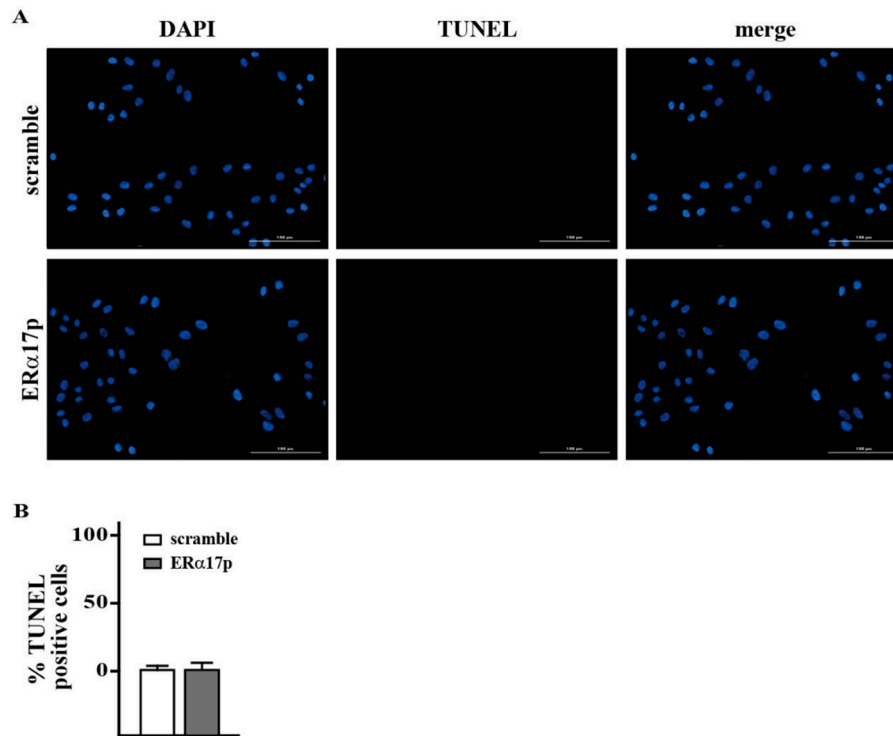


**Figure 2.** (**A**) Apoptosis detection by TUNEL (TdT-mediated dUTP nick-end-labeling) assay. (**B**) TUNEL staining (green) in SkBr3 cells treated for 72 h with 10 μM scramble peptide (control) and ERα17p. Nuclei were stained by 4′,6-diamidino-2-phenylindole (DAPI) (blue). Magnifications are indicated by horizontal bars (100 μm). Each experiment is representative of 20 random fields observed in each of three independent experiments. Bars graph represents the percentage of TUNEL-positive cells upon treatment versus vehicle. Values are the mean of three independent experiments.

*3.2. ERα17p and GPER Concomitant Staining at the Cell Membrane*

The cellular localization of ERα17p was explored by confocal microscopy using an N-terminal carboxyfluorescein-labeled version of the peptide (fluorescein-Ahx-ERα17p, Figure 3A). First, we confirmed that the fluorescein probe had no effect on the activity of the peptide. After 72 h of incubation, the labeled peptide (10 μM) induced 71% of viability (reference: ERα17p: 73%), confirming the absence of probe effect in the biological response. We observed a localization of the peptide at the membrane. The ERα17p fluorescence signal was superimposed with the immunofluorescent stain of the specific GPER antibody TA 55133, after 5 min of incubation (Figure 3B).
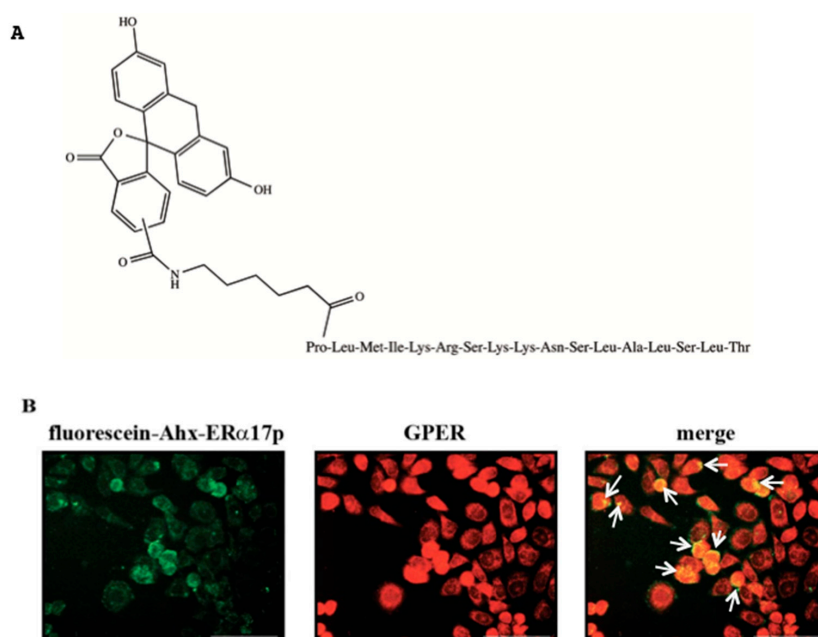
**Figure 3.** Fluorescence signal of the fluorescein-labeled peptide (carboxyfluorescein-Ahx-ERα17p). (**A**) Structure of the peptide ERα17p labeled at the C-terminus with Ahx (spacer) and carboxyfluorescein. The peptidic part of the molecule is written using the three letter code. (**B**) SkBr3 cells treated for 5 min with the peptide carboxyfluorescein-Ahx-ERα17p (10 μM, green signal, left) or immunostained with the anti-GPER antibody (red signal, middle). The overlay of the peptide carboxyfluorescein-Ahx-ERα17p and GPER signals generates the merge signal (in yellow) visualized in the right panel by white arrows. Each experiment is representative of 20 random fields observed in each of three independent experiments.

### 3.3. Absence of Interaction between ERα17p and Grb2 SH3 Domains

The GPER works in concert with growth factor receptors, which accept Grb2/Son of sevenless (Sos) as juxtamembrane mediators. We have used fluorescence spectroscopy to explore the interaction between ERα17p and the recombinant heterologous N- and C-terminal Sos-interacting Grb2 SH3 domains (SH3-SH2-SH3). Towards this aim, we have taken advantage of the presence of tryptophan in both Grb2 SH3 domains (Trp-36 and Trp-194 in the N- and C-terminal Grb2 SH3 domains, respectively) prone to fluorescence quenching under ligand association [53]. Fluorescence-based titration assay failed to reveal an interaction between Grb2 SH3 domains and the peptide ERα17p (Figure 4).
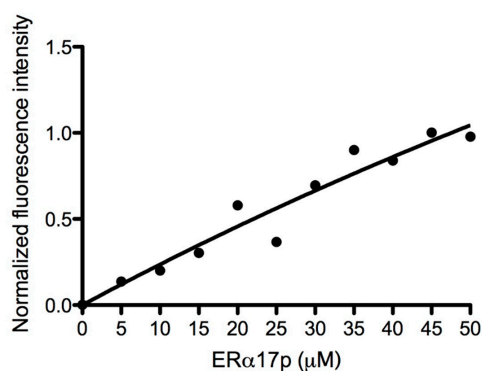


**Figure 4.** ERα17p/Grb2 SH3 domain interaction study by fluorescence spectroscopy. Fluorescence changes of the sole tryptophan of the Grb-SH3 domain (1 μM in 50 mM Tris buffer adjusted to pH 8) by ERα17p upon successive addition of 5 μL at $10^{-3}$ M in Tris buffer. Measurements were performed at 18 °C. The $\lambda_{exc}$ and $\lambda_{em}$ values were 280 nm and 350 nm, respectively. Experimental data points have been fitted with the software Prism 5.0a.

*3.4. ERα17p Downregulates GPER in a Proteasome-Dependent Manner and Decreases the Activation of EGFR and ERK1/2 as well as the Level of c-fos*

At a concentration of 10 µM and after 8 h of treatment, the peptide ERα17p drastically lowers the levels of GPER. It is noteworthy that both ERα17p and scramble peptide (10 µM) failed to decrease the level of GPER mRNA after 8 h of incubation (Figure 5A). Importantly, the proteasome inhibitor MG-132 prevents this decrease (Figure 5B). No effect was observed with the scramble peptide. ERα17p also abolishes the phosphorylation of EGFR (i.e., pEGFR) and ERK1/2 (i.e., pERK1/2), and decreases c-fos, as shown in Figure 5C (control: scramble peptide).
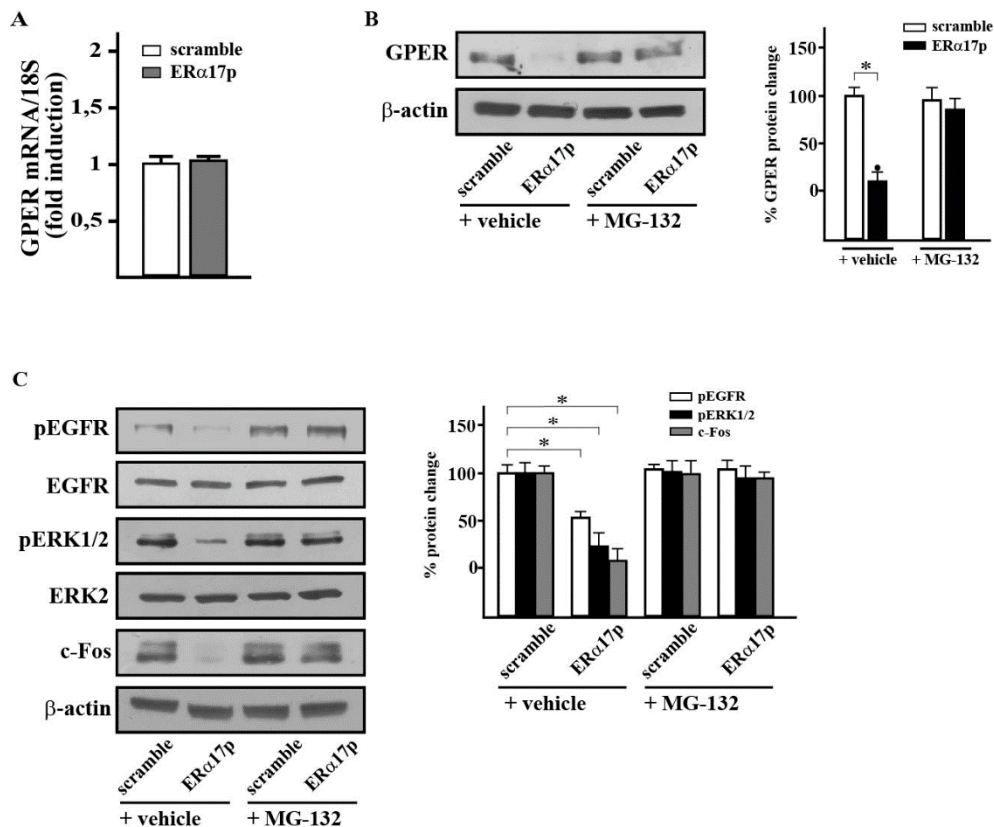


**Figure 5.** ERα17p downregulates proteins involved in GPER signaling in a proteasome-dependent manner. (**A**) The mRNA expression of GPER was evaluated by real-time PCR in SkBr3 cells treated for 8 h with either 10 µM scramble peptide (control) or 10 µM ERα17p. Results from three independent experiments, each in triplicate are normalized to actin and are shown as fold changes of mRNA expression induced by ERα17p with respect to cells treated with control scramble peptide (control). (**B**) Evaluation of the GPER protein level in SkBr3 cancer cells treated for 8 h with 10 µM scramble peptide (control) and 10 µM ERα17p, in the presence or in the absence of the proteasome inhibitor MG-132. Side panel shows densitometric analysis of the blot normalized to β-actin, which was used as a loading control. (**C**) Evaluation of pEGFR (phosphorylation of epidermal growth factor receptor), pERK1/2 (phosphorylation of extracellular signal-regulated kinase), and c-fos protein levels in SkBr3 cells treated for 8 h with 10 µM scramble peptide (control) and 10 µM ERα17p, in the presence or in the absence of the proteasome inhibitor MG-132. Side panel shows densitometric analysis of the blots normalized to EGFR, ERK2, and β-actin, which were used as loading controls for pEGFR, pERK1/2, and c-fos, respectively. Data are representative of at least two independent experiments. (∗) indicates $p < 0.05$.

### 3.5. ERα17p Diffuses Easily in Female Mice to Stain Mammary Glands

By using a cy5-labeled version of the peptide (H$_2$N-ERα17p-Pra(Cy5)-COOH, Figure 6A), a kinetic approach devoted to its distribution in mice shows that it localizes in the liver and bladder, when intraperitoneally injected at a dose of 2 mg/kg, after 15 min (Figure 6B). After 30 min, which corresponds to the incubation time for which a downregulation of GPER, pEGFR, pERK1/2, and c-fos is observed, it was almost exclusively found in the bladder (Figure 6B). After 30 min, we observed a moderate staining of the ovaries and of the uterus horn (Figure 6C). The labeling was even more impressive in the ventral skin, where the abdominal mammary glands were strongly stained (Figure 6C).
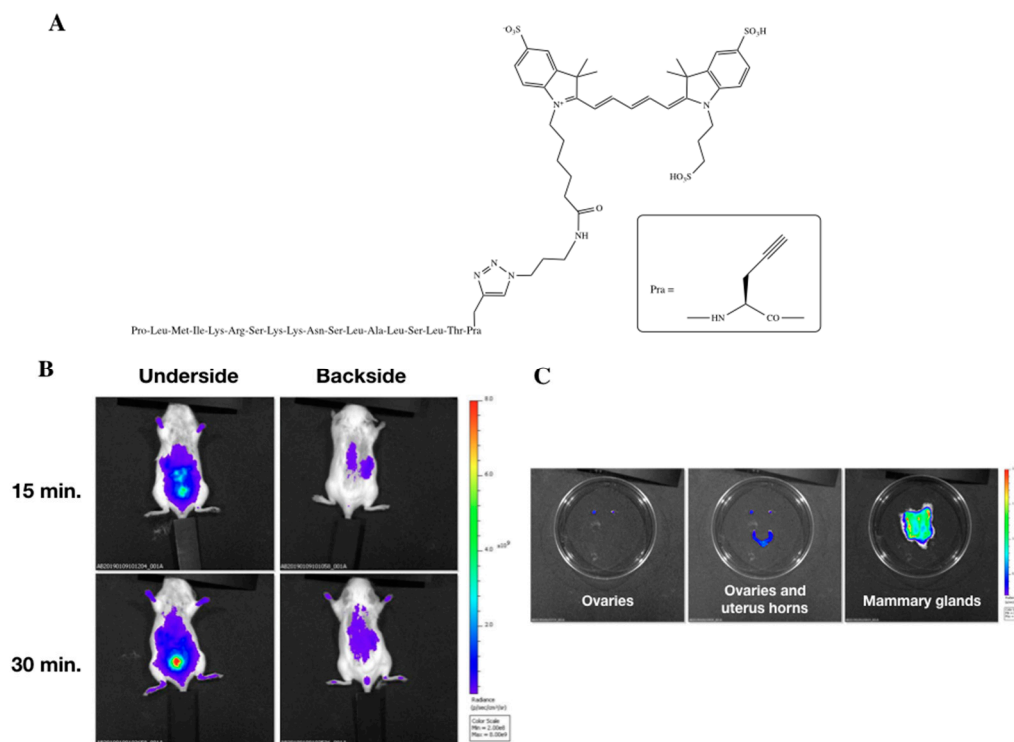


**Figure 6.** Distribution in mice of the peptide ERα17p at a dose of 2 mg/kg. (**A**) Structure of the Cy5-labeled peptide. (**B**) Pharmacokinetics of the Cy5-labeled peptide after 15 min and 30 min (underside and backside views). (**C**) Distribution of the peptide after 30 min in the ovaries (left), in the ovaries and uterus horns (middle), and in the mammary glands (right).

### 3.6. The PLMI Motif of ERα17p Supports the Anti-Proliferative Action of the Entire Peptide

We have evaluated the viability of SkBr3 cells in the presence of the N-terminal peptide fragment PLMI, over 72 h and at concentrations ranging from 10 to 100 μM. Remarkably, the tetrapeptide PLMI and the full-length peptide show comparable dose-dependent anti-proliferative effects (Figure 7A), strongly implying that the N-terminus of ERα17p is the driving force of action of the whole peptide. The scramble peptide, which was used as a control, was inactive.
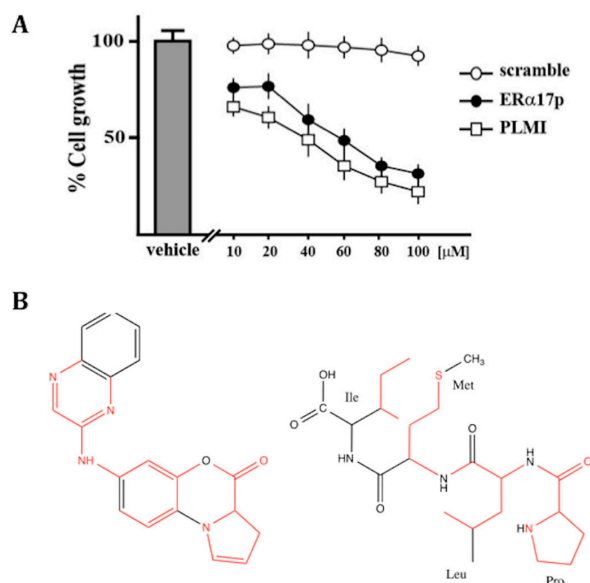
**Figure 7.** (**A**) The tetrapeptidic sequence PLMI inhibits the growth of breast cancer cells. SkBr3 cells were treated for 72 h with increasing concentrations of the scramble peptide (control), the ERα17p or the PLMI tetrapeptide. Cell viability is expressed as the percentage of cells upon exposure with ERα17p or PLMI with respect to cells treated with the scramble peptide (control). Values are mean ± SD of three independent experiments performed in triplicate. (**B**) Structural analogies (in red) between the GPR30 antagonist PBX1 (left) and the ERα17p-derived peptide motif PLMI (right).

*3.7. Docking and MD Studies of the PLMI Motif in the GPER*

The PLMI motif shares some structural similarities with the putative GPER antagonist 7-(quinoxalin-2-ylamino)-4*H*-benzo[b]pyrrolo [1,2-*d*][1,4]oxazin-7-one (PBX1) [36], as shown in Figure 8B. A blind search performed in a volume including the whole protein surface converged towards an interaction of the PLMI motif in the extracellular domain of the GPER and more particularly within the same cavity as other ligands, including PBX1 (Figure 8A). Predicted binding score values were found to be ~−6.5 kcal/mol (Table 1). The best structures fit with an alignment "head-first", where the N- and C-termini point towards the protein core and the solvent-exposed region, respectively. Accordingly, the proline and the leucine at the position 2 are deeply inserted in the protein with the two hydrophobic residues able to alternate positions (Figure 8B,C).

**Table 1.** Binding energies (in kcal/mol) of the PLMI motif obtained by molecular docking and MD simulation.

| Molecular Docking | | MD Simulation | |
|---|---|---|---|
| Structures N. | Score | Average | Standard Deviation |
| 1 | −6.5 | −5.7 | 0.7 |
| 2 | −6.5 | −5.6 | 0.6 |
| 3 | −6.5 | −3.7 | 0.4 |
| 4 | −6.3 | −4.2 | 0.5 |

Although the initial docked structures had similar binding scores, those structures numbered 3 and 4 showed, even after MD calculations, an energy >−4.3 kcal/mol, which corresponds to a Kd >$10^{-3}$ M (Table 1). The first two structures (N. 1 and 2, Table 1) showed more favorable binding energy (~−5.7 kcal/mol). The ligands PBX1 [36] and G-15 [54], which were used as references, were accommodated within the same protein site with energy values of −8.4 and −7.8 kcal/mol, respectively (Figure 8D, E). The mean values obtained in MD were systematically lower than those values predicted by molecular docking but were still consistent in predicting the association.
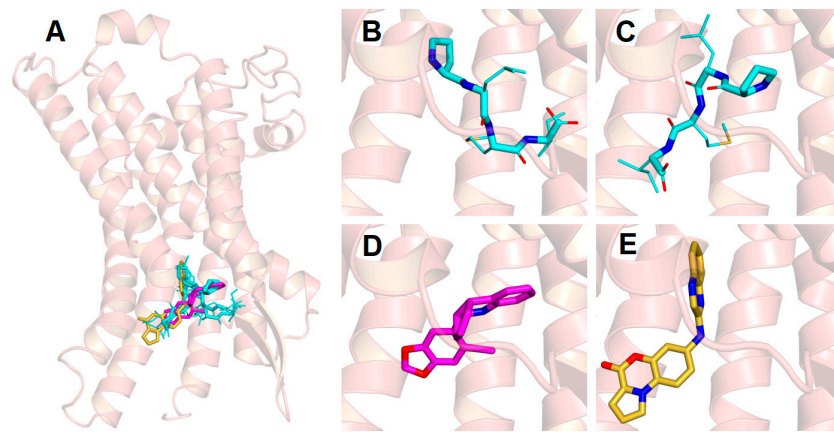
**Figure 8.** Docking and molecular dynamics (MDs) of ligands/GPER complexes. The GPER is shown as semi-transparent (ribbon), with the disordered region 1–50 omitted. Hydrogen atoms are omitted in all panels. Side chains are represented as smaller sticks compared to the backbone, with the exception of the ring of the proline that corresponds to the N-terminus. The oxygen and nitrogen atoms of the ligands are specified in red and blue, respectively. (**A**) Superimposition on the GPER model of the four most favorable docking structures of the tetrapeptide PLMI (cyan) and of two known GPER ligands (i.e., G-15 (magenta) and PBX1 (yellow)). (**B**, **C**) Details of the two main simulated binding modes of PLMI, with the N-terminus pointing towards the core of the GPER and with the side chain of the proline and the leucine 2 occupying alternate positions. (**D**, **E**) Binding modes of the selected compounds G-15 and PBX1, respectively.

As a control, we simulated the binding of the parent peptide ERα17p to the GPER. As shown in Figure 9, ERα17p, as with the PLMI motif, was oriented "head-first" in the same binding site, with the N-terminal region engulfed within the protein core. As in the case of the tetrapeptide, the proline and leucine residues that constitute the first two amino-acid residues could swap their position, determining for the N-terminal group two distinct binding configurations that interconverted during the simulated dynamics. The KRSKKNSLALSLT region of the full-length peptide was compacted at the entrance of the protein cavity. Strikingly, the binding energy was –7.2 kcal/mol, suggesting a Kd value in the low micromolar range.
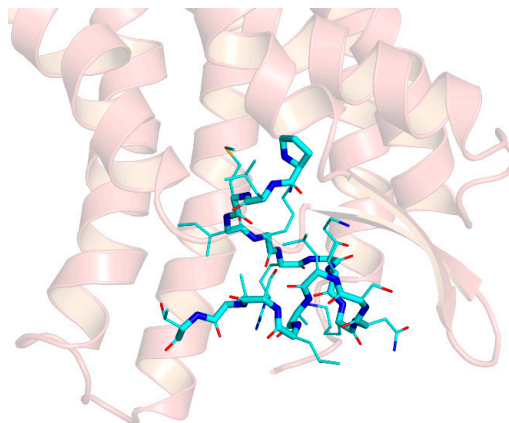


**Figure 9.** Model of binding of the peptide ERα17p (cyan) to the extracellular region of GPER. The GPER is shown as semi-transparent (ribbon), with the disordered region 1–50 omitted. Hydrogen atoms are omitted in all panels. Side chains are represented as smaller sticks compared to the main chain, with the exception of the ring of the N-terminal proline. The oxygen and nitrogen atoms of the ligands are specified in red and blue, respectively. The N-terminus of the peptide is inserted in the protein core, in a configuration with the first proline residues slightly more plunged within the protein core, whereas the C-terminus is at the entrance of the protein cavity.

## 4. Discussion

To distinguish the contribution of ERα from that of GPER, we have turned to the ERα-/GPER+ SkBr3 breast cancer cell line as it is classically used to explore GPER functionality [55,56]. Cell growth assays performed in the presence of ERα17p only, reveal an anti-proliferative activity when compared to those obtained in the absence of ligand (reference: 100% for the scramble peptide, Figure 1A,B). Thus, the GPER seems to harbor a constitutive (intrinsic) activity and implies an "inverse agonism" profile for ERα17p [57,58]. The intrinsic activity of the GPCR is well-documented [59–61]. In the same context, we have shown that the GPER antagonist G-36 was able to reduce the anti-proliferative potency of ERα17p (Figure 1A). Likewise, ERα17p abrogates the proliferation induced by E₂ and G-1 (Figure 1B). As cell growth values were systematically <100% (reference: 100% for the scramble peptide) when the peptide was used, we can conclude an "inverse agonism". As no synergistic effect was observed, an interaction within the same site as G-1 and G-36 seems likely. The "inverse" agonism profile of ERα17p could explain, at least partially, its opposing action in steroid-deprived conditions, where it stimulates breast cancer cell growth [19,62]. Importantly, the absence of biological response from the scramble peptide (reference), tested in the same experimental conditions as ERα17p, confirms that its action is sequence-dependent and not restricted to charge or other non-specific effects.

The ERα17p-induced decrease of the proliferation of the SkBr3 breast cancer cells logically resulting from either apoptosis or necrosis [35]. Terminal deoxynucleotidyl transferase dUTP Nick End Labeling (TUNEL), which is widely used to explore apoptosis, was carried out. As no small DNA fragments, which are a hallmark of apoptosis [63], were detected (Figure 2), a mechanism of action associated with necrosis must be proposed.

Over 30 min and 60 min, and at a peptide concentration of 10 μM, an ERα17p-induced downregulation of the GPER was detected. Such a phenomenon could result either from a genomic or a proteasome-dependent process. Since the level of GPER mRNA is not affected by the peptide (Figure 5C), a proteasome-dependent mechanism is likely. As the proteasome inhibitor MG-132 is capable of abrogating the GPER level reduction (Figure 5A), a post-translational mechanism is likely. As such, the activation of EGFR and of ERK2 (i.e., pEGFR and pERK2, respectively) as well as of the level of c-fos, were drastically decreased (Figure 5B). Hence, a desensitizing process of GPER should be evoked to explain the mechanism of action of ERα17p.

A crosstalk between GPER and growth factor receptors including EGFR has been demonstrated [64–66]. Activated growth factor receptors interact with the juxtamembrane adaptor protein Grb2, which, in turn, binds through its SH3 domains to the 1149–1158 carboxyl terminal polyproline II (PPII) region of Sos (Son of sevenless, sequence: V¹¹⁴⁹PPPVPPRRR¹¹⁵⁸) prior to the activation of the Shc/Ras/Raf/MEK/ERK/Elk-1/c-fos/c-jun transduction cascade [67–69]. Thus, we were interested in exploring a potential interaction between the peptide and the Grb2 SH3 domains. We were all the more motivated by this assay given that like the 1149–1158 SH3-interacting region of Sos, the ERα 295–311 sequence is partially structured in PPII [27]. As such, ERα17p could act as a Sos competitor with respect to Grb2. Fluorescence-based titration assays, which were previously described [53], failed to show an association of the peptide with Grb2, giving weight to a direct GPER-mediated mechanism (Figure 4).

In previous studies, we have shown that the peptide ERα17p was able to associate with both artificial anionic [24] and natural [35] membranes. On the basis of these preliminary results we wished to determine if the peptide localized at the membrane of ERα–/GPER+ SkBr3. We have thus used a fluorescein-labeled version of the peptide, where an Ahx (aminohexanoic acid, Figure 3A) was introduced between the fluorescent probe and the peptide to avoid any steric interference that would compromise protein–ligand interactions and, thereby, biological response. The fluorescent peptide was active with the same potency as the parent peptide, validating our approach. Localization of the peptide at the membrane was indeed observed, confirming our previous studies (Figure 3B) [35]. Such results could be related to its weak ability to internalize in cells [24,37,70]. Importantly, the fluorescence signal of the labeled peptide was shown to co-localize with the GPER, as highlighted by a concomitant

immunofluorescence stain using the specific GPER antibody TA 55,133 (Figure 3B). Hence, ERα17p membrane targeting may corroborate with a direct association of the peptide within the extracellular GPER ligand-binding site. The full-length 66 kDa ERα and its 36 kDa-truncated isoform, which both share the 295–311 sequence, associate physically with GPER [71–73].

A comparison of the structure of the ERα17p with a panel of putative GPER ligands [74] highlighted some structural analogies between the PLMI motif and the N-(4-oxo-4*H*-benzo[b]pyrrolo[1,2-*d*][1,4] oxazin-7-yl)benzamide (PBX1) GPER antagonist (Figure 7B) [36]. Thus, an interaction of the PLMI motif with the extracellular domain of the GPER, where other ligands (including PBX1) bind, is likely. Given these observations, we have used docking and molecular dynamics (MD) simulations to calculate the four most stable GPER/PLMI complexes. Our previous studies on GPER-ligand complexes [74] were also used as a benchmark to assess the accuracy of the theoretical model here used for the protein structure. A number of GPER ligands (including the agonists $E_2$ and G-1 and the antagonist G-15) were preliminarily tested to prove their binding within a common region already identified as the protein-binding site. Recognition of the PLMI motif by the extracellular ligand-binding site of the GPER was predicted in the same protein-binding site (Figure 8A–E). The docking procedure allowed us to estimate moderate Kd values (>1 μM). The fact that the mean MD values were lower than those values predicted by docking calculations emphasizes the importance of considering the dynamics of the whole molecular complex for a more accurate estimation of the binding energy. The standard deviations obtained for the two best structures were close to the energetic differences recorded by simple docking and MD simulations and were consistent with the energetic fluctuations resulting from thermal effects at room temperature (~0.6 kcal/mol). These results suggest that molecular docking captures only a static state of the complex corresponding to single isolated minima in the conformational landscape of the tetrapeptide. In other words, an entropic cost due to a decrease of flexibility under peptide/protein association seems likely. The fact that the tetrapeptide remains bound in the same site with a preserved "head-first" configuration during the calculation period validates our model [75,76]. Thus, we have tested the cell growth potency of the peptide PLMI in SkBr3. Importantly, the same effect as the parent peptide ERα17p was observed, further validating our model. These results suggest that only the part of the peptide deeply penetrating in the receptor is responsible for the action of the whole peptide.

The same calculations with the full-length peptide reveal a similar association with the GPER, with a predicted Kd in the micromolar range. The contribution of the first four N-terminal residues was predominant (–5.1 kcal/mol) as the entire peptide remains attached to the GPER ligand-binding site with the N-terminal proline projected towards the receptor core. Due to a significant energy contribution by ~1–3 kcal/mol depending upon the degree of compaction of the unstructured C-terminal region of the peptide (sequence KRSKKNSLALSLT) in the entrance of the protein cavity (Figure 9), we did not attempt to make an accurate estimate of the binding affinity. This effect might depend on finer detail in the parameterization of the solvent that cannot be easily corrected, as suggested by simulations with different water models obtained from a protocol recently developed for disordered peptides and protein regions [77,78].

In a previous work, we have shown that the peptide ERα17p was able to reduce by ~50% the volume of subscapularis xenografted human breast tumors obtained from ERα−/GPER+ MDA-MB-231 basal B TNBC cells [79] in mice without apparently affecting the liver. Thus, a specificity of the peptide for breast tissue seems likely [35]. In the present study, we were interested in exploring the distribution of the peptide in female organs by using an ERα17p peptide labeled at the C-terminus with the bright far-red fluorescent dye Cy5 (ERα17p-Pra(Cy5), Figure 6A), which is ideal for in vivo distribution studies. We observed that ERα17p diffuses easily with typical organ distribution in mice (Figure 6B) and a modest staining of the ovaries and uterus horns (Figure 6C). Likewise, a strong tropism of the peptide for the mammary glands, where GPER is widely expressed, was confirmed (Figure 6C).

In the present study, we have shown that the anti-proliferative action of the peptide ERα17p was mediated by the heptatransmembrane receptor GPER, with which it interacts. Since ERα17p is responsible for a proteasome-dependent downregulation of the GPER, we have concluded that a GPER

desensitization mechanism of action from the peptide is involved. A consequent decrease of the level of pEGFR, pERK1/2 as well as of GPER and c-fos was observed. In female mice, the peptide localizes rapidly in GPER rich tissues such as ovaries, uterus horns, and particularly the mammary glands. The N-terminal PLMI motif, which presents strong structural similarities with the putative GPER antagonist PBX1 was shown to support the anti-proliferative action of the whole peptide by locating within the same site of GPER as other ligands. These observations are consistent with the competitive effects of ERα17p with respect to G-1, G-36, and E$_2$. In fact, ERα17p acts as an inverse agonist. As such, the motif PLMI could open new avenues for the synthesis of GPER disruptors, which offer hope, as do other GPCR inhibitors, for the treatment of breast cancer [80]. Our work also raises the question as to whether the 295–311 sequence of ERα could correspond to a recruitment platform with the GPER. We would also like to draw attention to the fact that the PLMI motif is, to the best of our knowledge, the first peptidic GPER ligand identified to date.

**Author Contributions:** Y.J. and M.M. conceived the design of this study. R.L., F.G. and G.R.G. performed biochemical and pharmacological experiments. B.R. was in charge of modeling and docking studies. Y.J. and C.B. contributed to the chemical synthesis of peptides and labeled peptides. I.B. carried out fluorescence spectroscopy experiments. C.M., L.B and A.E. worked on in vivo experiments. Y.J. and M.M. analyzed and interpreted data. Y.J. and M.M. wrote the manuscript. All authors have read and approved the manuscript.

**Conflicts of Interest:** The authors declare no conflicts of interest.

## References

1. Bartos, J.R. *Estrogens: Production, Functions and Applications*; Nova Science Publishers, Inc.: New York, NY, USA, 2009; pp. 231–272.
2. Norman, A.W.; Mizwicki, M.T.; Norman, D.P.G. Steroid-hormone rapid actions, membrane receptors and a conformational ensemble model. *Nat. Rev.* **2004**, *3*, 27–41. [CrossRef] [PubMed]
3. Yan, Y.; Yu, L.; Castro, L.; Dixon, D. ERα36, a variant of estrogen receptor α, is predominantly localized in mitochondria of human uterine smooth muscle and leiomyoma cells. *PLoS ONE* **2017**, *12*, e0186078. [CrossRef] [PubMed]
4. Marino, M.; Ascenzi, P. Steroid hormone rapid signaling: The pivotal role of S-palmitoylation. *IUBMB Life* **2006**, *58*, 716–719. [CrossRef] [PubMed]
5. Wang, Z.; Zhang, X.; Shen, P.; Loggie, B.W.; Chang, Y.; Deuel, T.F. Identification, cloning, and expression of human estrogen receptor-alpha36, a novel variant of human estrogen receptor-alpha66. *Biochem. Biophys. Res. Commun.* **2005**, *336*, 1023–1027. [CrossRef] [PubMed]
6. Li, L.; Haynes, M.P.; Bender, J.R. Plasma membrane localization and function of the estrogen receptor alpha variant (ER46) in human endothelial cells. *Proc. Natl. Acad. Sci. USA* **2003**, *100*, 4807–4812. [CrossRef] [PubMed]
7. Carmeci, C.; Thompson, D.A.; Ring, H.Z.; Francke, U.; Weigel, R.J. Identification of a gene (GPR30) with homology to the G-protein-coupled receptor superfamily associated with estrogen receptor expression in breast cancer. *Genomics* **1997**, *45*, 607–617. [CrossRef] [PubMed]
8. Hsu, L.H.; Chu, N.M.; Lin, Y.F.; Kao, S.H. G-protein coupled estrogen receptor in breast cancer. *Int. J. Mol. Sci.* **2019**, *20*, 306. [CrossRef]
9. Molina, L.; Figueroa, C.D.; Bhoola, K.D.; Ehrenfeld, P. GPER-1/GPR30 a novel estrogen receptor sited in cell membrane: Therapeutic coupling to breast cancer. *Expert Opin. Ther. Targets* **2017**, *21*, 755–766. [CrossRef]
10. Zwart, W.; de Leeuw, R.; Rondaij, M.; Neefjes, J.; Mancini, M.A.; Michalides, R. The hinge region of the human estrogen receptor determines functional synergy between AF-1 and AF-2 in the quantitative response to estradiol and tamoxifen. *J. Cell Sci.* **2010**, *123*, 1253–1261. [CrossRef]

11. Popov, V.M.; Wang, C.; Shirley, L.A.; Rosenberg, A.; Li, S.; Nevalainen, M.; Fu, M.; Pestell, R.G. The functional significance of nuclear receptor acetylation. *Steroids* **2007**, *72*, 221–230. [CrossRef]

12. Ma, Y.; Fan, S.; Hu, C.; Meng, Q.; Fuqua, S.A.; Pestell, R.G.; Tomita, Y.A.; Rosen, E.M. BRCA1 regulates acetylation and ubiquitination of estrogen receptor-alpha. *Mol. Endocrinol.* **2010**, *24*, 76–90. [CrossRef] [PubMed]

13. Wang, C.; Tian, L.; Popov, V.M.; Pestell, R.G. Acetylation and nuclear receptor action. *J. Steroid Biochem. Mol. Biol.* **2011**, *123*, 91–100. [CrossRef] [PubMed]

14. Cui, Y.; Zhang, M.; Pestell, R.; Curran, E.M.; Welshons, W.V.; Fuqua, S.A. Phosphorylation of estrogen receptor α blocks its acetylation and regulates estrogen sensitivity. *Cancer Res.* **2004**, *64*, 9199–9208. [CrossRef]

15. Ward, R.D.; Weigel, N.L. Steroid receptor phosphorylation: Assigning function to site-specific phosphorylation. *Biofactors* **2009**, *35*, 528–536. [CrossRef] [PubMed]

16. Subramanian, K.; Jia, D.; Kapoor-Vazirani, P.; Powell, D.R.; Collins, R.E.; Sharma, D.; Peng, J.; Cheng, X.; Vertino, P.M. Regulation of estrogen receptor α by the SET7 lysine methyltransferase. *Mol. Cell* **2008**, *30*, 336–347. [CrossRef] [PubMed]

17. La Rosa, P.; Pesiri, V.; Marino, M.; Acconcia, F. 17β-estradiol-induced cell proliferation requires estrogen receptor (ER) α monoubiquitination. *Cell Signal.* **2011**, *23*, 1128–1135. [CrossRef]

18. Sentis, S.; Le Romancier, M.; Bianchin, C.; Rostan, M.C.; Corbo, L. Sumoylation of the estrogen receptor alpha hinge region regulates its transcriptional activity. *Mol. Endocrinol.* **2005**, *19*, 2671–2684. [CrossRef]

19. Gallo, D.; Jacquemotte, F.; Cleeren, A.; Laïos, I.; Hadiy, S.; Rowlands, M.G.; Caille, O.; Nonclercq, D.; Laurent, G.; Jacquot, Y.; et al. Calmodulin-independent, agonistic properties of a peptide containing the calmodulin binding site of estrogen receptor α. *Mol. Cell. Endocrinol.* **2007**, *268*, 37–49. [CrossRef]

20. Pierrat, B.; Heery, D.M.; Chambon, P.; Losson, R. A highly conserved region in the hormone-binding domain of the human estrogen receptor functions as an efficient transactivation domain in yeast. *Gene* **1994**, *143*, 193–200. [CrossRef]

21. Ylikomi, T.; Bocquel, M.T.; Berry, M.; Gronemeyer, H.; Chambon, P. Cooperation of proto-signals for nuclear accumulation of estrogen and progesterone receptors. *EMBO J.* **1992**, *11*, 3681–3694. [CrossRef]

22. Seielstad, D.A.; Carlson, K.E.; Kushner, P.J.; Greene, G.L.; Katzenellenbogen, J.A. Analysis of the structure core of the human estrogen receptor ligand binding domain by selective proteolysis/mass spectrometric analysis. *Biochemistry* **1995**, *34*, 12605–12615. [CrossRef] [PubMed]

23. Brandt, M.E.; Vickery, L.E. Cooperativity and dimerization of recombinant human estrogen receptor hormone-binding domain. *J. Biol. Chem.* **1997**, *272*, 4843–4849. [CrossRef] [PubMed]

24. Byrne, C.; Khemtémourian, L.; Pelekanou, V.; Kampa, M.; Leclercq, G.; Sagan, S.; Castanas, E.; Burlina, F.; Jacquot, Y. ERα17p, a peptide reproducing the hinge region of the estrogen receptor α associates to biological membranes: A biophysical approach. *Steroids* **2012**, *77*, 979–987. [CrossRef] [PubMed]

25. Conway, K.; Parrish, E.; Edmiston, S.N.; Tolbert, D.; Tse, C.K.; Geradts, J.; Livasy, C.A.; Singh, H.; Newman, B.; Millikan, R.C. The estrogen receptor-α A908G (K303R) mutation occurs at a low frequency in invasive breast tumors: Results from a population-based study. *Breast Cancer Res.* **2005**, *7*, R871–R880. [CrossRef] [PubMed]

26. Komagata, S.; Nakajima, M.; Tsuchiya, Y.; Katoh, M.; Kizu, R.; Kyo, S.; Yokoi, T. Decreased responsiveness of naturally occurring mutants of human estrogen receptor α to estrogens and antiestrogens. *J. Steroid Biochem. Mol. Biol.* **2006**, *100*, 79–86. [CrossRef] [PubMed]

27. Jacquot, Y.; Gallo, D.; Leclercq, G. Estrogen receptor alpha—Identification by a modelling approach of a potential polyproline II recognizing domain within the AF-2 region of the receptor that would play a role of prime importance in its mechanism of action. *J. Steroid Biochem. Mol. Biol.* **2007**, *104*, 1–10. [CrossRef] [PubMed]

28. Adzhubei, A.A.; Sternberg, M.J.; Makarov, A.A. Polyproline II helix in proteins: Structure and function. *J. Mol. Biol.* **2013**, *425*, 2100–2132. [CrossRef]

29. Bouhoute, A.; Leclercq, G. Modulation of estradiol and DNA binding to estrogen receptor upon association with calmodulin. *Biochem. Biophys. Res. Commun.* **1995**, *208*, 748–755. [CrossRef]

30. Li, L.; Li, Z.; Sacks, D.B. The transcriptionnal activity of estrogen receptor-α is dependent on $Ca^{2+}$/calmodulin. *J. Biol. Chem.* **2005**, *280*, 13097–13104. [CrossRef]

31. Teyssier, C.; Belguise, K.; Galtier, F.; Chalbos, D. Characterization of the physical interaction between estrogen receptor α and JUN protein. *J. Biol. Chem.* **2001**, *276*, 36361–36369. [CrossRef]

32. Zhou, D.; Ye, J.J.; Li, Y.; Lui, K.; Chen, S. The molecular basis of the interaction between the proline-rich SH3-binding motif of PNRC and estrogen receptor alpha. *Nucleic Acids Res.* **2006**, *34*, 5974–5986. [CrossRef] [PubMed]

33. De Leon, J.T.; Iwai, A.; Feau, C.; Garcia, Y.; Balsiger, H.A.; Storer, C.L.; Suro, R.M.; Garza, K.M.; Lee, S.; Kim, Y.S.; et al. Targeting the regulation of androgen receptor signaling by the heat shock protein 90 cochaperone FKBP52 in prostate cancer cells. *Proc. Natl. Acad. Sci. USA* **2011**, *108*, 11878–11883. [CrossRef] [PubMed]

34. Byrne, C.; Henen, M.A.; Belnou, M.; Cantrelle, F.X.; Kamah, A.; Qi, H.; Giustiniani, J.; Chambraud, B.; Baulieu, E.E.; Lippens, G.; et al. A β-turn motif in steroid hormone receptor's ligand-binding domains interacts with the peptidyl-prolyl isomerase (PPIase) catalytic site of the immunophilin FKBP52. *Biochemistry* **2016**, *55*, 5366–5376. [CrossRef] [PubMed]

35. Pelekanou, V.; Kampa, M.; Gallo, D.; Notas, G.; Troullinaki, M.; Duvillier, H.; Jacquot, Y.; Stathopoulos, E.N.; Castanas, E.; Leclercq, G. The estrogen receptor alpha-derived peptide ERα17p ($P_{295}$-$T_{311}$) exerts pro-apoptotic actions in breast cancer cells in vitro and in vivo, independently from their ERα status. *Mol. Oncol.* **2011**, *5*, 36–47. [CrossRef] [PubMed]

36. Maggiolini, M.; Santolla, M.F.; Avino, S.; Aiello, F.; Rosano, C.; Garofalo, A.; Grande, F. Identification of two benzopyrroloxazines acting as selective GPER antagonists in breast cancer cells and cancer-associated fibroblasts. *Future Med. Chem.* **2015**, *7*, 437–448. [CrossRef] [PubMed]

37. Leiber, D.; Burlina, F.; Byrne, C.; Robin, P.; Piesse, C.; Gonzalez, L.; Leclercq, G.; Tanfin, Z.; Jacquot, Y. The sequence Pro295-Thr311 of the hinge region of oestrogen receptor α is involved in ERK1/2 activation via GPR30 in leiomyoma cells. *Biochem. J.* **2015**, *472*, 97–109. [CrossRef] [PubMed]

38. Guilloteau, J.P.; Fromage, N.; Ries-Kautt, M.; Reboul, S.; Bocquet, D.; Dubois, H.; Faucher, D.; Colonna, C.; Ducruix, A.; Becquart, J. Purification, stabilization, and crystallization of a modular protein: Grb2. *Proteins* **1996**, *25*, 112–119. [CrossRef]

39. Hewitson, T.D.; Bisucci, T.; Darby, I.A. Histochemical localization of apoptosis with in situ labeling of fragmented DNA. *Methods Mol. Biol.* **2006**, *326*, 227–234. [PubMed]

40. Lappano, R.; Sebastiani, A.; Cirillo, F.; Rigiracciolo, D.C.; Galli, G.R.; Curcio, R.; Malaguarnera, R.; Belfiore, A.; Cappello, A.R.; Maggiolini, M. The lauric acid-activated signaling prompts apoptosis in cancer cells. *Cell Death Discov.* **2017**, *3*, 17063. [CrossRef]

41. Zhang, J.; Yang, J.; Jang, R.; Zhang, Y. GPCR-I-TASSER: A hybrid approach to G protein-coupled receptor structure modeling and the application to the human genome. *Structure* **2015**, *23*, 1538–1549. [CrossRef]

42. Abraham, M.J.; Murtola, T.; Schulz, R.; Páll, S.; Smith, J.C.; Hess, B.; Lindahl, E. GROMACS: High performance molecular simulations through multi-level parallelism from laptops to supercomputers. *SoftwareX* **2015**, 19–25. [CrossRef]

43. Trott, O.; Olson, A.J. AutoDock Vina: Improving the speed and accuracy of docking with a new scoring function, efficient optimization, and multithreading. *J. Comput. Chem.* **2010**, *31*, 455–461. [CrossRef] [PubMed]

44. Koide, A.; Abbatiello, S.; Rothgery, L.; Koide, S. Probing protein conformational changes in living cells by using designer binding proteins: Application to the estrogen receptor. *Proc. Natl. Acad. Sci. USA* **2002**, *99*, 1253–1258. [CrossRef] [PubMed]

45. Grande, F.; Rizzuti, B.; Occhiuzzi, M.A.; Ioele, G.; Casacchia, T.; Gelmini, F.; Guzzi, R.; Garofalo, A.; Statti, G. Identification by molecular docking of homoisoflavones from *Leopoldia comosa* as ligands of estrogen receptors. *Molecules* **2018**, *23*, 894. [CrossRef] [PubMed]

46. Lindorff-Larsen, K.; Piana, S.; Palmo, K.; Maragakis, P.; Klepeis, J.L.; Dror, R.O.; Shaw, D.E. Improved side-chain torsion potentials for the Amber ff99SB protein force field. *Proteins* **2010**, *78*, 1950–1958. [CrossRef] [PubMed]

47. Wang, J.; Wolf, R.M.; Caldwell, J.W.; Kollman, P.A.; Case, D.A. Development and testing of a general amber force field. *J. Comput. Chem.* **2004**, *25*, 1157–1174. [CrossRef] [PubMed]

48. Pantusa, M.; Bartucci, R.; Rizzuti, B. Stability of trans-resveratrol associated with transport proteins. *J. Agric. Food Chem.* **2014**, *62*, 4384–4391. [CrossRef] [PubMed]

49. Evoli, S.; Mobley, D.L.; Guzzi, R.; Rizzuti, B. Multiple binding modes of ibuprofen in human serum albumin identified by absolute binding free energy calculations. *Phys. Chem. Chem. Phys.* **2016**, *18*, 32358–32368. [CrossRef] [PubMed]

50. Dennis, M.K.; Field, A.S.; Burai, R.; Ramesh, C.; Petrie, W.K.; Bologa, C.G.; Oprea, T.I.; Yamaguchi, Y.; Hayashi, S.I.; Sklar, L.A.; et al. Identification of a GPER/GPR30 antagonist with improved estrogen receptor counterselectivity. *J. Steroid Biochem. Mol. Biol.* **2011**, *127*, 358–366. [CrossRef]

51. Bologa, C.G.; Revankar, C.M.; Young, S.M.; Edwards, B.S.; Arterburn, J.B.; Kiselyov, A.S.; Parker, M.A.; Tkachenko, S.E.; Savchuck, N.P.; Sklar, L.A.; et al. Virtual and biomolecular screening converge on a selective agonist for GPR30. *Nat. Chem. Biol.* **2006**, *2*, 207–212. [CrossRef]

52. Vivacqua, A.; Bonofiglio, D.; Recchia, A.G.; Musti, A.M.; Picard, D.; Andò, S.; Maggiolini, M. The G protein-coupled receptor GPR30 mediates the proliferative effects induced by 17beta-estradiol and hydroxytamoxifen in endometrial cancer cells. *Mol. Endocrinol.* **2006**, *20*, 631–646. [CrossRef]

53. Jacquot, Y.; Broutin, I.; Miclet, E.; Nicaise, M.; Lequin, O.; Goasdoué, N.; Joss, C.; Karoyan, P.; Desmadril, M.; Ducruix, A.; et al. High affinity Grb2-SH3 domain ligand incorporating $C^\beta$-substituted prolines in a Sos-derived decapeptide. *Bioorg. Med. Chem.* **2007**, *15*, 1439–1447. [CrossRef]

54. Dennis, M.K.; Burai, R.; Ramesh, C.; Petrie, W.K.; Alcon, S.N.; Nayak, T.K.; Bologa, C.G.; Leitao, A.; Brailoiu, E.; Deliu, E.; et al. In vivo effects of a GPR30 antagonist. *Nat. Chem. Biol.* **2009**, *5*, 421–427. [CrossRef]

55. Prossnitz, E.R.; Maggiolini, M. Mechanisms of estrogen signaling and gene expression via GPR30. *Mol. Cell. Endocrinol.* **2009**, *308*, 32–38. [CrossRef]

56. Chimento, A.; Casaburi, I.; Rosano, C.; Avena, P.; De Luca, A.; Campana, C.; Martire, E.; Santolla, M.F.; Maggiolini, M.; Pezzi, V.; et al. Oleuropein and hydroxytyrosol activate GPER/GPR30-dependent pathways leading to apoptosis of ER-negative SKBR3 breast cancer cells. *Mol. Nutr. Food Res.* **2014**, *58*, 478–489. [CrossRef]

57. Bosier, B.; Hermans, E. Versatility of GPCR recognition by drugs: From biological implications to therapeutic relevance. *Trends Pharmacol. Sci.* **2007**, *28*, 438–446. [CrossRef]

58. Sato, J.; Makita, N.; Iiri, T. Inverse agonism: The classic concept of GPCRs revisited. *Endocr. J.* **2016**, *63*, 507–514. [CrossRef]

59. Zhang, B.; Albaker, A.; Plouffe, B.; Lefebvre, C.; Tiberi, M. Constitutive activities and inverse agonism in dopamine receptors. *Adv. Pharmacol.* **2014**, *70*, 175–214.

60. Takezako, T.; Unal, H.; Karnik, S.S.; Node, K. Current topics in angiotensin II type 1 receptor research: Focus on inverse agonism, receptor dimerization and biased agonism. *Pharmacol. Res.* **2017**, *123*, 40–50. [CrossRef]

61. Riddy, D.M.; Cook, A.E.; Shackleford, D.M.; Pierce, T.L.; Mocaer, E.; Mannoury la Cour, C.; Sors, A.; Charman, W.N.; Summers, R.J.; Sexton, P.M.; et al. Drug-receptor kinetics and sigma-1 receptor affinity differentiate clinically evaluated histamine $H_3$ receptor antagonists. *Neuropharmacology* **2019**, *144*, 244–255. [CrossRef]

62. Gallo, D.; Haddad, I.; Duvillier, H.; Jacquemotte, F.; Laïos, I.; Laurent, G.; Jacquot, Y.; Vinh, J.; Leclercq, G. Trophic effect in MCF-7 cells of ERα17p, a peptide corresponding to a platform regulatory motif of the estrogen receptor α—Underlying mechanisms. *J. Steroid Biochem. Mol. Biol.* **2008**, *109*, 138–149. [CrossRef]

63. Zhang, J.H.; Xu, M. DNA fragmentation in apoptosis. *Cell Res.* **2000**, *10*, 205–211. [CrossRef]

64. Lappano, R.; de Marco, P.; de Francesco, E.M.; Chimento, E.; Pezzi, V.; Maggiolini, M. Cross-talk between GPER and growth factor signaling. *J. Steroid. Biochem. Mol. Biol.* **2013**, *137*, 50–56. [CrossRef]

65. Magruder, H.T.; Quinn, J.A.; Schwartzbauer, J.E.; Reichner, J.; Huang, A.; Filardo, E.J. The G protein-coupled estrogen receptor-1, GPER-1, promotes fibrillogenesis via Shc-dependent pathway resulting in anchorage-independent growth. *Horm. Cancer* **2014**, *5*, 390–404. [CrossRef]

66. de Marco, P.; Cirillo, F.; Vivacqua, A.; Malaguarnera, R.; Belfiore, A.; Maggiolini, M. Novel aspects concerning the functional cross-talk between the insulin/IGF-I system and estrogen signaling in cancer cells. *Front. Endocrinol. (Lausanne)* **2015**, *6*, 30. [CrossRef]

67. Miclet, E.; Jacquot, Y.; Goasdoue, N.; Lavielle, S. Solution structural study of a proline-rich decapeptide. *C. R. Chim.* **2008**, *11*, 486–492. [CrossRef]

68. Gril, B.; Vidal, M.; Assayag, F.; Poupon, M.F.; Liu, W.Q.; Garbay, C. Grb2-SH3 ligands inhibit the growth of HER2+ cancer cells and has antitumor effects in human cancer xenografts alone and in combination with docetaxel. *Cancer Ther.* **2007**, *121*, 407–415. [CrossRef]

69. Ijaz, M.; Shahabz, M.; Jiang, W.; Fathy, A.H.; Nesa, E.U.; Wang, D.; Wang, F. Oncogenic role of Grb2 in breast cancer and Grb2 antagonists as therapeutic drugs. *Cancer Ther. Oncol. Int. J.* **2017**, *3*, 1084–1095.

70. Notas, G.; Kampa, M.; Pelekanou, V.; Troullinaki, M.; Jacquot, Y.; Leclercq, G.; Castanas, E. Whole transcriptome analysis of the ER synthetic fragment P$_{295}$-T$_{311}$ (ERα17p) identifies specific ERα-isoform (ERα, ERα36)-dependent and -independent actions in breast cancer cells. *Mol. Oncol.* **2013**, *7*, 595–610. [CrossRef]

71. Vivacqua, A.; Lappano, R.; De Marco, P.; Sisci, D.; Aquila, S.; De Amicis, F.; Fuqua, S.A.; Andòs, S.; Maggiolini, M. G protein-coupled receptor 30 expression is up-regulated by EGF and TGF alpha in estrogen receptor alpha-positive cancer cells. *Mol. Endocrinol.* **2009**, *23*, 1815–1826. [CrossRef]

72. Irsik, D.L.; Carmines, P.K.; Lane, P.H. Classical estrogen receptors and ERα splice variants in the mouse. *PLoS ONE* **2013**, *8*, e70926. [CrossRef]

73. Pelekanou, V.; Kampa, M.; Kiagiadaki, F.; Deli, A.; Theodoropoulos, P.; Agrogiannis, G.; Patsouris, E.; Tsapis, A.; Castanas, E.; Notas, G. Estrogen anti-inflammatory activity on human monocytes is mediated through cross-talk between estrogen receptor ERα36 and GPR30/GPER1. *J. Leukoc. Biol.* **2016**, *99*, 333–347. [CrossRef]

74. Rosano, C.; Ponassi, M.; Santolla, M.F.; Pisano, A.; Felli, L.; Vivacqua, A.; Maggiolini, M.; Lappano, R. Macromolecular modelling and docking simulations for the discovery of selective GPER ligands. *AAPS J.* **2016**, *18*, 41–46. [CrossRef]

75. Rizzuti, B.; Bartucci, R.; Sportelli, L.; Guzzi, R. Fatty acid binding into the highest affinity site of human serum albumin observed in molecular dynamics simulation. *Arch. Biochem. Biophys.* **2015**, *579*, 18–25. [CrossRef]

76. Kotev, M.; Lecina, D.; Tarragó, T.; Giralt, E.; Guallar, V. Unveiling prolyl oligopeptidase ligand migration by comprehensive computational techniques. *Biophys. J.* **2015**, *108*, 116–125. [CrossRef]

77. Santofimia-Castaño, P.; Rizzuti, B.; Abián, O.; Velázquez-Campoy, A.; Iovanna, J.L.; Neira, J.L. Amphipathic helical peptides hamper protein-protein interactions of the intrinsically disordered chromatin nuclear protein 1 (NUPR1). *Biochim. Biophys. Acta Gen. Subj.* **2018**, *1862*, 1283–1295. [CrossRef]

78. Pantoja-Uceda, D.; Neira, J.L.; Contreras, L.M.; Manton, C.A.; Welch, D.R.; Rizzuti, B. The isolated C-terminal nuclear localization sequence of the breast cancer metastasis suppressor 1 is disordered. *Arch. Biochem. Biophys.* **2019**, *664*, 95–101. [CrossRef]

79. Chavez, K.J.; Garimella, S.V.; Lipkowitz, S. Triple negative breast cancer cell lines: One tool in the search for better treatment of triple negative breast cancer. *Breast Dis.* **2010**, *32*, 35–48. [CrossRef]

80. Lappano, R.; Jacquot, Y.; Maggiolini, M. GPCR modulation in breast cancer. *Int. J. Mol. Sci.* **2018**, *19*, 3840. [CrossRef]